The University Of Sheffield.

A Fundamental Understanding of the Factors Controlling the Chemical Performance of Model Polymer Networks

S Knox

Thesis submitted in partial fulfillment for the degree of Doctor of Philosophy

The University of Sheffield,

Faculty of Engineering,

Department of Mechanical Engineering

2018

Acknowledgements

I would like to thank my supervisor Prof Patrick Fairclough for all his help, advice, time and passion over the past eight years of undergraduate and then postgraduate study. At the risk of being overly sentimental, he is a very very clever man but an even nicer person and that's why I've loved doing science with him across all of the projects/tutorials.
p.s. I'll never forget the importance of **UNITS** again I promise.

Thanks go to my industrial sponsor, AkzoNobel, and especially Colin Cameron and Tony Wright for all of their wise and valued input (as well as a range of others who have helped over the course of the PhD!).

The Fairclough group as a whole is also deserving of lots of thanks—particularly Ryan Seabright, Alec Shackleford, Rhys Williams, Yas Khalil and, from way back when, Tom Sydney for lots of lunches, chats and bad quality office games. A special mention is given to the physics to my chemistry, Alec Shackleford. It's been a pleasure working together so much, as well as multiple trips to Newcastle and fighting snow and ice to Didcot. Thanks also to the other people who I've shared an office with over the PhD—especially Luke Fox and Ryan Brown for lots of football, food and FIFA, as well as helpful chats and what-have-yous about polymery things.

In the chemistry department, a thank you to Babs and Prykey for all of their help and generosity in terms of lab and office space, as well as brews, games of cribbage and high sodium content sustenance. Thanks also go to Rob Hanson for his analytical help, and to Rory Campbell & Zoe Smallwood for a range of assistance/loans/donations. Rod and Joel in Materials also very much thanked for all of their help and DMA kindness!

I've also had the pleasure of being part of the Polymer CDT in Sheffield and would like to thank Prof Steve Armes and Dr Joe Gaunt for all they have done in coordinating the scheme and supporting our study, as well as the rest of my cohort - Luke, Matt, Kat, Amy and Dom - without whom seminars and conferences would have been far less fun.

So many friends have also been cracking—too many if I'm going to keep this to a page but I'm grateful to so many for lunches, dinners, beers and coffees—especially Sam, Tay, Clive, Fred, Si, Ben, Grant, Liam...

Finally, I'd like to thank my family - first my cracking brother and sister Phil and Debz who are always there if I need them and even pretend to be interested in chemistry for me (sometimes). Second, my Mum and Dad who blessed me so much with their love and support growing up. I am so grateful for the legacy my Dad left and the continued love my Mum shows. Finally, finally, Nic, my amazing, beautiful, funny and kind wife. Thank you for your love, support and understanding over our first two years of marriage. I love you so much and am so grateful for all you are and do.

Abstract

A range of bisphenol based epoxy resin monomers were cured with a range of amines to investigate the influence of nuanced chemical changes of constituent molecules upon the chemical performance of networks.

Initially, the curing process was optimised in order to reduce the influence of oxidation and carbamation. Moving away from a stoichiometric formulation was found to result in a slight decrease in chemical performance. Networks cured under an air atmosphere swelled faster, and were more vulnerable to failure.

Networks based on DGEBF monomers rather than DGEBA were generally found to exhibit an improved chemical performance. Chain extension of epoxy resin monomers was demonstrated to result in less dense networks which showed lower and slower solvent uptake.

Aromatic amines were found to give denser networks which showed reduced and slower sorption (vs. aliphatic analogues). 1,3- substitution of six-membered rings was found to produce networks of a higher performance than 1,4- analogues, irrespective of similar densities.

Complete isomeric separation from an industrial DGEBF based resin was not possible by any scalable means, but purified mixtures were obtained. Furthermore, individual isomers were synthesised. Networks produced with these isomers (as well as mixtures of different compositions) demonstrated the reduced performance caused by ortho- substitution. Particular emphasis is drawn to the comparison of para-para-DGEBF (ppDGEBF) to ortho-ortho-DGEBF (ooDGEBF) which shows the dramatic effect that nuanced chemical changes can have upon chemical performance—the oo was shown to have a much higher rate of sorption and ultimate uptake.

Across the work it was demonstrated that none of the individual physical/thermal properties probed (T_g, density, crosslink density, T_β) offered an effective indicator (in isolation) of chemical performance, though a combination of properties indicating a well-packed network gave a good indication of performance. Density was shown to be the most important of these factors.

Contents

List of abbreviations

1,3-BAC - 1,3-bis(aminomethyl)cyclohexane

1,4-BAC - 1,4-bis(aminomethyl)cyclohexane

3,3'-DDS - 3,3'-diaminodiphenyl sulfone

4,4'-DDS - 4,4'-diaminodiphenyl sulfone

AFM - Atomic force microscopy

C1 - Cycle one

C2 - Cycle two

DDM - diaminodiphenyl methane

DER 332 - Dow Epoxy Resin 332

DER 354 - Dow Epoxy Resin 354

DGEBA - diglycidyl ether of bisphenol A

DGEBF - diglycidyl ether of bisphenol F

DMA - Dynamic mechanical analysis

DSC - Differential scanning calorimetry

D_{sor} - Diffusion coefficient of sorption

D_{des} - Diffusion coefficient of desorption

E828 - Epikote 828

ECH - Epichlorohydrin

EEW - Epoxide equivalent weight

F1 - Fraction one

F2 - Fraction two

HMD - hexamethylenediamine

HPLC - High performance liquid chromatography

IR - Infrared

LM33 - A mixture of the n=0 DGEBF isomers with a pp : po : oo ratio of 33 : 50 : 17

LM37 - A mixture of the n=0 DGEBF isomers with a pp : po : oo ratio of 37 : 47 : 16

M_c - mass between crosslinks

MW - molecular weight

MXDA - meta-xylylenediamine

NIR - Near infrared

NMR - Nuclear magnetic resonance

oo - ortho-ortho-

ooDGEBF - ortho-ortho-diglycidyl ether of bisphenol F

PACM - bis(para-aminocyclohexyl) methane

po - para-ortho-

poDGEBF - para-ortho-diglycidyl ether of bisphenol F

pp - para-para-

ppBPF - para-para-bisphenol F

ppDGEBA - para-para-diglycidyl ether of bisphenol A

ppDGEBF - para-para-diglycidyl ether of bisphenol F

pppo - an approximately 1:1 mixture of the para-para- and para-ortho- isomers of DGEBF

PTFE - Poly(tetrafluroethylene)

PXDA - para-xylylenediamine

PY306 - Araldite PY306

R_f - Retardation factor

SANS - Small angle neutron scattering

SAXS - Small angle x-ray scattering

T - temperature

T_β - β-transition temperature

TBAB - Tetrabutylammonium bromide

T_g - Glass transition temperature

TGA - Thermogravimetric analysis

UV - Ultraviolet

vdW - van der Waal's

List of Figures

List of Tables

Chapter 1

Introduction

1.1 Background

1.1.1 Polymers

Polymers are macromolecules which are formed from the repeated reaction of monomers, in polymerisation.[1] The repeating structure formed gives rise to properties different to other species. There are two main mechanisms of formation—step or chain growth polymerisations (Figure 1.1). Chain growth involves the creation of a reactive centre, which reacts with monomer (generally rapidly) until a final termination reaction to prevent any further reaction (Figure 1.1a). Examples of this type of polymerisation are radical and ionic polymerisations. Step growth polymerisations involve the reaction of functional groups in a stepwise manner. This means that before any macromolecules are formed, smaller oligomers are formed (Figure 1.1b), and as such, a high proportion of reactive groups must react in order to obtain high molecular weight polymers (Figure 1.1c).

Polymerisations can form one of two main types of polymers: thermoplastics or thermosets. Examples of thermoplastics include polyethylene, polystyrene and nylon. The molecules in thermoplastics, whilst large, are distinct. Therefore, upon heating they will melt and flow.[2] Thermosets, on the other hand are a class of polymer which do not flow upon heating, due to crosslinking reactions.[1] Upon reaching a sufficiently high temperature, thermosets will degrade - in air, this results in burning. They include the first fully synthetic polymer, Bakelite – made in 1909.[3] In polymerisation, a molecule of "infinite" molecular weight (considered so relative to the other molecules within the vessel) is formed.[2,4] The polymer formed is insoluble in any solvent, though it will swell in compatible solvents.

(i) Initiation $I^* + M \longrightarrow IM^*$

(ii) Propagation $IM^* + nM \longrightarrow IM_nM^*$

(iii) Termination $IM_nM^* \longrightarrow IM_nM$

(a)

monomer + monomer → dimer
monomer + dimer → trimer
dimer + dimer → tetramer
trimer + monomer → tetramer
trimer + dimer → pentamer
etc.

(b)

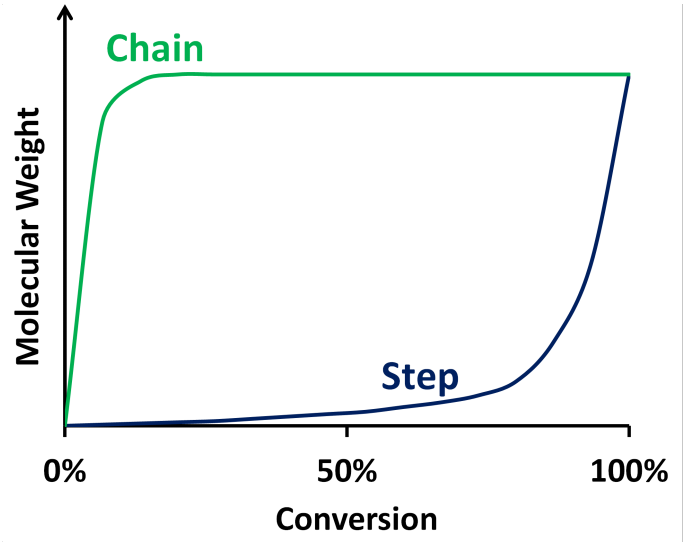

(c)

Figure 1.1: Generalised mechanisms of polymerisation for (a) chain growth and (b) step growth polymerisations and (c) the development of molecular weight with monomer conversion for step and chain polymerisations

1.1.2 Thermosetting networks

Generally, thermosets are stiff and strong, and have a high resistance to both mechanical and chemical attack. Such materials have wide ranging applications such as barrier materials and adhesives. Howsoever they may be formed, whether by a combination of multiple components or a simple homopolymerisation, there is a critical extent of reaction (i.e. the point at which this "infinitely" large molecule is formed), where the material becomes a solid; the gel-point. With regard to step growth polymerisation, multifunctional monomers or oligomers allow for the formation of such a molecule. Equation 1.1 shows the result of Flory and Stockmayer's work on the subject, based on the assumptions that (a) molecular weight has no bearing on the reactivity of a functional group and (b) intramolecular reactions are neglected.[4–7] This states that in a system where functional group A reacts with group B (e.g. epoxy-amine reaction), the extent of reaction at which gelation occurs relies solely on the stoichiometric ratio of the reactants, r, and the site average functionality of the reactants, $f_s(X)$. In a two component reaction mixture (M_A & M_B) this simplifies to the functionalities (i.e. the maximum number of times something can react) of M_A & M_B.

$$P_{gel} = \frac{1}{\sqrt{r(f_s(A)-1)(f_s(B)-1)}} \tag{1.1}$$

Extent of reaction at the gel point (P_{gel}) of an A + B polymerisation, where r is the stoichiometry ($[M_A]/[M_B]$), $f_s(X)$ is the site average functionality of component X[4–7]

Upon gelation, theoretically viscosity becomes infinite, and a molecule which interconnects all of the boundaries of the system is formed (the aforementioned "infinite" molecular weight species).[2] The system can then be thought of as two main components; the macromolecular network, and the "sol". The sol is made up of the remaining collection of "finite" (soluble) molecules, i.e. the remaining unreacted monomers and any solvent that might be present. The relative amount of sol, quantified as the sol fraction, decreases as the network continues to grow as the cure progresses.

Degree of cure is used to describe the progress of reaction and is given as the ratio

of reacted groups to the total number of possible reactive groups. Any chains that are not connected at both ends to the network are known as "dangling ends", though they are still part of the gel, rather than the sol.

1.1.3 Coatings

A very common application of thermosets is as coatings. There are two main reasons for coating a substrate. The first is decorative, to improve its appearance, such as decorative paint. The second is protective, to extend the longevity of the substrate, or its resistance to a particular variety of attack.[8,9] One example of an application of protective coatings is in chemical tanks. These tanks can range in size from lab-scale few litre tanks, to industrial settings. One such setting are tanks used in marine chemical transport—where they can carry millions of litres of chemicals.

The primary concern with regards to a decorative coating, usually a paint or varnish, is its appearance. This is usually controlled by the surface roughness, and the refractive index of the components of the coatings. Usually, it is the addition of a pigment that achieves the colour, and a change in surface roughness that adjusts the "finish" of the coating.

Protection can be offered from mechanical ageing or chemical damage and the effectiveness of that protection is described by the coatings performance. Mechanical performance is split into many different categories, from friction to impact resistance.[10] Which of these is most important is application dependent, but there exists a plethora of tests in order to fully characterise a coating's mechanical performance. How a coating maintains its properties over time is also crucial. Ageing can be weathering related, including (but not limited to) exposure to oxygen, sunlight (UV), heat, pollutants and cleaning chemicals. Finally, chemical performance describes the resistance of a coating to a variety of substances.

Chemical performance

The range of possible chemical environments is vast. Potential aggressors can be solid, liquid or gaseous and vary in temperature, pH or polarity. Approaches to chemical protection are either aggressor specific or general. An example of a specialised approach is the selection of a highly non-polar coating for a polar chemical. This would discourage mixing, meaning that the chemical is less likely to damage the coating. A more universal approach is the use of highly crosslinked networks, or thermosets. These networks must not have any bonds or linkages that are readily degraded by common aggressors (such as easily hydrolysed groups). By their nature these networks are insoluble in any solvent, and hence offer protection across a wider variety of aggressors.[2] However, ingress of solvent molecules into the networks is possible, which causes swelling, this swelling induces a stress in the coating and in turn damage—therefore, longevity of the coating will be inversely related to the solvent uptake.[11,12] Furthermore, the presence of an solvent plasticises the network. This leads to a decrease in the glass transition temperature and a reduction in mechanical properties.

1.1.4 Diffusion

Since it is the sorption of a chemical species that leads to a stress exerted on a network,chemical performance in thermoset polymers is often tested using solvent uptake measurements. Of note here is that the uptake of mass is not limited to either absorption nor adsorption and therefore, the terms sorption or uptake are preferred.[13]

The most common theory used to described the diffusion processes which govern the solvent uptake is Fick's laws.[14] Fick's first law (Equation 1.2) states that a species will move from an area of high concentration to an area of low concentration. The rate of this motion is governed by the concentration gradient—as described by Fick's second law (Equation 1.3). Therefore, the rate of diffusion of a species into an environment will always be highest when it is first exposed to that environment. As the concentration gradient decreases, so too will the rate.

As discussed, one way by which to measure the diffusion of a material into a solid

$$\mathbf{J} = -D \frac{\partial C}{\partial x} \tag{1.2}$$

$$\frac{\partial C}{\partial t} = D \frac{\partial^2 C}{\partial x^2} \tag{1.3}$$

Fick's first (1.2) and second (1.3) laws. **J** *is the diffusive flux,* **D** *is the diffusion coefficient,* **C** *is the concentration* **t** *is time and* **x** *is the position.*

medium is by the mass uptake of the medium. At short times, for Fickian diffusion, the mass uptake can be shown to be directly proportional to the square root of time—the rate of diffusion therefore slowing with time (as the concentration gradient decreases).

It has been shown by Shen and Springer that Equation 1.4 describes the uptake of a material displaying Fickian behaviour, at short times.[15] Hence, the diffusion coefficient can be determined by the plotting of $\frac{M_t}{M_\infty}$ against the square root of time where M_t is the mass at any time and M_∞ is the ultimate mass absorbed.

$$\frac{M_t}{M_\infty} = \frac{4}{s}\sqrt{\frac{Dt}{\pi}} \tag{1.4}$$

Approximation of the diffusion coefficient at short times with Fickian diffusion, where $\mathbf{M_t}$ *is the mass at any time,* $\mathbf{M_\infty}$ *is the ultimate mass absorbed,* **s** *is twice the thickness of the sample for a sample exposed on one side or the thickness of the sample if it is exposed on both sides,* **D** *is the diffusion coefficient and* **t** *is time.*

Solubility

The speed and amount of uptake can generally be attributed to two key factors—solubility and the diffusion coefficient.[13,16] These are influenced by both the polymer network and by the potential penetrant. In uptake, solubility refers to the miscibility of the network with the penetrant. The major influencing factor is the polarity of both components - similarity in polarity leads to good miscibility. This can be quantified by the use of a solubility parameter (δ), such as the Hansen solubility parameter.[17] This theory, which built upon work by Hildebrand among others, makes use of three

components - the contributions towards the cohesive energy of a substance (to which the solubility is directly related) made by (i) dispersion forces, (ii) polar forces and (iii) hydrogen bonding—as shown in Equation 1.5. Similar values for the cohesive energies of two components means mixing is favoured.[18]

$$\delta^2 = \delta_d^2 + \delta_p^2 + \delta_h^2 \tag{1.5}$$

The determination of the individual components of Equation 1.5 is not facile. The methodology applied by Hansen uses an indirect measurement of each component. Using the absence of any polar or hydrogen bonding groups in hydrocarbons, it is assumed that the dispersive contribution of any substance is equal to its corresponding hydrocarbon—i.e. one of similar structure. The polar and hydrogen bonding components were then separated empirically. The solubilities of a range of polymers in a range of solvents was determined, and δ_p & δ_h adjusted until all good solvents for a specific polymer were in close proximity when plotted upon a three dimensional plot of δ_d, δ_p & δ_h. There are a number of values available in the literature, for both polymers and solvents.[19–22]

Both Hoftyzer & Van Krevelen and Hoy offer methods by which to achieve prediction of solubility based on this work.[18,23,24] Both methods identify the functional groups present in a substance and then sum dispersive, polar and hydrogen bonding contributions made by those groups to predict a value for each of the total contributions to the solubility parameter. Hoftyzer & Van Krevelen's method first predicts the three contributing values and then takes the sum of squares to obtain a figure. By contrast, the Hoy method first predicts the total solubility parameter, the hydrogen bonding contribution and the polar contribution. Finally, the dispersive contribution is found by subtraction of the latter two components from the former. The usefulness of such methods lies in their ability to make predictions for the majority of polymers. However, it provides only a useful guide, it is not a cover-all method for solubility determination.

Diffusion coefficient

The diffusion coefficient is not wholly separate to solubility, in that it again relates to interaction between a penetrant and a uptaking medium. Where solubility is particularly low, the diffusion coefficient will be low, as any mixing will be highly disfavoured. However, in cases where mixing is favoured, a pathway for sorption must be possible for uptake to occur. Therefore, the "free volume" of a medium is relevant to its ability to uptake small molecules. It also follows that the size of such penetrants is also relevant to the sorption.

As is illustrated by Jackson *et al.*, where a solvent is larger than the characteristic free volume in a substance, the prospect of sorption is substantially reduced, regardless of solubility (illustrated by the use of substances with very similar chemical compositions but a difference in free volume).[25]

Diffusion in polymers

When considering diffusion in polymers, further complications are introduced by the elastic behaviour of the polymer. In rigid solids, diffusion is entirely governed by the flux of the penetrant.[26] However, polymers are by no means rigid and so the flux calculations also need to account for the kinetic coefficients of the polymer. Further, the sorption of solvent in polymers results in a change in the properties of the polymer. The disruption of the polymer-polymer interactions plasticises the network—so-called due to the associated decrease in T_g. Upon swelling, there is an associated "decrease in chain configurational entropy".[27,28] This decrease in entropy is counteracted by the energetic favourability of solvent-polymer mixing. There is extensive mathematical treatment of the entropic changes, but the qualitative picture can be explained in terms of the two opposing driving forces. Upon swelling, an elastic force builds in the network as chains stretch to facilitate the presence of the penetrant.[29] This restrictive force acts in opposition to the osmotic pressure causing uptake—and the plateau in uptake is observed when these opposing forces balance (the osmotic pressure is driven by the energetic favourability of mixing).

The change in free volume caused by solvent ingress results in deviations from Fickian

diffusion for some polymeric systems. A number of non-Fickian processes are shown in Figure 1.2. The most extreme case of those shown is Case II (d)—the expected decrease in sorption is not observed. Instead the mass uptake is proportional to time and not the square root of time.[30] As is alluded to, swelling processes drive this unexpected finding—since glassy polymers are not at equilibrium, there are relaxation processes facilitated by the ingress, allowing further such ingress.[26,29] Further work, such as that by Rossi & Mazich shows that the sigmoidal mode of uptake can be described by Fickian theory, when the mobility of the network (i.e. swelling) is accounted for.[31]

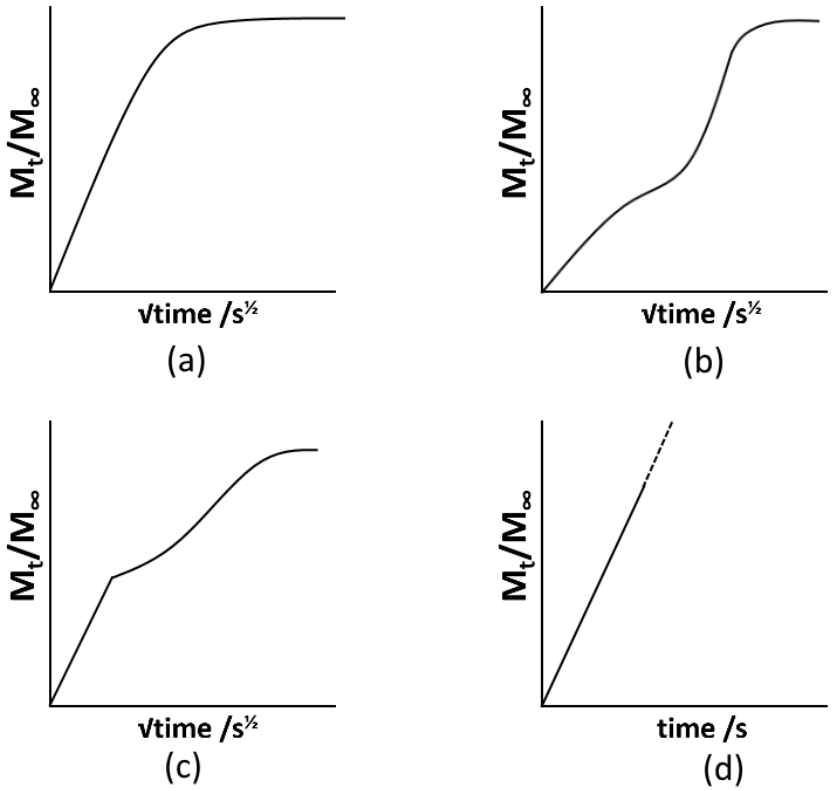

Figure 1.2: Different classes of sorption: (a) Fickian, (b) sigmoidal, (c) two-step, (d) Case II.[29]

1.1.5 Epoxy resins

The term "epoxy resins" is used to describe both (a) a group of epoxide end functionalised monomers and oligomers which form the basis for thermosets used ubiquitously in coatings, adhesives and paints, and (b) the thermosets themselves.[32–34] For the purposes of this work, epoxy resin monomers will be used to describe (a), the functionalised monomers; and crosslinked epoxy resins or epoxy networks used to describe (b) the prepared thermoset networks. The high reactivity of the epoxide group with both nucleophiles and electrophiles is the basis for network formation.[2] Networks are formed with homopolymerisation upon heating with a suitable catalyst (such as a tertiary amine) or, more commonly, with a wide variety of co-reactants, called curing agents or "hardeners".

Bisphenol based epoxy resins

Bisphenol based glycidyl ethers (such as the diglycidyl ether of bisphenol F, DGEBF, and the diglycidyl ether of bisphenol A, DGEBA) are made with the reaction of epichlorohydrin (ECH) and the relevant bisphenol (Scheme 1.1).[35] This reaction also leads to the formation of higher oligomers, as the phenolic groups can attack the epoxide (the product is shown in Figure 1.3b).

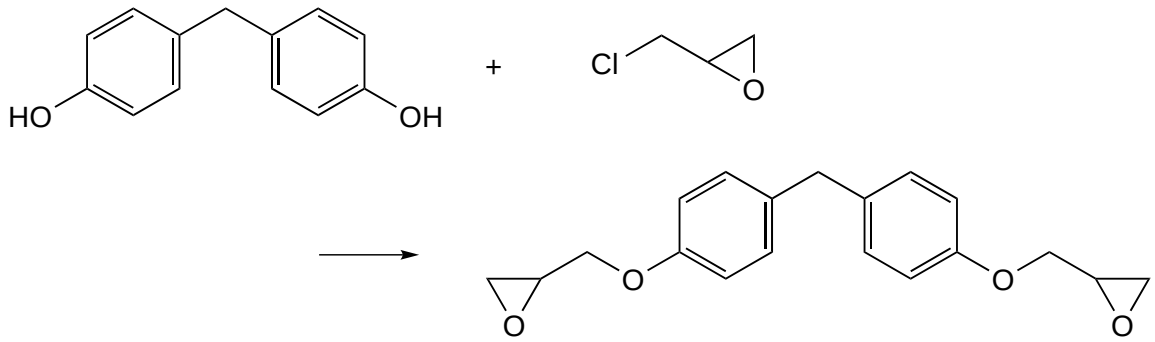

Scheme 1.1: The synthesis of para-para-diglycidyl ether of bisphenol F (ppDGEBF) from para-para-bisphenol F (ppBPF) and epichlorohydrin

In the case of epoxy resins based on bisphenol F, there are further structural complications introduced by the regioisomerism possible around the phenyl rings. This variation is not found in bisphenol A based resins. The possible isomers are para-para- (pp), para-ortho- (po) and ortho-ortho- (oo) -DGEBF, and are shown in Figure 1.3a.

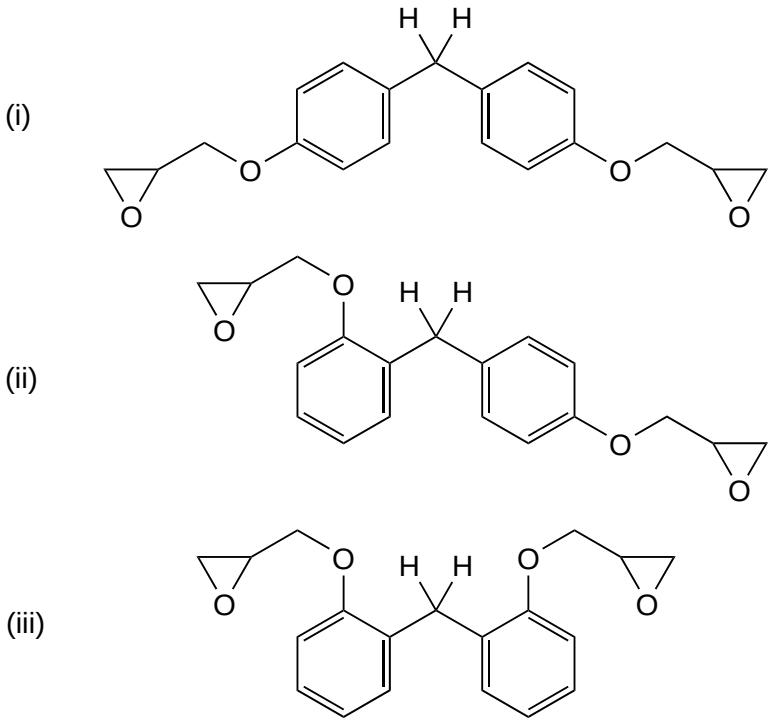

(a) The three isomers of DGEBF, (i) para-para (pp), (ii) para-ortho (po), (iii) ortho-ortho (oo). The methylene protons on the bridging carbon are explicitly shown. These have different NMR environments and so can be used to find the ratio of the isomers in any mixtures.

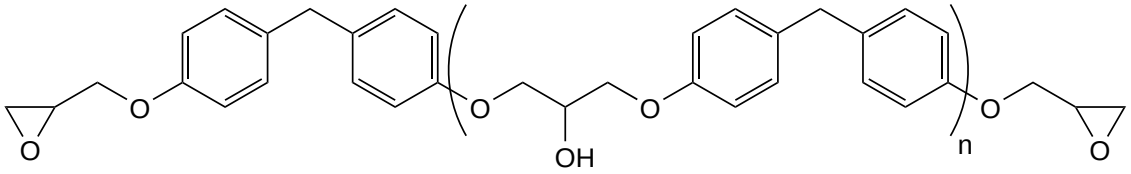

(b) The structure of "chain extended" isomers when only considering para- substitution in DGEBF.

Figure 1.3: Sources of chemical variability in bisphenol F based epoxy resins

Dow Epoxy Resin 354 (DER 354) is an industrially available bisphenol F based resin. The degree of chain extension is quantified by the value for n shown in Figure 1.3. For DER 354 this is 0.11 (found by titration). When considering only the $n = 0$ isomers, the ratio of the pp : po : oo isomers is 40 % : 45 % : 15 %, as found by high performance liquid chromatography. (For more detailed methods used to find these values, see Section 3.1.1). It is worth noting that with all the chemical possibilities available, there is likely to be variation between bisphenol F based resins from different suppliers, and even potentially between different batches.

Characterisation of epoxy resin monomers

As a result of the above discussed chain extension, reactant mixtures can show variability in the molecular weight of the epoxide species. Hence, the parameter epoxide equivalent weight (EEW, in units of mass per mole of epoxide) is commonly used. This can be determined by titration, infrared (IR) spectroscopy or ^{1}H nuclear magnetic resonance (NMR) spectroscopy.[36–38] EEW is useful when epoxides are used in tandem with hardeners, as stoichiometry can then be effectively calculated and adjusted accordingly.

Two other measurements of note with regard to epoxy resin monomers are hydroxyl and chlorine content.[39] Hydroxyl groups are present simply as a result of the ring opening of the epoxide group, as with the above mentioned formation of higher oligomers. They may introduce complexity as they react with some hardeners, and the epoxide group itself, alongside catalysing of other epoxide reactions. Chlorine present is usually as a result of an abnormal addition of ECH, or through the reaction of ECH with an intermediate. It can affect final properties of the cured resin, most generally as a resin with lower functionality: the EEW is increased- this can lead to less efficient packing in the network. This is turn leads to a degradation in the barrier properties.

1.1.6 Epoxy-amine reactions

The epoxy-amine system is the most commonly used in producing epoxy networks and is consequently well-studied. As shown in Scheme 1.2, both primary and secondary amines react with epoxide groups; at similar rates if the amines are aliphatic.[2] This reaction is autocatalytic: the presence of hydroxyl groups increases the rate, with the formation of a trimolecular transition state (Scheme 1.3), though reaction in the absence of hydroxyl is also possible.[40–42]

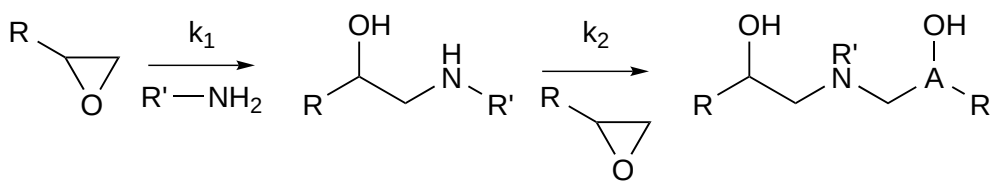

Scheme 1.2: Basic reaction scheme in epoxy-amine network formation

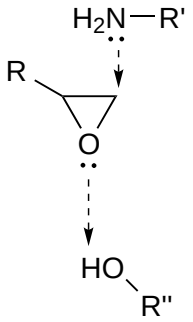

Scheme 1.3: Trimolecular transition state of hydroxyl catalysed epoxy-amine reaction

Mechanistic considerations

A range of different mechanistic schemes have been developed for amine-epoxy network formation. General agreement is found with a number of considerations. Homopolymerisation of the epoxide is neglected in the absence of Lewis acids/bases. Etherification (see Scheme 1.4), where hydroxyl groups produced in earlier reactions then ring open the epoxide ring is also generally negligible, except in certain circumstances: when there is a stoichiometric excess of epoxy groups, the higher activation barrier (vs. amine-epoxy reaction) ceases to prevent competition as long as the temperature is sufficiently high.[43]

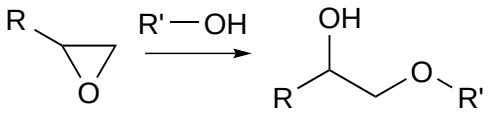

Scheme 1.4: Etherification in epoxy resin curing

The amine-epoxy reaction is by no means as simplistic as it at first glance appears. As stated above, autocatalysis is seen due to the formation of hydroxyl groups, though this is not the only possible route. Initial treatments from Horie et al. and Smith completely discount bimolecular reactions.[40,44] These authors state that only trimolecular reactions involving hydrogen donors are relevant. This treatment has also been supported by a number of authors, including Arutyunyan, Mijovic and Rozenberg, who all account for reaction in the absence of hydroxyl groups with a second amine acting as the hydrogen donor – justified by a quadratic dependence of the rate upon amine concentration.[42,45,46] Cole added to this position by also explicitly accounting for etherification, for those situations where there is an excess of epoxy with high temperatures.[47]

However, further study, for example that by Paz-Abuin et al., describes a much more important role played by the bimolecular reaction.[48] Scheme 1.5 shows this treatment, with both catalysed and uncatalysed processes accounted for. Steps (3) and (4) show the uncatalysed reactions between amines and epoxides. Their findings disagree explicitly with the claim of a quadratic dependence of the rate on the amine concentration, stating they could not "...find any good theoretical or experimental agreement." A theoretical study from Ehlers et al. also agrees that the uncatalysed route is likely to play a part, especially in the absence of hydroxyls.[49]

The reason for the disagreement is most likely a variation in the reactivity of the amines investigated. This can have a major effect on the relative rates of reaction. A large disparity between the catalysed and uncatalysed rates is seen with aromatic amines, Rozenberg reports the catalysed being 40-50 times faster.[42] In stark contrast, Paz-Abuin et al. found a much smaller disparity when using the aliphatic amine 1,3-bis(aminomethyl)-cyclohexane (1,3-BAC).[48] They report the catalytic reaction to only be around twice as fast as the uncatalysed.

The study completed by Ehlers et al. also presents some interesting findings regarding the nature of the transition states.[49] It was found computationally that the acyclic route was much more likely to produce a reaction than the cyclic. Activation energies were substantially lower - in the case of the hydroxyl catalysed reaction, half the energy.

The complexity described above means a fully accurate and complete model has not been produced, though there are some general features that are agreed upon, or that are used regularly across many different studies. Equation 1.7 is one such feature, which can be derived from the Horie model. It is also possible to derive from Scheme 1.5, assuming (a) there is no evaporation, (b) the formulation is stoichiometric (i.e. the initial concentration of epoxide $[E]_0$ is double that of primary amine, $([E]_0 = 2[A_1]_0)$ and (c) the ratio of the rate constants for primary and secondary reaction is independent of route and, as an ideal case, equal to a half (i.e. $\frac{k_2}{k_1} = \frac{k_2'}{k_1'} = \frac{1}{2}$.). The explicit suggestion is that primary & secondary amine hydrogens are of equal reactivity. However, this ideal case certainly does not hold in all circumstances, with the secondary amine commonly

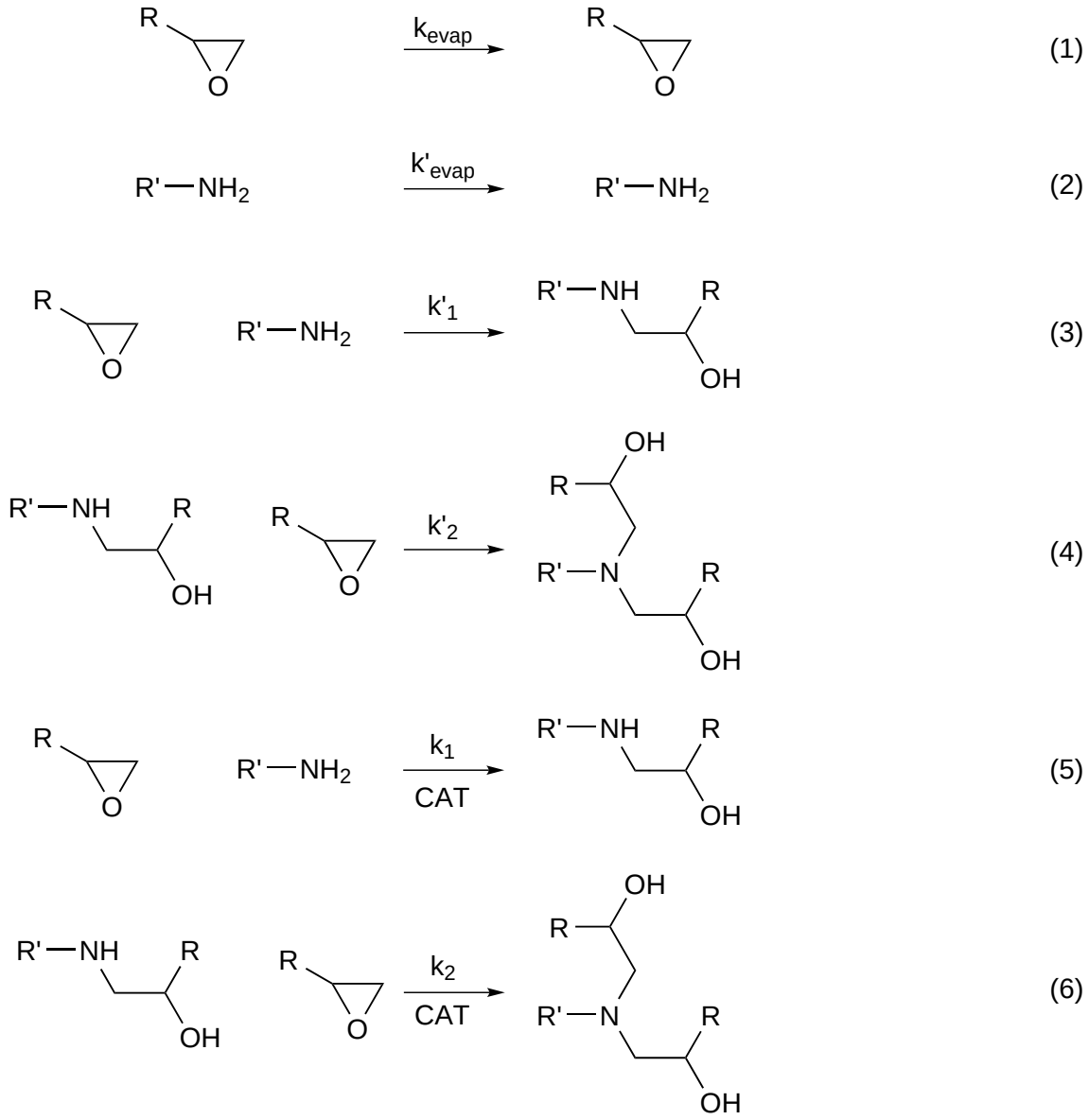

Scheme 1.5: Kinetic scheme from Paz-Abuin et al.[48] for reaction of amine with epoxide. Steps (1) & (2) represent evaporation of both monomers; (3) & (4) uncatalysed reactions between epoxides and amines; (5) & (6) the catalysed reactions. In the scheme it is accepted that OH groups are the catalytic groups

found to be less reactive.[46,48,50] This is explained by Ehlers and co-workers as a solvent effect, and not due to steric or electronic effects.[49]

$$\alpha = \frac{[E]_0 - [E]}{[E]_0} \tag{1.6}$$

α, the extent of reaction, defined in terms of epoxide consumption, where $[E]$ is the epoxide concentration, and $[E]_0$ is the initial epoxide concentration

$$\frac{d\alpha}{dt} = \left(\frac{1}{2}k_1'[E]_0 + \frac{1}{2}k_1{[E]_0}^2\right)(1-\alpha)^2 \tag{1.7}$$

Rate of consumption of epoxide, relative to the rate constants of the uncatalysed (k'_1) and catalysed (k_1) reactions. α is the extent of reaction as defined in Equation 1.6, and $[E]_0$ denotes the initial concentration of epoxide.

Approaches to kinetic investigation

There have been a number of experimental approaches in order to observe the epoxide reaction with amines and extract relevant kinetic information. A very common approach is to simply use monofunctional analogues of the components of the reactive mixture.[44,51] For example, Horie and co-workers used phenyl glycidyl ether in place of DGEBA and butylamine for a variety of aliphatic diamines (Figure 1.4). This ensures there is not the same increase in viscosity and gelation, so the kinetics of the individual reactions can be studied (for example, those outlined in Scheme 1.5).

Other experimental studies simply use the multifunctional compounds in the cure, but do not run to full conversion, or only fit their kinetic model to partial conversions.[48,52] The advantage here is the use of the actual system of interest, but no kinetic information can be obtained in the later stages of reaction, as it becomes diffusion limited. This might impair investigation of the reaction of secondary amines with epoxides to form the tertiary amine bridge points. Both systems allow for investigation of the rates of reaction between amines and epoxides. Observation of the progress of reaction (or of the degree of cure) is most commonly achieved using near-IR spectroscopy or differential

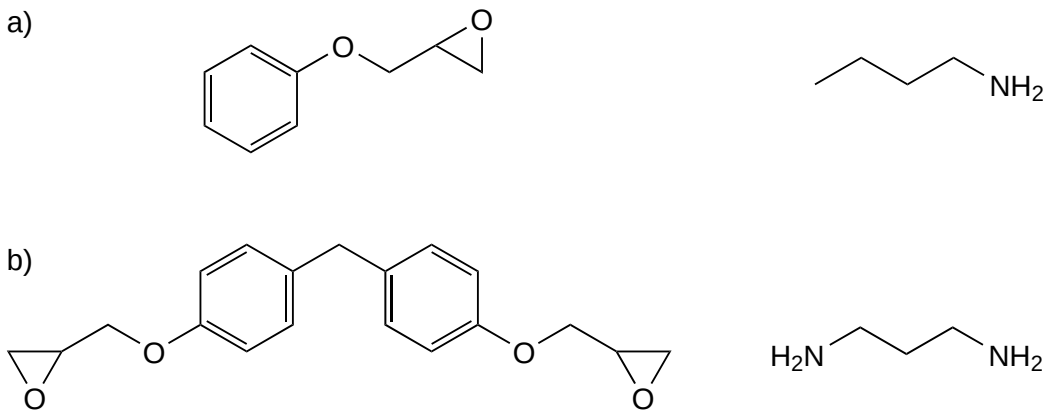

Figure 1.4: a) Monofunctional analogues of b) their multifunctional counterparts for both an epoxy (left) and an amine (right)

scanning calorimetry (DSC).[51,53–55] There are many other methods, including Raman spectroscopy and rheometric studies.[56,57]

1.1.7 Structure of crosslinked epoxy resins

One defining characteristic of thermosets is the crosslink density, inversely related to the mass between crosslinks, M_c. An increased crosslink density leads to higher strength and stiffness, as well as an increase in glass transition temperature (T_g).[7,11] For this reason, the T_g is a good indicator for degree of cure.[2] Epoxy resins generally have a higher crosslink density than typical elastomer networks.[32] It is from this that a number of their beneficial properties arise.[11,58] For example, the increase leads to an increase in some mechanical properties (higher strength and stiffness, for example) and results in a reduction of solvent uptake, however this does tend to make the networks more brittle.

Achieving a high crosslink density is primarily achieved by ensuring the formulation is stoichiometric (i.e. the ratio of hardener reactive sites to epoxy reactive sites is 1).[32] Hence, in an ideal system, all of the functional groups will have reacted, and each pair replaced by a crosslink. However, this ideality is reliant on full conversion, which is hindered by the connected nature of the network and is on the whole arrested upon vitrification of the network. Ensuring the coating is heated to above its ultimate glass transition temperature ($T_g(\infty)$) during the cure will go some way to achieving a high crosslink density, by preventing vitrification, though chain mobility is still inhibited in the

rubbery state upon gelation.

It has been claimed that variations throughout the network in crosslink density result in a nodular, inhomogeneous structure.[59,60] Initial evidence was drawn from "granular" electron microscopy images which show features between 5 and 100 nm in size.[32,61]

Using atomic force microscopy (AFM), Vanlandingham and co-workers also observed the presence of microgel particles which are highly crosslinked. These 10nm particles aggregate to give features up to 70 μm in size, surrounded by a lower density phase. They found the T_g of the polymer is highly dependent on the proportion of the second less dense phase. Even a small amount of this softer phase leads to a substantial suppression of the T_g of the network. It does not however result in a significant change in mechanical properties (as indicated by the flexural storage modulus).

However, there is a conflict of opinion regarding the existence of the microgel particles. The origin of this disagreement lies in work by a number of researchers.[62,62,63] They found that when using electron microscopy (i) similar nodular features are seen in amorphous thermoplastic polymers and (ii), perhaps more compellingly, nodules are only seen in lower vacuums. This demonstrates that the electrons are etching the polymer, and producing the inhomogeneity within the system. Furthermore, they call into question the conclusions drawn by Vanlandingham et al. By outlining a variety of drawbacks with the AFM methodology used, they draw the conclusion that sample preparation is responsible for the inhomogeneity observed.

Further evidence in support of both sides is found in work using scattering techniques such as small angle neutron scattering (SANS) and small angle x-ray scattering (SAXS).[64,65]

For nodules to be present, there must be a mechanism by which they form. Whilst their conclusions regarding homogeneity differ somewhat, Bahrami et al. and Sahagan and Morgan both describe such a mechanism.[58,66,67] As earlier discussed, the network growth reaction is autocatalytic; hydroxyl groups are formed which then catalyse further amine-epoxy reactions. As such, after initial reaction, further activity will tend to occur in close proximity to these already formed crosslinks. This leads to clusters (or nodules)

of crosslinked materials, separated by unreacted monomers. Upon gelation, linkages are formed between these nodules, giving the heterogeneous material observed so commonly. The difference in these two pieces of work lies in their description of fully cured networks, as both agree that nodules initially form, and are present at lower degrees of cure. However, Bahrami and co-workers found the fully reacted network to be homogeneous whereas Sahagun and Morgan found a heterogeneous final network upon complete cure.

To summarise, a valid mechanism for the formation of regions of higher crosslink density in some epoxy systems has been presented and proven to cause, at least initially, nodules to form. Therefore, these nodules will be present at the gel point, which occurs well before full conversion. It follows that the final product will be nodular unless there is a stress-relieving mechanism (e.g. shrinkage, cracking), or that the regions of low crosslink density are of an equal or higher molecular density. This is because high crosslink density regions grow at the expense of molecules from regions of lower crosslink density regions.

Nanostructure of crosslinked epoxy resins

The nanostructure of crosslinked epoxy resins will clearly be governed by the chemical structure of its constituent parts (some of the details of which were discussed in Setion 1.1.5). In terms of the probing of this structure, aside from kinetic investigation of the reaction (Section 1.1.6), low temperature thermal analysis is used to probe the mobility of small chain segments (such as the phenylene rings in bisphenol based resins).[68,69] At lower temperatures than the glass transition, two other transitions are observed. Nomenclature is varied; in this work the sub-ambient transition at approximately -50 °C is denoted the β-transition. The third transition is found in between the T_g and the β-transition temperature (T_β).

The temperature and area of the β-transition provides information about the type and amount of molecular motion present in a polymer. Tu *et al.* found for a DGEBA/4,4'-DDS network, the β-transition to consist of three main motions which occur with increasing temperature. First, the phenylene ring flip of the bisphenol moiety, then a motion associated with the glycidyl ether segment and finally, at the higher end of the

transition, a phenylene ring motion of the the DDS (Figure 1.5).[68]

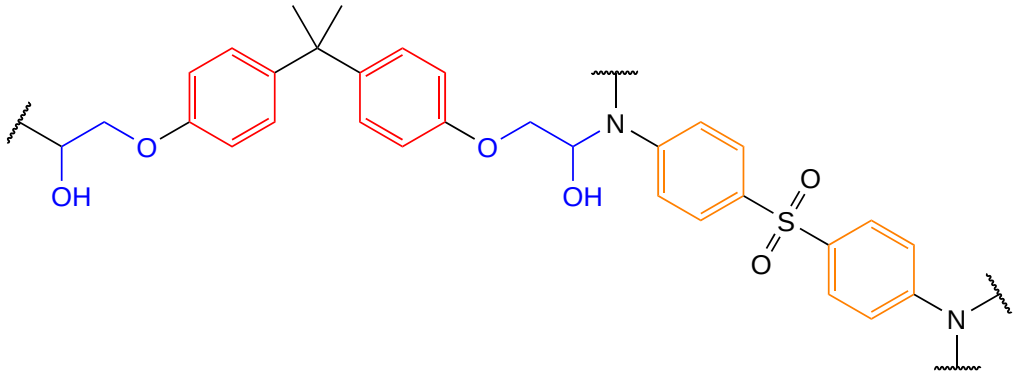

Figure 1.5: A single DGEBA-4,4'-DDS linkage. The bisphenol phenylene groups are coloured red, the glycidyl ether moiety, blue, and the DDS phenylene, orange. DGEBA - diglycidyl ether of bisphenol A; 4,4-DDS - 4,4'-diaminodiphenylsulfone.[68]

1.1.8 Factors influencing the structure and performance of crosslinked epoxy resins

The high level of chemical performance (also referred to as chemical resistance) of epoxy networks is commonly referenced in the literature; commonly cited as the result of a high crosslink density.[7] However, there is a good deal of variation between the performance of different epoxy networks. The relationships that exist between structural features and the performance of a network are not always simplistic.

Chemical reactivity of components

The structure of a network will be dramatically influenced by the way in which its constituent monomers bind—its connectivity. It follows that we would expect connectivity to impact upon the chemical performance of a network. The connectivity of the network is defined by crosslinks. A crosslink is defined when there is a branching unit (which would originally have been a monomer) which has at least three separate branches to the infinite network.[2] Intrinsically, the crosslink density (and hence structure) will rely upon the functionality of the monomers used and their potential to react (i.e. the ratio of functional groups).

Functionality Generally, the mass between crosslinks decreases as functionality increases, leading to an increase in crosslink density. A study by Frank *et al.* showed that this generally results in a decrease in the average hole size throughout the polymer, and a decrease in the diffusion coefficient.[11] However, an increase in ultimate water uptake is also observed, attributed to an increase in the fractional free volume irrespective of the lowering of the average hole size.

(a)

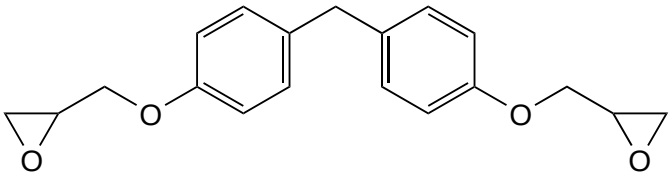

(b)

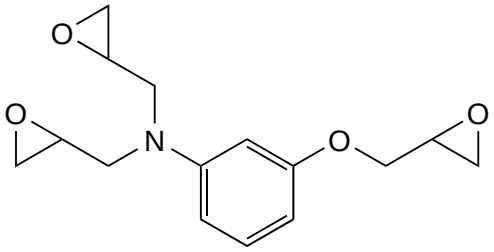

(c)

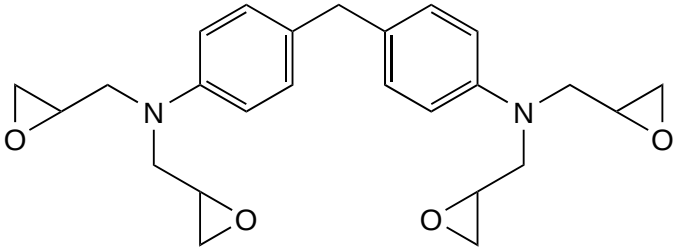

Figure 1.6: Examples of epoxy monomers of different functionalities (a) DGEBF, two-functional; (b) mTGAP (m-triglycidylaminophenol), three-functional and (c) N,N,N',N'-tetraglycidyl-4,-4'-diaminodiphenylmethane

Stoichiometry As has been discussed above, off-stoichiometric ratios result in a lower crosslink density—inherently "dangling ends" will produce a higher mass between crosslinks. Frank and Wiggins showed this expected reduction in crosslink density, when formulating with an amine deficiency. However, they also found a concurrent increase in the ultimate uptake of water, which, as above, might not initially be expected.[43] A similar finding is described by Vanlandingham *et al.*—they found the lowest ultimate uptake occurs in an amine deficient system—at a stoichiometry of approximately 0.75

amine hydrogens : 1.25 epoxy.[59]

Etherification In the stoichiometric study by Frank *et al.*, etherification is identified as a likely influence for the off-stoichiometric formulations—which would result in a more tightly packed network and hence the lower the free volume available for the penetrant. This is because it alters the functionality of the resin in question—a hydroxyl group is produced with each epoxy-amine reaction. They also note that while the general trend shows some increased performance from a move to amine deficiency, that this is not observed for the highest performing stoichiometric formulation, based on a DGEBF resin.

Morsch *et al.* also showed that for increased cure time (and therefore further crosslinking) of an industrial epoxy resin, there was an increase in the ultimate water uptake attributed to the creation of more free volume.[70] The arguments presented are that either (a) there is a reduced packing efficiency in the regions in close proximity to crosslinks; or (b) a side-effect of the higher T_g is an increased free volume in the glass. That is, since the T_g is higher, a greater amount of free volume is frozen into the network upon cooling below T_g, since the polymer is further from equilibrium, upon the "freezing" (i.e. vitrification) process.

Reaction conditions

The study by Morsch *et al.* shows the conditions of reaction to be a strong influencer in network properties and chemical performance. Ultimately it is the kinetics of the reaction that determine the degree of cure—the two key variables are the temperature(s) of cure and the time spent at those temperatures. The method employed by Morsch *et al.* is perhaps the simplest manipulation of degree of cure, by editing the time spent at a set temperature.

Temperature An increased temperature of cure leads to an increased degree of cure when the cure temperature is lower than the ultimate T_g of the material.[71] This is because vitrification limits any further reaction below T_g. There is insufficient molecular

mobility to allow migration of reaction groups to one another.

Pethrick *et al.* showed that an increase in the cure temperature leads again to an increase in reaction extent and therefore increased crosslink density.[72] A consequent decrease in density and increase in water uptake is also observed.

Sahagun and Morgan have shown cure temperature can have further impact than simply degree of cure.[67] Using atomic force microscopy and fracture measurements, they show that different structures are formed at different cure temperatures, with a "peak" in homogeneity at a certain temperature and the increased presence of nodules at both lower and higher cure temperatures (see Section 1.1.7). If present, an inhomogeneous structure is said to facilitate uptake as the less dense phase will less effectively resist any sorption.[59]

Schedule There is variation seen between coatings cured with a different schedule—that is, the adjustment of the thermal profile in cure. The simplest profile is of course an isothermal cure—a cure at a single temperature. The first complication can be introduced by starting at a lower temperature and a ramp to the cure temperature. Childers *et al.* showed that the rate of this ramp can have subtle influence upon some micro-scale features such as the average hole size and chain packing.[73] However, the impact on more macro-scale properties such as T_g was negligible.

A commonly used curing technique is a post-cure—where a resin is cured at an initial temperature (the *cure temperature*) and then the temperature increased further for a post-cure. When comparing the properties of a resin cured isothermally or in a two-step cure (i.e. one with a post-cure), we see good variation in water uptake, among other properties, as shown by Frank and Wiggins.[43] They showed higher crosslink density and higher ultimate water uptake for some samples cured in a two step process (125 °C, then 200 °C) rather than an isothermally cured sample (at 180 °C). However, for a different resin subjected to the same two cure schedules, very little variation is observed in water ultimate uptake, in spite of a increase in crosslink density when cured isothermally. This is attributed to different "network growth kinetics" between the two reactive mixtures used found by Jackson.[74] The above mentioned study by Sahagun and Morgan also

refer to different possible growth mechanisms, where the growth of linear regions or crosslinked regions can be favoured by an adjustment of the temperature.[67]

Atmosphere There are a number of side reactions possible during epoxy cure. The primary concern that this presents is the consumption of the reactive components, so the stoichiometry formulated for is not that which reacts. The two most commonly observed problems are those of carbamation and oxidation. Carbamation refers to the reaction of amines with carbon dioxide, in the presence of water, and is also referred to as amine blushing/blooming.[75,76] Where water is absent, curing is largely unaffected by carbamation (even in carbon dioxide atmospheres), since the reaction is water-catalysed. Oxidation refers to the reaction of the epoxy with oxygen, though there is not a specific reaction—rather a range of different processes, which can occur after network formation is complete.[77] The literature on the impact of such processes upon properties is limited, especially regarding chemical performance. Due to low permeabilities, both will be primarily surface effects, especially for carbamation, since the formation of carbamate is likely to make the amine insoluble in the resin and hence cause phase separation.

Chemical structure

Outside of the functionality of the monomers, the chemical structure of the remainder of the molecules will have a large effect upon the structure of the resin. The two key features to consider are the polarity of the constituent bonds and the geometry of the molecules, chiefly affected by the number and type of bonds between the functional groups. When considering the formed network, the geometry of connectivity is described as the topology.

Polarity There are some polar bonds in epoxy-amine networks by definition - since they are formed by the reaction of an epoxide with an amine, an amine is incorporated into the network backbone and a pendant hydroxyl group is also formed. The potential for hydrogen bonding might be reduced by etherification of the hydroxyl group, but an ether group would still be incorporated into the network. Polarity can be further influenced

by other side groups, such as additional hydroxyl groups, or carbonyl containing groups. Zhang *et al.* showed that where a hydroxyl pendant group was replaced by an ester, water uptake was substantially reduced—demonstrating that miscibility of the network with the penetrant is very important in determining ultimate uptake.[78] If we are to consider this in terms of the solubility parameter, it is worth noting that more than polarity is adjusted here, with the hydrogen bonding capability of a hydroxyl being substantially higher than that of an ester.

Soles *et al.* also report that the polarity is the primary influencing factor in water uptake.[79–81] They found that a non-amine based system sorbed less than difunctional epoxy-amine systems, which sorbed less than a trifunctional epoxy-amine system—directly commensurate with polarity increases. However, between the difunctional systems where polarity is more similar, there is still variation observed in ultimate uptake, attributed to the topology of the network.

Topology In the study by Soles *et al.*, they show that the use of flexible amine hardener (hexamethylenediamine (HMD), Figure 1.7a(i)) leads to an increase in moisture uptake, relative to a more rigid amine (diaminodiphenylmethane (DDM), Figure 1.7a(ii)).[79] In contrast to this finding, Toscano and co-workers found the increased flexibility in a DGEBF based resin relative to a DGEBA based network led to lower moisture uptake. It is worth noting that this change is substantially more subtle than the change from HMD to DDM; and that the comparison is clouded by the regioisomerism found in DGEBF based resins (which is neglected in this study). Where Soles *et al.* reduce the rigidity in a more subtle way, they also showed a small decrease in mass uptake (though there is a reasonably large variation in the amine structures).

The para and meta substituted isomers of diaminodiphenylsulphone (4,4'-DDS and 3,3'-DDS respectively) are both commonly used hardeners (for structures see Figure 1.7b). The use of meta isomers in barrier materials have been shown by a number of authors to have improved properties, including solvent uptake.[43,69,82] Indeed, Frank and Wiggins show a reduced free volume and lower water uptake for 3,3'-DDS relative to 4,4'-DDS. Ramsdale-Capper and Foreman observed improved mechanical properties in spite of a

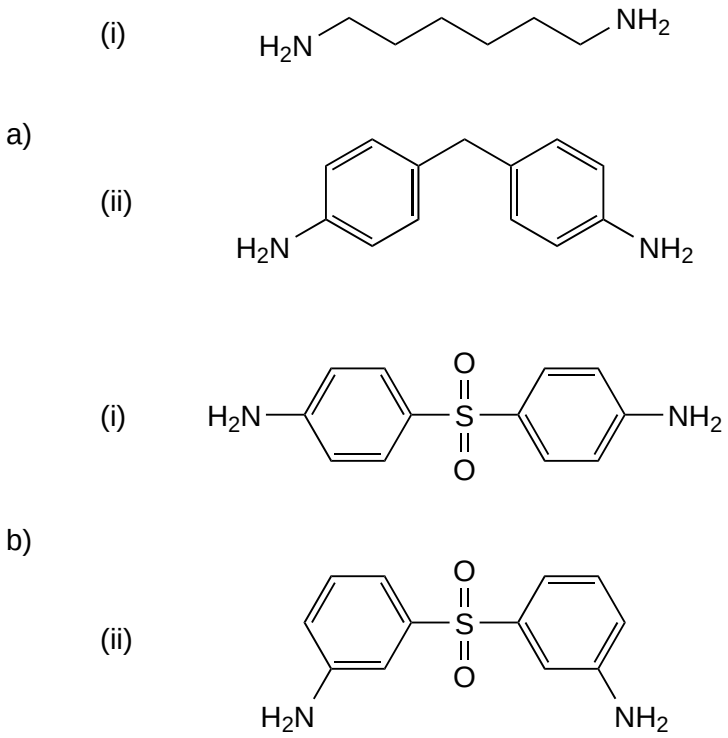

Figure 1.7: Diamines of variable **a) flexibility**, *(i) hexamethylenediamine, (ii) diaminodiphenylmethane; and* **b) molecular geometry**, *(i) 4,4'-diaminodiphenylsulfone, (ii) 3,3'-diaminodiphenylsulfone.*

T_g reduction— which they attributed to improved chain packing in the meta- substituted networks. Regioisomerism around a single phenyl ring was also shown to produce significant changes in T_g by Riad *et al.*.[83]

A clear illustration of the importance of topology is shown by Jackson *et al.* (also described in Section 1.1.4), whereby the relationship between hole size and penetrant size is shown to significantly affect the solvent uptake behaviour (Figure 1.8).[25] Where the solvent van der Waal's (vdW) volume exceeds the average hole size, uptake is drastically reduced.

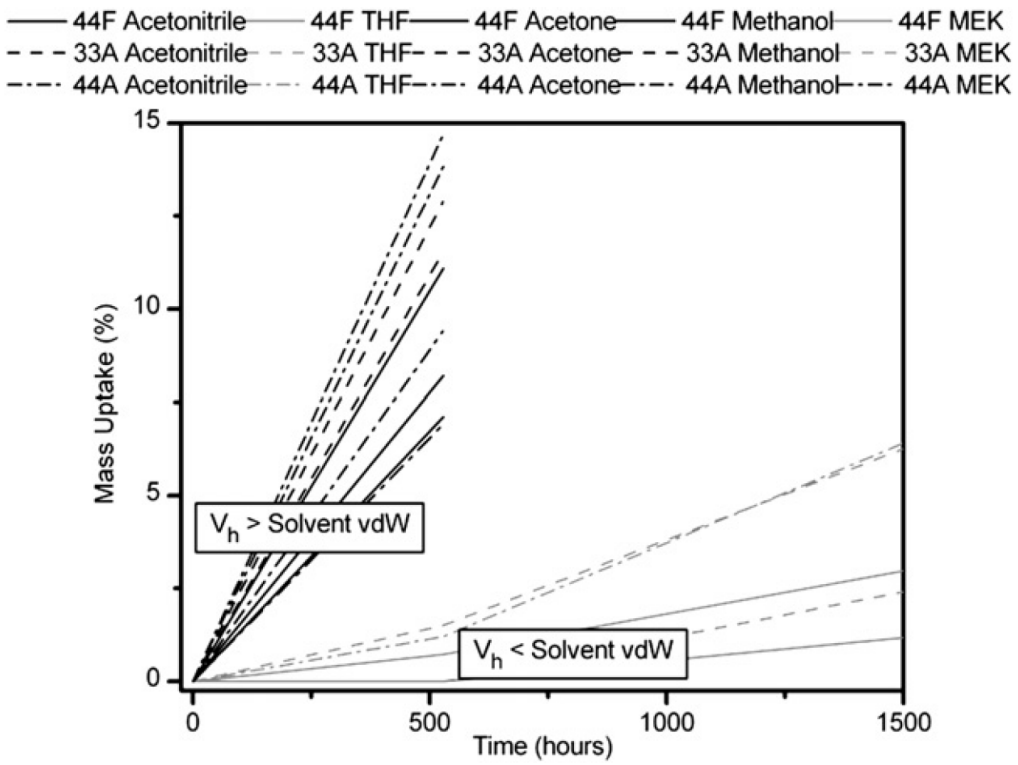

Figure 1.8: A range of networks composed of combinations of 4,4-DDS/3,3'-DDS (44 or 33 in labelling) with DGEBF/DGEBA (A or F in labelling) in a range of solvents. The rate of solvent uptake is shown to dramatically reduce when the solvent vdW volume is larger than the average free volume hole size. (reproduced from Jackson et al. with permission)[25]

To summarise across the range of factors discussed, there are a few key features and trends to draw out. One such feature is that there is a complicated relationship between the crosslink density and the chemical performance. As is suggested by traditional theory (and indeed intuitively), at low degrees of cures, any increase in the crosslink density by reaction leads to the network becoming more dense.[70] However, as the reaction moves to higher degrees of cures, there is an increase in the free volume of the system.[84] This generally results in a higher uptake of water or other penetrants.

Another key consideration is the weighing of the influence of polarity and topology. Some studies find the chemical structure, in particular the polarity, to be the governing factor, though others weigh much more heavily on the topology. Where we discuss water uptake, the work by Soles *et al.* is compelling in showing the importance of polarity above topology.[79–81] However, the work by Jackson clearly demonstrates that as we diversify in terms of penetrant, the topology will be a much more significant factor to account

for.[25]

One area of limitation in the literature is the lack of diversity amongst the epoxy monomers used. Generally, the studies completed have relied upon the use of commercially available resins and amines, and therefore it has been difficult to isolate individual factors affecting the network performance. Extensive work has been completed using industrially supplied bisphenol based resins, though there are few other bifunctional epoxies used. Further there is little or no regard given to the diversity of isomers present in an industrial mixture of DGEBF.

1.2 Current work

This work sets out to better understand the influence of nanoscale topology upon the subsequent performance of the network. That is, it seeks to identify the effect of chemical changes made to the epoxy resin monomers or hardeners - especially those which give very little change to the "bulk" properties such as polarity or constituent atoms.

The three key novel areas which will be investigated are:

A. Geometry of molecules - generally edited by the position of substituents on six-membered rings

B. Nature of chemistry - by changing the nature of six-membered rings from aromatic to aliphatic, and changing the type of bisphenol

C. Distance between bonds - inherent to a change of geometry, the distance between reactive groups will also be varied. This can also be achieved by editing the epoxy resin.

The primary chemical "tools" that will be employed to achieve these aims will be the constituent isomers of DGEBF and a range of monocycle amines of varying geometry and bond type. The effects of changing the isomers of DGEBF is of particular interest as the literature generally neglects any consideration of the resin composition.[12,43,85–87]

The purpose of such work is to better inform epoxy resin formulators, especially where formulating for chemically resistant applications. A better understanding of how chemical structure influences chemical performance will enable more strategic formulation and design of better coatings.

References

[1] Odian, G. *Principles of polymerization*. Wiley InterScience electronic collection. Wiley, Hoboken, 4th edition (2004). ISBN 9780471478744.

[2] Pascault, J. P., Sautereau, H., Verdu, J. & Williams, R. J. J. *Thermosetting Polymers*. Plastics engineering. Taylor & Francis, New York (2002). ISBN 9780203908402.

[3] Baekeland, L. H. The synthesis, constitution, and uses of Bakelite. *Journal of Industrial and Engineering Chemistry (Washington, D. C.)*, **1**(Copyright (C) 2014 American Chemical Society (ACS). All Rights Reserved.), 149–61 (1909).

[4] Flory, P. J. Molecular size distribution in three dimensional polymers. I. Gelation. *Journal of the American Chemical Society*, **63**(11), 3083–3090 (1941).

[5] Stockmayer, W. H. Theory of molecular size distribution and gel formation in branched-chain polymers. *The Journal of Chemical Physics*, **11**(2), 45 (1943).

[6] Stockmayer, W. H. Theory of molecular size distribution and gel formation in branched polymers II. General cross linking. *The Journal of Chemical Physics*, **12**(4), 125 (1944).

[7] Cameron C., A. B. P. Film formation. In Marrion, A., editor, *The Chemistry and Physics of Coatings*, pages 46–63. The Royal Society of Chemistry, Cambridge, 2nd edition (2004). ISBN 978-0-85404-604-1.

[8] van Westing, E., Ferrari, G. & de Wit, J. The determination of coating performance with impedance measurements-I. Coating polymer properties. *Corrosion Science*, **34**(9), 1511–1530 (1993).

[9] Sørensen, P. A., Kiil, S., Dam-Johansen, K. & Weinell, C. E. Anticorrosive coatings: a review. *Journal of Coatings Technology and Research*, **6**(2), 135–176 (2009).

[10] Port, A. B. & Cameron, C. Performance Properties of Coatings. In Marrion, A., editor, *The Chemistry and Physics of Coatings*, pages 64–95. Royal Society of Chemistry, Cambridge, 2nd edition (2004).

[11] Frank, K., Childers, C., Dutta, D., Gidley, D., Jackson, M., Ward, S., Maskell, R. & Wiggins, J. Fluid uptake behavior of multifunctional epoxy blends. *Polymer*, **54**(1), 403–410 (2013).

[12] Alessi, S., Toscano, A., Pitarresi, G., Dispenza, C. & Spadaro, G. Water diffusion and swelling stresses in ionizing radiation cured epoxy matrices. *Polymer Degradation and Stability*, **144**(Supplement C), 137–145 (2017).

[13] Chin, J. W., Nguyen, T. & Aouadi, K. Sorption and diffusion of water, salt water, and concrete pore solution in composite matrices. *Journal of Applied Polymer Science*, **71**(3), 483–492 (1999).

[14] Atkins, P. & de Paula, J. *Physical Chemistry*. OUP Oxford, Oxford, 9th edition (2010). ISBN 9780199543373.

[15] Shen, C.-H. & Springer, G. S. Moisture Absorption and Desorption of Composite Materials. *Journal of Composite Materials*, **10**, 2 (1976).

[16] Apicella, A. & Nicolais, L. Effect of water on the properties of epoxy matrix and composite. *Advances in Polymer Science*, **72**(Epoxy Resins Compos. 1), 69–77 (1985).

[17] Hansen, C. *The Three Dimensional Solubility Parameter and Solvent Diffusion Coefficient*. Ph.D. thesis, Copenhagen (1967).

[18] Van Krevelen, D. W. & Te Nijenhuis, K. Chapter 7 - Cohesive Properties and Solubility. In Van Krevelen, D. W. & Te Nijenhuis, K. B. T., editors, *Properties of Polymers*, pages 189–227. Elsevier, Amsterdam (2009). ISBN 978-0-08-054819-7.

[19] Small, P. A. Some factors affecting the solubility of polymers. *Journal of Applied Chemistry*, **3**(2), 71–80 (1953).

[20] van Krevelen, D. W. Chemical structure and properties of coal. XXVIII. Coal constitution and solvent extraction. *Fuel*, **44**(4), 229–242 (1965).

[21] Hoy, K. L. New values of the solubility parameters from vapor pressure data. *Journal of Paint Technology*, **42**(541), 76–118 (1970).

[22] Fedors, R. F. A method for estimating both the solubility parameters and molar volumes of liquids. *Polymer Engineering and Science*, **14**(2), 147–154 (1974).

[23] Hoftyzer, P. & Van Krevelen, D. Paper (Nr 111a-15) presented at the International Symposium on Macromolecules. *IUPAC, Leiden* (1970).

[24] Hoy, K. L. Solubility parameter as a design parameter for water borne polymers and coatings. *Journal of Coated Fabrics*, **19**, 53–67 (1989).

[25] Jackson, M., Kaushik, M., Nazarenko, S., Ward, S., Maskell, R. & Wiggins, J. Effect of free volume hole-size on fluid ingress of glassy epoxy networks. *Polymer*, **52**(20), 4528–4535 (2011).

[26] Neogi, P. *Diffusion in Polymers*. Plastics Engineering. Taylor & Francis, New York (1996). ISBN 9780824795306.

[27] Flory, P. J. & Rehner, J. Statistical mechanics of cross-linked polymer networks II. Swelling. *The Journal of Chemical Physics*, **11**(11), 521–526 (1943).

[28] James, H. M. & Guth, E. Simple presentation of network theory of rubber, with a discussion of other theories. *Journal of Polymer Science*, **4**(2), 153–182 (1949).

[29] De Kee, D., Liu, Q. & Hinestroza, J. Viscoelastic (non-Fickian) diffusion. *The Canadian Journal of Chemical Engineering*, **83**(6), 913–929 (2005).

[30] Alfrey, T., Gurnee, E. F. & Lloyd, W. G. Diffusion in glassy polymers. *Journal of Polymer Science Part C: Polymer Symposia*, **12**(1), 249–261 (1966).

[31] Rossi, G. & Mazich, K. A. Macroscopic description of the kinetics of swelling for a cross-linked elastomer or a gel. *Physical Review E*, **48**(2), 1182–1191 (1993).

[32] LeMay, J. D. & Kelley, F. N. Structure and ultimate properties of epoxy resins. In Dušek, K., editor, *Epoxy Resins and Composites III SE - 4*, volume 78 of *Advances in Polymer Science*, pages 115–148. Springer Berlin Heidelberg (1986). ISBN 978-3-540-15936-0.

[33] Weiss, K. D. Paint and coatings: A mature industry in transition. *Progress in Polymer Science*, **22**(2), 203–245 (1997).

[34] Marrion, A. R. Binders for conventional coatings. In Marrion, A., editor, *The Chemistry and Physics of Coatings*, pages 96–150. Royal Society of Chemistry, Cambridge, 2nd edition (2004).

[35] Tanaka, Y., Okada, A. & Tomizuka, I. Synthesis and characteristics of epoxides. In *Epoxy Resins: Chem. Technol.*, pages 9–134,737–740. Dekker (1973).

[36] Brennan, D. J., White, J. E. & Brown, C. N. High-barrier poly(hydroxy amide ethers): effect of polymer structure on oxygen transmission rates. 3. *Macromolecules*, **31**(23), 8281–8290 (1998).

[37] Jay, R. R. Direct titration of epoxy compounds and aziridines. *Analytical Chemistry*, **36**(3), 667–668 (1964).

[38] Garcia, F. G. & Soares, B. G. Determination of the epoxide equivalent weight of epoxy resins based on diglycidyl ether of bisphenol A (DGEBA) by proton nuclear magnetic resonance. *Polymer Testing*, **22**(1), 51–56 (2003).

[39] Ellis, B. Introduction to the chemistry, synthesis, manufacture and characterization of epoxy resins. In Ellis, B., editor, *Chemistry and Technology of Epoxy Resins SE - 1*, pages 1–36. Springer Netherlands (1993). ISBN 978-94-010-5302-0.

[40] Smith, I. T. The mechanism of the crosslinking of epoxide resins by amines. *Polymer*, **2**, 95–108 (1961).

[41] Vladimirov, L., Artemenko, S., Ivanov, V., Zelenetskii, A., Oleinik, E. & Salamatina, O. Mechanism of reactions between epoxy compounds and amines. *Polymer Science U.S.S.R.*, **22**(1), 254–261 (1980).

[42] Rozenberg, B. A. Kinetics, thermodynamics and mechanism of reactions of epoxy oligomers with amines. *Advances in Polymer Science*, **75**, 113–165 (1986).

[43] Frank, K. & Wiggins, J. Effect of stoichiometry and cure prescription on fluid ingress in epoxy networks. *Journal of Applied Polymer Science*, **130**(1), 264–276 (2013).

[44] Horie, K., Hiura, H., Sawada, M., Mita, I. & Kambe, H. Calorimetric investigation of polymerization reactions. III. Curing reaction of epoxides with amines. *Journal of Polymer Science Part A-1: Polymer Chemistry*, **8**(6), 1357–1372 (1970).

[45] Arutyunyan, K., Tonoyan, A., Davtyan, S., Rozenberg, B. & Yenikolopyan, N. Kinetics and mechanism of the reaction of phenyl glycidyl ether with aniline. *Polymer Science U.S.S.R.*, **17**(8), 1892–1900 (1975).

[46] Mijovic, J., Fishbain, A. & Wijaya, J. Mechanistic modeling of epoxy-amine kinetics. 1. Model compound study. *Macromolecules*, **25**(2), 979–985 (1992).

[47] Cole, K. C. A new approach to modeling the cure kinetics of epoxy/amine thermosetting resins. 1. Mathematical development. *Macromolecules*, **24**(11), 3093–3097 (1991).

[48] Paz-Abuin, S., Pellin, M. P., Paz-Pazos, M. & Lopez-Quintela, A. Influence of the reactivity of amine hydrogens and the evaporation of monomers on the cure kinetics of epoxy-amine: kinetic questions. *Polymer*, **38**(15), 3795–3804 (1997).

[49] Ehlers, J.-E., Rondan, N. G., Huynh, L. K., Pham, H., Marks, M. & Truong, T. N. Theoretical study on mechanisms of the epoxy-amine curing reaction. *Macromolecules*, **40**(12), 4370–4377 (2007).

[50] Grillet, A., Galy, J., Pascault, J. & Bardin, I. Effects of the structure of the aromatic curing agent on the cure kinetics of epoxy networks. *Polymer*, **30**(11), 2094–2103 (1989).

[51] Mijovic, J. & Andjelic, S. A study of reaction kinetics by near-infrared spectroscopy. 1. Comprehensive analysis of a model epoxy/amine system. *Macromolecules*, **28**(8), 2787–2796 (1995).

[52] Zvetkov, V. L. A modified kinetic model of the epoxy-amine reaction. *Macromolecular Chemistry and Physics*, **203**(3), 467–476 (2002).

[53] Sourour, S. & Kamal, M. Differential scanning calorimetry of epoxy cure: isothermal cure kinetics. *Thermochimica Acta*, **14**(1-2), 41–59 (1976).

[54] Zvetkov, V., Simeonova-Ivanova, E. & Calado, V. Comparative DSC kinetics of the reaction of DGEBA with aromatic diamines IV. Iso-conversional kinetic analysis. *Thermochimica Acta*, **596**, 42–48 (2014).

[55] Younes, M., Wartewig, S., Lellinger, D., Strehmel, B. & Strehmel, V. The curing of epoxy resins as studied by various methods. *Polymer*, **35**(24), 5269–5278 (1994).

[56] Rocks, J., Rintoul, L., Vohwinkel, F. & George, G. The kinetics and mechanism of cure of an amino-glycidyl epoxy resin by a co-anhydride as studied by FT-Raman spectroscopy. *Polymer*, **45**(20), 6799–6811 (2004).

[57] Morell, M., Ramis, X., Ferrando, F. & Serra, À. Effect of polymer topology on the curing process and mechanical characteristics of epoxy thermosets modified with linear or multiarm star poly(ϵ-caprolactone). *Polymer*, **52**(21), 4694–4702 (2011).

[58] Sahagun, C. M., Knauer, K. M. & Morgan, S. E. Molecular network development and evolution of nanoscale morphology in an epoxy-amine thermoset polymer. *Journal of Applied Polymer Science*, **126**(4), 1394–1405 (2012).

[59] Vanlandingham, M. R., Eduljee, R. F. & Gillespie, J. W. Moisture diffusion in epoxy systems. *Journal of Applied Polymer Science*, **71**(5), 787–798 (1999).

[60] Vanlandingham, M. R., Eduljee, R. F. & Gillespie Jr., J. W. Relationships between stoichiometry, microstructure, and properties for amine-cured epoxies. *Journal of Applied Polymer Science*, **71**(5), 699–712 (1999).

[61] Morgan, R. J. & O'Neal, J. E. The microscopic failure processes and their relation to the structure of amine-cured bisphenol-A-diglycidyl ether epoxies. *Journal of Materials Science*, **12**(10), 1966–1980 (1977).

[62] Dušek, K. Are cured thermoset resins inhomogeneous? *Die Angewandte Makromolekulare Chemie*, **240**(1), 1–15 (1996).

[63] Oberlin, A., Ayache, J., Oberlin, M. & Guigon, M. High-resolution dark-field imaging in epoxy and polyimide systems. *Journal of Polymer Science: Polymer Physics Edition*, **20**(4), 579–591 (1982).

[64] Bai, S. Crosslink distribution of epoxy networks studied by small-angle neutron scattering. *Polymer*, **26**(7), 1053–1057 (1985).

[65] Wu, W.-l. & Bauer, B. J. Network structure of epoxies — a neutron scattering study: 2. *Polymer*, **27**(2), 169–180 (1986).

[66] Bahrami, A., Morelle, X., Hông Minh, L. D., Pardoen, T., Bailly, C. & Nysten, B. Curing dependent spatial heterogeneity of mechanical response in epoxy resins revealed by atomic force microscopy. *Polymer*, **68**, 1–10 (2015).

[67] Sahagun, C. M. & Morgan, S. E. Thermal control of nanostructure and molecular network development in epoxy-amine thermosets. *ACS Applied Materials & Interfaces*, **4**(2), 564–572 (2012).

[68] Tu, J., Tucker, S. J., Christensen, S., Sayed, A. R., Jarrett, W. L. & Wiggins, J. S. Phenylene ring motions in isomeric glassy epoxy networks and their contributions to thermal and mechanical properties. *Macromolecules*, **48**(6), 1748–1758 (2015).

[69] Ramsdale-Capper, R. & Foreman, J. P. Internal antiplasticisation in highly crosslinked amine cured multifunctional epoxy resins. *Polymer*, **146**, 321–330 (2018).

[70] Morsch, S., Lyon, S., Greensmith, P., Smith, S. & Gibbon, S. Water transport in an epoxy–phenolic coating. *Progress in Organic Coatings*, **78**, 293–299 (2015).

[71] Marks, M. J. & Snelgrove, R. V. Effect of conversion on the structure-property relationships of amine-cured epoxy thermosets. *ACS Applied Materials & Interfaces*, **1**(4), 921–926 (2009).

[72] Pethrick, R. A., Hollins, E. A., McEwan, I., Pollock, E. A., Hayward, D. & Johncock, P. Effect of cure temperature on the structure and water absorption of epoxy/amine thermosets. *Polymer International*, **39**(4), 275–288 (1996).

[73] Childers, C. H., Hassan, M. K., Mauritz, K. A. & Wiggins, J. S. Molecular scale cure rate dependence of thermoset matrix polymers. *Arabian Journal of Chemistry*, **9**(2), 206–218 (2016).

[74] Jackson, M. *Effects of molecular architecture on fluid ingress behavior of glassy polymer networks*. Ph.D. thesis, University of Southern Mississippi (2011).

[75] Dinnissen, T. Amine blushing and blooming of epoxy binder systems. *Pitture e Vernici, European Coatings*, **82**(8), 15–21 (2006).

[76] Croll, S. G. Atmospheric gases and the hardening of an amine-cured epoxy coating. *Journal of Coatings Technology*, **52**, 65–69 (1980).

[77] Celina, M. C., Dayile, A. R. & Quintana, A. A perspective on the inherent oxidation sensitivity of epoxy materials. *Polymer*, **54**(13), 3290–3296 (2013).

[78] Zhang, S.-Y., Ding, Y.-F., Li, S.-J., Luo, X.-W. & Zhou, W.-F. Effect of polymeric structure on the corrosion protection of epoxy coatings. *Corrosion Science*, **44**(4), 861–869 (2002).

[79] Soles, C. L., Chang, F. T., Bolan, B. A., Hristov, H. A., Gidley, D. W. & Yee, A. F. Contributions of the nanovoid structure to the moisture absorption properties of epoxy resins. *Journal of Polymer Science Part B: Polymer Physics*, **36**(17), 3035–3048 (1998).

[80] Soles, C. L. & Yee, A. F. A discussion of the molecular mechanisms of moisture transport in epoxy resins. *Journal of Polymer Science Part B: Polymer Physics*, **38**(5), 792–802 (2000).

[81] Soles, C. L., Chang, F. T., Gidley, D. W. & Yee, A. F. Contributions of the nanovoid structure to the kinetics of moisture transport in epoxy resins. *Journal of Polymer Science Part B: Polymer Physics*, **38**, 776–791 (2000).

[82] Brennan, D. J., White, J. E., Haag, A. P., Kram, S. L., Mang, M. N., Pikulin, S. & Brown, C. N. Poly(hydroxy amide ethers): New high-barrier thermoplastics. *Macromolecules*, **29**(11), 3707–3716 (1996).

[83] Riad, K. B., Schmidt, R., Arnold, A. A., Wuthrich, R. & Wood-Adams, P. M. Characterizing the structural formation of epoxy-amine networks: The effect of monomer geometry. *Polymer*, **104**, 83–90 (2016).

[84] Gupta, V. & Brahatheeswaran, C. Molecular packing and free volume in crosslinked epoxy networks. *Polymer*, **32**(10), 1875–1884 (1991).

[85] Kravchenko, O., Li, C., Strachan, A., Kravchenko, S. & Pipes, R. Prediction of the chemical and thermal shrinkage in a thermoset polymer. *Composites Part A: Applied Science and Manufacturing*, **66**, 35–43 (2014).

[86] Toscano, A., Pitarresi, G., Scafidi, M., Di Filippo, M., Spadaro, G. & Alessi, S. Water diffusion and swelling stresses in highly crosslinked epoxy matrices. *Polymer Degradation and Stability*, **133**, 255–263 (2016).

[87] Oya, Y., Kikugawa, G. & Okabe, T. Clustering approach for multidisciplinary optimum design of cross-linked polymer. *Macromolecular Theory and Simulations*, **26**(2), 1600072 (2017).

Chapter 2

Model network optimisation using a sample system

2.1 Results and Discussion

Overview

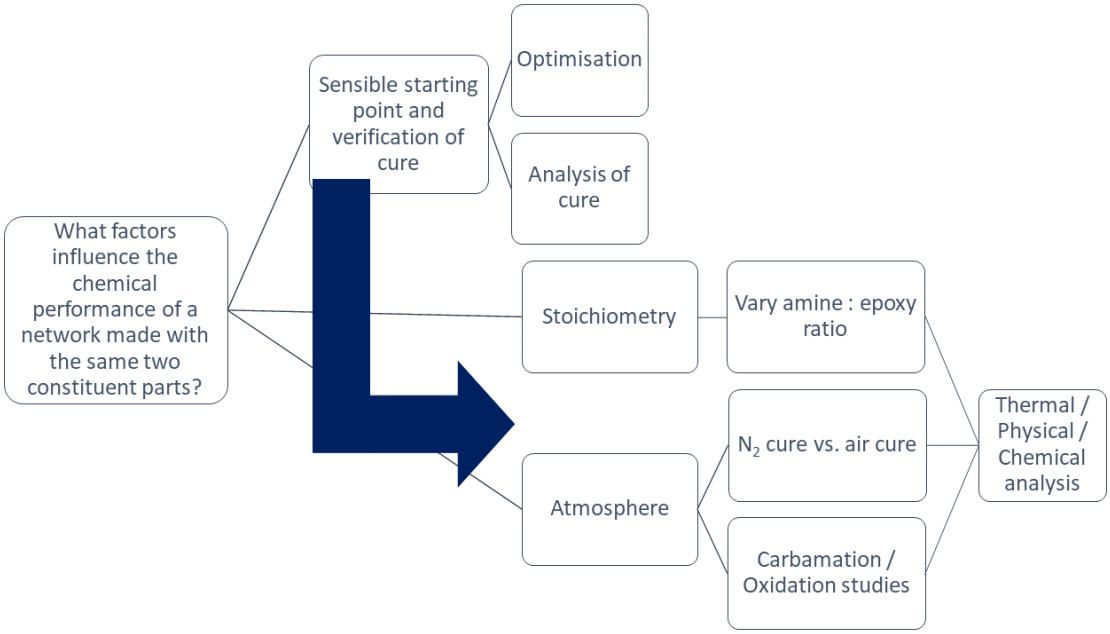

In order to effectively understand the variation in properties caused by nuanced chemical adjustments, an understanding of the other factors that might affect network performance is important. The degree of influence that factors such as atmosphere and stoichiometry might have on the performance of a network is of interest in and of itself, and will also inform the amount of control required for subsequent research, adjusting chemistries—in order that any performance variation can be attributed to any change in chemistry and not these factors.

PART A: Network preparation

There are a number of considerations in curing an epoxy resin. A range of properties may be attainable from a single chemical system, while defects and unwanted reactions may also be introduced without any change to the chemical components. In order to effectively compare the chemical performance of a range of networks, a set of optimum conditions must be established.

The goal in optimisation is the reproducible formation of a network with as high a crosslink density as is achievable for a system, in order that the systems be comparable. A high crosslink density is generally achieved by using a stoichiometric or near-stoichiometric ratio (see Section 1.1.7). Moving away from an approximately stoichiometric network will inherently limit the achievable crosslink density as full reaction of all components would not be possible. Further, ensuring maximum reaction between amine and epoxy groups is key. This can be divided further into two:

(i) ensuring the reactive groups are not kinetically frozen apart

(ii) preventing any other reactions in which epoxide or amine groups might participate.

The first of these two goals is achieved with control of the temperature of cure - cure above the ultimate glass transition temperature (T_g) ensure mobility in the network is maintained throughout the cure, and hence the majority of reactive groups are able to react. Of interest, then is whether a temperature slightly above the ultimate T_g is sufficient to obtain full reaction, or whether a substantial gap is needed.

The second goal has a much wider scope - both epoxides and primary amines are reactive groups and thus competing reactions are inevitable. Competing reactions which consume epoxide or amine groups will also limit the achievable crosslink density as they will adjust the stoichiometry of the system. Therefore, how best to eliminate these side reactions was investigated.

2.1.1 Cure optimisation

Selection of cure temperature and time

The system chosen for this work was DER 354 and meta-xylylenediamine (MXDA). Generally the maximum achievable T_g of such systems was found to be between 100 and 115 °C. Therefore to investigate the question posed above (whether a minimal or larger difference in cure temperature and ultimate T_g is needed), the two selected cure temperatures were 120 °C and 160 °C. Excessively high temperatures can give rise to degradation processes, so 40 °C above T_g was selected as the upper limit to this experiment.[1–3]

Figure 2.1 shows the T_gs obtained for the two different cure temperatures, at different cure times. In all cases, the higher cure temperature led to a higher T_g indicating increased reaction. Therefore, 160 °C was selected as the cure temperature. For the 160 °C cure, it can be seen there is a peak in T_g at 180 minutes (3 hours). This was selected as the cure time.

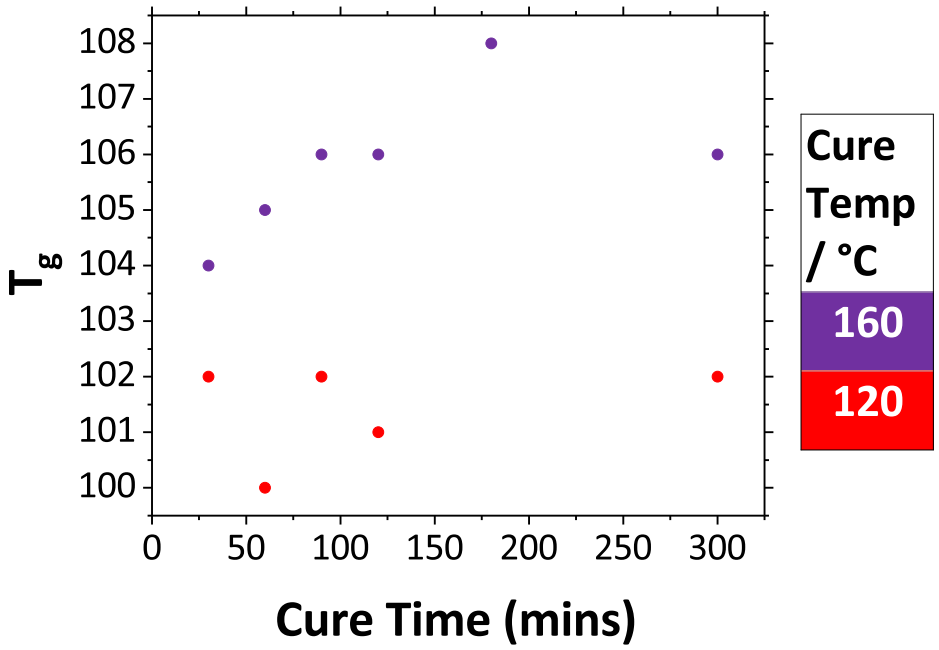

Figure 2.1: A comparison of the glass transition temperature (T_g) obtained, varying cure time for a cure temperature of either 120 °C or 160 °C

Optimisation of preparation parameters

The basic method for preparing networks in this optimisation is outlined in Section 2.2.3. A number of experiments were carried out in order to achieve goal (ii) as laid out above - that is, to eliminate chemical processes other than the desired reaction. The primary qualifier of success was the network's optical appearance. In an ideal reaction, a uniform, clear and colourless polymer is produced.

The preparation parameters that were optimised include the atmosphere of cure, initial temperature in the oven and the ramp rate (i.e. the rate of temperature increase) from initial temperature to cure temperature (160 °C), as well as the pot-time (the amount of time between mixing of the chemical components and application to slides).

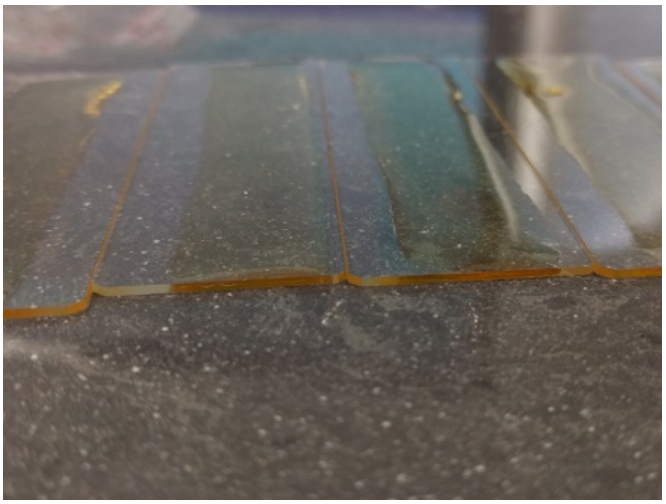

Start Temp	Ambient
Hold Temp	160 °C
Ramp rate	20 °C min^{-1}
Oven	Fan
Atmosphere	Air
Pot time	1 hr 15 m

Figure 2.2: Slides cured in run 1 and cure conditions (Slides are 26 mm wide)

Run 1 was cured in a standard lab fan oven, as per the conditions used for the selection of cure temperature and time (Section 2.1.1), with a high ramp rate (20 °C min^{-1}). As is shown in Figure 2.2, the slide finish is clear, but yellow. This is indicative of oxidation reactions taking place alongside the desired epoxy-amine reaction.[4]

In order to remove the yellowing produced by oxidation, run 2 was conducted under an inert atmosphere of nitrogen. In order to do this, a vacuum oven purged with nitrogen was used for cure. This vacuum oven had a maximum ramp rate of 1 °C min^{-1}, so the same schedule was used, with that slower ramp rate. As can be seen in Figure 2.3 the networks produced had minimal yellowing. However, the top surface was generally

white, characteristic of carbamation - the reaction of an amine with carbon dioxide (Scheme 2.1). This shows that the trace amounts of carbon dioxide found in the nitrogen used were sufficient to cause carbamation issues.

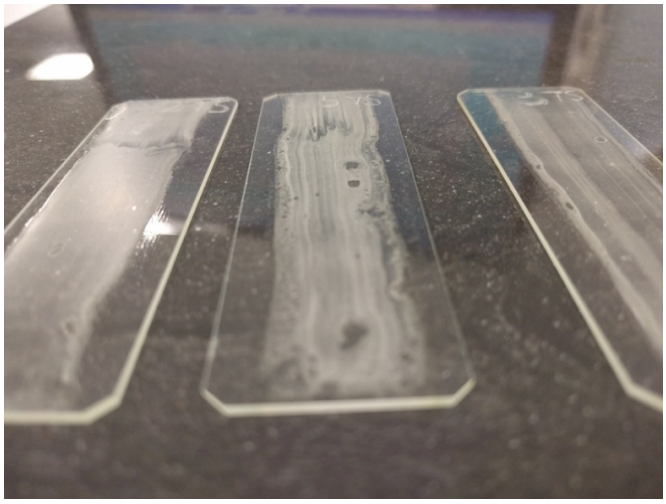

Start Temp	Ambient
Hold Temp	160 °C
Ramp rate	1 °C min^{-1}
Oven	Vacuum
Atmosphere	Nitrogen
Pot time	1 hr 15 m

Figure 2.3: Slides cured in run 2 and cure conditions (Slides are 26 mm wide)

Scheme 2.1: Carbamation of an amine

Run 3, the same experiment as run 2 but in an air atmosphere, shows similar levels of carbamation (as well as the expected yellowing) - leading us to conclude that carbamation results from the slower ramp rate, as all other variables are identical to those in run 1. This leads us to conclude that the carbamation reaction best competes with the epoxy-amine reaction at ambient temperature. Hence, it was decided to avoid exposure of the reaction mixture to air as much as possible. One way by which this was achieved was the sealing of the reaction mixture in the pot using Parafilm®. It was also important to minimise how much the mixture is exposed to air at room temperature once applied to slides, by placing in a hot oven immediately following the drawdown.

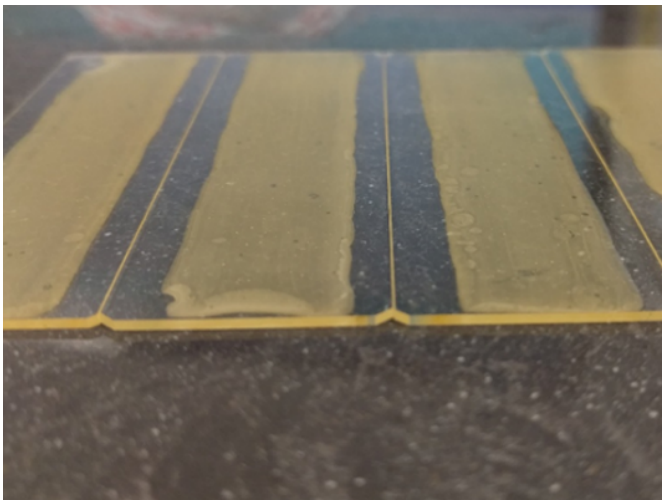

Start Temp	Ambient
Hold Temp	160 °C
Ramp rate	1 °C min^{-1}
Oven	Fan
Atmosphere	Air
Pot time	1 hr 15 m

Figure 2.4: Slides cured in run 3 and cure conditions (Slides are 26 mm wide)

Figure 2.5 shows the results of eliminating the ramp in cure, by placing the slides into an oven at temperature. In addition the pot-time was varied, with a shorter, 20 minute pot-time and a much extended 3 hour 35 minute time. The appearance shows a clearer, more colourless coating, indicating reduced carbamation and oxidation. Clearly there is an issue with dewetting, as a result of the high initial temperature, which is more pronounced for the shorter pot time. In addition, the slides were weighed immediately after drawdown and again after cure and showed significant mass loss - 7 % of the network mass in run 4 and, for run 5, a reduced 4 % as a result of the longer pot-time used. As can be seen in Figure 2.6, this is much higher than what might normally be expected. Therefore, an initial temperature above room temperature but much below 160 °C was used for the following cures.

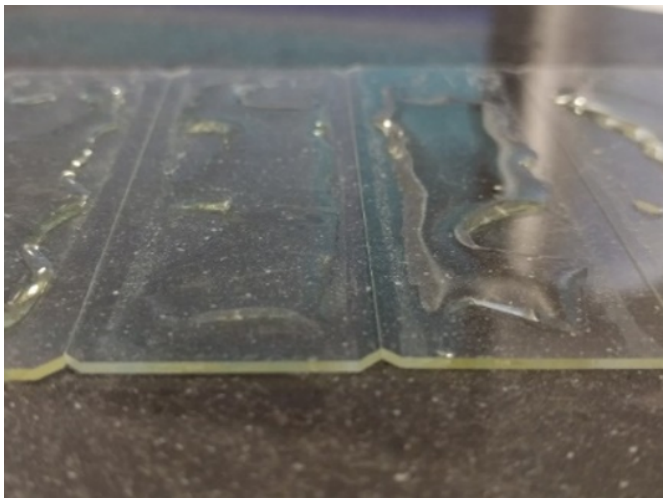

Start Temp	160 °C
Hold Temp	160 °C
Ramp rate	n/a
Oven	Vacuum
Atmosphere	Nitrogen
Pot time	20 mins

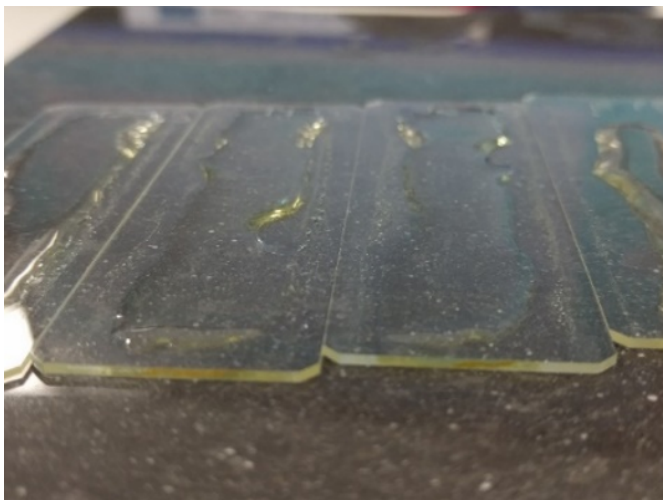

Start Temp	160 °C
Hold Temp	160 °C
Ramp rate	n/a
Oven	Vacuum
Atmosphere	Nitrogen
Pot time	3 hr 35 m

Figure 2.5: Slides cured in runs 4 (top) and 5 (bottom) and cure conditions (Slides are 26 mm wide)

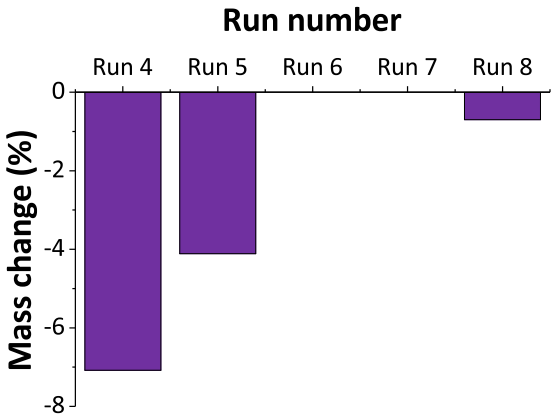

Figure 2.6: Mass change upon cure for runs 4 - 8

Figure 2.7 shows the networks produced with the adjustment to a lower initial temperature. Both show a negligible mass change, with small levels of yellowing. There is limited carbamation in both cases, though it is more prevalent in run 6. Some dewetting was also observed - especially shown on the far-right slide in the images. A small mass loss is expected for cure, as there are small amounts of volatiles in both components (see Figure 2.9b and Section 2.1.2). The absence of any change in mass is likely to be as a result of carbamation.

The reduction in carbamation and general improvement in appearance from run 6 to run 7 shows a longer pot-time to be beneficial. In order to address the dewetting seen, the substrate (i.e. glass surface) needed to be adjusted.

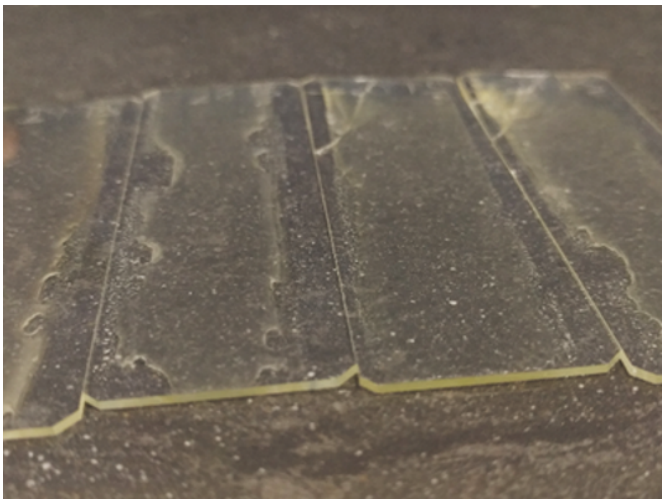

Start Temp	50 °C
Hold Temp	160 °C
Ramp rate	1 °C min^{-1}
Oven	Vacuum
Atmosphere	Nitrogen
Pot time	5 mins

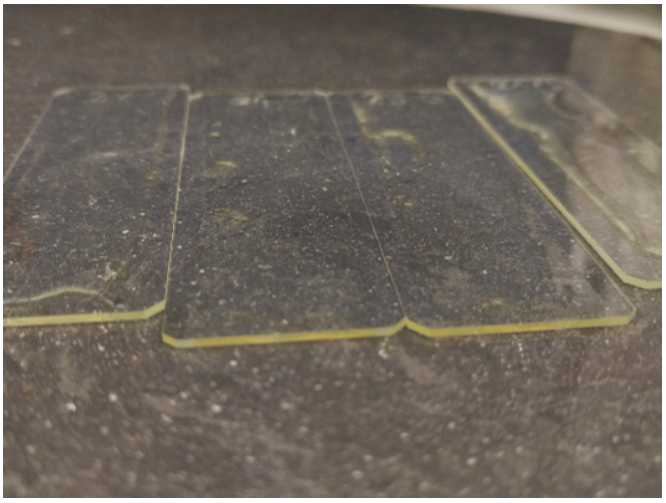

Start Temp	50 °C
Hold Temp	160 °C
Ramp rate	1 °C min^{-1}
Oven	Vacuum
Atmosphere	Nitrogen
Pot time	3 hr 55 m

Figure 2.7: Slides cured in runs 6 (top) and 7 (bottom) and cure conditions (Slides are 26 mm wide)

The optimised conditions are shown in Figure 2.8 as those used in run 8. The pot time was extended by freezing the mixture after 3 hours, and then removed from the freezer the following morning. Therefore, the true pot time in terms of reaction completed is greater, as the mixture will take time to cool down in the freezer and then will take to time to warm up again. A slightly higher nitrogen flow than that used for previous runs was employed, as well as slide treatment. The slides were treated with piranha solution (sulfuric acid mixed with hydrogen peroxide - see Section 2.2.5 for method details). This performs two functions; firstly to clean the surface and secondly to functionalise the surface by producing hydroxyl groups.[5] This will result in better wetting of the surface by the resin. The increase of initial temperature by 10 °C to 60 °C, also further reduces the competition of carbamation with the desired reaction, without a significantly adverse effect on dewetting or component evaporation. This is shown by the small mass loss at 0.7%.

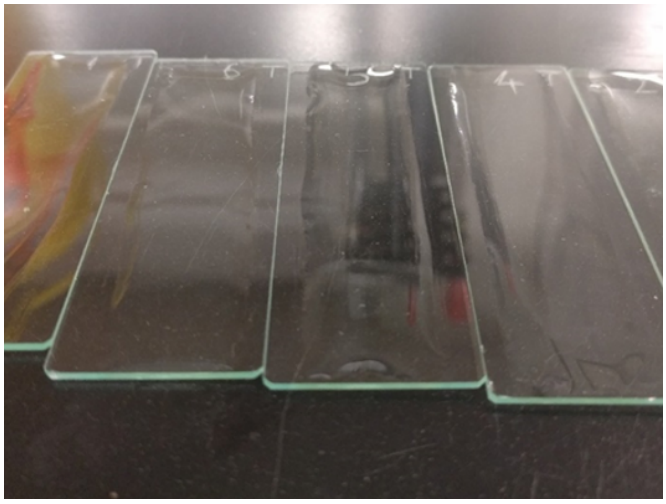

Start Temp	60 °C
Hold Temp	160 °C
Ramp rate	1 °C min^{-1}
Oven	Vacuum
Atmosphere	Nitrogen
Pot time	3 hr*

*Figure 2.8: Slides cured in run 8 and cure conditions (Slides are 26 mm wide). *Pot-time was extended by placing sealed mixture in a freezer after 3 hours, and then drawn-down after warming to room temperature.*

2.1.2 Themogravimetric analysis (TGA) of cure & cure components

The gravimetric variation between cure under the different atmospheres is shown below (Figure 2.9a). Both traces begin with a sharp decrease in mass (relative to the rest of the cure). In the nitrogen cure the initial mass loss is 0.3 %, and then a discontinuity followed by a further, smaller mass loss, with an ultimate mass loss of 0.5 %. In the air cure, the initial mass loss is around 0.2 %, followed by a mass increase to 100.3 % of the initial mass.

Following this, thermogravimetric analysis was performed on pure MXDA, when subjected to the cure schedule as above and when held at the start temperature, 60 °C. These traces are shown in Figure 2.9b. A similar initial mass loss followed by a discontinuity is shown in both MXDA traces, indicating that there is a small volatile loss upon heating to 60 °C, followed by a constant rate of evaporation. Therefore, the further mass loss shown in the nitrogen cure is more likely to be loss of the hardener itself. The mass gain associated with the cure in air is most likely as a result of carbamation of the amine (Scheme 2.1, Section 2.1.1), with the much higher concentration of carbon dioxide. Oxidation may also provide a mechanism for mass gain, but the exact chemical reactions are not as well-defined.

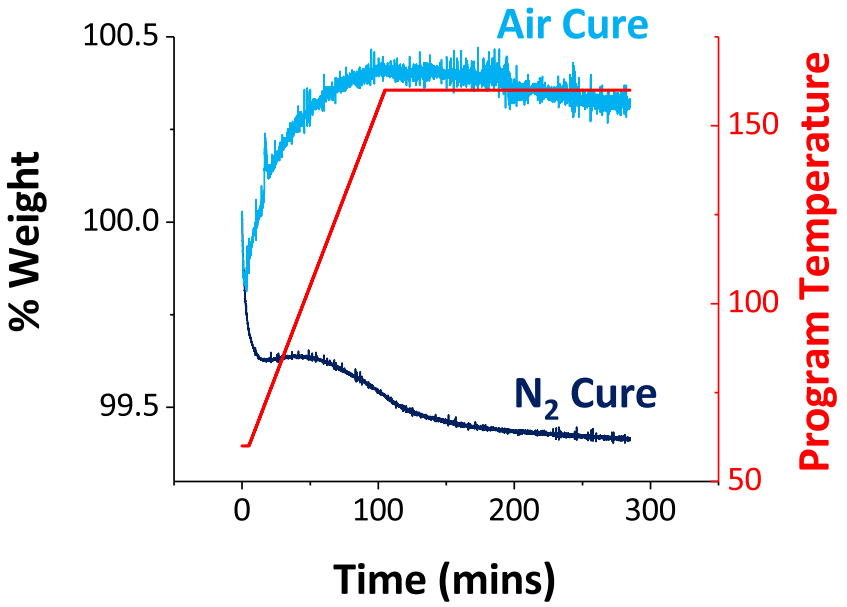

(a)

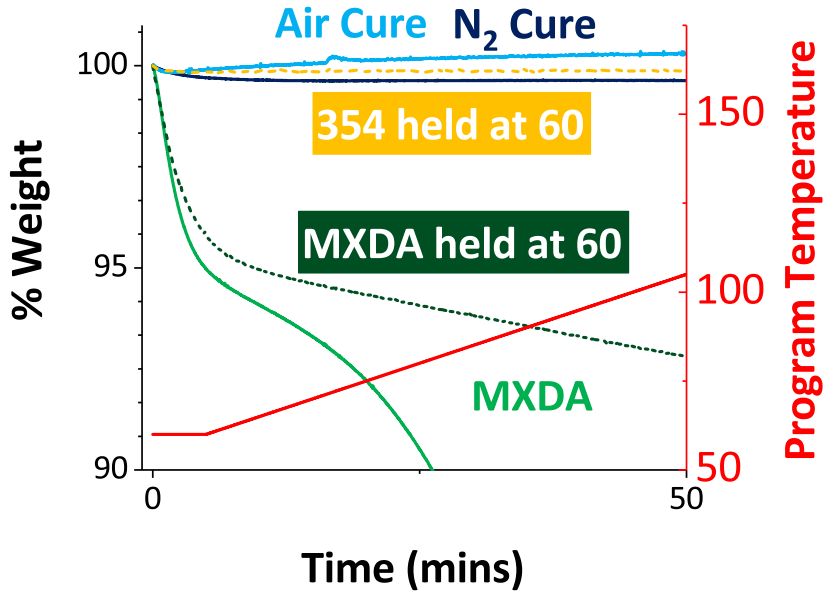

(b)

Figure 2.9: Thermogravimetric traces for a stoichiometric mixture of DER 354/MXDA cured under air and nitrogen and of pure MXDA, for the temperature gradient shown (red trace) and MXDA & DER 354 held at 60 °C under nitrogen. Figure 2.9a shows the whole cure for the stoichiometric mixture. Figure 2.9b shows the initial 50 minutes of cure (solid lines, temperature gradient in red), and MXDA and DER 354 held at 60 °C

2.1.3 Near-infrared spectroscopy

Near-infrared (NIR) spectroscopy was used to monitor the curing reactions, in order to measure the degree of reaction of epoxide groups (or "degree of cure"). Figure 2.10a shows the spectrum of DER 354. The key peak used to monitor conversion is found at approximately 4529 cm^{-1}, highlighted yellow. The adjacent peak, highlighted red is related to the phenyl ring content and as such can be used as a reference peak, since phenyl ring content remains constant throughout cure. This absorption is also found in the spectrum of MXDA, highlighted red in Figure 2.10b. The other peaks of interest relate to primary amine (green) and a band relating to both primary and secondary amines (blue).

The evolution of the NIR spectrum during cure is shown in Figure 2.11. The epoxide peak at 4529 cm^{-1} can been seen to decrease sharply. There is a decrease in amine concentration, as shown by the decrease in the signal for primary amines at $\sim$4940 cm^{-1} and the expected slower decrease of the signal for primary and secondary amines at $\sim$6515 cm^{-1}. It is expected since the secondary amine concentration is expected to persist longer into the cure reaction. Also observed is an increase in signals relating to hydroxyl (-OH) groups ($\sim$7000 cm^{-1} & 4700-4900 cm^{-1}). Finally, the signal at 4618 cm^{-1} is related to the phenyl group content and so does not change during cure. Therefore, it was selected as an internal standard to normalise all scans to.

The hydroxyl signal at 4700-4900 cm^{-1} interferes with the primary amine signal at $\sim$4940 cm^{-1}. A comprehensive measurement of the cure progression relies on this signal since it is generally the only peak by which to differentiate between primary and secondary amines. Further, as can be seen in Figure 2.10b, there is a small absorption at $\sim$4530 cm^{-1} in the amine spectrum which can be subtracted by using the amine concentration (which would usually be calculated from the 4940 cm^{-1} peak). However, approximate conversion can be calculated by disregarding this contribution for two reasons: (i) the contribution made by amine is much smaller, shown quantitatively by the extinction coefficients calculated below (Section 2.1.3); (ii) the majority of epoxide group consumption will correspond to consumption of an amine group, hence any contribution

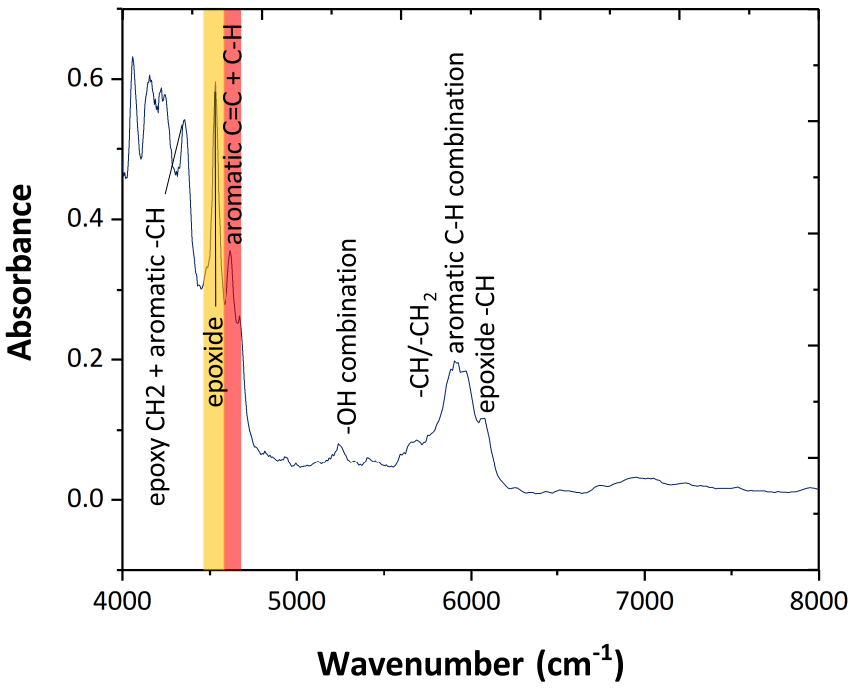

(a)

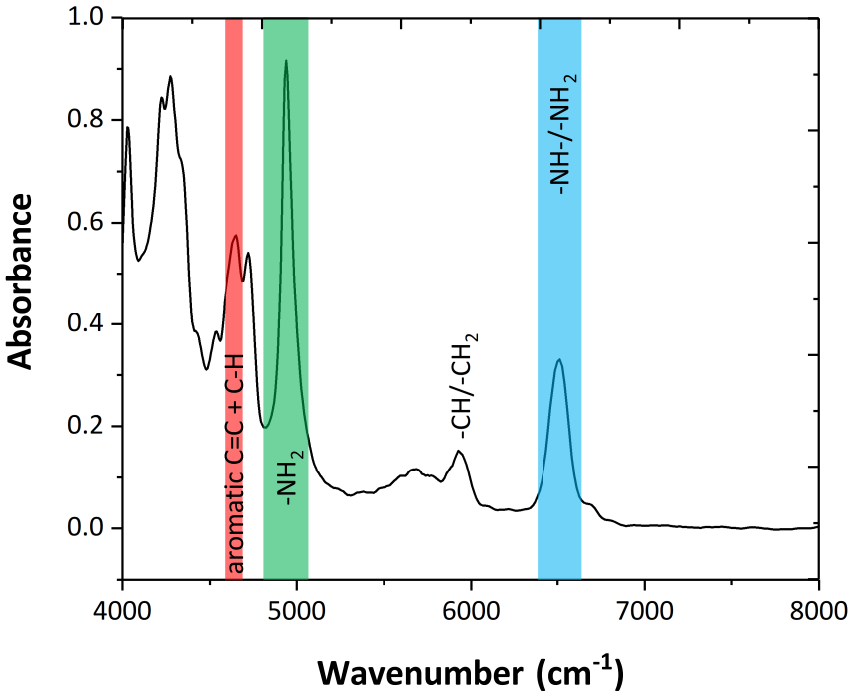

(b)

Figure 2.10: The near-infrared spectrum (4000 - 8000 cm^{-1}) of (a) DER 354 and (b) MXDA with peaks assigned to the chemical groups responsible.

made by amine to the peak area will be equally removed by that reaction. However, care must be taken where there is a realistic prospect of a high quantity of amine relative to epoxide—such as for non-stoichiometric formulations.

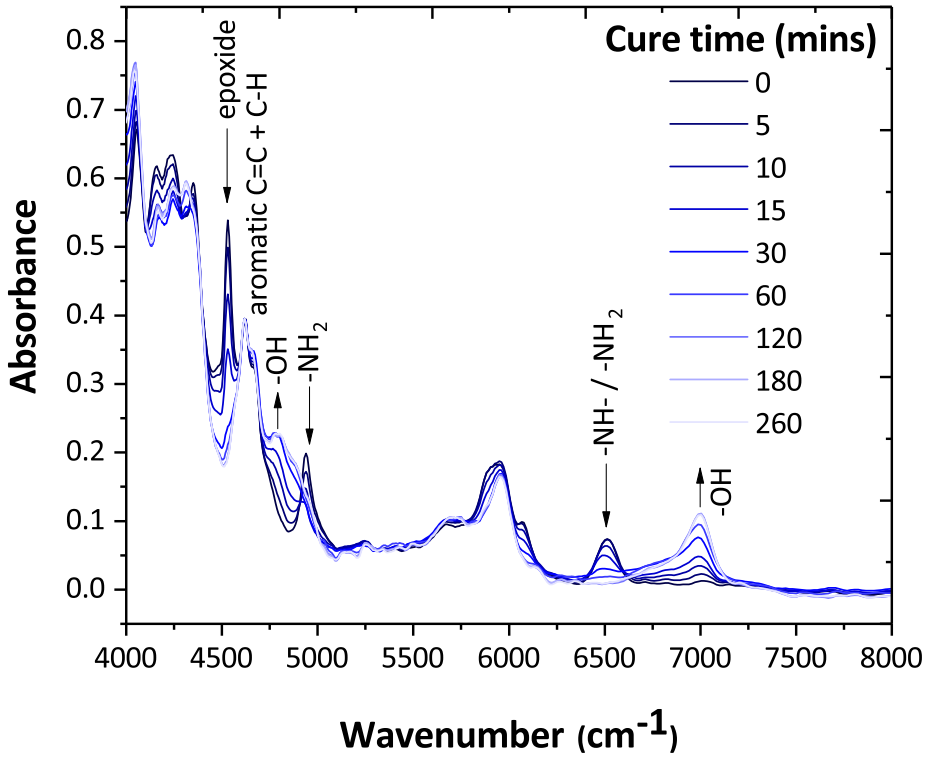

Figure 2.11: Near-infrared spectra collected during the cure of MXDA and DER 354 in a 99 % stoichiometric ratio (i.e. 0.99 amine : 1.01 epoxide—see Section 2.1.4), with the chemical groups assigned to peaks. The direction of arrow shows whether the peak increases or decreases wit cure time.

Quantitative treatment of the NIR data

The development of the epoxide absorbing peak is shown in Figure 2.12. We observe a decrease in the size of the peak, until the apparent disappearance of the peak from 180 minutes. However, quantitative interpretation of this data is not trivial—as the baseline is complicated by the presence of neighbouring peaks, most notably those relating to the phenyl ring at 4618 & 4665 cm^{-1} and the strong aromatic absorption at 4350 cm^{-1}.

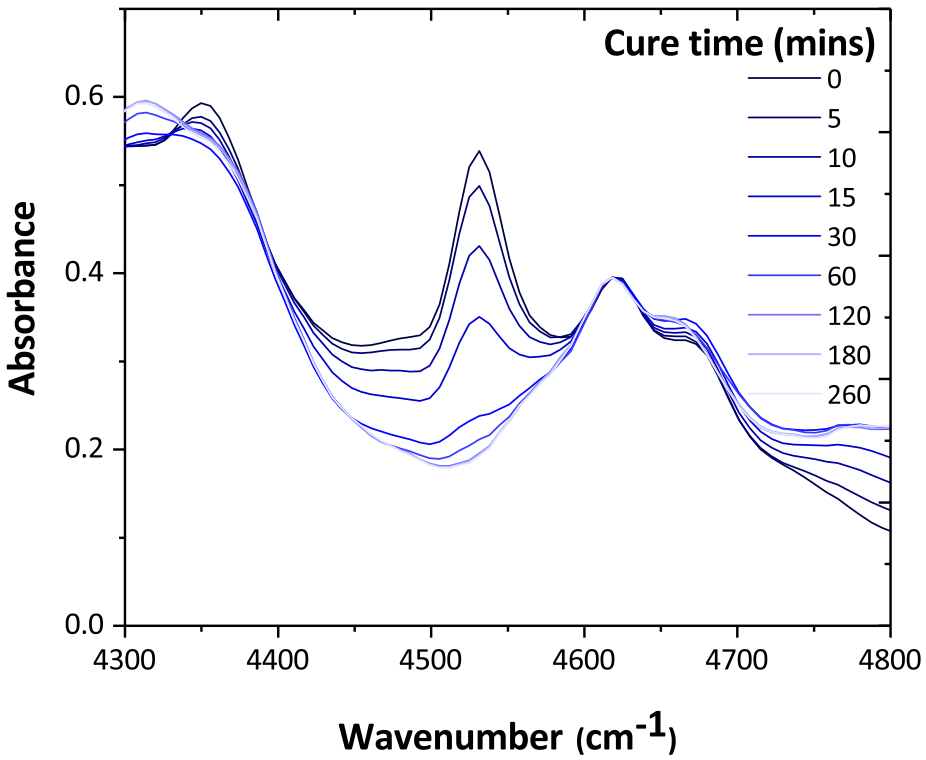

Figure 2.12: The development of the epoxide absorbing peak at ~4529 cm^{-1} during the cure of MXDA and DER 354 in a 99 % stoichiometric ratio.

The simplest approach that can be employed in NIR is using peak intensity to determine concentration. In this case, this is not appropriate, since the overlap leads to a non-zero absorbance, regardless of the fact that there is no apparent peak at the point of interest. Therefore, as is consistent with the literature, the peak area was used in the conversion to concentration (via the Beer-Lambert law).[6–8]

Since the region of interest occupies a trough in the later measurements, the simplistic approach of selecting the two points on the extremes of the peaks and integrating

between them is fruitless, since it returns (impossible) negative values of concentration. Therefore, fitting of the region of interest is necessary to ascertain the contribution made by the epoxide group to any individual scanning (e.g. Figure 2.13).

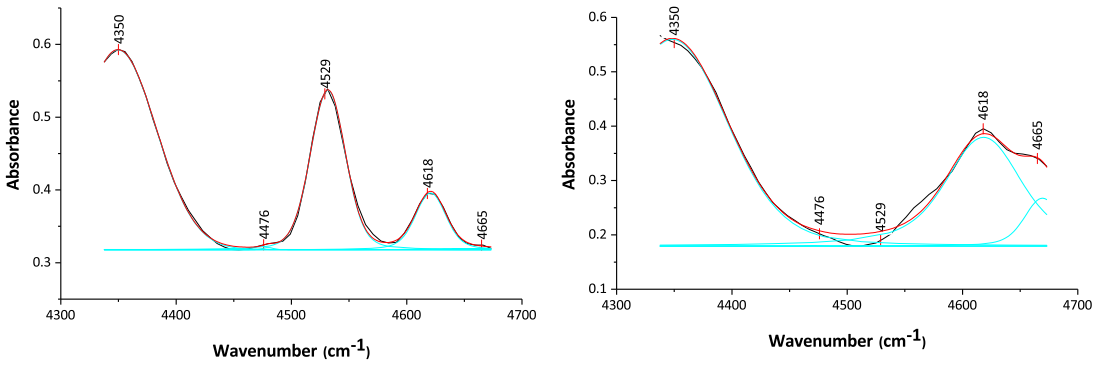

Figure 2.13: Initial fitting of the peaks surrounding the epoxide peak for (a) the initial scan (t = 0 mins) and (b) the final scan (t = 260 mins) in Figure 2.12 for the cure of MXDA and DER 354 in a 99 % stoichiometric ratio

Fitting was completed using OriginPro 2017, using Voigt fits of each of the peaks.[9] The first fit developed is shown in Figure 2.13. Fitting the whole spectrum was not considered since (i) it is very computationally demanding and (ii) when considering the number of peaks present, there are multiple permutations that would give a successful fit. Without attempting to fit the whole spectra, using zero absorbance as the baseline is not possible because of the many signals overlapping at both extremes of the region of interest. Therefore, the selected background was the local minimum.

Five peaks were initially identified. The four that have already been mentioned, phenyl peaks at 4618 and 4665 cm^{-1}, as well as another phenyl related peak at 4350 cm^{-1} and the epoxide peak at 4529 cm^{-1}. The final addition is seen as a small bump at 4476 cm^{-1}, which clearly has a much stronger impact at high conversions (Figure 2.13b). The weakest part of the fit is shown to some extent on the initial scan, but is shown clearly on the final scan—there is a peak at approximately 4670 cm^{-1}, which is dwarfed in the initial scan by the highly absorbing epoxide. Therefore, a fit incorporating this peak into the scan was developed, and is shown in Figure 2.14. These fitting methods were compared when determining the extinction coefficient for this peak for DER 354.

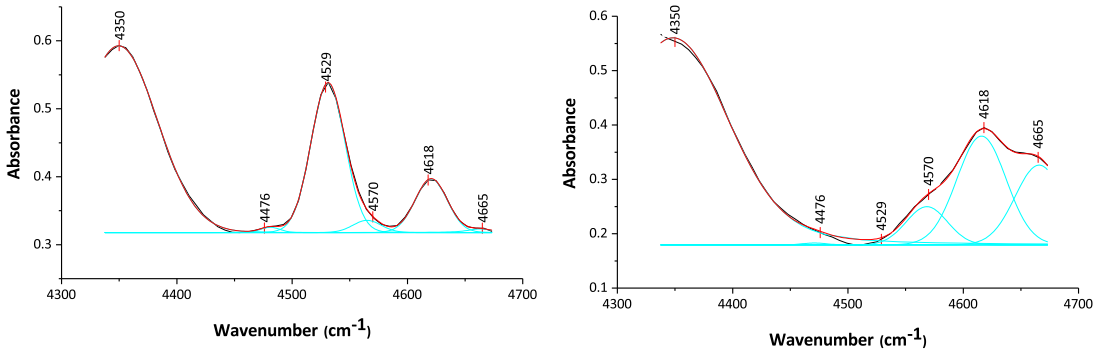

Figure 2.14: Fitting of the peaks surrounding the epoxide peak for (a) the initial scan (t = 0 mins) and (b) the final scan (t = 260 mins) in Figure 2.12, incorporating the peak at ~4570 cm^{-1} for the cure of MXDA and DER 354 in a 99 % stoichiometric ratio

Extinction coefficient determination

In order to determine the extinction coefficient of the peak at 4529 cm^{-1}, cells of various path length were prepared, using microscope slides and PTFE spacers. A scan of the NIR spectrum was collected for each path length and the data fitted. A plot of peak area vs. path length was produced. According to the Beer-Lambert law, the gradient is equal to the molar extinction coefficient multiplied by the concentration. The plots using both fit methods are shown in Figure 2.15—both give a similar gradient, but the intercept is different. The Beer-Lambert law has no additional component and so an intercept is not expected (Equation 2.1). This supports the use of the six peak fit, since that has an intercept much closer to zero. Using this method, the extinction coefficient for epoxide at 4529 cm^{-1} was determined to be 43.27 kg mol^{-1} cm^{-1} or 36.36 dm^3 mol^{-1} cm^{-1}. This is similar to the values found in the literature: Jackson *et al.* found it to be 36.64 dm^3 mol^{-1} cm^{-1}, Sahagun *et al.* found it to be 58.8 kg mol^{-1} cm^{-1} and Poisson *et al.* found it to be 34.9 kg mol^{-1} cm^{-1}.[6–8] For amine, at the same wavenumber, the extinction coefficient was found to be 6.21 kg mol $^{-1}$ cm^{-1} or 6.01 dm^3 mol^{-1} cm^{-1}. In this case, there were no available references for the amine used.

$$A = \varepsilon c l \tag{2.1}$$

The Beer-Lambert law, where A is the absorbance, ε is the molar extinction coefficient, c the concentration and l the path length.

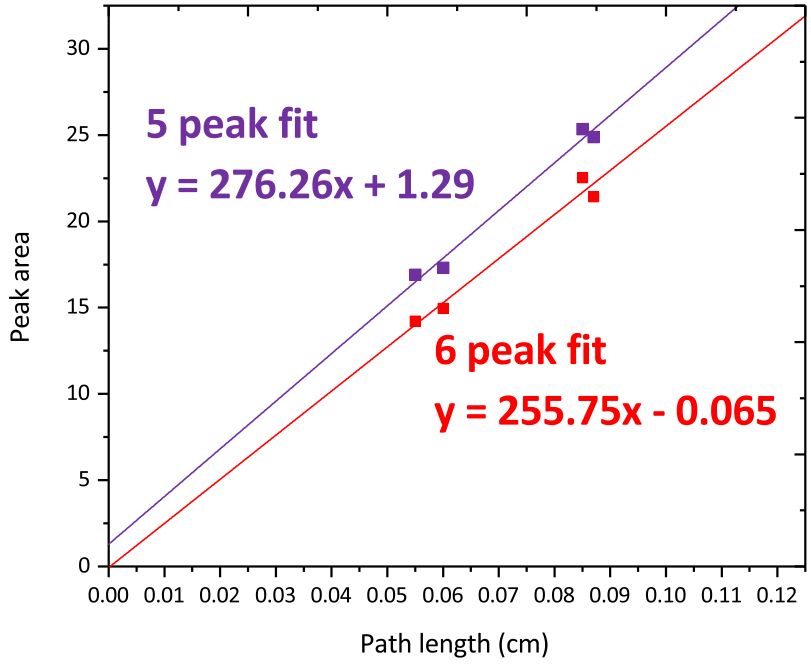

Figure 2.15: Determination of the extinction coefficient of the epoxide peak at 4529 cm^{-1} using a five peak fit (purple) and a six peak fit (red)

Conversion

The conversion quantifies the amount of a functional group that has been consumed, or *converted*, in a chemical reaction. Measuring the conversion relies on knowing the initial amount (or concentration) of a reactant used as well as the amount remaining (Equation 2.2).

$$\alpha = 1 - \frac{C_t}{C_0} \tag{2.2}$$

Conversion, α, using the remaining concentration, $\mathbf{C_t}$*, and the initial concentration,* $\mathbf{C_0}$

In the literature, there is use of both mass and volume concentrations for epoxy cure conversion.[7,8,10–12] The use of mass concentration is perhaps unexpected at first glance. This is because the physically correct method is to use the volume concentration. However, the determination of the volume concentration in a reactive mixture is not necessarily possible. It either requires a unique (i.e. belonging to one component) identifying

peak which does not change throughout the reaction, or a spectrum obtained before any reaction has taken place, which is fundamentally impossible for reaction mixtures which react quickly, or require any treatment following initial mixing before application. This is true of the samples in this study, which require repeated mixing over the first hour of reaction, without which phase separation occurs, resulting in a very different reaction. This was observed through dramatically different T_gs obtained from samples only mixed once versus samples mixed >5 times over the first hour. The usefulness of mass concentration lies in the ease of determination of the initial concentration, from the quantities measured before mixing in formulation.

Using mass concentration relies on a minimal change in density of the material over the course of the reaction. Since the density of DER 354 is 1.19 g cm^{-3} and the highest density obtained in any resin produced was 1.22 g cm^{-3}, this assumption is reasonable. In any case, the only possible inaccuracy is an underestimation of the conversion, since the material is at its densest (and therefore most absorbing) at the final time-point. This is acceptable as we are seeking to ascertain whether there are any unreacted epoxide groups, and a slight overestimation of this still gives a good physical picture of the network. Where conversion is near-complete (97 % or larger), it will have a negligible effect on the value obtained.

We can calculate the concentration in Equation 2.2 at any given time from the peak area using the molar extinction coefficient calculated above and the Beer-Lambert law. Plotting the results of Equation 2.2 against time of cure (for the 99 % MXDA/DER 354 mixture used in the examples above), where t = 0 relates to the beginning of the oven cure, we obtain Figure 2.16. The conversion begins at 30 % since the initial reaction occurs during the pot-time, when mixing is carried out. Reaction was rapid; 77 % of reaction by 15 minutes and 95 % of the reaction was completed within the first half hour of cure, in spite of the temperature only having reached 90 °C. 98 % conversion had occurred by one hour, with the temperature at 120 °C. By 2 hours, after 20 minutes at the "cure temperature", the conversion was found to be 100 %.

For this study, NIR is employed primarily to ascertain degree of cure, and so profiles

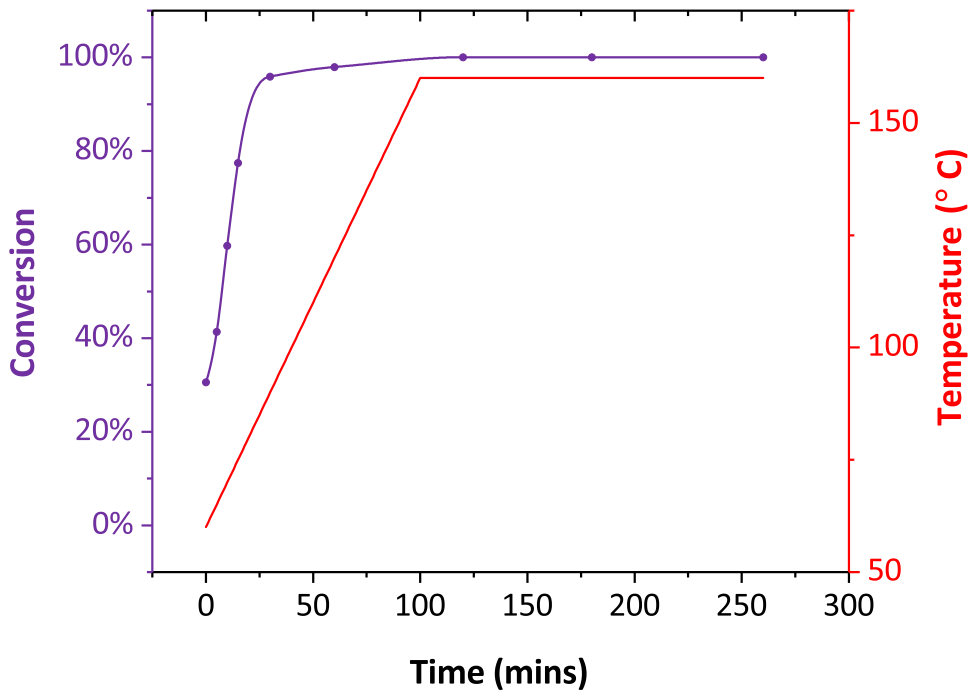

Figure 2.16: Conversion of epoxide group as measured by NIR spectroscopy during cure, with the temperature profile of cure shown in red, for the cure of MXDA and DER 354 in a 99 % stoichiometric ratio

such as this will not be presented for each cure.

2.1.4 Cures completed - Degree of Cure

A range of networks were prepared using DER 354 and MXDA , whilst varying atmosphere and stoichiometry (for a schematic of network preparation see Figure 2.17). Stoichiometry in this study is described as the molar percentage of amine relative to epoxy. For example a molar ratio of 0.94 amine hydrogens : 1.06 epoxy groups is referred to as "94 %". The epoxide equivalent weight (EEW—see Section 1.1.5), as calculated by titration was used for the relative amount of epoxy (see Section 2.2.2 for method).

The properties of an epoxy resin network are chiefly derived from the high degree of crosslinking, which directly results from the epoxy-amine reaction. Indeed, network properties and structure are highly reliant on reaction extent (see Sections 1.1.7 & 1.1.8). NIR spectroscopy was employed in order to measure the degree of cure—in order to ensure that the desired reaction is realised.

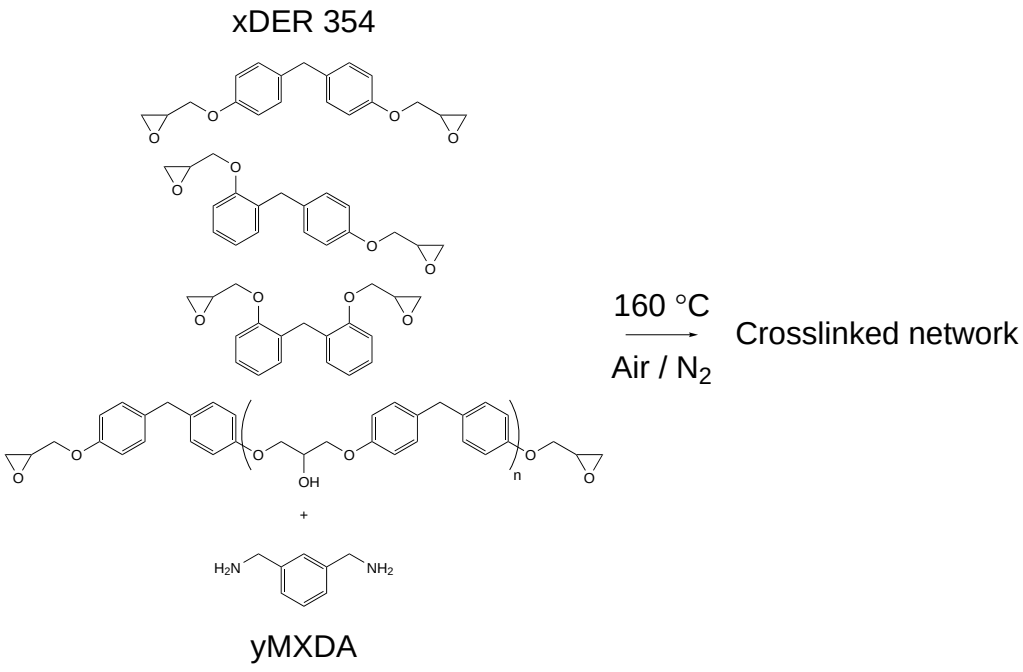

(a)

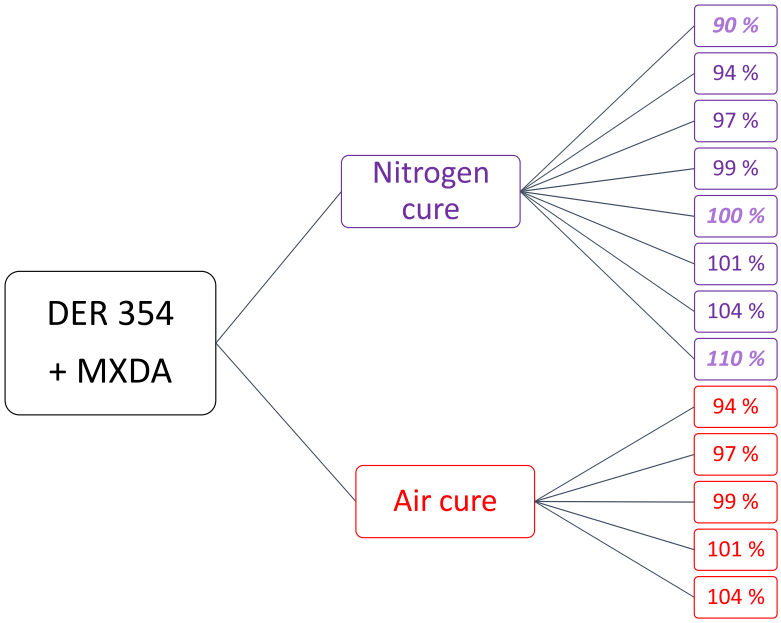

(b)

Figure 2.17: Schematic illustrating the preparation of the networks prepared in this study. (a) shows the general reaction scheme, and (b) shows the specific samples prepared, in terms of stoichiometry and atmosphere of cure. For the chain extended isomer in (a), only para-para substitution is considered, though other regioisomers will also be present. The italicised nitrogen cured samples were added after the initial study to provide further information.

All networks were prepared as in Section 2.2.3, and the degree of cure found as laid out in Section 2.1.3. In order to obtain a quantitative measurement from NIR spectroscopy, it is necessary to have a fixed path length, which was achieved by using a cell. However, this means that it is not possible (by this method) to obtain quantitative NIR data for a network exposed to an atmosphere—the cell prevents any interaction between reaction mixture and atmospheric species. Therefore, only one conversion was obtained per stoichiometry.

The conversions obtained are shown in Figure 2.18. From the amine deficient systems, we find higher degrees of conversion than would be expected if we only consider epoxy-amine reactions. This is a likely to be the result of etherification—reaction of epoxides with hydroxyl groups (see Section 1.1.6). As is expected, the epoxide conversion for near-stoichiometric formulations show the highest conversions.

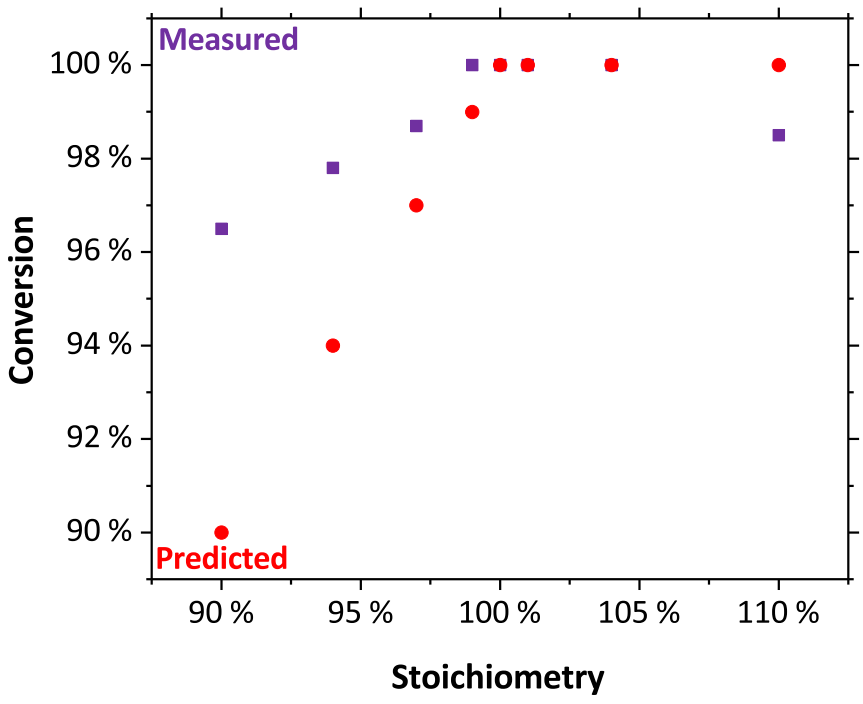

Figure 2.18: Measured and predicted epoxide conversions for each formulation. Predictions are based on the assumption that there are no reactions aside from the desired epoxy-amine reaction. Each of the amine deficient formulations show conversion to be higher than expected.

The lower than expected conversion for the 110 % sample most likely results from

absorption by the amine, at the analysed peak at 4529 cm^{-1}. While this absorption is small compared to epoxide (Section 2.1.3), it will have a bearing when there is markedly more amine than epoxide in the system, as is expected here with this excess of amine. This can be confirmed by observation of the peak at 6500 cm^{-1}, which is still prominent in this spectrum, where it is not in the majority of other samples (Figure 2.19). The assumption that it is negligible in near-stoichiometric formulations is supported by the 104 % sample, which shows 100 % conversion while showing a small signal at 6500 cm^{-1}, and therefore we can continue to rely on this assumption in these cases.

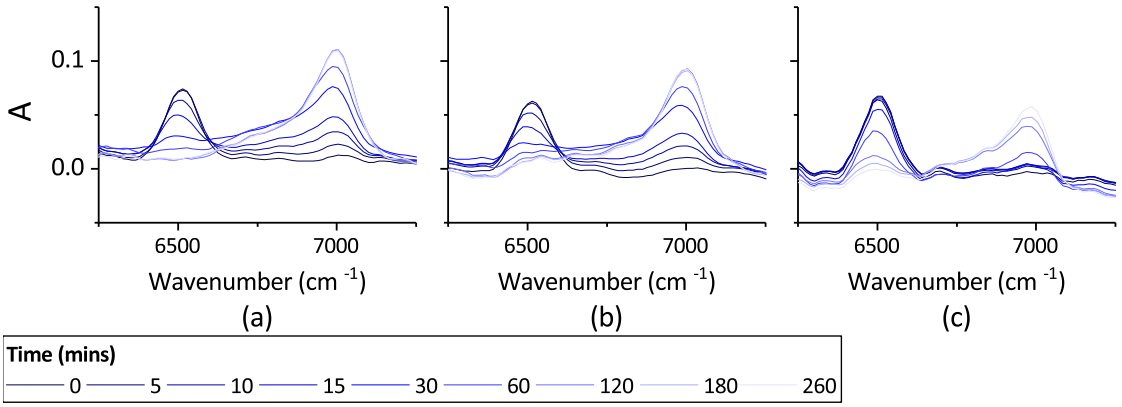

Figure 2.19: The development of the -NH_2/-NH- peak at ~6500 cm^{-1} and -OH peak at ~7000 cm^{-1} in the NIR spectra of a MXDA / DER 354 curing system, for three different formulations: (a) 99 % - an amine deficient system; (b) 104 % - an amine excess; and (c) 110 % - a large amine excess

In any case, the results confirm near-complete reaction for the near-stoichiometric reaction, with a reduction in reaction as we move away from stoichiometry. It follows that we would expect reduced performance from the off-stoichiometric samples, relative to those with conversion >99 %.

PART B: Analysis of cured networks

2.1.5 Thermal and physical properties of cured networks

Glass transition temperatures

The T_gs of the produced networks were obtained from a Lorentzian fit of the peak in tan δ from DMA, placing sample in an aluminium pouch - an example is shown in Figure 2.20. The obtained T_g are shown in Table 2.1.

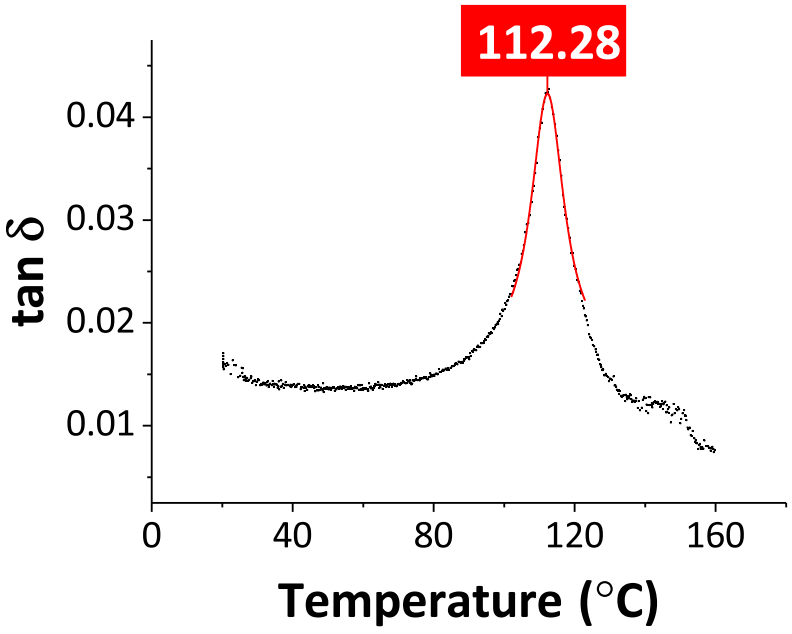

Figure 2.20: Tan δ against temperature for a cured sample (black), with a heating rate of 3 °C min^{-1}, and the Lorentzian fit used to find the peak (red). Here the T_g is 112 °C

There is a small variation in T_g seen between the air and nitrogen cured samples, though each T_g changes by a maximum of 3 °C and a similar but not identical trend is seen. In the directly comparable systems, the lowest T_g in both cases is the most amine deficient system (94 %). As amine concentration is increased in the nitrogen cured samples an increase is seen as stoichiometry is approached, followed by a decrease past ideality to epoxy excess. In the case of the air cure, a continuous increase is observed where both of the epoxy excess materials have the highest T_g. This is consistent with the theory that there are side reactions which use up amine groups when curing under an air atmosphere, as the highest T_g is expected when all reactive groups have reacted

Stoich	N_2 sample T_g /°C	Air sample T_g /°C
90 %	98	
94 %	107	105
97 %	109	110
99 %	114	111
100 %	114	
101 %	112	114
104 %	112	114
110 %	111	

Table 2.1: Glass transition temperatures (T_g) obtained for cures with varying stoichiometry and atmosphere. The percentage stoichiometry refers to the ratio of the amine to the epoxy (i.e. 0.9:1.1 of amine:epoxy = 90 %).

with one another, forming the most tightly packed network possible.

When the stoichiometric range was extended for the nitrogen cured samples, from 90 % to 110 %, the obtained T_g was found to be 98 °C for 90 % and 111 °C for the 110 %. The reason for this large disparity between the epoxy excess samples and the amine excess samples is largely due to the functionality of the reactant molecules. The functionality is the number of reactive sites per molecule. If none of the reactive groups in a molecule react, the molecule will contribute to the sol fraction, and if only one of the reactive groups in a molecule react with the network, a chain end is produced. Both of these two possibilities lead to a decrease in the crosslink density and hence a reduction in T_g.

The amine has twice the functionality (i.e. reactive sites) (4), than the epoxy (2). In both of the extreme formulations a minimum of 10 % (0.1) of the reactive groups will be unreacted. Assuming only amine-epoxy reaction, in the case of the epoxy component, this means that there is a 1 % (0.1^2) chance that both epoxide groups on any particular molecule will remain unreacted, contributing to the sol fraction. The remaining unreacted epoxide groups will produce chain ends, with the associated decrease in crosslink density. By contrast, the chances of a completely unreacted amine molecule are 0.1^4 - a negligible

0.01 %. Further, the likelihood of only a single reaction sits at just 0.1 %. Hence, whilst the average mass between crosslinks (M_c) will increase somewhat, the number of molecules not contributing to the network structure as sol or dangling ends is much lower. In addition, the definition of a crosslink is given as a branching unit which has at least three separate branching units to the infinite network. As such, where only one of the four reactive sites present in a MXDA molecule fails to react, a crosslink is still formed, irrespective of any other physical changes this may cause.

Crosslink Density

Further investigation of the cured properties were obtained using beams of sample of a known thickness, in order to obtain modulus values. The rubbery plateau modulus of the sample can then be used to calculate crosslink density.[13] Figure 2.21 shows the crosslink densities obtained for both atmospheres of cure. The data shows a loose relationship between T_g and crosslink density. Variation between samples was generally high, leading to a large error—generally all samples within 4 % of stoichiometry were of the same crosslink density within error.

There was a significant fall off in crosslink density with amine deficiency as would be expected since the amines form the basis for any crosslink. The highest crosslink densities were found for samples cured under a nitrogen atmosphere, though for the amine deficient samples, the air cured samples were found to have a higher value. Under air there are a number of reactions which the amine can undergo, so we would not expect this increase. It is suggestive of a fundamental difference to the network structure formed under each atmosphere, though the cause of this is unknown. We can speculate that there may be an overall increase in the crosslink density due to consumption of epoxide groups under air, or that there is a higher propensity for etherification.

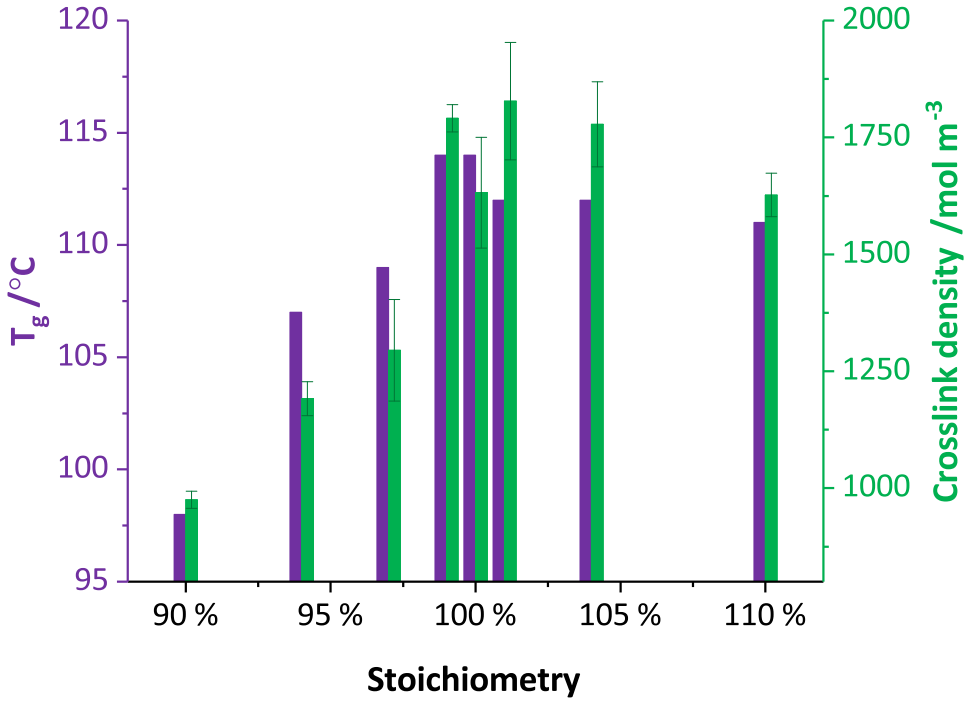

(a)

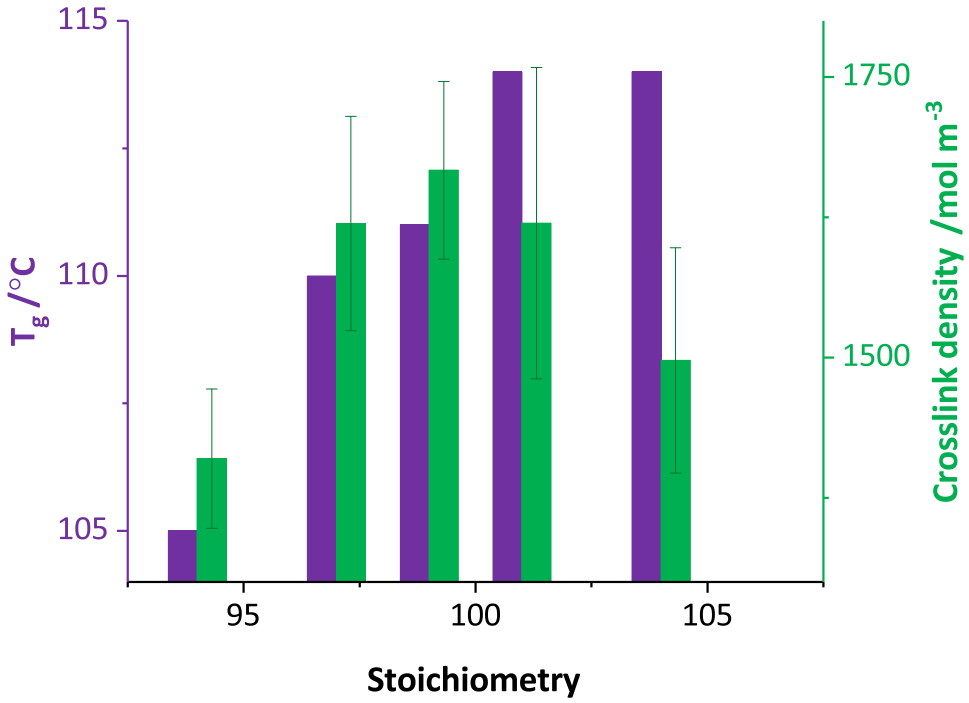

(b)

Figure 2.21: The glass transition temperature, T_g and the crosslink density of DER 354 / MXDA networks made with varied stoichiometries cured under (a) a nitrogen atmosphere and (b) an air atmosphere. Error bars show standard error of three samples.

Bulk density

Bulk density was measured by helium pycnometry. Figure 2.22 shows the variation in density between networks of different stoichiometries and cure atmospheres. Generally the variation is small—the range is 0.4 % of the average. The only difference of note is observed with the 100 and 101 % stoichiometry, nitrogen cured samples when compared to the other samples. They show a reduction in density relative to all of the other samples. This is in agreement with Gupta & Brahatheeswaran, Pethrick *et al.* and Morsch *et al.*, who found that at high conversions, increased reaction leads to a reduction in density.[14–16] To reiterate that discussed in Section 1.1.8, this decrease in density is associated with either free volume directly associated with the region immediately surrounding crosslinks, or an increase in free volume present at the point of vitrification, as a result of the increase in T_g.

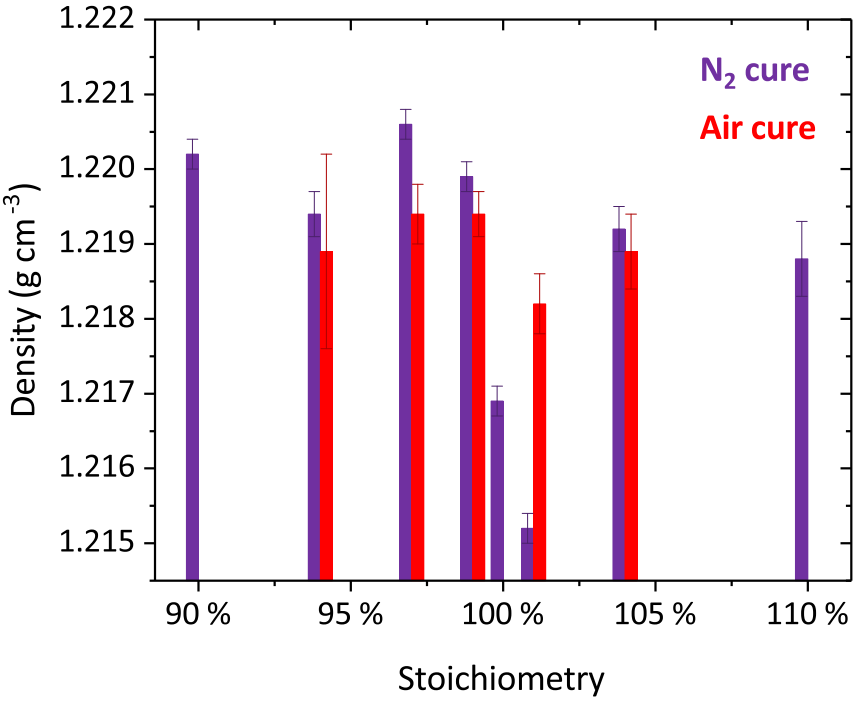

Figure 2.22: Density obtained from helium pycnometry for DER 354 / MXDA networks of different stoichiometries, cured under nitrogen (N_2—purple)) and air (red). Error bars show standard deviation of ten measurements of a single sample.

When comparing the different atmospheres, the densities are slightly lower than those for nitrogen cured samples (aside from the larger variation for the stoichiometric samples

discussed above). However, the differences are minimal.

2.1.6 Solvent uptake studies: (i) Methanol uptake

$$J = -D \frac{\partial C}{\partial x} \tag{2.3}$$

$$\frac{\partial C}{\partial x} = D \frac{\partial^2 C}{\partial x^2} \tag{2.4}$$

Fick's first (2.3) and second (2.4) laws. **J** *is the diffusive flux,* **D** *is the diffusion coefficient,* **C** *is the concentration and* **x** *is the position.*

For a network exposed to a solvent on one side it has been shown by Shen and Springer that Equation 2.5 describes the uptake of a material displaying Fickian behaviour, at short times.[17] Hence, the diffusion coefficient can be determined by the plotting of $\frac{M_t}{M_\infty}$ against the square root of time where M_t is the mass at any time and M_∞ is the ultimate mass absorbed.

$$\frac{M_t}{M_\infty} = \frac{4}{s}\sqrt{\frac{Dt}{\pi}} \tag{2.5}$$

Approximation of the diffusion coefficient at short times with Fickian diffusion, where $\mathbf{M_t}$ *is the mass at any time,* $\mathbf{M_\infty}$ *is the ultimate mass absorbed,* **s** *is twice the thickness of the sample (for a sample exposed on both sides it is simply the thickness of the sample),* **D** *is the diffusion coefficient and* **t** *is time.*

Stoichiometric variation for inert cure networks

Figure 2.23 shows the methanol sorption and desorption for the networks cured under a nitrogen atmosphere (for stoichiometries between 94 and 104 %). The initial slopes are fitted as per Equation 2.5.

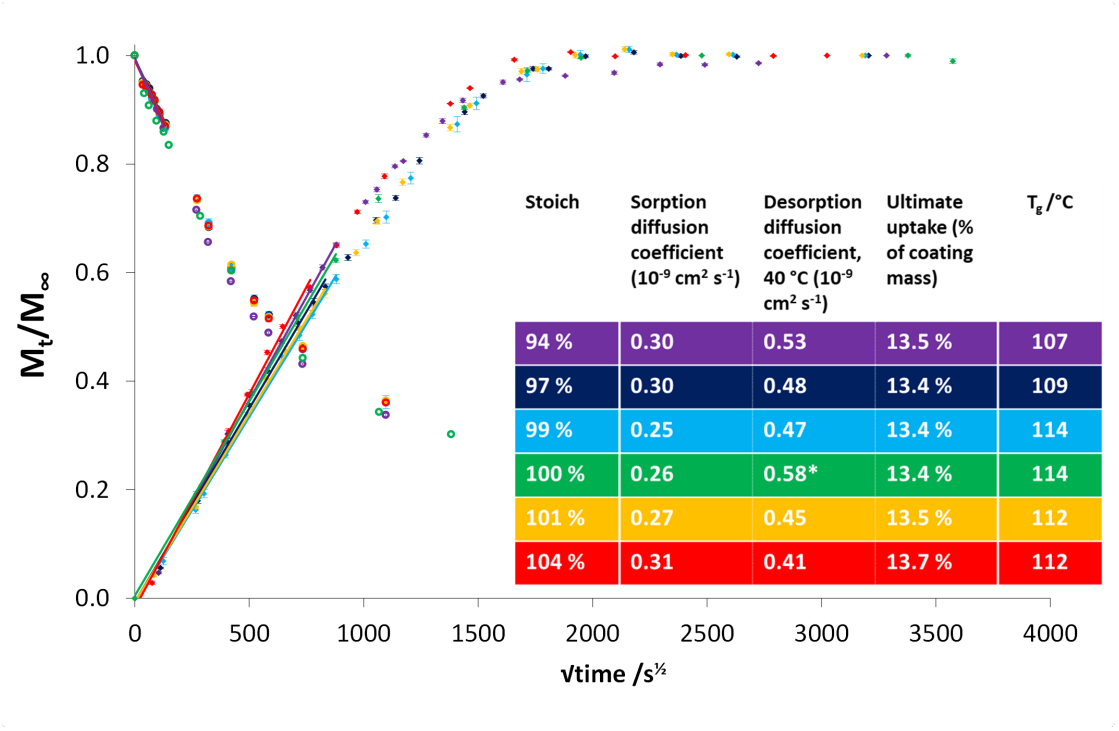

Stoich	Sorption diffusion coefficient (10^{-9} cm^2 s^{-1})	Desorption diffusion coefficient, 40 °C (10^{-9} cm^2 s^{-1})	Ultimate uptake (% of coating mass)	T_g /°C
94 %	0.30	0.53	13.5 %	107
97 %	0.30	0.48	13.4 %	109
99 %	0.25	0.47	13.4 %	114
100 %	0.26	0.58*	13.4 %	114
101 %	0.27	0.45	13.5 %	112
104 %	0.31	0.41	13.7 %	112

Figure 2.23: Methanol sorption and desorption of DER 354 / MXDA networks on glass slides made with varying stoichiometries of the two components. Sorption begins at the origin with a positive slope and desorption at $\frac{M_t}{M_\infty} = 1$*, with a negative slope. Error bars show standard error of three samples. The diffusion coefficients, D, were calculated from the gradient of the initial linear fits (Equation 2.5) and are shown in the inset table. Ultimate uptake and glass transition temperature,* T_g*, are shown for each sample. *the desorption for the 100 % sample was performed in a different oven environment, and so is not directly comparable to the values obtained for the other samples.*

An alternative approach to diffusion coefficient determination presented by Shen and Springer is to fit the entire diffusion curve, using the approximation shown in Equation 2.6.[17] An example of this method is shown in Figure 2.24a.

$$\frac{M_t}{M_\infty} = 1 - \exp\left[7.3\left(\frac{D_x t}{s}\right)^{0.75}\right] \tag{2.6}$$

There is a small reduction in the diffusion coefficient calculated by this method relative to using the initial slope, but the same general trend is shown (Figure 2.24b).

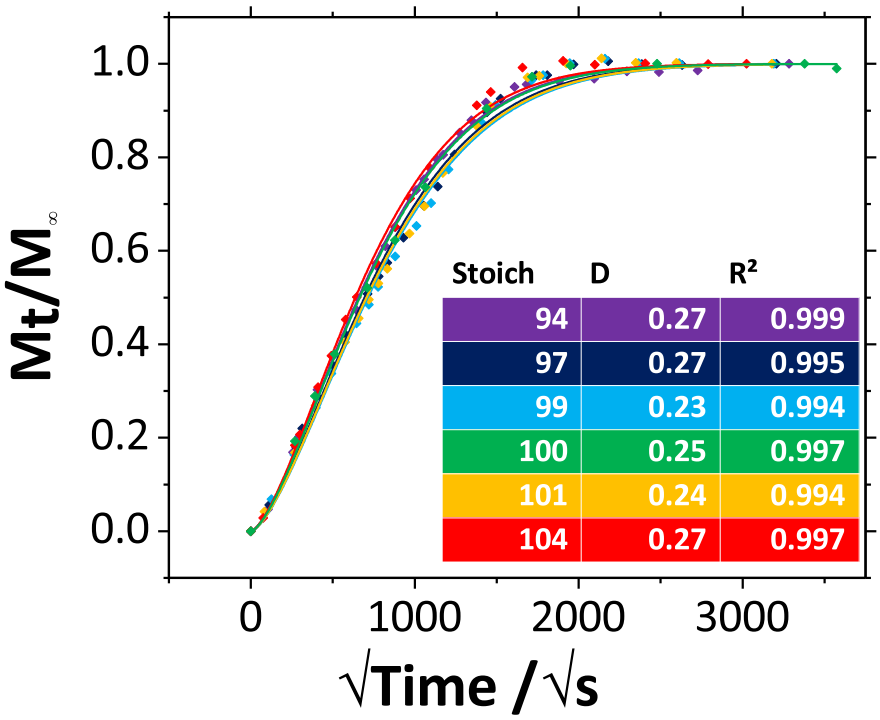

(a) Methanol sorption curves for DER 354 / MXDA networks on glass slides made with varying stoichiometries of the two components, fitted using Equation 2.6. The diffusion coefficient calculated from the fit (with units of 10^{-9} cm^2 s^{-1}) are shown in the inset table.

Stoich	Sorption diffusion coefficient (10^9 cm^2 s^{-1}) Linear fit	Curve fit
94 %	0.30 ± 0.004	0.27 ± 0.004
97 %	0.30 ± 0.005	0.27 ± 0.007
99 %	0.25 ± 0.004	0.23 ± 0.007
100 %	0.26 ± 0.005	0.25 ± 0.008
101 %	0.27 ± 0.004	0.24 ± 0.007
104 %	0.31 ± 0.007	0.27 ± 0.006

(b) Comparison of methanol sorption diffusion coefficients obtained by an initial linear fit, using Equation 2.5 or a fit of the entire curve, using Equation 2.6.

Figure 2.24

Therefore, the simpler initial slope method was selected as an appropriate tool to compare the networks. Each sample was immersed in methanol until an equilibrium mass was reached, and then dried in an oven (C1). Following a complete drying in a vacuum oven, this process was then repeated in a second cycle (C2).

Cycle one (C1)

There is limited variation in diffusion between the different stoichiometries, for either the diffusion coefficients or the ultimate uptake. The lowest diffusion coefficient for sorption (D_{sor}) is seen for the 99 % sample, with 104 % having the highest, though all are within 10 % of one another. As perhaps might be expected, the diffusion coefficient reaches a minimum around stoichiometry (99/100/101 % samples), with higher values for D_{sor} obtained when moving further away from stoichiometry.

The ultimate uptake is reasonably consistent throughout the samples, with only a 2 % variation across the samples—the highest is 13.7 % and the lowest 13.4 %. Again a minimum around the samples closer to stoichiometry is observed.

The desorption diffusion coefficients (D_{des}) are of a greater magnitude than the sorption as a result of the desorption being conducted at a higher temperature. This helps ensure that the environment is constant, rather than being subject to atmospheric variations. Perhaps surprisingly, the lowest desorption diffusion coefficient is seen for 104 %, which has the highest sorption coefficient. The variation for D_{des} is $\sim$20 %. The oven environment was adjusted in between obtaining the data for the 100 % sample and the other samples, leading to a larger value. If we ignore this, the highest D_{des} is for the 94 %, and the trend is an increase as we reduce the stoichiometry (i.e. decrease amine content).

Cycle two (C2)

The comparison of C1 and C2 is shown by Figure 2.25. It is observed that the general trend is very similar. The ultimate uptake measurements reveal very little variation in trend, but there is a small reduction in the average uptake, from 13.5 % to 13.3 %.

In comparing the sorption diffusion coefficient, we find very similar coefficients for all samples (i.e. within error), excluding the two extremes of stoichiometry. For the 104 % sample, we observe a 10% decrease in sorption coefficient. For the 94 % sample we see the reverse: a 17 % increase in sorption coefficient.

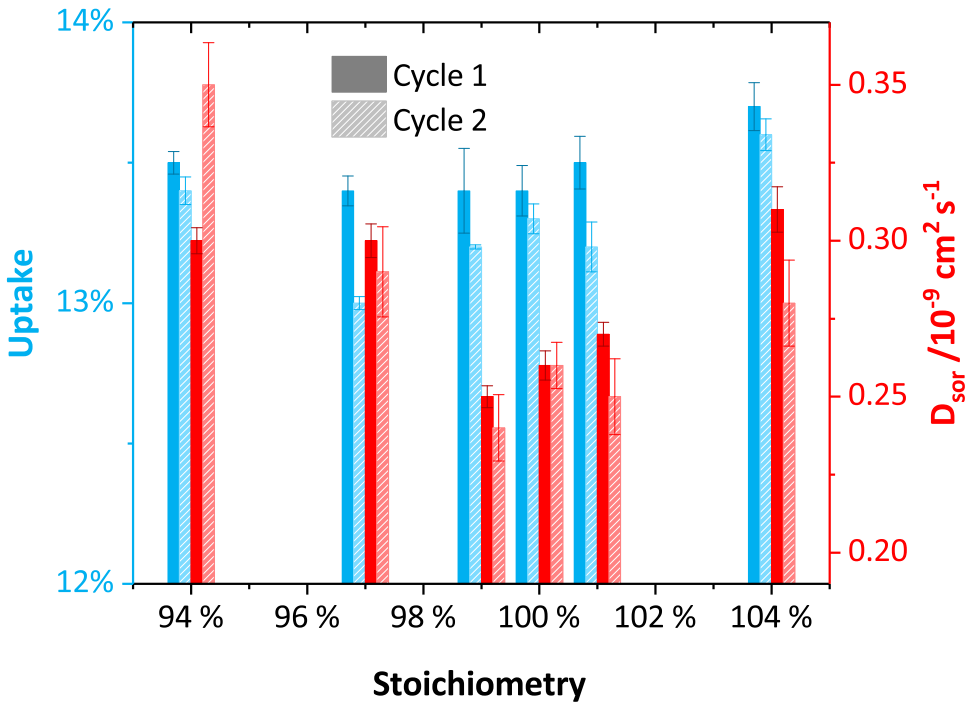

Figure 2.25: Ultimate uptake (blue) and sorption diffusion coefficients (D_{sor} - red) for MXDA/DER 354 networks, cured under a nitrogen atmosphere, immersed in methanol immediately after cure (cycle 1) and after reaching equilibrium and rigorous drying in a vacuum oven (cycle 2). Error bars show standard error of three samples.

The general decrease in ultimate uptake is expected - in order to remove all solvent from the sample, each network was heated above its T_g—to 120 °C under reduced pressure for 24 hours. This prolonged period above T_g provides the opportunity for post-cure - if there are any unreacted epoxide groups, reaction with any unreacted amine or hydroxyl groups is likely to take place. It also provides an opportunity for molecular relaxation to occur, which could result in a denser network.

When we compare the sorption coefficients, the decrease seen for the 104 % sample can be justified by a similar way to the ultimate uptake findings. That is, that the drying of the networks provided a post-cure. Further, the sorption coefficient data is likely to be

influenced by the small amounts of residual solvent that was found in some, but not all of the networks. The average was found to be 0.10 % of the network mass. This initial mass means the concentration gradient is less steep and therefore would serve to slow the diffusion of the methanol. The change for 94 % is much more unexpected. In terms of post-cure we would expect the amine-deficient sample to have the highest proportion of unreacted epoxide groups which would possibly undergo etherification (reaction of epoxide and hydroxyl). It is even more unexpected considering the reduction in ultimate uptake.

The desorption results are not directly comparable as a result of the aforementioned change in oven environment and therefore are not shown in Figure 2.25. However, the trend is broadly the same, with the 99 % sample deviating slightly.

Overall trends

The overall results show small variations in diffusion characteristics between the samples of various stoichiometries, in spite of a good degree of variability in T_g. From the degree of cure obtained by NIR spectroscopy this might be expected—even the 94 % sample shows a 98 % conversion of epoxide groups. However, there are small but noticeable changes, more clearly in D_{sor} but also ultimate uptake, with minima around approximately ($\pm 1\%$) stoichiometric formulations.

In order to probe the limits of these findings, networks further from stoichiometry (by 10 %) were prepared under nitrogen. The T_g, ultimate uptake and D_{sor} are shown in Figure 2.26. The decrease in T_g and crosslink density is discussed in Section 2.1.5—we see a much sharper decrease in both with an amine deficiency, than an excess due to the higher functionality of MXDA relative to DER 354.

The inclusion of the more extreme deviations from stoichiometry show the limited nature of the variation for the other samples analysed. Both exhibit an increased ultimate uptake and D_{sor}. The 90 % sample showed uptake of $>$15 % by mass, the highest of any network probed across this work, which is consistent with the greater reduction in thermal properties relative to the 110 % sample (uptake = 13.9 %). However, D_{sor} was

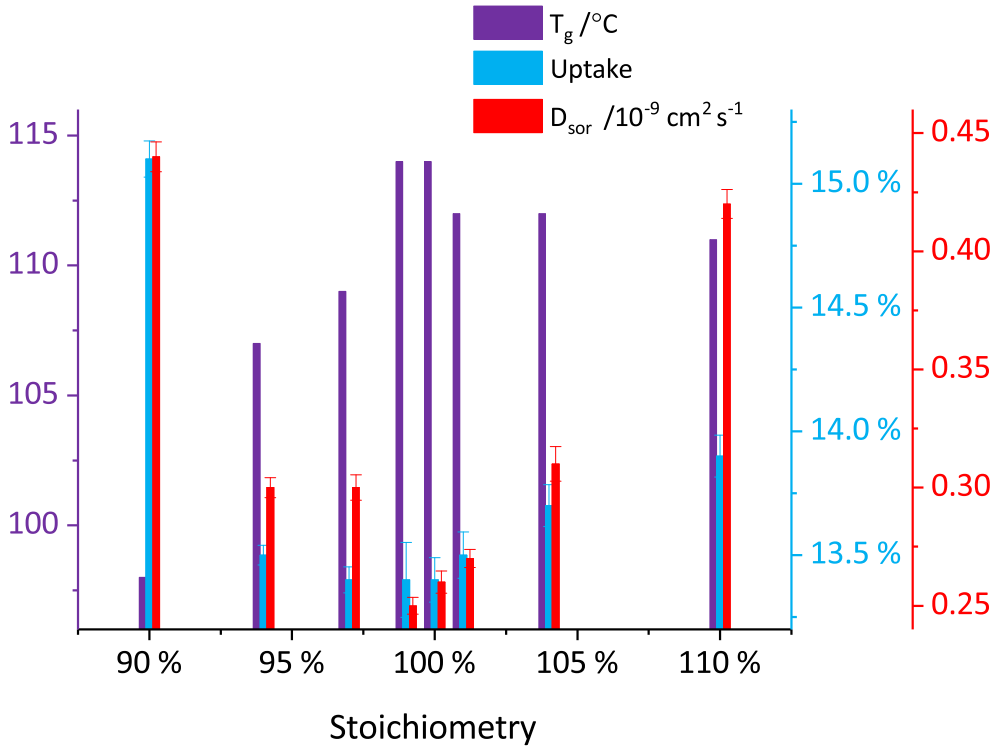

Figure 2.26: The T_gs (purple), ultimate uptake (blue) and diffusion coefficient for sorption (D_{sor}) for MXDA / DER 354 networks of varied stoichiometries (for the cycled samples, only the first cycle is shown). Error bars show standard error of three samples.

similar for both samples. This is unexpected in light of the thermal properties—and is suggestive that there is little dependence of the rate of diffusion upon crosslink density when we diverge from an "ideal" network. Instead the relationship appears to be based upon degree of reaction, whether crosslinks are produced or not.

If we only consider the amine deficient systems (90 - 100 %), we observe that there are trends between degree of cure and subsequent properties, including T_g (Figure 2.27). However, when considering the amine excess samples, the T_g remains high even with a large divergence from 100 % stoichiometry, as a result of the above-discussed variation in functionality—there is a remaining concentration of amine hydrogens but since these are incorporated into the network, they neither plasticise nor increase the proportion of dangling ends.

Therefore, in assessing the quality and likely performance of a network the T_g must be used with caution. It is seen to correlate well with epoxide conversion, but shows much less dependence on the degree of amine reaction. However, chemical performance

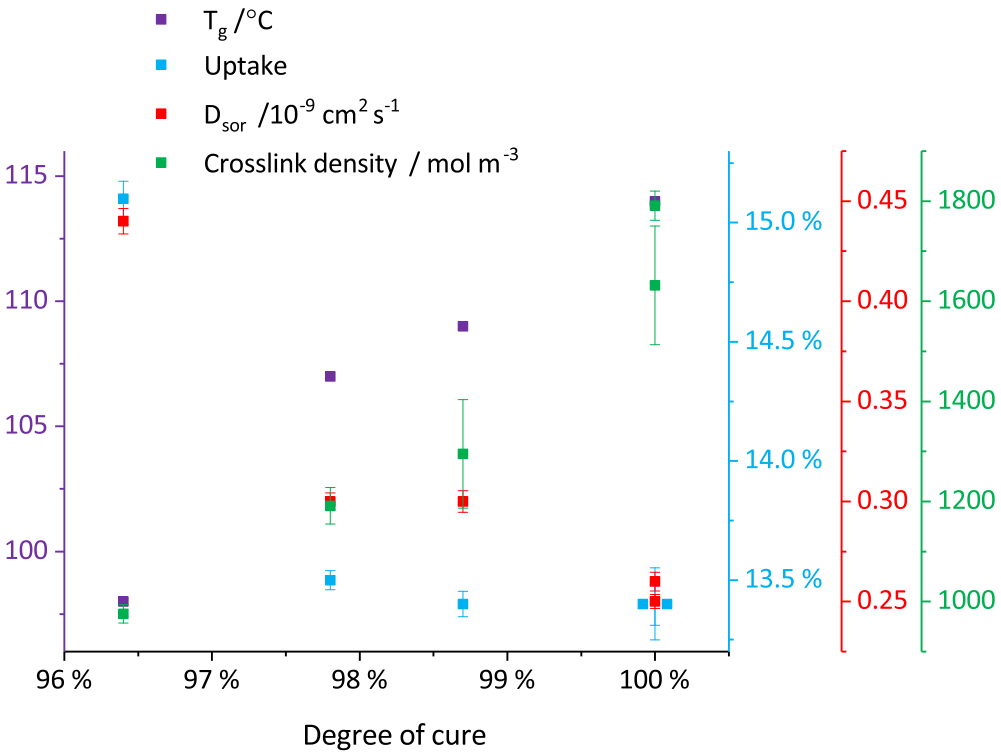

Figure 2.27: The T_gs (purple), ultimate uptake (blue), diffusion coefficient for sorption (D_{sor}-red) and crosslink density (green) for MXDA / DER 354 networks of different degrees of cure—as a result of changing stoichiometry. All networks shown were formulated with an amine deficiency. Error bars show standard error of three samples.

is shown to decrease where full reaction of either component is not achieved, with the lowest and slowest uptake achieved for approximately stoichiometric formulations. Samples formulated <6 % from 100 % stoichiometry illustrate the robustness of the chemical system selected—that the majority of performance will be maintained until there is a greater disparity in the ratio of reactive groups. However, the most extreme samples show that upon the disparity reaching a certain point, there is a marked drop-off in performance. Ensuring the maximum amount of epoxy-amine reaction is of most importance in improved performance.

Stoichiometric variation for air cure

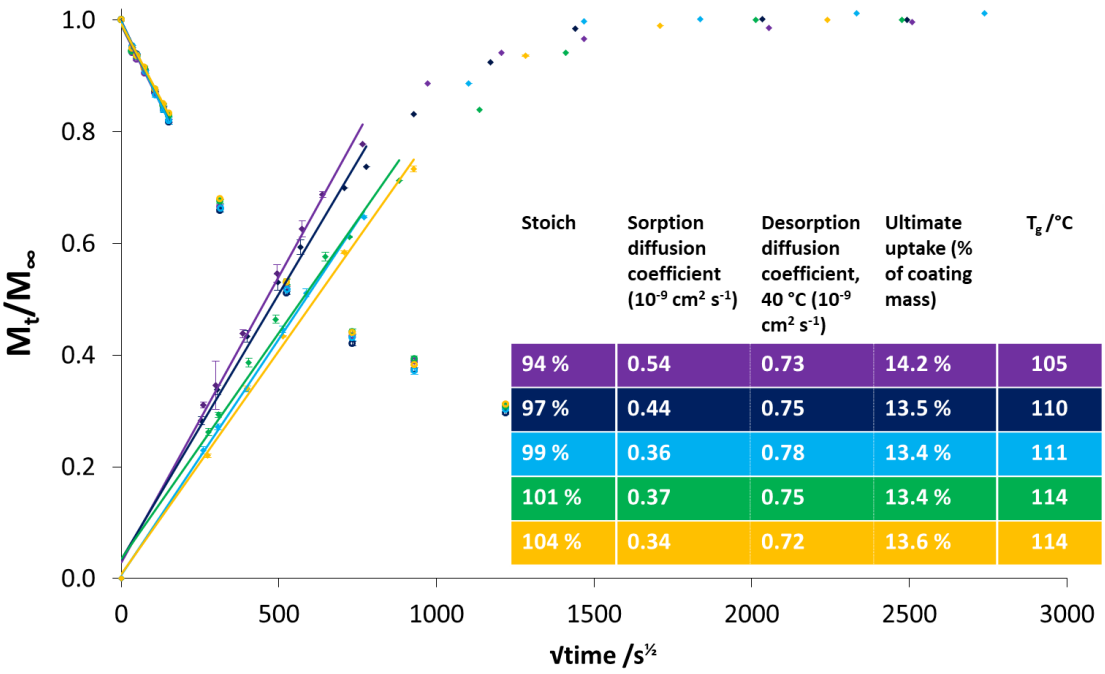

Stoich	Sorption diffusion coefficient (10^{-9} cm^2 s^{-1})	Desorption diffusion coefficient, 40 °C (10^{-9} cm^2 s^{-1})	Ultimate uptake (% of coating mass)	T_g /°C
94 %	0.54	0.73	14.2 %	105
97 %	0.44	0.75	13.5 %	110
99 %	0.36	0.78	13.4 %	111
101 %	0.37	0.75	13.4 %	114
104 %	0.34	0.72	13.6 %	114

Figure 2.28: Methanol sorption and desorption of DER 354 / MXDA networks on glass slides made with varied stoichiometries of the two components, cured under an atmosphere of air. Sorption begins at the origin with a positive slope and desorption at $\frac{M_t}{M_\infty} = 1$, *with a negative slope. Error bars show standard error of three samples. The diffusion coefficients, D, were calculated from the gradient of the initial linear fits (Equation 2.5) and are shown in the inset table. Ultimate uptake and glass transition temperature,* T_g, *are shown for each sample.*

Cycle one (C1)

Figure 2.28 shows the methanol sorption and desorption for the air cured samples in C1. Here we see some more pronounced differences between the varied stoichiometries for sorption, with the diffusion coefficient increasing with amine deficiency. The 94 % stoichiometry in particular had a much higher D_{sor} - ∼50 % higher than the 99, 101 and 104 % samples. Further to this the same sample had a higher ultimate uptake - at 14.2%, relative to approximately 13.5 % found for all the other samples.

However, the desorption data shows much less variation, less than 10 % between all the values for D_{des}. The fastest desorption happened for the 99 % sample, with desorption slower for the 94 % sample, in spite of faster sorption and higher ultimate

uptake.

Cycle two (C2)

The cycling of the air slides shows some similarities to the cycling of nitrogen cured slides discussed above but also key differences between the networks, as is shown in Figure 2.29. As with the majority of the nitrogen cured samples, the sorption coefficient is seen to decrease by 13-23 %. However, mass uptake slightly increases (by 0.7-3 %) in all but the 94 % sample, which shows a small decrease. This increase is suggestive of some degradation of the network, resulting in the creation of free volume. A concurrent decrease in the diffusion coefficient is not necessarily expected, but there is evidence in the literature that lowering crosslink density can lead to slower diffusion.[15,16] It may also be that while there is degradation, molecular relaxation caused by heating could improve polymer chain packing.

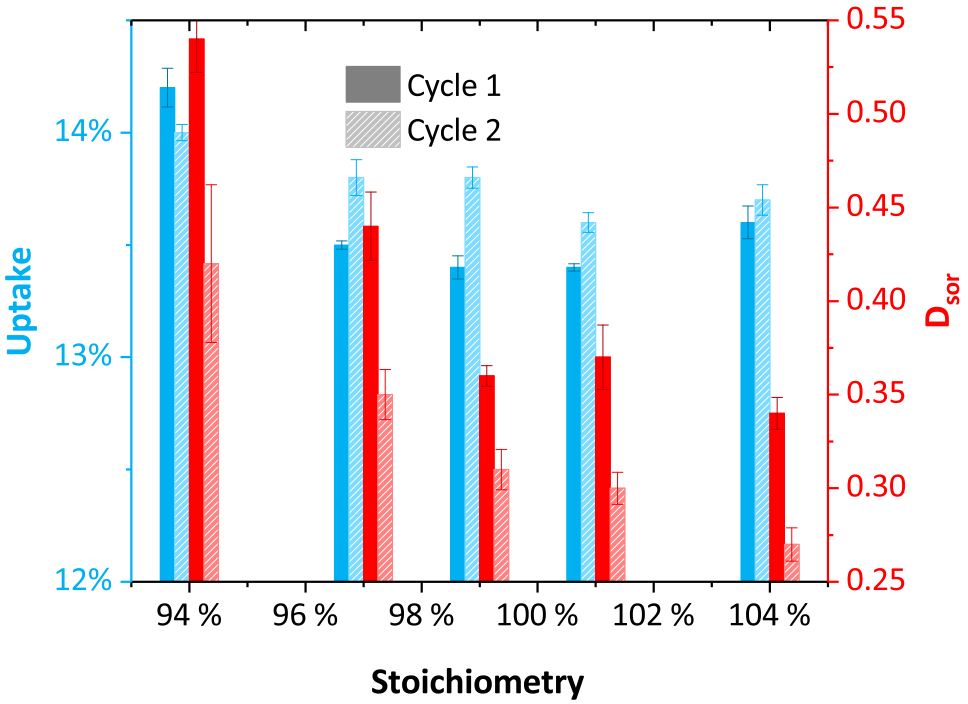

Figure 2.29: Ultimate uptake (blue) and sorption diffusion coefficients (D_{sor} - red) for MXDA/DER 354 networks, cured under an air atmosphere, immersed in methanol immediately after cure (cycle 1) and after reaching equilibrium and rigorous drying in a vacuum oven (cycle 2)

Overall trends

As described in Section 2.1.5, for the air-cured samples, the trend in T_g suggests the presence of side-reactions which consume amine groups whilst not contributing to the network structure (such as carbamation and oxidation). This causes those formulations which are already amine deficient to become even more so. This leads to the substantial inferiority (both in terms of ultimate uptake and D_{sor}) of the 94 % sample relative to the other samples. All of the other samples showed very similar results in terms of solvent uptake, which would be expected considering: (i) the similarity in T_g; (ii) that the crosslink density values were found to be within error of one another; (iii) and a limited bulk density variation (Figure 2.30).

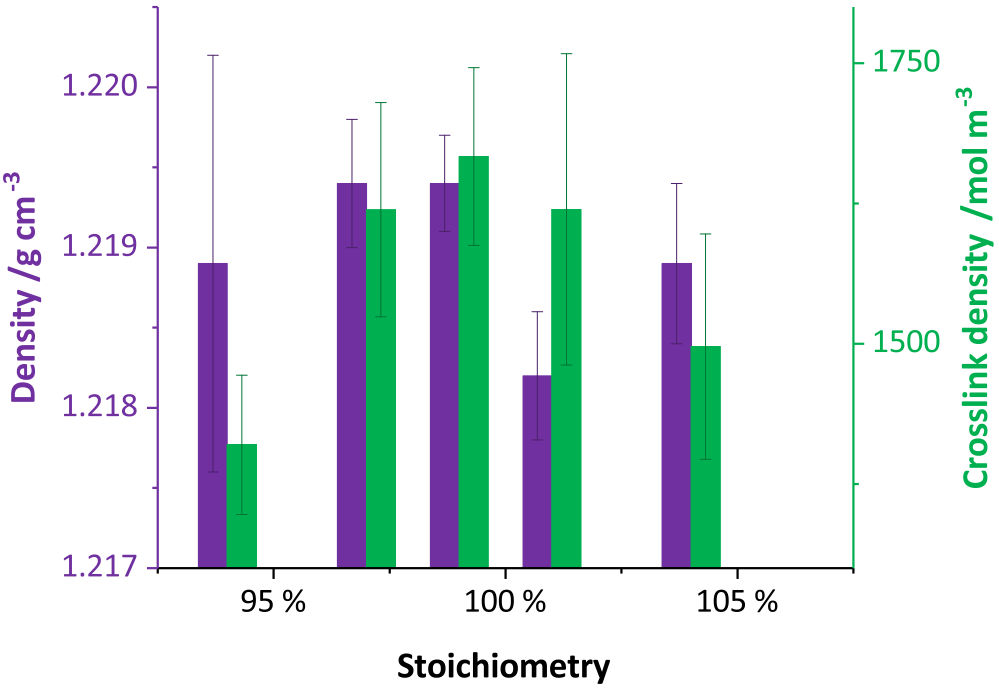

Figure 2.30: Density and crosslink density of DER 354 / MXDA networks made with different stoichiometries cured under an air atmosphere. Error bars show standard deviation of ten measurements for density and standard error of three samples for crosslink density.

Comparison between different atmosphere cures

Of greatest interest from these studies is the comparison between the different cure atmospheres. As is shown in Figures 2.23 & 2.28 there is a marked difference between the sorption and desorption coefficients - that the air cured samples have larger diffusion coefficients for both cases. This is shown in Figure 2.31.

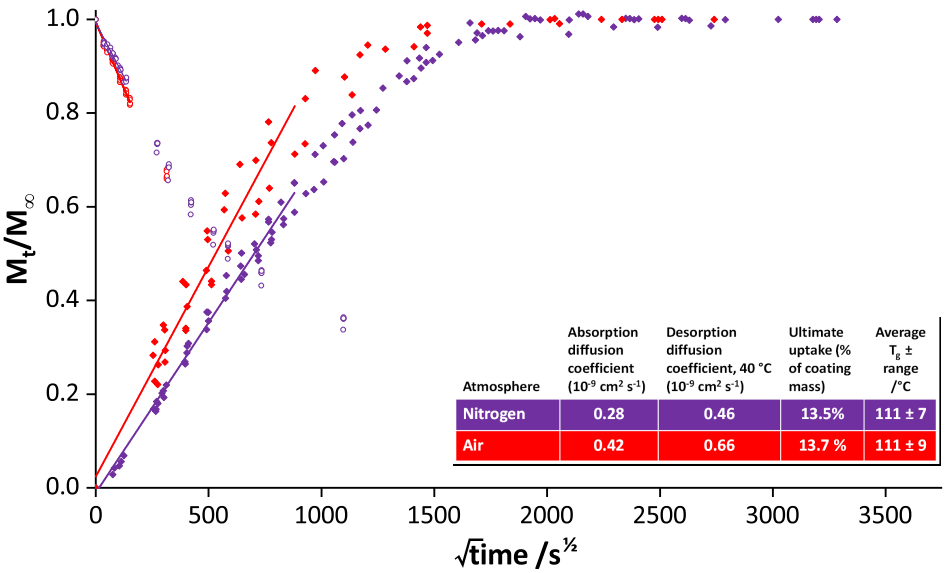

Figure 2.31: Methanol sorption and desorption of DER 354 / MXDA networks on glass slides made with varying stoichiometries (94 % - 104 %) of the two components under an atmosphere of air (red) or nitrogen (purple). Sorption begins at the origin with a positive slope and desorption at $\frac{M_t}{M_\infty} = 1$*, with a negative slope. The diffusion coefficients, D, were calculated from the gradient of the initial linear fits (Equation 2.5) and are shown in the inset table. Average ultimate uptake and glass transition temperature,* T_g*, are shown for each sample.*

These results show an interesting phenomenon, that a sample of a lower T_g shows slower solvent sorption and desorption, than one with a higher T_g - as is shown by the 94 % nitrogen cured vs. the 101 % air cured. This supports the idea that the T_g is by no means an indicator of the nanoscale structure which governs the sorption of solvent, and instead shows a measure of the uniformity of the overall structure.

2.1.7 Solvent uptake studies: (ii) Ethanol uptake

In spite of long uptake times (>400 days for the nitrogen cured samples), an ultimate uptake has not been obtained. Therefore, it is not possible to calculate a diffusion coefficient by the method used above. However, we can perform a comparison of the uptake at set time-points, and of the uptake curve as a whole.

The data shows a clear difference between the samples cured in a nitrogen atmosphere and those in an air atmosphere (Figure 2.32). Uptake is much higher in the air-cured samples, and the variation between the different air-cured samples substantially greater than the variation in the N_2-cured samples. The uptake by mass at approximately 200 days is between 2.1 % and 2.4 % for the nitrogen cured samples, where this value varies between 2.8 % and 4.7 % for those cured under air.

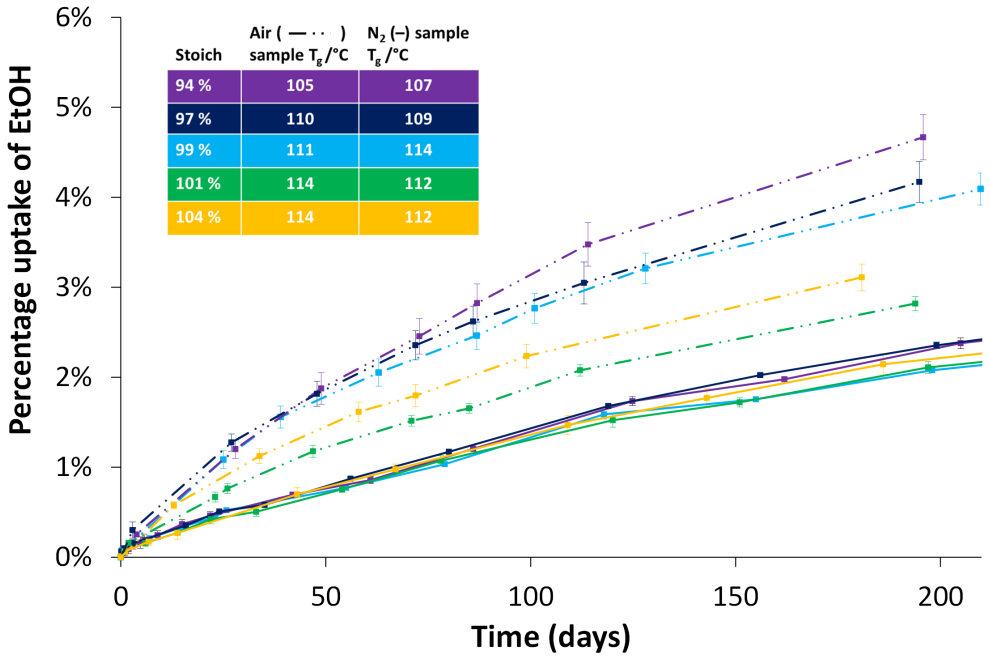

Figure 2.32: Ethanol sorption vs time for DER 354 / MXDA networks on glass slides made with varying stoichiometries of the two components under an atmosphere of air or nitrogen. Error bars show standard error of three samples.

Between the different stoichiometries of nitrogen-cured samples there is little variation, but the better performance centres around stoichiometry, where T_g is greater—here, T_g is generally shown to be a good predictor for the performance. The two most-uptaking samples (of ethanol) are the 94 % and 97 % samples, which are the two lowest T_g ma-

terials. The 99 % and 101 % are the least-uptaking and the 104 % third.

The trend within the air-cured samples also generally follows the T_g. The most uptaking is the 94 %, followed by the 97 % and the 99 %. The least uptaking is the 101 %, with the 104 % sample uptaking second-least. For networks cured under both atmospheres then, while the 101 % and the 104 % have the same T_g, the 101 % is better performing. Within the air cured samples, the most unexpected data in light of the methanol uptake data, is the amount of uptake in the 99 % samples. This showed the joint lowest uptake and diffusion coefficient across all the samples when exposed to methanol. However, when exposed to ethanol, its performance is much more similar to the worse performing 97 % stoichiometry.

When the data is plotted against the square root of time, we observe that it is not linear (Figure 2.33). This shows us that unlike the methanol uptake it is not Fickian. This is generally explained by the plasticisation of the network by the aggressor.[18,19] That the traces for mass uptake against time (Figure 2.32) are not linear shows the uptake is not Case II. The traces are most similar to the sigmoidal mode of diffusion.

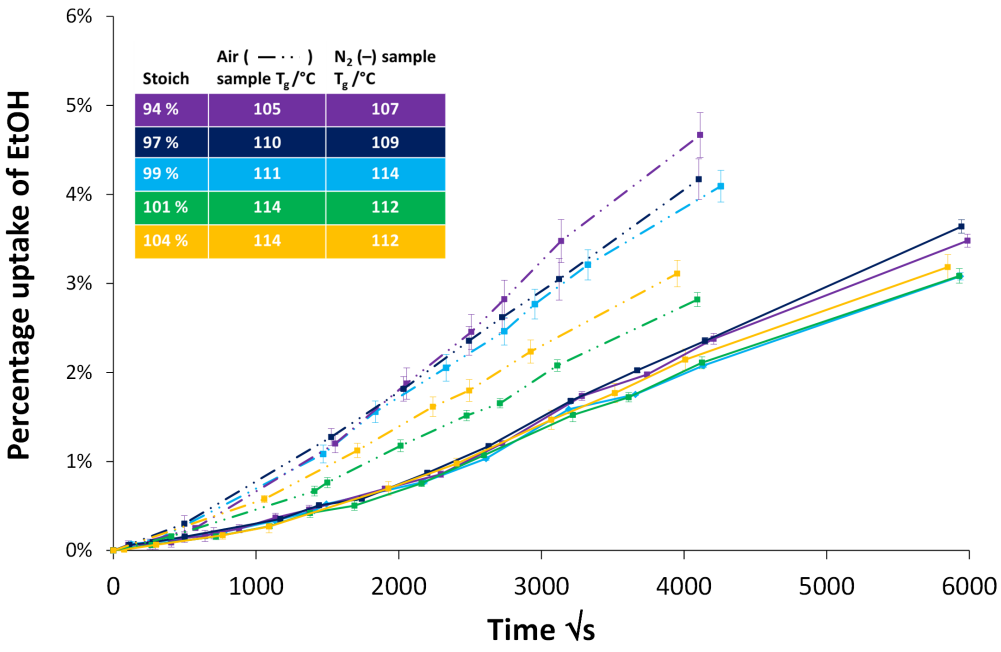

Figure 2.33: Ethanol sorption vs the square root of time for DER 354 / MXDA networks on glass slides made with varying stoichiometries of the two components under an atmosphere of air or nitrogen. Error bars show standard error of three samples.

Further to this mass uptake evidence, enhanced swelling exhibits itself with cracking

of the network, indicating there is degradation occurring (Figure 2.34). This supports that there is a fundamental weakness inherent to samples cured under air, which was suggested by the increase in methanol uptake seen between cycles (Section 2.1.6).

Figure 2.34: Photograph of two MXDA/DER 354 networks on microscope slides cured under an atmosphere of (l) nitrogen and (r) air, and immersed in ethanol for >200 days. Cracking is evident for the air cured sample and is highlighted by red boxes.

The ethanol uptake demonstrates a fundamental difference between the air and nitrogen cured samples. This is illustrated not only by the increased average uptake, but by the variation between stoichiometries. It is suggestive of some degradation—and also highlights the reduction in the robustness of the system when curing in air.

2.1.8 Oxidation and carbamation studies

The two processes that are likely to take place under air are oxidation (i.e. reaction with oxygen) or carbamation (reaction with carbon dioxide). In order to assess the contributions made by oxidation and carbamation on the chemical performance a study was performed to isolate and enhance each of these processes.

Oxidation study

In order to vary the levels of oxidation, whilst avoiding carbamation, networks were made according to the method used for the nitrogen cure (see Section 2.2.3). Then these samples were divided into three and treated in the oven under different atmospheres, according to the schematic in Figure 2.35a. Upon increasing amounts of time exposed to air, the yellowing of the networks was shown to increase (Figure 2.35b). These networks were then exposed to methanol and uptake monitored. Figure 2.36 shows the uptake for the three samples.

The control sample (i.e. not oxidised at all) showed the slowest uptake, and the 1.5 h sample showed slower uptake than the 3h sample. However, the magnitude of the variation between the control sample and the oxidised samples is substantially less than that observed within the atmosphere of cure study. Desorption showed no variation outside of error.

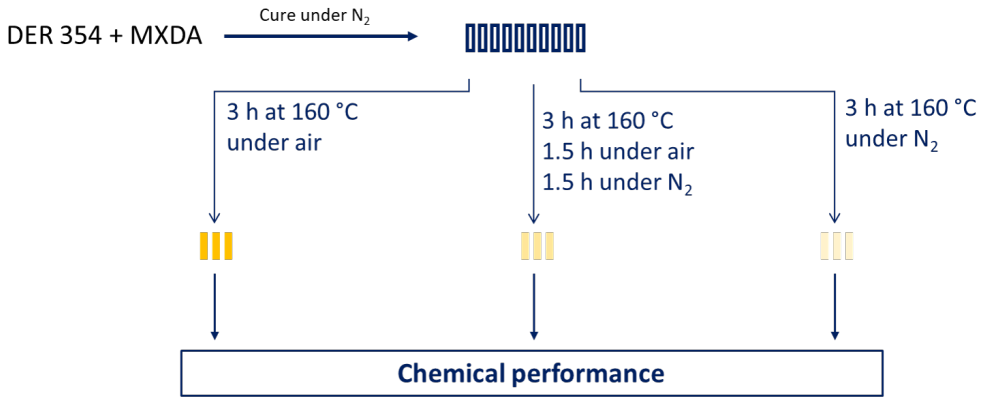

(a) Schematic of the experimental procedure undertaken to vary the yellowing of a 354/MXDA network.

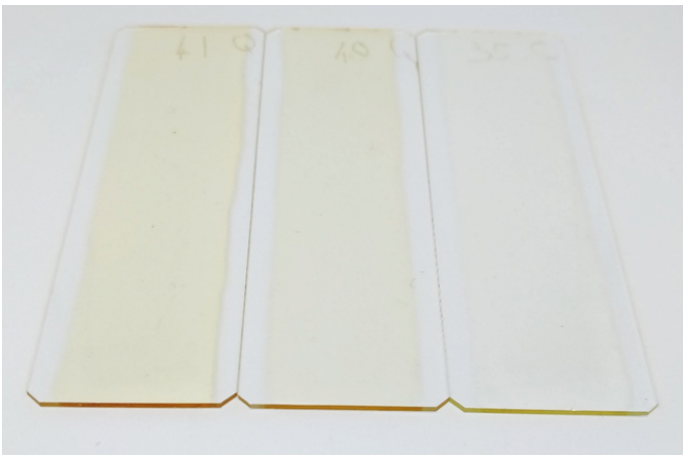

(b) Image showing the slides following oxidative treatment at 160 °C for 3 h, 1.5 h and 0 h (r-l). As oxidative treatment time increases, yellowing of the networks increases.

Figure 2.35

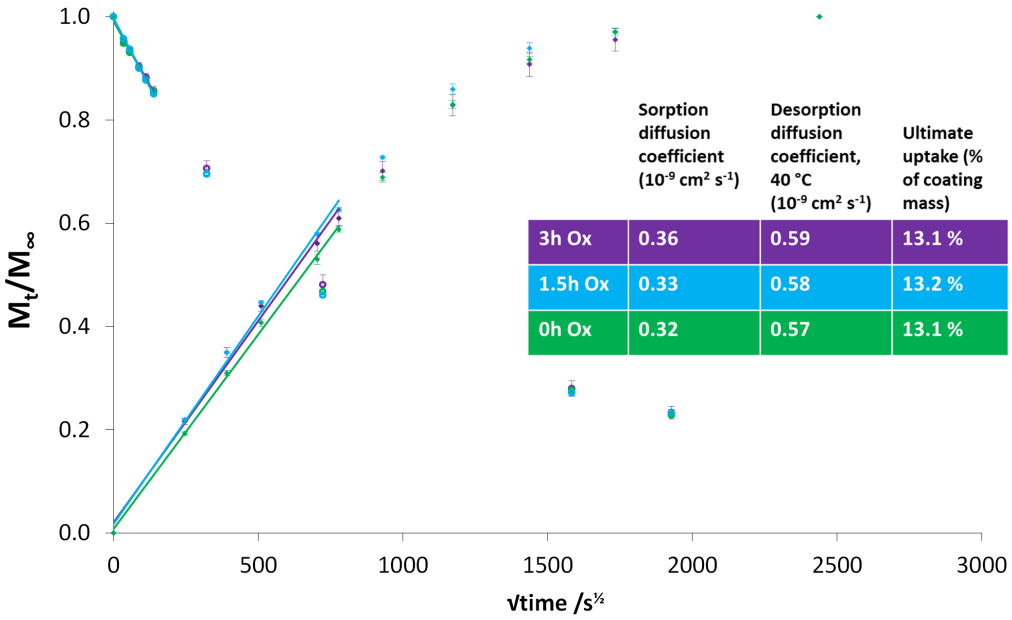

Figure 2.36: Methanol sorption and desorption of DER 354 / MXDA networks on glass slides which have been treated according to Figure 2.35. Sorption begins at the origin with a positive slope and desorption at $\frac{M_t}{M_\infty} = 1$*, with a negative slope. Error bars show standard error of three samples. The diffusion coefficients, D, were calculated from the gradient of the initial linear fits (Equation 2.5) and are shown in the inset table. Standard error for all values of* D_{sor} *was found to be 0.01* 10^{-9} cm^2 s^{-1}*, and was no higher than 0.03* 10^{-9} cm^2 s^{-1} *for* D_{des}*.*

Carbamation study

Carbamation requires the presence of both water vapour and carbon dioxide. As the surface area to volume area increases, the amount of material available to react with water vapour and carbon dioxide increases. Further, competition between carbamation and the cure reactions is higher at lower temperatures (see Section 2.1.1). Therefore, carbamation levels were varied by exposure of thin films of the same reactive mixture to air at room temperature for different time periods prior to cure. Three groups were prepared—40 minutes exposure, 10 minutes exposure and 0 minutes exposure (40m, 10m, 0m).

As the time exposed to air at room temperature increases, the networks showed an increase in opacity, as increasing amounts of the carbamate salt form on the surface of the network. The appearance of the networks produced is shown in the photograph in Figure 2.37a. These samples were then exposed to methanol and the uptake recorded, as

shown by Figure 2.37b. There is no appreciable trend in terms of the sorption diffusion coefficient (D_{sor}), though the slowest uptake was recorded for the 0m sample. The ultimate uptake is higher for the samples with increased carbamation levels, though only marginally so. In both cases the variation is very limited. The desorption diffusion coefficients (D_{des}) show an unexpected minimum for the 10m sample, which displayed the highest D_{sor}. The highest D_{des} was found for the 0m sample which had the lowest D_{abs}.

The marginal increase in ultimate uptake is of the same order of magnitude as that seen for the divergence from stoichiometry. This suggests that the only impact that carbamation has is to use up amine reactive sites, which serves to shift the formulation to an off-stoichiometric ratio. Due to the highly polar nature of a carbamate, it is likely that the product of carbamation will be immiscible, or less miscible with the bulk of the material. This means that any reaction is less likely to disrupt the network as a whole, as the produced carbamate will rise to the surface—if it is not already at the surface as a result of reaction at the air-resin interface. This is supported by the surface finish shown in Figure 2.37a. The rest of the mixture is then free to react as it would have otherwise done—albeit with a reduced amine concentration.

Oxidation/Carbamation experiment conclusion The limited effect upon both ultimate uptake and rate of diffusion shows that carbamation is not responsible for the step change in diffusion coefficients seen when varying the atmosphere of cure. It is also worth noting that the surface finish on the air cured samples does not show the clouding as seen in the 40 and 10 minutes samples from the carbamation experiment. Further, the oxidation study shows that the oxidation of the formed epoxy network can have an effect on the diffusion rate, though again the magnitude of change is not observed. Therefore, it is not the responsible factor in producing a network with such an increased sorption rate. The flaw in such an experiment is the inability to consider the impact of oxidation of the unreacted epoxy and amine groups. By the process of elimination (using the combined findings of both studies), we can suggest that the oxidation of these groups is likely to have an effect stronger than that of oxidation of the cured network.

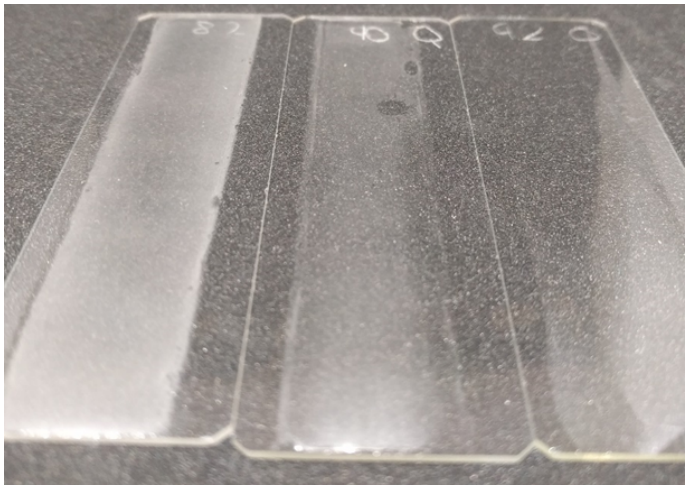

(a) Image showing the networks produced following exposure to air at room temperature for different time periods (40 mins, 10 mins and 0 mins, l-r), for the carbamation study.

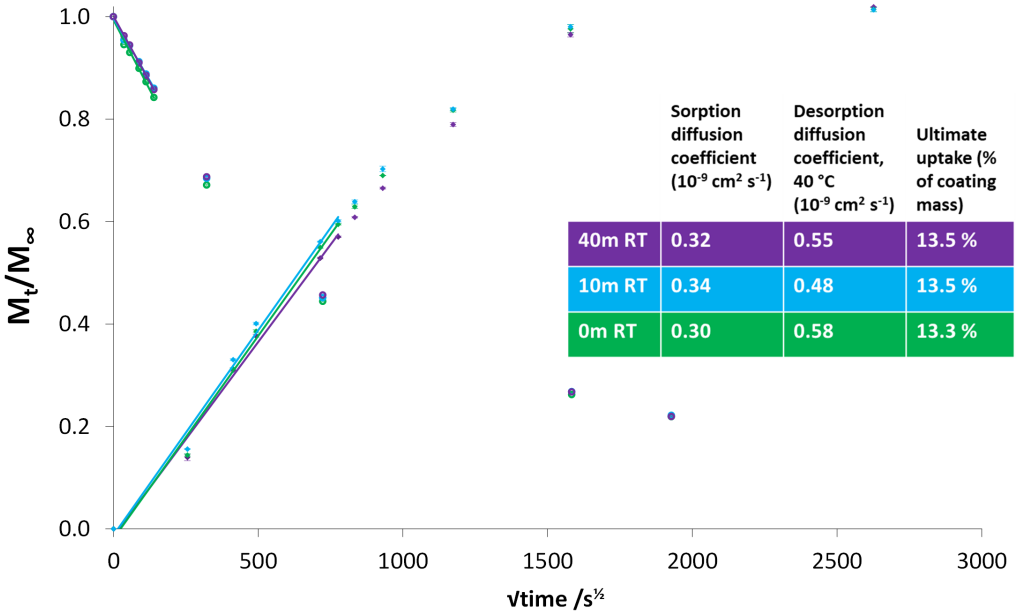

	Sorption diffusion coefficient (10^{-9} cm^2 s^{-1})	Desorption diffusion coefficient, 40 °C (10^{-9} cm^2 s^{-1})	Ultimate uptake (% of coating mass)
40m RT	0.32	0.55	13.5 %
10m RT	0.34	0.48	13.5 %
0m RT	0.30	0.58	13.3 %

(b) Methanol sorption and desorption of DER 354 / MXDA networks on glass slides which were exposed to an air atmosphere at room temperature for varied time periods before cure. Sorption begins at the origin with a positive slope and desorption at $\frac{M_t}{M_\infty} = 1$, with a negative slope. The diffusion coefficients, D, were calculated from the gradient of the initial linear fits (Equation 2.5) and are shown in the inset table. Standard error for all values of the sorption diffusion coefficient was found to be 0.01 10^{-9} cm^2 s^{-1}, and was no higher than 0.03 10^{-9} cm^2 s^{-1} for the desorption diffusion coefficient.

Figure 2.37

2.1.9 Conclusions

The primary influence on chemical performance of a network composed of the same chemistry is the amount of epoxy-amine reaction. This can be affected by the initial ratio of these groups that are combined, as shown by the stoichiometric study, or by unwanted consumption of either reactive group by a third party.

The stoichiometric studies showed that mixing of components in an approximately 1:1 ratio (± 1 %) gives the highest T_g materials and those of the highest chemical performance, when considering ultimate uptake and sorption coefficients. However, the performance changes caused are comparably small until larger (>10 %) variations in stoichiometry are considered. In contrast the atmospheric study showed an unexpected change in chemical performance, when considering the similarity in T_gs obtained—the nitrogen cured samples showed slower sorption of both methanol and ethanol and a greater resistance to failure when exposed to methanol and (even more so) ethanol relative to the air cured samples.

Subsequent atmospheric studies went some way to explaining these findings, showing that both oxidation and carbamation can influence a networks chemical properties in a damaging way. However, the magnitude of the effects observed did not serve to fully explain the step change observed in the two stoichiometric studies in different atmospheres. Carbamation provides a route to consumption of amine. However, it was observed that this is primarily a surface effect, that the carbamated species are found at the surface. As such, carbamation does not disrupt the bulk network structure, and does not damage the chemical performance past that which would occur by formulating with an amine deficiency. Where the oxidation study observed the oxidative processes in already fully cured resin, there are more oxidative processes possible during cure, as there are unreacted epoxy and amine groups present. These processes could be the root of the reduced performance.

This can be further supported by observing the T_g trends found for stoichiometries in the original comparison of cures under different atmospheres. A higher T_g gives an indication of a higher degree of cure.[20] For the nitrogen cured samples, the peak in T_g

comes at 99 and 100 %, whereas for the air cured samples the peak is with an excess of amine (at 101 and 104 %). This (combined with TGA—Figure 2.9a) suggests a consumption of amine groups by another mechanism when curing under an atmosphere of air. Since the networks cured are clear and show little evidence of clouding on the surface, it is likely that this is as a result of oxidative processes rather than that of carbamation. In any case, the changes in performance are attributed to a reduction in the amount of amine-epoxy reaction, as reactive groups are consumed by reaction with atmospheric gases.

Impact on subsequent work

From these findings, for the remainder of this work, all networks will be cured according the optimised conditions established in Section 2.1.1, under nitrogen and at $\sim$100 % stoichiometry, to promote the amine-epoxy reaction as far as possible.

2.2 Methods/Materials

2.2.1 Materials

Dow Epoxy Resin 354 (DER 354) was obtained from the Olin Corporation and used as supplied. It is the reaction product of bisphenol F and epichlorohydrin.

Meta-xylylenediamine (MXDA , 99%) was obtained from Sigma Aldrich Co. LLC., and used as supplied.

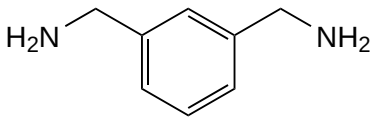

Figure 2.38: meta-Xylylenediamine (MXDA)

2.2.2 Titration for epoxide equivalent weight[21]

Tetraethylammonium bromide (98 %) and glacial acetic acid were obtained from Fisher Scientific and used as supplied. Crystal violet solution (0.5 % solution in glacial acetic acid, >96 %) was obtained from Sigma Aldrich Co. Ltd. and used as supplied. Perchloric acid (0.1 mol l^{-1} solution in acetic acid, 99.5 %) was obtained from VWR International.

Tetraethylammonium bromide (40g, 0.19 mol) was dried for approx. one hour at 100 °C. It was then dissolved with warming in acetic acid (450 cm^3) and allowed to cool. 8 drops of 0.5 % crystal violet solution in acetic acid were added, and the mixture neutralised to an emerald green colour using 0.1 mol dm^{-3} perchloric acid in acetic acid (approx 5 cm^3). Samples of DER 354 (∼0.1 g) were dissolved in this mixture and then titrated with 0.1 mol dm^{-3} perchloric acid in acetic acid to the emerald green end-point. The epoxide equivalent weight (EEW) was then calculated from Equation 2.7

$$EEW(g\ mol^{-1}) = \frac{Sample\ weight\ (g)}{Titre\ (dm^3) \times Concentration\ of\ perchloric\ acid\ (mol\ dm^{-3})} \quad (2.7)$$

Mass DER 354 used /g	Titre /cm^3	EEW /g mol^{-1}
0.1143	6.75	169.3
0.1035	6.13	168.8
0.1296	7.65	169.4

Table 2.2: Quantities used in EEW measurements

2.2.3 Network Preparation

Initial cure temperature optimisation

DER 354 was added to meta-xylylenediamine with an approximately 1:1 stoichiometric ratio of epoxide groups to amine hydrogens, and then mixed using a stirring rod (for quantities see Table 2.3). The resulting mixture was left to react. Following this, the mixture was drawn-down onto glass slides, which were placed in an oven and heated to 120°C or 160 °C. Slides were then removed at time intervals: 30 mins, 60 mins, 90 mins, 120 mins, 180 mins and 300 mins. The T_g of these networks was obtained from the peak in tan δ measured by dynamic mechanical analysis (DMA) (approx 15 mg of sample placed in an aluminium pouch).

Cure Temperature	Mass (amine) /g	Moles (amine) /mol	Mass (epoxy) /g	Moles (epoxy) /mol	Stoichiometry
120	7.082	2.09×10^{-1}	35.440	2.08×10^{-1}	99.3%
160	6.995	2.07×10^{-1}	35.070	2.05×10^{-1}	99.1%

Table 2.3: Quantities used in cures for initial cure temperature optimisation

Optimisation of preparation parameters

A general method is given below. For more details regarding variations to this method see Section 2.1.1.

DER 354 was added to meta-xylylenediamine with an approximately 1:1 stoichiometric ratio of epoxide groups to amine hydrogens, and then mixed using a stirring rod. The resulting mixture was left to react. Following this, the mixture was drawn-down onto

glass slides, which were placed in an oven and heated to 160 °C.

Network preparation for solvent sorption/desorption studies

DER 354 was added to meta-xylylenediamine (for quantities see Table 2.4), and then mixed using a stirring rod. The resulting mixture was left, with occasional mixing, at room temperature, and covered using parafilm. After 3 hours, the mixture was sealed and stored overnight at -20 °C in a freezer. The following morning, whilst sealed (to avoid condensation contaminating the mixture), the vessel was brought to room temperature, and then drawn-down onto prepared glass slides (see section 2.3) using a drawdown cube. The drawdown cube was obtained from Sheen Instruments, with a 400 μm slot. The slides were then placed in an oven and cured under the desired atmosphere (see Table 1). For a nitrogen (N_2) atmosphere, oxygen free nitrogen, obtained from BOC, was purged through the oven at $\sim$5 cm^3 min^{-1}. The cure schedule was an initial temperature of 60 °C, with a ramp of 1 °C min^{-1} to 160 °C, where the oven was held for three hours. Upon completion of the three hours, the samples were removed from the oven and allowed to cool. Any samples not immediately analysed were placed in a desiccator over phosphorus pentoxide to prevent moisture uptake.

2.2.4 Near-infrared (NIR) spectroscopy

NIR spectroscopy was performed on an Ocean Optics NIRQuest 2500. Spectra were sampled using an integration time of 10ms, and taking 100 scans to average. Sample cells were prepared by the use of a PTFE spacer between glass slides, which were fastened together using a small amount of epoxy resin.

For the molar extinction coefficient determination with varied path length, different thicknesses (approx. 0.55 mm, 0.6 mm, 0.8 mm, 0.85 mm) of PTFE were used to make the cells.

For degree of cure measurements, cells with a path length of 0.55-0.6 mm were used, and cure completed in a heated cell, using the same cure schedule as that described as the above section. Spectra were obtained throughout cure.

Mass (DER 354)	Mass (MXDA)	Stoichiometry (% amine)	Atmosphere
11.672	2.223	94.6%	N_2
27.780	5.443	97.4%	N_2
28.878	5.764	99.2%	N_2
11.289	2.299	101.2%	N_2
7.983	1.678	104.5%	N_2
11.454	2.173	94.3%	Air
11.471	2.244	97.2%	Air
10.08	2.013	99.2%	Air
11.609	2.366	101.3%	Air
8.601	1.804	104.2%	Air

Table 2.4: Cure conditions used in network preparation

2.2.5 Glass slide preparation

Hydrogen peroxide was added with care and gentle stirring to sulfuric acid in a 1:3 ratio to produce "piranha solution". Slides (as supplied) were placed in the "piranha solution" and left for 15 minutes before rinsing thoroughly with deionised water. The treated slides were placed in a rack and dried at 50 °C in an oven, and stored there until use.

2.2.6 Thermogravimetric analysis (TGA)

Thermogravimetric analysis was performed on a PerkinElmer Pyris 1. Samples of 5 $\pm$ 3 mg were placed in a crucible and then heated under an atmosphere of nitrogen or air, while the mass was recorded.

2.2.7 Dynamic mechanical analysis (DMA)

Dynamic mechanical analysis was performed on a PerkinElmer DMA8000, using single cantilever mode where the dynamic response to a sinusoidal force applied at a frequency of 1 s^{-1} recorded. For basic glass transition temperature (T_g) measurements, samples

were prepared in aluminium pouches and measured. The T_g was taken as the peak in the tan δ trace, from a Lorentzian fit of the peak using OriginLab 2017. For crosslink density, three beams were prepared for each sample, approximately 10 mm wide and 1.6 mm thick and measured.

Crosslink density can then be calculated from Equation 2.8.

$$\nu = \frac{E}{3RT} \tag{2.8}$$

Crosslink density, ν, where E is the storage modulus at T_g + 40 K, R is 8.314 J mol^{-1} K^{-1} and T is the temperature in K

2.2.8 Differential scanning calorimetry (DSC)

DSC measurements were made on a PerkinElmer DSC 8500, and analysis performed on Pyris DSC software. Samples of 15 $\pm$ 5 mg were weighed into a aluminium pan and then measurements taken using the calorimeter.

2.2.9 Helium pycnometry

Helium pycnometry was performed on a Micrometrics AccuPyc 1330, using approximately 0.4 g of sample in a sample cell of 1 cm^3 and a standard of known mass and volume for calibration.

2.2.10 Solvent sorption/desorption

Coated glass slides were placed in solvent and weighed at time intervals, ranging from 2 hours to 65 weeks (See Table 2.5). Intervals between measurements were increased as time increased due to the slowing of mass uptake. Upon reaching a plateau in mass, these samples were removed from solvent and placed in an oven at 40 °C, and weighed at time intervals, until a reasonable plateau was obtained. No plateau was achieved for ethanol immersed slides, and therefore no cycling was performed. In order to repeat the sorption and desorption process, samples were placed in a vacuum oven above their

T_g (approx. 130 °C) under vacuum, and left until a stable mass, approximate to their original mass was obtained. The process was then repeated.

No. in series	Time (days) - Methanol uptake	Time (days) - Ethanol uptake
0	0	0
1	0.25	3
2	1	20
3	2	39
4	4	63
5	7	90
6	11	120
7	17	160
8	25	200
9	36	260
10	50	320
11	86	400

Table 2.5: Example weighing schedule for methanol and ethanol sorption

2.2.11 Oxidation experiment

DER 354 (19.025 g, 0.112 mol) was added to meta-xylylenediamine (3.828 g 0.112 mol), and then mixed using a stirring rod. The resulting mixture was left, with occasional mixing, at room temperature, and covered using parafilm. After 3 hours, the mixture was sealed and stored overnight at -20 °C in a freezer. The following morning, whilst sealed (to avoid condensation contaminating the mixture), the vessel was brought to room temperature, and then drawn-down onto prepared glass slides (see section 2.2.5) using a drawdown cube. The drawdown cube was obtained from Sheen Instruments, with a 400 μm slot. The slides were then placed in an oven and cured. Oxygen free nitrogen, obtained from BOC, was purged through the oven at $\sim$5 cm^3 min^{-1}. The cure schedule was an initial temperature of 60 °C, with a ramp of 1 °C min^{-1} to 160 °C, where the oven was held for three hours. Upon completion of the three hours, the samples were

removed from the oven and allowed to cool. Any samples not immediately analysed were placed in a desiccator over phosphorus pentoxide to prevent moisture uptake. Further treatment of these slides was completed by placing in an oven held at 160 °C for 3 hours under varying atmosphere. The first of three groups was held under an atmosphere of N_2 for all 3 hours, the second an atmosphere of air for 3 hours and the final group, an atmosphere of air for 1.5 hours, followed by an atmosphere of air for 1.5 hours. This is laid out schematically in Figure 2.35a in Section 2.1.8.

2.2.12 Carbamation experiment

DER 354 (22.230 g, 0.131 mol) was added to meta-xylylenediamine (4.474 g 0.131 mol), and then mixed using a stirring rod. The resulting mixture was left, with occasional mixing, at room temperature, and covered using parafilm. After 2 hours 20 minutes, the mixture was sealed and stored overnight at -20 °C in a freezer. The following morning, whilst sealed (to avoid condensation contaminating the mixture), the vessel was brought to room temperature, and then drawn-down onto prepared glass slides (see section 2.3) using a drawdown cube. The drawdown cube was obtained from Sheen Instruments, with a 400 μm slot. The slides were assigned to one of three groups. For the first of these groups, the drawdown was performed as soon as the mixture was returned to room temperature. The second was drawn down 30 minutes later and the final group a further 10 minutes later, at which point all slides were placed in an oven and cured. This means the three groups of networks were exposed to atmospheric conditions for 40, 10 and 0 minutes. Oxygen free nitrogen, obtained from BOC, was purged through the oven at $\sim$5 cm^3 min^{-1}. The cure schedule was an initial temperature of 60 °C, with a ramp of 1 °C min^{-1} to 160 °C, where the oven was held for three hours. Upon completion of the three hours, the samples were removed from the oven and allowed to cool. Any samples not immediately analysed were placed in a desiccator over phosphorus pentoxide to prevent moisture uptake.

References

[1] Vanlandingham, M. R., Eduljee, R. F. & Gillespie Jr., J. W. Relationships between stoichiometry, microstructure, and properties for amine-cured epoxies. *Journal of Applied Polymer Science*, **71**(5), 699–712 (1999).

[2] Frank, K., Childers, C., Dutta, D., Gidley, D., Jackson, M., Ward, S., Maskell, R. & Wiggins, J. Fluid uptake behavior of multifunctional epoxy blends. *Polymer*, **54**(1), 403–410 (2013).

[3] Celina, M. C., Dayile, A. R. & Quintana, A. A perspective on the inherent oxidation sensitivity of epoxy materials. *Polymer*, **54**(13), 3290–3296 (2013).

[4] Mailhot, B., Morlat-Thérias, S., Ouahioune, M. & Gardette, J.-L. Study of the degradation of an epoxy/amine resin, 1. *Macromolecular Chemistry and Physics*, **206**(5), 575–584 (2005).

[5] Seu, K. J., Pandey, A. P., Haque, F., Proctor, E. A., Ribbe, A. E. & Hovis, J. S. Effect of surface treatment on diffusion and domain formation in supported lipid bilayers. *Biophysical Journal*, **92**(7), 2445–2450 (2007).

[6] Sahagun, C. M., Knauer, K. M. & Morgan, S. E. Molecular network development and evolution of nanoscale morphology in an epoxy-amine thermoset polymer. *Journal of Applied Polymer Science*, **126**(4), 1394–1405 (2012).

[7] Poisson, N., Lachenal, G. & Sautereau, H. Near- and mid-infrared spectroscopy studies of an epoxy reactive system. *Vibrational Spectroscopy*, **12**(2), 237–247 (1996).

[8] Jackson, M., Kaushik, M., Nazarenko, S., Ward, S., Maskell, R. & Wiggins, J. Effect of free volume hole-size on fluid ingress of glassy epoxy networks. *Polymer*, **52**(20), 4528–4535 (2011).

[9] Meier, R. J. On art and science in curve-fitting vibrational spectra. *Vibrational Spectroscopy*, **39**(2), 266–269 (2005).

[10] Min, B.-G., Stachurski, Z., Hodgkin, J. & Heath, G. Quantitative analysis of the cure reaction of DGEBA/DDS epoxy resins without and with thermoplastic polysulfone modifier using near infra-red spectroscopy. *Polymer*, **34**(17), 3620–3627 (1993).

[11] Mijovic, J. & Andjelic, S. A study of reaction kinetics by near-infrared spectroscopy. 1. Comprehensive analysis of a model epoxy/amine system. *Macromolecules*, **28**(8), 2787–2796 (1995).

[12] Sahagun, C. M. & Morgan, S. E. Thermal control of nanostructure and molecular network development in epoxy-amine thermosets. *ACS Applied Materials & Interfaces*, **4**(2), 564–572 (2012).

[13] Frank, K. & Wiggins, J. Effect of stoichiometry and cure prescription on fluid ingress in epoxy networks. *Journal of Applied Polymer Science*, **130**(1), 264–276 (2013).

[14] Gupta, V. & Brahatheeswaran, C. Molecular packing and free volume in crosslinked epoxy networks. *Polymer*, **32**(10), 1875–1884 (1991).

[15] Pethrick, R. A., Hollins, E. A., McEwan, I., Pollock, E. A., Hayward, D. & Johncock, P. Effect of cure temperature on the structure and water absorption of epoxy/amine thermosets. *Polymer International*, **39**(4), 275–288 (1996).

[16] Morsch, S., Lyon, S., Greensmith, P., Smith, S. & Gibbon, S. Water transport in an epoxy–phenolic coating. *Progress in Organic Coatings*, **78**, 293–299 (2015).

[17] Shen, C.-H. & Springer, G. S. Moisture Absorption and Desorption of Composite Materials. *Journal of Composite Materials*, **10**, 2 (1976).

[18] Rossi, G., Pincus, P. A. & de Gennes, P.-G. A Phenomenological Description of Case-II Diffusion in Polymeric Materials. *Europhysics Letters (EPL)*, **32**(5), 391–396 (1995).

[19] Friedman, A. & Rossi, G. Phenomenological Continuum Equations To Describe Case II Diffusion in Polymeric Materials. *Macromolecules*, **30**(1), 153–154 (1997).

[20] Pascault, J. P., Sautereau, H., Verdu, J. & Williams, R. J. J. *Thermosetting Polymers*. Plastics engineering. Taylor & Francis, New York (2002). ISBN 9780203908402.

[21] Cameron, C. Private communication. *AkzoNobel* (2014).

Chapter 3

Variation of epoxy resin and amine monomers using commercially available materials

3.1 Results and Discussion

Overview

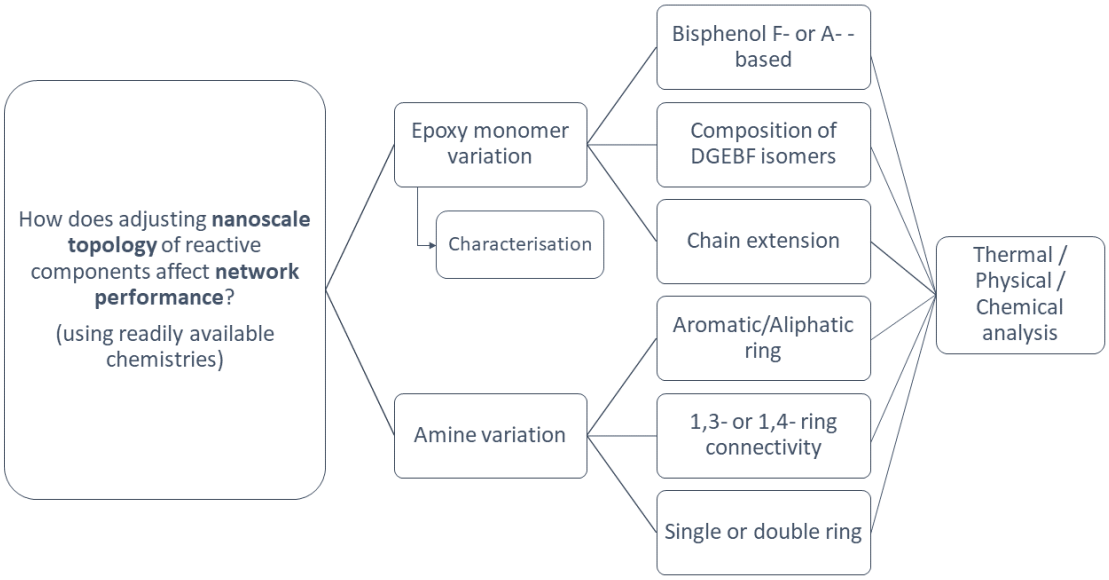

There is a wide range of epoxy resin monomers and amines readily available to formulators. In the context of this study, subtle changes are of greatest interest, in order to isolate the root cause of changes in performance, especially in cases where solubility differences are negligible. Since the basis of the initial work is a network made from Dow Epoxy Resin 354 (DER 354) and meta-xylylenediamine (MXDA), candidates for variation were selected based on their similarity to these monomers. Figure 3.1 shows the structures of the amines and the base structures of the epoxy monomers. Key points of interest are the nature of bonding and distance between crosslinks; i.e. whether six membered rings are aromatic or aliphatic, the connectivity of such rings and the role that introducing a second ring might play. Further, as has been described in Section 1.1.5, there is a great diversity in the chemical species present in an industrially produced epoxy resin. Some aspects of this diversity will be investigated here with the use of four different industrial bisphenol based resins. The more striking difference between diglycidyl ether of bisphenol F (DGEBF) and diglycidyl ether of bisphenol A (DGEBA) based resins will be considered, as well as the introduction of a second DGEBF based mixture and the use of a purer DGEBA resin (with very limited chain extension).

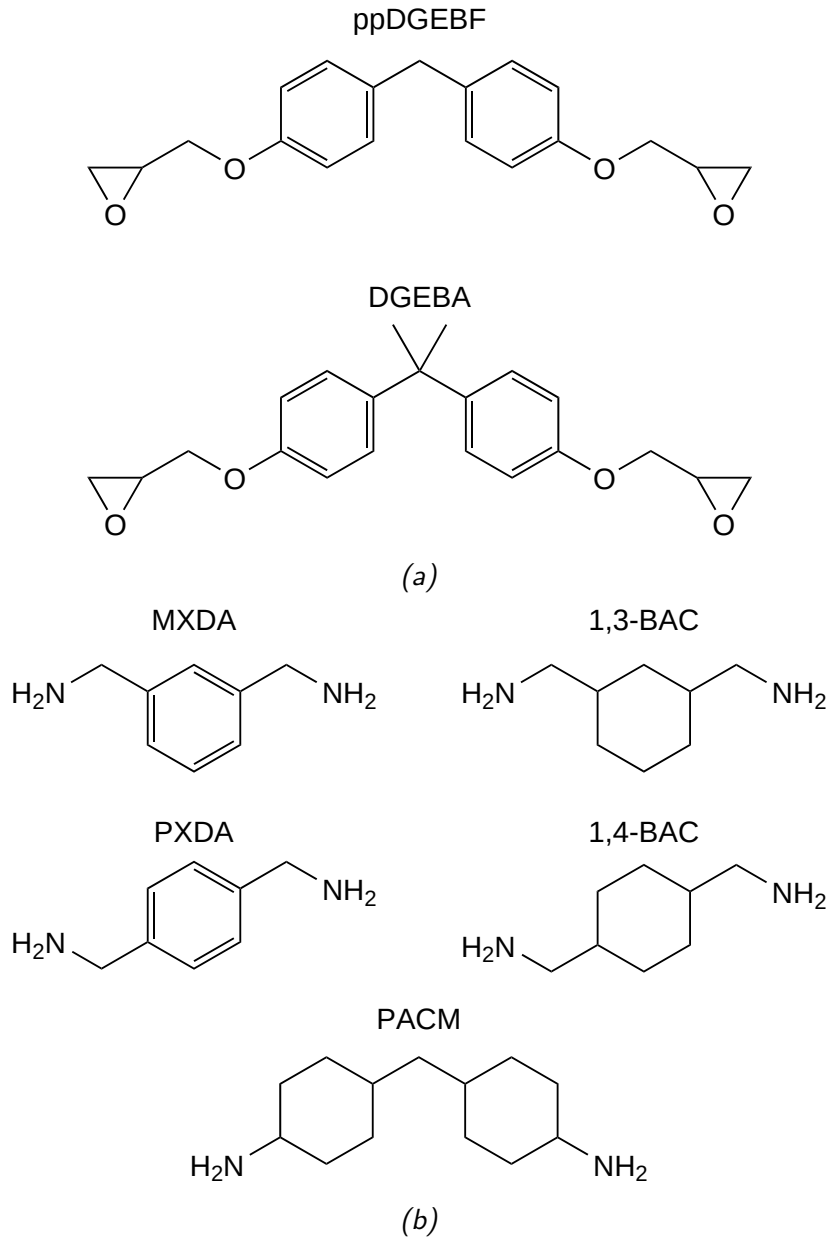

Figure 3.1: (a) Base structures of epoxy resin monomers and (b) the structures of amine monomers used in this chapter— Key: **ppDGEBF**- *para-para-diglycidyl ether of bisphenol F;* **DGEBA**- *diglycidyl ether of bisphenol A;* **MXDA**- *meta-xylylenediamine;* **1,3-BAC**- *1,3-bis(aminomethyl)cyclohexane,* **PXDA**- *para-xylylenediamine;* **1,4-BAC**- *1,4-bis(aminomethyl)cyclohexane;* **PACM**- *bis(para-aminocyclohexyl) methane.*

3.1.1 Chemistry of DGEBF based epoxy resins

There are many chemical species contained within an industrially available diglycidyl ether of bisphenol F (DGEBF) based epoxy resin. The two primary complications when considering the chemical composition are (a) regioisomerism around the phenyl rings (Figure 3.2a) and (b) chain extension to incorporate two or more bisphenol units into a single molecule, resulting in a higher molecular weight (MW) (Figure 3.2b).

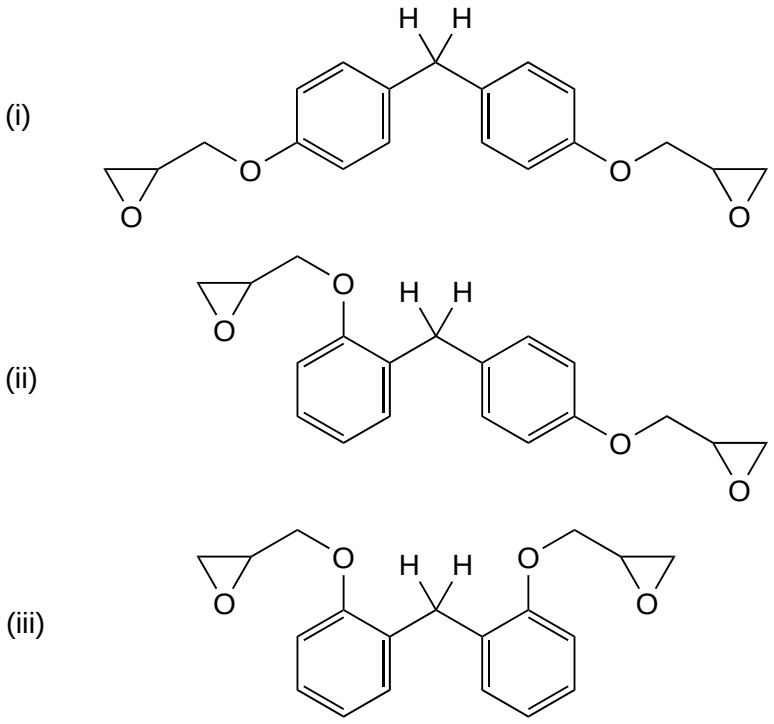

(a) The three isomers of DGEBF, (i) para-para (pp), (ii) para-ortho (po), (iii) ortho-ortho (oo). The methylene protons on the bridging carbon are explicitly shown. These have different NMR environments and so can be used to find the ratio of the isomers in any mixtures.

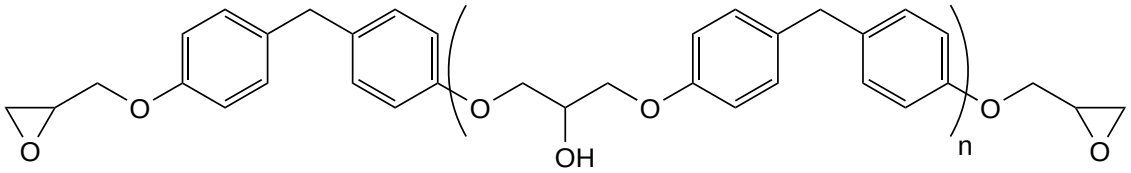

(b) The structure of "chain extended" isomers when only considering para- substitution in DGEBF.

Figure 3.2: Sources of chemical variability in DGEBF based epoxy resins

^{1}H nuclear magnetic resonance (NMR) spectroscopy can be used to calculate the ratio of the pp, po and oo isomers (para-para-, para-ortho- and ortho-ortho—see Figure 3.2a) of DGEBF, using the ratio of the peaks of the bridging methylene protons. DER 354 contains these isomers in a 3.5 : 3.0 : 1 ratio respectively (47 % : 40 % : 13 %). In d-

chloroform, this determination is not possible, as there is significant overlap between the diglycidyl ether signals and the methylene protons. However, using deuterated benzene as the solvent resolves this problem because of the aromatic solvent induced shift, as described by Domke.[1] It is worth noting that this method gives the overall ratio of the isomers across the material, not the ratio of any single molecules - this is as a result of the second complication - chain extension.

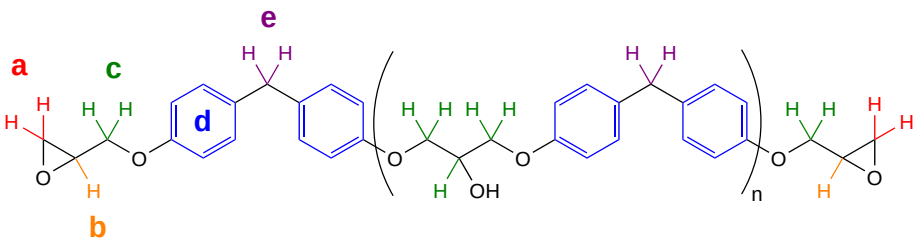

(a) The structure of DGEBF with generalised proton environments

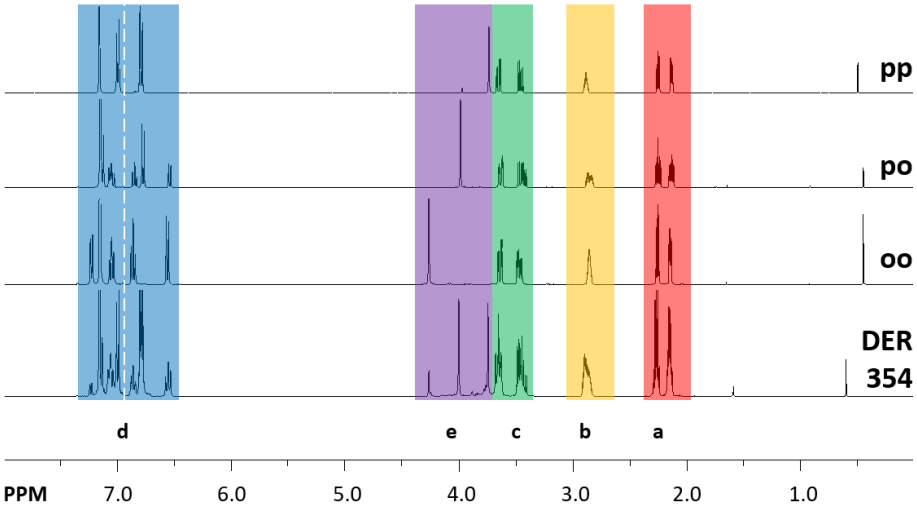

(b) ^{1}H NMR spectra of DER 354 and of the three n = 0 component isomers (para-para-, para-ortho- and ortho-ortho). The isomers exhibit a different signal for the bridging methylene protons, environment e (purple), oo at the highest ppm, then po and finally pp. The epoxide equivalent weight can be calculated using the integrated ratio of the right hand portion of environment 'd' (blue) and environments a and b. (yellow/red)

Figure 3.3

Chain extension is evident in the ^{1}H NMR spectrum—it can be seen in the distinct absence of ideality in peak integration of the different proton environments - seen most clearly by a comparison of the aromatic peaks around 7 ppm and the epoxide multiplet around 3 ppm. It is also shown in titrations to find the epoxide content of the material—quantified in the epoxide equivalent weight (EEW). This gives the relative quantity of

epoxide groups in a certain mass of compound - a direct measure of the reactivity of the resin. Assuming that each molecule in the system contains two epoxide groups, this can be used to calculate a degree of extension—giving an average value for n. For DER 354, the epoxide equivalent weight was found to be 169.2 g mol^{-1} by titration (for method see Section 3.2.2). Using the molecular weights of the "n" segment (that is, the portion within the brackets in Figure 3.2b) and the n = 0 isomer (as shown in Equation 3.1), n was found to be 0.11 for DER 354.

$$n = \frac{(f \times EEW) - MW_{n=0}}{MW_{n\ segment}} \tag{3.1}$$

*Equation used to find the average degree of extension (**n**) from the epoxide equivalent weight (**EEW**) and functionality (**f**) of a given resin, and the molecular weights of the n = 0 molecule ($\mathbf{MW_{n=0}}$) and the n segment of that resin ($\mathbf{MW_{n\ segment}}$)*

^{1}H NMR spectroscopy can also be used to calculate the epoxide equivalent weight for an epoxy, as shown by Garcia and Soares.[2] They compare the ratio of all aromatic protons to those in the epoxide bond and from this the EEW can be derived. Some adjustment to their method was required due to the use of a DGEBF based resin, which led to a change in solvent to deuterated benzene. This peak sufficiently disrupts the aromatic peaks that it is no longer possible to integrate for all aromatic peaks. Therefore, the right-hand side of the aromatic signals (as shown by the white line in Figure 3.3b) was used in this study since there is no disruption from outside influences and it corresponds to exactly half of the aromatic signal in each isomer. The EEW found by this method was 169.0 g mol^{-1}, very similar to that obtained by titration.

High performance liquid chromatography of DER 354

High performance liquid chromatography (HPLC) has been shown to achieve isomer separation for DGEBF.[3] Using analytical-HPLC, separation was demonstrated with an acetonitrile/water solvent system. The order of elution is governed by the distribution between retention by the stationary phase and solubility in the mobile phase.[4] A reverse-phase column was used and hence in terms of polarity, more polar substances elute first.

The size of molecules also influences the retention, and lower molecular weight molecules will elute faster.

This is observed in the chromatogram (Figure 3.4) which shows a good resolution of the peaks relating to the three isomers which elute as pp- first, followed by po- and then oo- DGEBF (11.5, 13 and 14.3 mins respectively). At a faster elution time (approx. 5 mins), the peaks for the three isomers of bisphenol F are identifiable by their similarity in distribution as the longer isomers. These elute faster as a result of their hydroxyl groups and lower MW. In order to elute the higher MW components, the solvent system was moved to pure acetonitrile, and they are seen in the broader, multicomponent peak at 23-26 minutes. The complexity of this peak in terms of individual signals displays the increased molecular diversity in longer chains. Addition of one bisphenol unit to another is not limited to those of the same regioisomer, hence a pp isomer can bind to another pp isomer, or either of the other isomers. For the po isomer, addition can be to either end, introducing still more diversity. Hence, there are 9 possible n = 1 isomers and as n increases, the possibilities increase combinatorially.

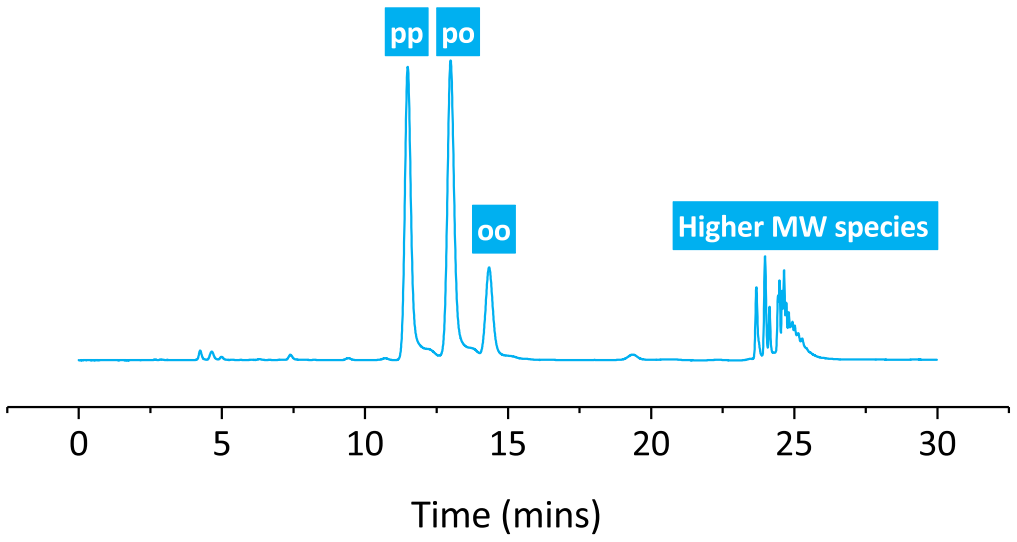

Figure 3.4: The HPLC chromatogram for DER 354 using an 50:50 acetonitrile:water isocratic solvent system. The major peaks are labelled with the responsible component of a DGEBF based mixture.

The ratio of the three peaks relating to the n = 0 isomers gives a route to the direct determination of the ratio of those isomers. When integrated to give the area, the ratio

was found to be 40 % : 45 % : 15 % (pp : po : oo). This shows a difference to the determination of the overall ratio by ^{1}H NMR which found the ratio to be 47 % : 40 % : 13 %. A possible explanation for this might be that the para-para moiety is found more commonly in the chain extended isomers, whereas it is not the dominant structure in the lowest molecular weight structures. A hypothesis for this is that the steric hindrance experienced by ortho- moieties in the chain extension reactions causes a higher prevalence of the pp- isomer. However, there remains the possibility that other impurities contaminate the peak found at 3.7 ppm in the ^{1}H NMR spectrum, corresponding to the methylene signal in ppDGEBF, leading to a higher integration.

It is reasonable to assume that the absorption of the 280 nm light would be very similar between the regioisomers and therefore using the relative peak areas as a judge of abundance is reasonable. However, since the structures of the higher MW species are different, especially in terms of the amount of aromatic rings, comparing the area of the peak at 23-26 mins to the n = 0 isomer peaks is not justifiable.

Comparison of epoxy monomers

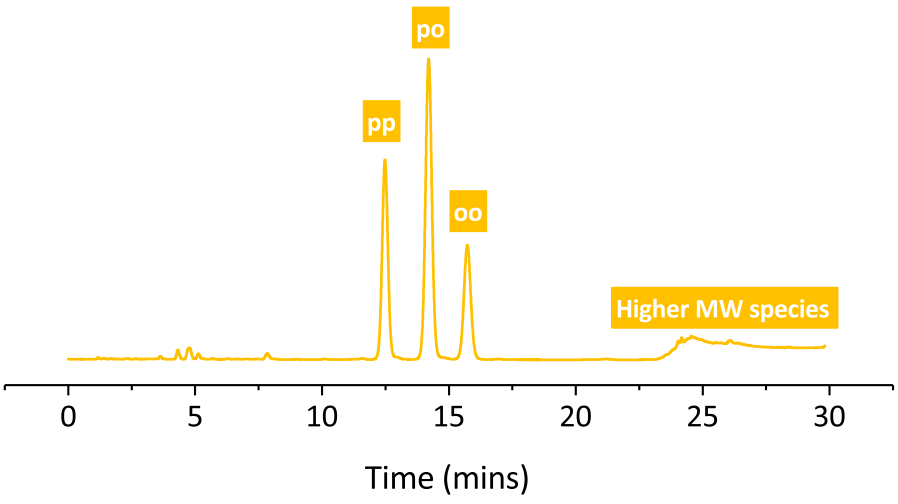

Figure 3.5: HPLC chromatogram for PY306 using an 50:50 acetonitrile:water isocratic solvent system. The major peaks are labelled with the responsible component of a DGEBF based mixture.

DGEBF based networks Comparing the HPLC chromatograms and ^{1}H NMR spectra of DER 354 and Araldite PY306 (PY306) shows there is a higher proportion of ortho- substitution in the PY306—both as po- and oo- isomers. When using ^{1}H NMR spectroscopy, the pp : po : oo ratio was 36 % : 49 % : 14 %. From HPLC, as with DER 354, an increased proportion of ortho- substitution is observed, at 30 % : 50 % : 20 % (Figure 3.5). Further, there is a slight reduction in the n value (vs. DER 354), whether obtained from titration (0.08), or ^{1}H NMR spectroscopy (0.07) This reduction is shown in the HPLC also—further there is a blurring of the signal, the cause of which is unknown.

DGEBF based networks The two resins based on diglycidyl ether of bisphenol A (DGEBA) used in this study are Epikote 828 (E828) and Dow Epoxy Resin 332 (DER 332) There is no regioisomerism in DGEBA, as the two methyl groups prevent ortho-substitution.[5] n was determined to be 0.13 for E828 by titration—slightly larger than both DER 354 and PY306. In contrast, DER 332 is by and large one molecule with very limited chain extension, as n = 0.02 by EEW titration. The HPLC chromatograms shown in Figure 3.6 illustrate the relative compositions—where DER 332 only shows one major peak, there are multiple peaks to the right of the main peak for E828 illustrating the presence of higher MW structures. Both traces indicate the absence of regioisomerism.

3.1.2 Network preparation

A range of networks were produced while varying either amine or epoxy monomer. In all cases, the formulations were stoichiometric. When varying epoxy monomer, the amine used was MXDA and the epoxy varied between DER 354, PY306, E828 and DER 332. Where the amine was varied, DER 354 was used as the epoxy. The amines used were MXDA, PXDA, 1,3-BAC, 1,4-BAC and PACM.

The optimised preparation method from Section 2.1.1 was used as the basis for cures, with some small variations. The same cure schedule was used for all cures, though pot-time was adjusted to account for the varied reactivity of the components used. Further,

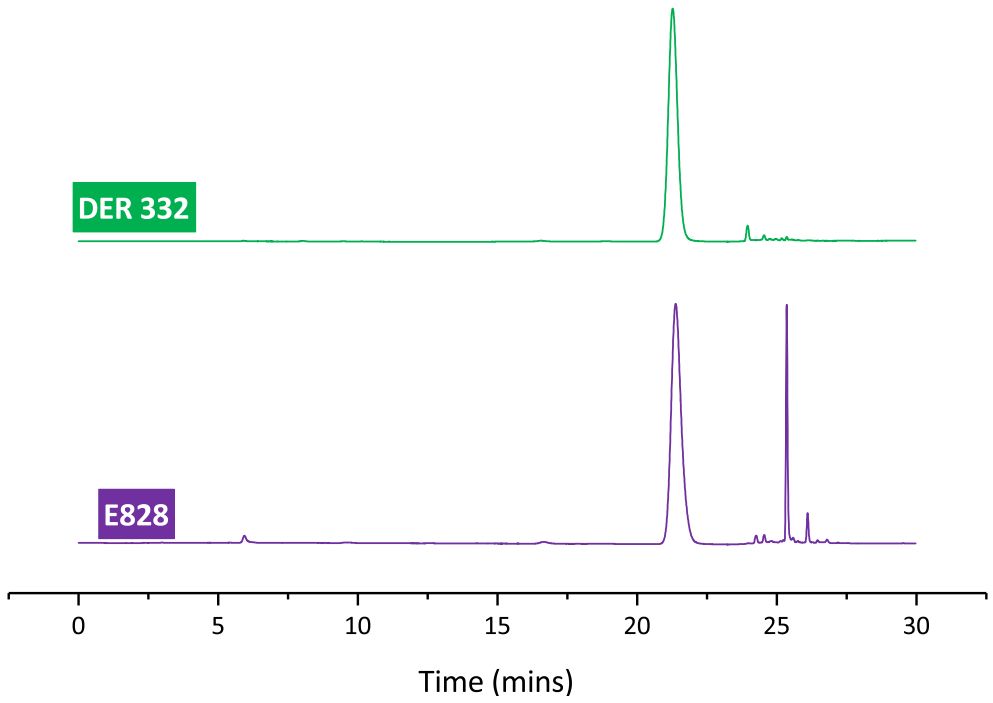

Figure 3.6: HPLC chromatograms for Epikote 828 (E828) and Dow Epoxy Resin 332 (DER 332) using an 50:50 acetonitrile:water isocratic solvent system. The absence of high MW components of DER 332 is illustrated by the presence of a single main peak, compared to the multiple peaks observed for E828

PXDA is a solid at room temperature, and so a new method had to be developed to successfully produce coatings.

Epoxy monomer variation

The maximum amount of time that can be allowed before application (pot-time) is related to the viscosity. Where the viscosity becomes too high, the mixture can no longer be applied effectively. Since E828 and DER 332 are more viscous, they reach this point sooner than the DGEBF based networks and thus a shorter pot-time is required, though the variation is limited.

Amine variation

The pot-time varied substantially more across the range of amines. The amines with aliphatic rings were more reactive than the aromatic analogues and as such reached the limit of their usability at shorter times. Further, as mentioned earlier, PXDA is a

solid at room temperature (m.p. 60-64 °C), and as such required different treatment. This primarily consisted of initial melting of the PXDA, rapid addition and mixing of warm DER 354, achieved by adding approximately 75 % of the resin and mixing before accurately weighing the final portion of resin. Further, an elevated pot temperature of 30 °C was used to prevent recrystallisation of PXDA. This lead to a much reduced pot time of 1 hour.

Further, a heated drawdown block was designed in order to hold the slides at an elevated temperature, to prevent recrystallisation upon drawdown—it is shown in Figure 3.7. The heating is controlled by a temperature controller, using thermocouples and cartridge heaters, and a groove for slides, with a removal bar for easy manipulation.

(a) *(b)*

Figure 3.7: Heated aluminium drawdown block. (a) shows the top, which has a groove to hold slides in place and a bar to enable easy removal of slides. (b) shows the back, with cartridge heaters supplying heat (grey wires) and thermocouples to monitor temperature (green wires).

NIR spectroscopy

Since in the NIR spectroscopy method it is only the epoxide peak that is considered, no new extinction coefficients need to be calculated, since the local chemical environment of the epoxide is identical in all of the epoxides used, with the chemical structure as whole only adjusted very slightly. The conversions for all networks produced were in excess of 99 % and are shown in Table 3.1

Epoxy	Amine	Final Conversion
DER 354	MXDA	100.0 %
PY306	MXDA	99.8 %
E828	MXDA	100.0 %
DER 332	MXDA	100.0 %
DER 354	PXDA	99.6 %
DER 354	1,3-BAC	100.0 %
DER 354	1,4-BAC	99.8 %

Table 3.1: The epoxide conversion obtained for each network prepared by NIR spectroscopy

3.1.3 Properties and performance—epoxy monomer variation

The chemical structure and composition of the epoxy monomers used in this study are described in Section 3.1.1. The key variations are (i) the chemical structure in terms of bisphenol used, (ii) the regioisomeric composition of DGEBF based resins and (iii) the effect of chain extension in DGEBA based resins. All were cured using MXDA as the hardener.

Thermal and physical properties

DGEBF based networks The DER 354 / MXDA sample showed a higher glass transition temperature (T_g) than the PY306 / MXDA (Figure 3.8). Further, it also exhibited a higher beta transition temperature (T_β). The crosslink density of the PY306 sample was found to be 1421 $\pm$ 72 mol m^{-3}, again lower than that for DER 354 (1632 $\pm$ 118 mol m^{-3}). Finally, a very small reduction in bulk density is observed for the PY306 sample.

The two differences between the chemistries is the relative isomer content and the slight reduction in chain extension for the PY306. A reduction in chain extension would be expected to yield a higher crosslink density and a higher value for T_g. Therefore, the reduction in these properties is attributed to the increased ortho- substitution in the bisphenol rings, as is contributed by the increase of both po and oo isomers relative

to pp. The change in T_β is suggestive that the ortho- moiety influences the smallscale molecular motion within the polymer, which may influence solvent uptake properties. A reduction in T_β indicates that the responsible molecular motion has a smaller energetic barrier.

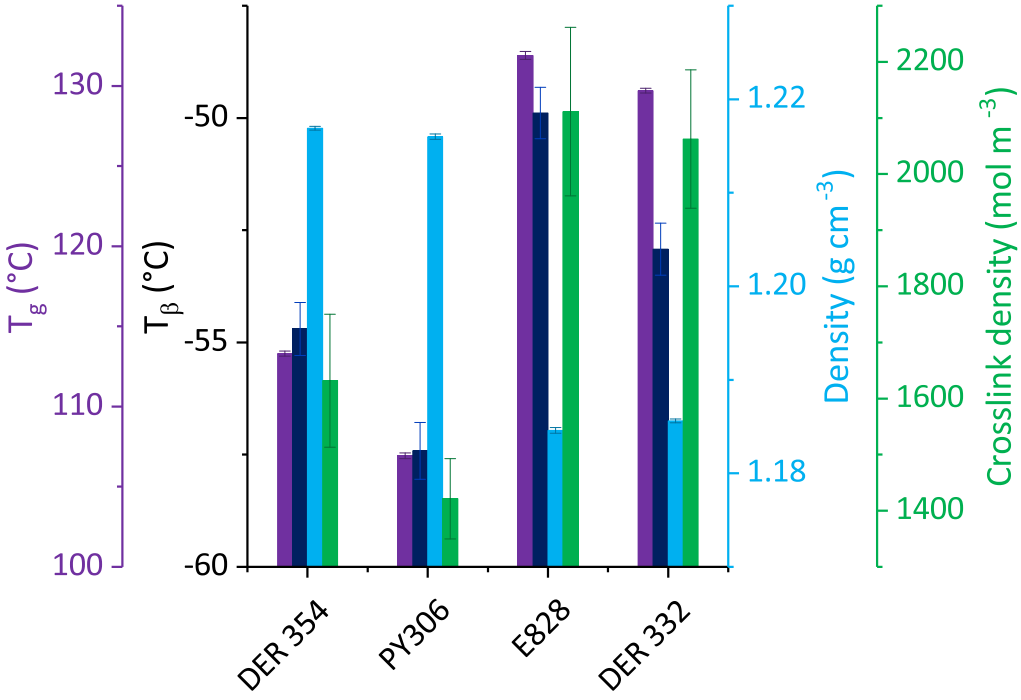

Figure 3.8: The T_g, T_β, crosslink density (all as found by DMA) and density (as found by helium pycnometry) of networks prepared with varied epoxy resin monomers (cured with MXDA). Error bars show standard error of three measurements for the values obtained by DMA, and standard deviation of ten measurements of a single sample for density.

DGEBA based networks The DGEBA based networks showed very similar T_gs, at 131 °C for E828 / MXDA and 130 °C for DER 332 / MXDA (Figure 3.8)). This shows that the degree of chain extension has a minimal impact upon T_g, which also supports the above argument that the T_g difference observed between PY306 and DER 354 is as a result of the relative isomer concentrations. The crosslink densities obtained for both DGEBA based networks were within error of one another (for the E828: 2111.2 $\pm$ 150.1 mol m^{-3}; for the DER 332: 2062.4 $\pm$ 123.3 mol m^{-3}) The densities of both networks were found to be similar, with a slightly higher value observed for DER 332, showing the anticipated densification of a network with an average shorter distance between

crosslinks, though only slightly. The T_β was found to be lower for the DER 332, than the E828, suggesting the chain extended isomers have more complex molecular motions which require more energy to mobilise. Further, the peak area of the β-transition is larger for the 828, with additional peak components present on the high temperature side of the peak. This suggests there is greater motion present at ambient temperatures for the E828.

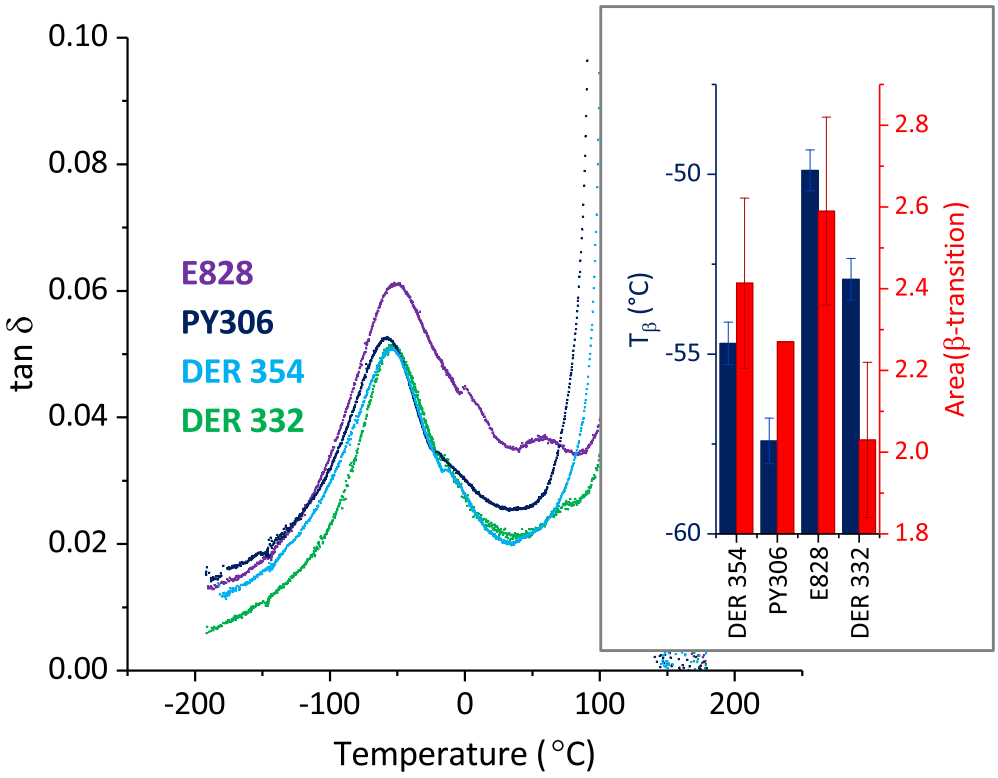

Figure 3.9: DMA traces of tan δ against temperature for networks prepared with varied epoxy resin monomer (cured with MXDA), showing the response for the β-transition. Inset: The T_β and area of the β-transition for those networks. Error bars show standard error of two samples

Comparison of DGEBA and DGEBF based networks There are clear differences between the two resin types—DGEBA based networks have a higher T_g & T_β, higher crosslink density but a lower density. The most notable differences in chemical structure are the methyl groups on the bridging carbon in the bisphenol unit, and the presence of a mixture of regioisomers for DGEBF. In order to deconvolute the factors, an isomerically pure DGEBF is needed, and the comparison will be discussed in Section 6.2.2.

Methanol uptake

DGEBF based networks The methanol sorption is shown in Figure 3.10a. DER 354 / MXDA is both the lowest and slowest absorbing material. Surprisingly, the performance of the other DGEBF based network, PY306 / MXDA, is substantially different, in spite of broadly similar chemistries. It has a much higher sorption diffusion coefficient (D_{sor}) and a higher ultimate uptake. The T_g of the PY306 (106 °C) is suggestive of a less well packed network relative to the DER 354, considering the similar chemistry. As previously referred to, the two DGEBF based resins show a different proportion of ortho- substitution (higher in PY306). These data show that changing the proportion of the DGEBF isomers can have a substantial impact upon the chemical performance of a network—as it did for the thermal and physical properties discussed above. Whether this results from the increased diversity in constituent chains or is directly linked to the nature of the ortho- moieties is uncertain, though the observed change in T_β is suggestive of the latter, as the β transition is generally attributed to local cooperative motions (e.g. motion of individual phenylene rings).[6] It is certainly cause for further investigation using greater chemical control—this is explored in Chapter 5.

DGEBA based networks E828 / MXDA shows increases in D_{sor} and ultimate uptake relative to both DGEBF based networks, in spite of a substantially higher T_g and a higher crosslink density (Figure 3.10). Density measurements provide the likely cause of the large reduction in chemical performance. Where the DGEBF based networks have a density of 1.22 g cm^{-3}, the E828 has a lower density of 1.1846 g cm^{-3}. The results for DER 332 / MXDA ow the impact that removing chain extended isomers has upon the chemical performance. D_{sor} for DER 332 is much reduced relative to E828, and there is a smaller reduction for D_{des}. Ultimate uptake is also lower than for the E828.

The shorter time period used to find the initial gradient of the E828 sample was used because of the different sorption mode of uptake found for it. This mode change is illustrated in Figure 3.11. The deviation observed at $\frac{M_t}{M_\infty} \approx 0.5$ shows the diffusion mode to be two-step (see Section 1.1.4)—whilst similar to the sigmoidal mode, instead

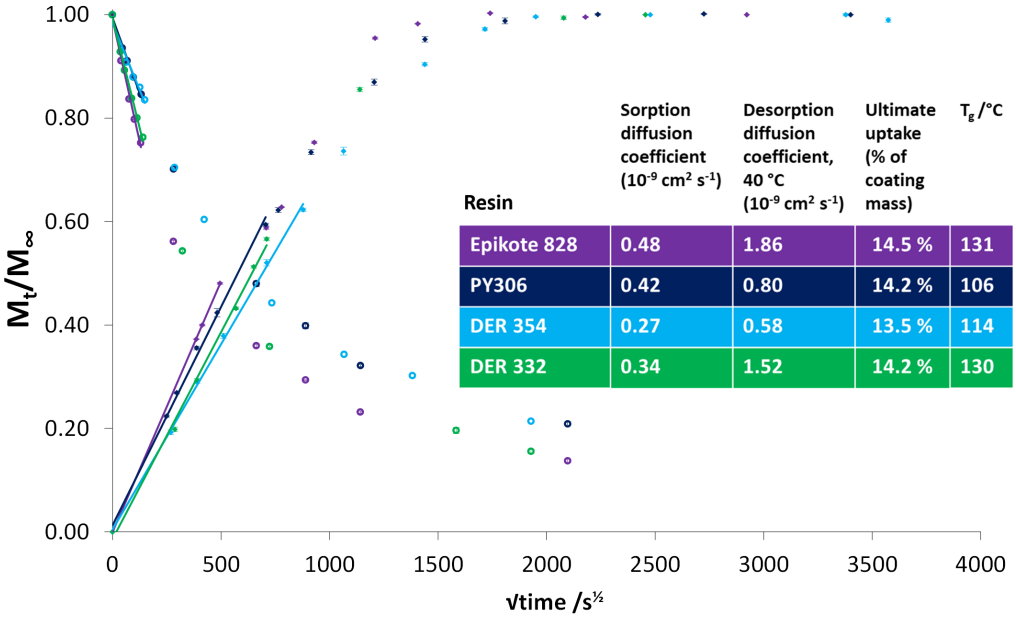

Resin	Sorption diffusion coefficient (10^{-9} cm^2 s^{-1})	Desorption diffusion coefficient, 40 °C (10^{-9} cm^2 s^{-1})	Ultimate uptake (% of coating mass)	T_g /°C
Epikote 828	0.48	1.86	14.5 %	131
PY306	0.42	0.80	14.2 %	106
DER 354	0.27	0.58	13.5 %	114
DER 332	0.34	1.52	14.2 %	130

(a) Methanol sorption and desorption of networks on glass slides made with varying epoxy resin monomers and MXDA. Sorption begins at the origin with a positive slope and desorption at $\frac{M_t}{M_\infty} = 1$*, with a negative slope. Error bars show standard error of three samples. The diffusion coefficients, D, were calculated from the gradient of the initial linear fits and is shown in the inset table. Ultimate uptake and glass transition temperature,* T_g*, are shown for each sample.*

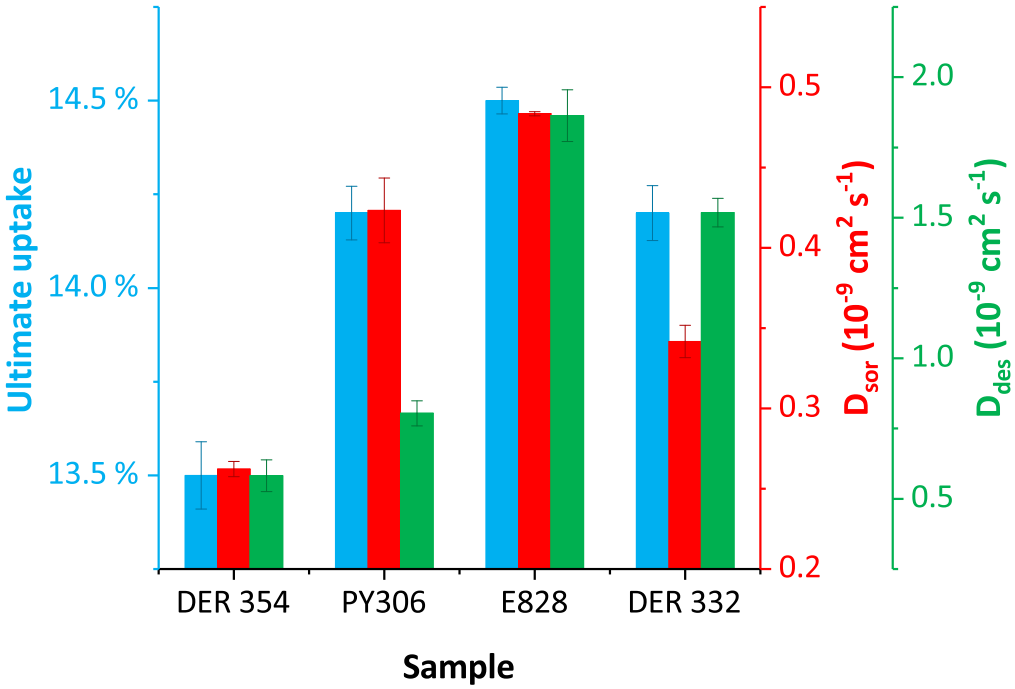

(b) Summary of methanol uptake parameters for networks made with a range of epoxy resin monomers and MXDA. Error bars show standard error of three samples.

Figure 3.10

of an increase, this mode has a decrease in gradient following a discontinuity. The literature regarding such diffusion is limited, but Neogi relates it to the presence of inhomogeneities.[7] The qualitative justification for this would be that there is an initial rapid sorption of penetrant into a less dense phase, followed by slower sorption into higher density regions of the material. The higher degree of chain extension might provide a plausible mechanism for regions with a higher free volume; the regions where the n>1 isomers are present in the network. The gradient of the second period of constant sorption for the E828 sample vs. $\sqrt{time}$ (700-1250 $s^{\frac{1}{2}}$) is remarkably similar to the gradient obtained for the DER 332. This further supports the idea that chain extension might produce less dense regions, as the more dense regions would be expected to perform very similarly to the DER 332 network (since DER 332 consists solely of the n = 0 DGEBA molecule that is found in E828).

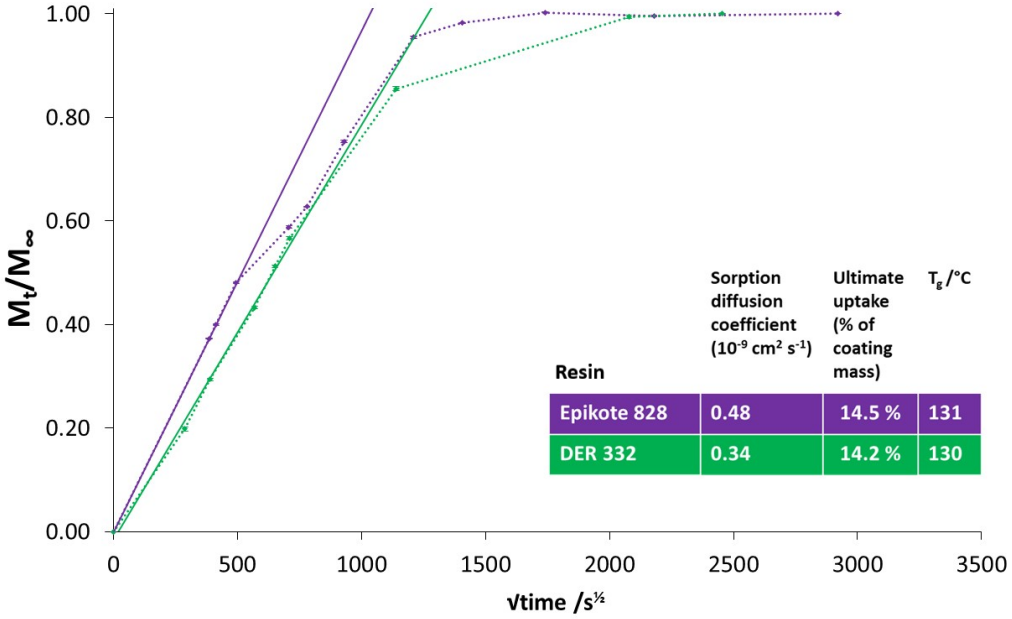

Figure 3.11: Uptake curves for networks based on E828 and DER 332 cured with MXDA. Initial slopes are projected to $\frac{M_t}{M_\infty} = 1$. The trace for E828 is seen to deviate from the initial slope at a much lower $\frac{M_t}{M_\infty}$ than the Fickian curves observed for DER 332. The individual points taken for each series are connected by the straight dotted lines.

Ethanol uptake

The DER 354 based network showed the best performance in ethanol, with a much slower uptake than that found for all of the other resins (Figure 3.12). The sorption for both DGEBF based networks was found to be lower than those based on DGEBA. Perhaps surprisingly, the DER 332 sample performed very similarly to the E828 in spite of the variation observed for methanol uptake. In the case of all resins, the sigmoidal mode of sorption is clearly observed, though the gradient change is much more drastic in DGEBA resins, and is greater for the PY306 network than for the DER 354.

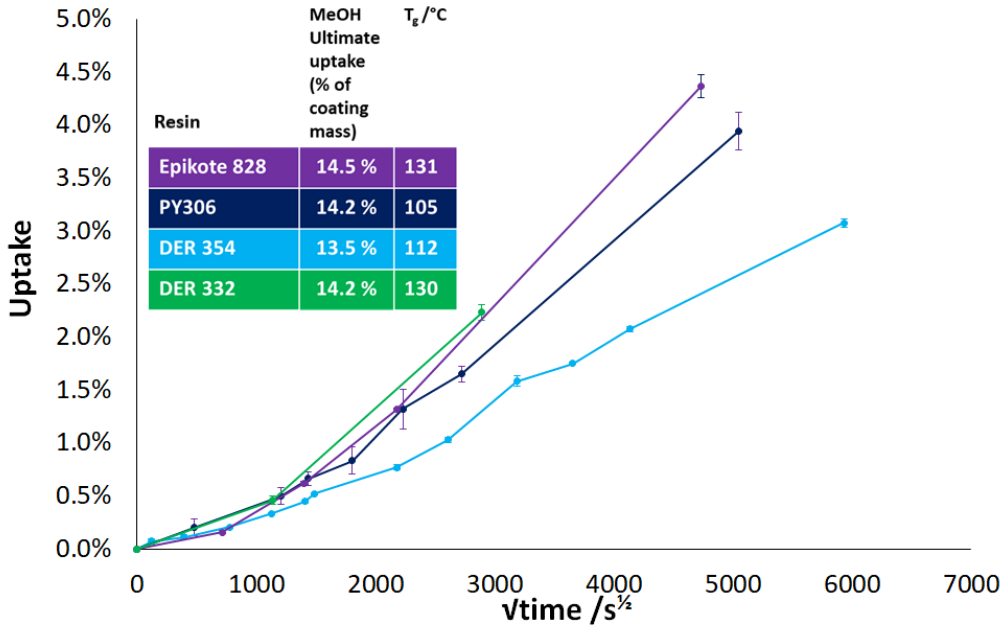

Figure 3.12: Ethanol sorption of networks on glass slides made with varying epoxy resin monomers and MXDA. For reference, ultimate uptake for methanol sorption and glass transition temperature, T_g, are shown for each sample in the inset table.

Summary

The results from comparing the networks based on E828 and DER 332 show a marked improvement in resistance to methanol with the removal of chain extended components in spite of similar thermal/physical properties. However, the same change is not observed for ethanol uptake. The different modes of methanol uptake indicate different network structures for the two DGEBA based networks. The DER 354 / PY306 compar-

ison illustrates the impact that regioisomerism can have—the mixture comprising more ortho- substituted DGEBF species (PY306) performed worse. The variation in the β-transition suggests that this is due to fundamentally different molecular behaviour from the regioisomers of DGEBF, though the impact of diversity of species is not discounted.

The variability between the networks based on the chemically similar DER 354 and PY306 shows that much caution is required in comparing either to the (effectively) isomerically pure DER 332, especially in drawing any firm conclusions. However, where DGEBA and DGEBF based networks are compared, the importance of chemical structure is illustrated in the differences in performance between the resins. Despite DER 354 containing a mixture of isomers and chain extension, when cured with MXDA, its chemical performance is still found to be superior to DER 332 / MXDA, in both methanol and ethanol. The crosslink density is higher in the DER 332 network, but this is accompanied by a relatively large reduction in density. This can be attributed to the methyl groups on the bridging carbon of the bisphenol unit—the free volume imparted is shown to be a greater influence than any regioisomeric factor or the diversity of chemical species.

3.1.4 Properties and performance—amine variation

This investigation seeks to understand the impact of two main factors: (i) the impact of regioisomerism of six-membered ring containing amines between 1,3- and 1,4- substitution (MXDA vs PXDA and 1,3-BAC vs 1,4-BAC) and (ii) the impact of the bonding type (aromatic vs aliphatic—MXDA vs 1,3-BAC / PXDA vs 1,4-BAC). Finally, PACM is included to observe the impact of the introduction of a second six membered ring. Chemical structures of the amines are shown in Figure 3.13. For the purposes of this comparison, all were cured with DER 354.

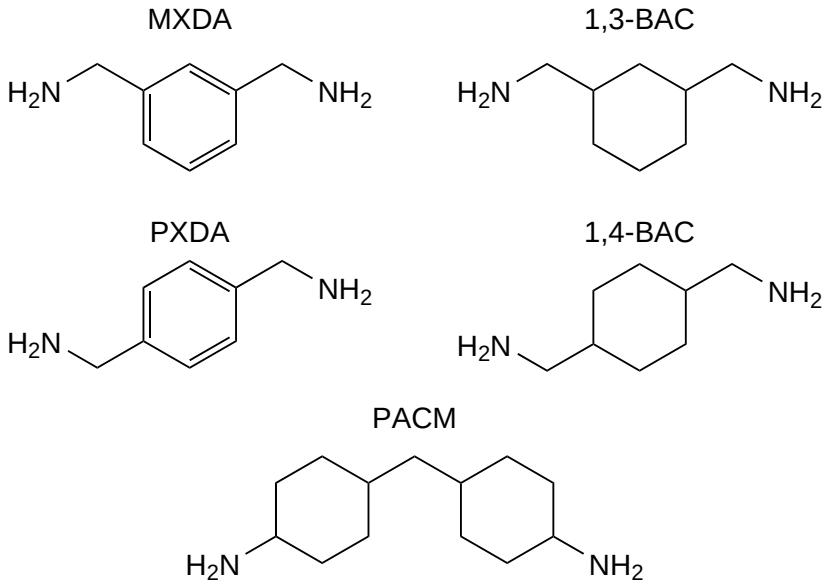

Figure 3.13: The chemical structures of the amines investigated. Key: **MXDA**- *meta-xylylenediamine;* **1,3-BAC**- *1,3-bis(aminomethyl)cyclohexane,* **PXDA**- *para-xylylenediamine;* **1,4-BAC**- *1,4-bis(aminomethyl)cyclohexane;* **PACM**- *bis(para-aminocyclohexyl) methane.*

Thermal and physical properties

Amine regioisomerism The trends identified were mixed (Figure 3.14). Density showed no real change with regioisomerism. This suggests the space filling of 1,3- and 1,4- isomers is very similar, when considering aromatic and aliphatic systems in isolation. The T_g was similar for the aliphatic systems—with the DER 354 / 1,3-BAC network having a slightly higher T_g (127 °C) than the DER 354 / 1,4-BAC (125 °C). However, in the case of the aromatic systems, there is a larger change for meta- and para- substitution

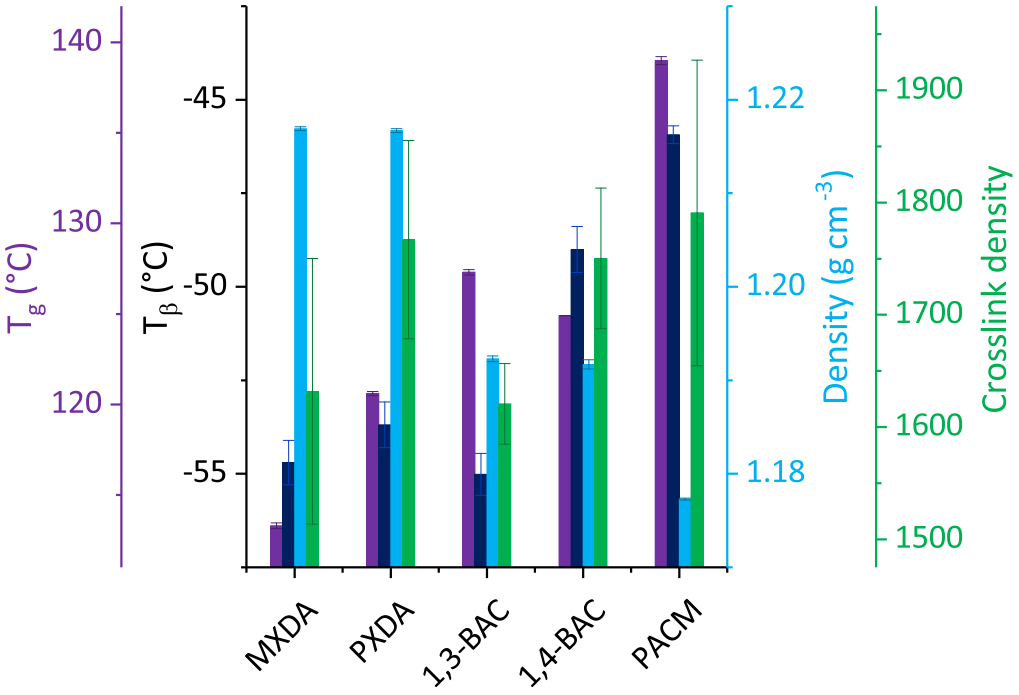

Figure 3.14: The T_g, T_β, crosslink density (all as found by DMA) and density (as found by helium pycnometry) of the five different networks prepared with varied amine hardeners (and DER 354). Error bars show standard error of three measurements for the values obtained by DMA, and standard deviation of ten measurements of a single sample for density.

(i.e. 1,3- and 1,4- aromatic substitution). The DER 354 / MXDA network had a lower T_g (113 °C) than the DER 354 / PXDA (121 °C). This T_g change was not mirrored by any other changes in the properties measured. Perhaps unexpectedly then, T_β varied substantially more for the aliphatic regioisomers than for the aromatics. T_β was found to be 5 °C lower for the 1,3-BAC network relative to the 1,4-BAC network. This indicates a change in nanostructure between 1,3- and 1,4- substituted aliphatic amines, causing a change to small-scale molecular motion. The energetic barrier to motion is lower in the 1,3-BAC network. This is accompanied by an increase in crosslink density for the 1,4-BAC network (vs. 1,3-BAC), (but is not reflected in the T_g, which is higher for the 1,3-BAC). For the aromatics, T_β was slightly higher for the PXDA based network (vs. MXDA), but within error. An observation of the β-transition (Figure 3.15), shows that the area of the transition is lower for the 1,3- substituted structures relative to the 1,4-. This is indicative of the absence of a particular molecular motion, such as a phenylene ring flip.[6,8]

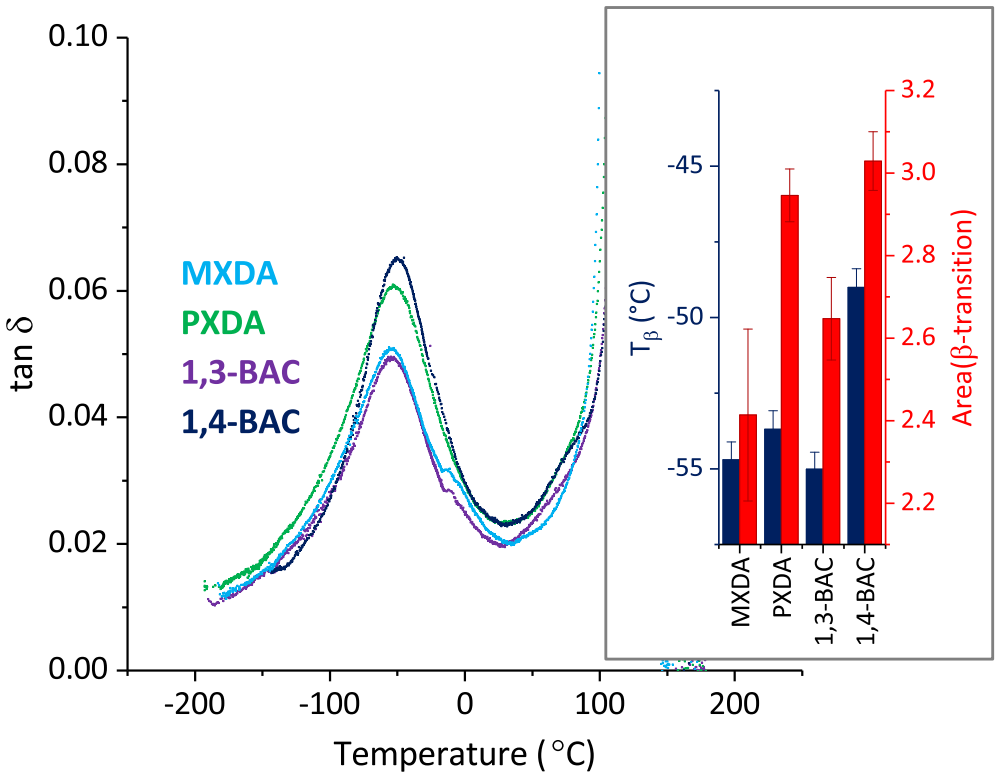

Figure 3.15: DMA traces of tan δ against temperature for networks prepared with varied amine hardener (and DER 354), showing the response for the β-transition. Inset: The T_β and area of the β-transition for those networks. Error bars show standard error of two samples

Aromatic/Aliphatic bonding The aromatic and aliphatic samples showed large differences for T_g, T_β and density, in spite of a largely similar crosslink density. Whilst there is variation between the aromatic samples, the T_gs for the aliphatic samples are both higher. This is an unusual observation—where aromaticity is included in a polymer backbone, generally T_g is seen to increase, for the rigidity provided, such as for poly(ethylene terephthalate) and its aliphatic analogue, shown in Figure 3.16. This finding was extensively studied, questioned and re-examined using a number of different cure methods and analytical approaches and shown repeatedly to be the case.

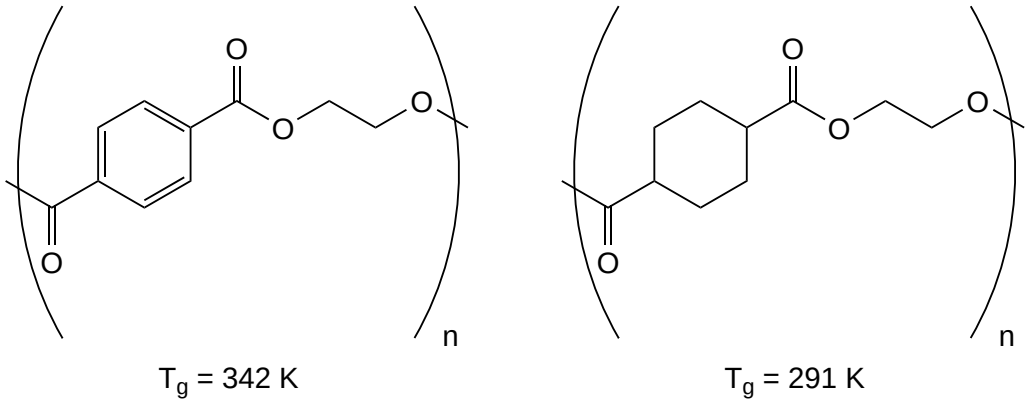

Figure 3.16: The chemical structure and glass transition temperatures (T_g) of poly(ethylene terephthalate) (left) and its aliphatic analogue (right).[9]

A similar trend is observed for the T_βs. Conversely, the densities of the aromatic based networks are much higher than the aliphatic systems, indicating that the space-filling of aromatic species is much more effective relative to aliphatic species. MXDA and 1,3-BAC networks show similar T_βs, though the PXDA network exhibits a lower T_β than the 1,4-BAC. This difference would be attributed to the contribution of a molecular motion involving the amine ring—the lower density for the 1,4-BAC suggests the ring fills more space, which in turn would require more energy to mobilise. Further, the reduction in T_β seen for 1,3- substitution (vs. 1,4- substitution) can then also be tentatively attributed to a ring flip which is not possible for 1,3- moieties, and therefore the same change for 1,3-BAC vs. MXDA is not observed.

PACM The DER 354 / PACM sample was found to have the lowest density, whilst having both the highest T_g and T_β. This suggests a stiffer structure imparted by the

amines being directly bound to the ring (resulting in higher T_g/T_β), with more free volume produced by the larger unit between the branch points of the molecular segment. Again, crosslink density is similar to the other samples explored.

Methanol uptake

Amine regioisomerism In both aromatic and aliphatic systems, there is a reduction in chemical performance with 1,4- substitution relative to 1,3- substitution (Figure 3.17). There is an increase in ultimate uptake for the PXDA network vs. MXDA and for the 1,4-BAC vs. 1,3-BAC. Further, there are marked increases in D_{sor} and D_{des}. The PXDA network showed a 5 % relative increase in ultimate uptake compared to the MXDA and the 1,4-BAC showed a 3.5 % relative increase (vs. 1,3-BAC). In terms of D_{sor}, increases of 50 % and 44 % were observed for the 1,4- substituted structure (vs. the 1,3-) for the aromatic and aliphatic species respectively. D_{des} was 84 % larger for the PXDA network vs the MXDA, though the increase for the 1,4-BAC (vs. 1,3-BAC) was much smaller, at 15 %.

Aromatic/Aliphatic bonding The aliphatic systems showed reduced chemical performance compared to their aliphatic analogues. The 1,3-BAC network showed a 5 % relative increase in uptake compared to the MXDA and the 1,4-BAC network showed a 3.5 % increase relative to the PXDA. D_{sor} and D_{des} were also higher for aliphatic species than for aromatic species—both the 1,3-BAC and 1,4-BAC showed substantial increases in sorption and desorption rates relative to their aromatic analogues (all $>$70 %).

PACM The PACM network showed the joint highest ultimate uptake with the 1,4-BAC (14.7 %) but had a much reduced D_{sor}, relative to the 1,4-BAC. D_{des} was by far the highest found, at almost four times the value for MXDA. As might be expected, this suggests the structure of this network is different to the others.

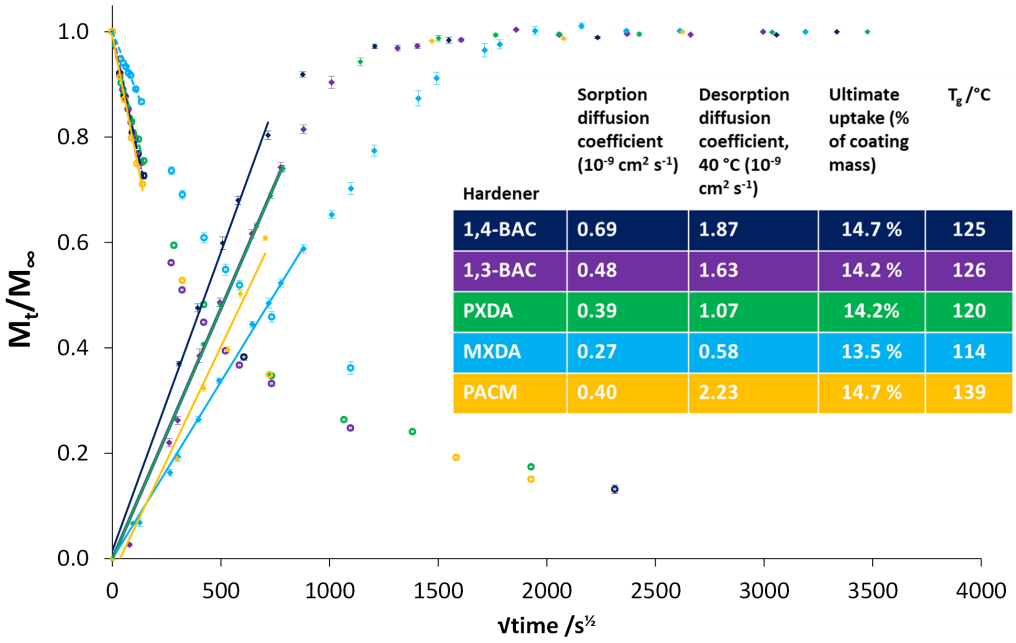

Hardener	Sorption diffusion coefficient (10^{-9} cm^2 s^{-1})	Desorption diffusion coefficient, 40 °C (10^{-9} cm^2 s^{-1})	Ultimate uptake (% of coating mass)	T_g /°C
1,4-BAC	0.69	1.87	14.7 %	125
1,3-BAC	0.48	1.63	14.2 %	126
PXDA	0.39	1.07	14.2%	120
MXDA	0.27	0.58	13.5 %	114
PACM	0.40	2.23	14.7 %	139

(a) Methanol sorption and desorption of networks on glass slides made with varying amines and DER 354. Sorption begins at the origin with a positive slope and desorption at $\frac{M_t}{M_\infty} = 1$, with a negative slope. Error bars show standard error of three samples. The diffusion coefficients, D, were calculated from the gradient of the initial linear fits and is shown in the inset table. Ultimate uptake and glass transition temperature, T_g, are shown for each sample.

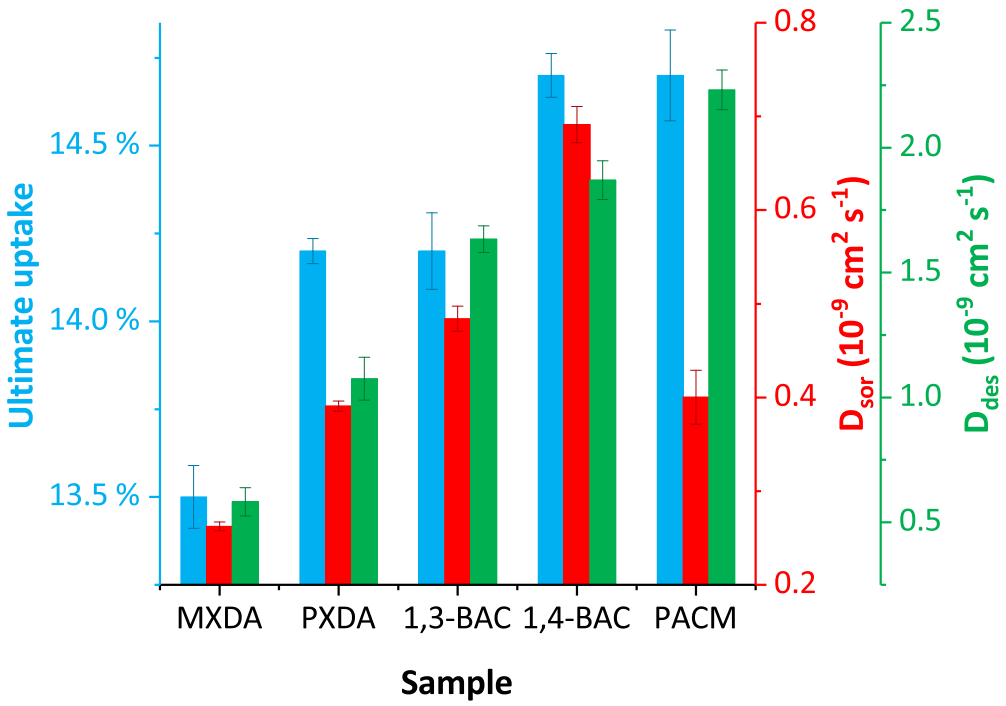

(b) Summary of methanol uptake parameters for networks made with a range of amines and DER 354. Error bars show standard error of three samples

Figure 3.17

Ethanol uptake

The sorption of ethanol by the networks made with varied amines provides insight into the network structure. Time constraints prevented the PACM sample being investigated in this study. For all samples, sigmoidal sorption is again observed—that is there is a discontinuity in gradient, where a steepening of the curve is seen—as a result of swelling. However, there is variation both in terms of initial performance and the magnitude of the change in gradient.

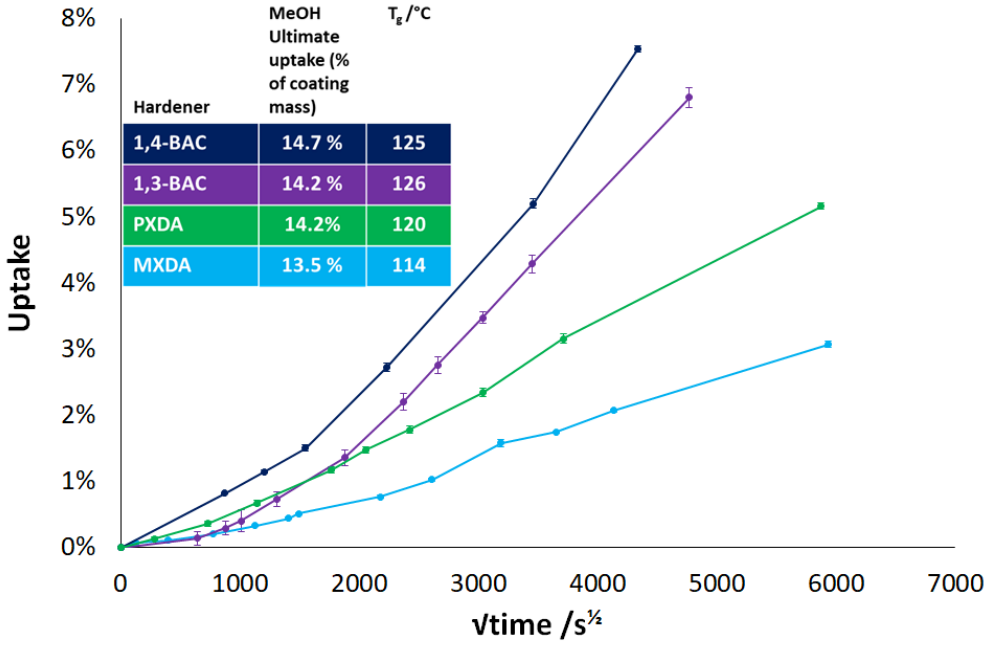

Figure 3.18: Ethanol uptake for networks on glass slides made with varying amines and DER 354. For reference, ultimate uptake for methanol sorption and glass transition temperature, T_g, are shown for each sample in the inset table.

Amine regioisomerism Where only regioisomers are considered, a very similar mode of uptake (i.e. the uptake curve shape is similar) is observed. The change in gradient for both the networks based on aromatic species (MXDA & PXDA) and aliphatic species (1,3-BAC & 1,4-BAC) is similar. Again, as found for methanol uptake, the 1,3-substituted species uptake less than the 1,4- species in both cases.

Aromatic/Aliphatic bonding The most striking difference between the aliphatic and aromatic species is the dramatic steepening of uptake for the aliphatic samples

relative to the aromatic. This is best illustrated by comparing the MXDA and 1,3-BAC based networks. They show an initially similar uptake, but the 1,3-BAC shows much increased ethanol uptake as a result of the much greater upturn in gradient. This upturn is sufficiently large, that the 1,3-BAC curve crosses the PXDA curve, which begins initially steeper. The 1,4-BAC network shows the fastest uptake, with both the steepest initial gradient and subsequent steeper gradient. Since the increase in gradient is related to swelling, the data is indicative that aliphatic networks are much more vulnerable to swelling. This is perhaps expected in light of the lower density observed for aliphatic species (Section 3.1.4).

Summary

Chemical performance was found to improve with 1,3-substitution of amines and for aromatic systems relative to aliphatic systems. When this is considered in light of the physical properties of the networks, a large density drop from the aromatic systems to aliphatics is observed, which is likely to result in a reduced chemical performance. Swelling of the network was observed for ethanol uptake in the aliphatic systems, further supporting this claim.

In identifying other differences between the 1,3- and 1,4- systems, there is a slight reduction in crosslink density (which has been linked to a reduction in solvent uptake), though this is very limited. There is also a reduction in the intensity of the beta transition for 1,3- substituted species, suggesting less ambient molecular motion. Since diffusion in polymers is dependent on kinetic constants for both the solvent and polymer, this is likely to impact on the ingress of any aggressors and therefore is suggested as a justification to the results above.

PACM was shown to produce a stiffer network which showed favourable methanol uptake properties relative to its physical properties (in particular, the lowest density of any network produced across this work). Further, it showed a large disparity between sorption and desorption coefficients—with the desired low sorption as well as high desorption. In terms of use as a coating this is beneficial, as any cargo solvent will uptake slowly whilst

carried, but upon removal will be able to be removed quickly.

3.2 Methods/Materials

3.2.1 Materials

meta-Xylylenediamine (MXDA , 99%) and 1,3-bis(aminomethyl)cyclohexane (1,3-BAC, 98 %) were obtained from Sigma Aldrich Co. LLC., and used as supplied. para-Xylylenediamine (PXDA, >99%) and 1,4-bis(aminomethyl)cyclohexane (1,4-BAC, >98%) were obtained from Tokyo Chemical Industry UK Ltd. and used as supplied. DER 354 was obtained from the Olin Corporation and used as supplied. Epikote 828 (E828) was obtained from Delta Resins Ltd. and used as supplied. Araldite PY306 (PY306) was obtained from Huntsman International LLC and used as supplied.

3.2.2 Chemical analysis of monomers

Nuclear magnetic resonance spectroscopy

All nuclear magnetic resonance spectroscopy was completed using a Bruker Avance 400 MHz spectrometer. Chemical shifts are given relative to the lock solvent. Samples of approximately 10 mg were dissolved in $\sim$1 cm^3 C_6D_6.

High performance liquid chromatography (HPLC)

A Varian Pro Star HPLC system was used, with a 230 pump and a 310 UV detector. The autosampler used was a 410 model, with a 100 μl injection loop. The column (4.6 x 250 mm) was a Waters XBridge™ C18 5 μm. The detector was operated at 280 nm, and the system was run at a flow rate of 1.0 ml min^{-1}. Samples of $\sim$1 mg were dissolved in $\sim$1 cm^3 of acetonitrile, and injected into the column. A 50:50 acetonitrile:water mixture was used for 19 minutes, whereupon the system was moved to 100 % acetonitrile for a further 10 minutes.

Titration for epoxide equivalent weight (EEW)[10]

Titration for epoxide equivalent weight was performed as in Chapter 2—see Section 2.2.2.

3.2.3 Network Preparation

Glass slide preparation

Hydrogen peroxide was added with care and gentle stirring to sulfuric acid in a 1:3 ratio to produce "piranha solution". Slides (as supplied) were placed in the "piranha solution" and left for 15 minutes before rinsing thoroughly with deionised water. The treated slides were placed in a rack and dried at 50 °C in an oven, and stored there until use.

Network preparation for solvent sorption/desorption studies—Liquid isomers

Formulation Epoxy resin was added to an amine (for identities/quantities see Table 3.2), and then mixed using a stirring rod. The resulting mixture was covered using parafilm, and left, with further mixing (initially every five minutes, then less regularly), at room temperature. After a pot time of 2-3 hours (see Table 3.2), the mixture was sealed and stored overnight at -20 °C in a freezer.

Application to glass slides The following morning, whilst sealed (to avoid condensation contaminating the mixture), the vessel was brought to room temperature, and then drawn-down onto prepared glass slides (see section 3.2.3) using a drawdown cube. The drawdown cube was obtained from Sheen Instruments, with a 400 μm slot. The slides were then placed in an oven and cured under a nitrogen atmosphere. Oxygen free nitrogen, obtained from BOC, was purged through the oven at $\sim$5 cm^3 min^{-1}. The cure schedule was an initial temperature of 60 °C, with a ramp of 1 °C min^{-1} to 160 °C, where the oven was held for three hours. Upon completion of the three hours, the samples were removed from the oven and allowed to cool. Any samples not immediately analysed were placed in a desiccator over phosphorus pentoxide to prevent moisture uptake.

Network preparation for solvent sorption/desorption studies—PXDA (solid amine)

Formulation PXDA was added to a sample tube and melted (m.p. 60-64 °C). Some DER 354 was added immediately with stirring, and the mixture brought to 30 °C. The remainder of the DER 354 was then added (for quantities see Table 3.2), and then

Amine	Mass (amine) /g	Moles (amine) /mol	Epoxy	Mass (epoxy) /g	Moles (epoxy) /mol	Stoich	Pot time
MXDA	1.9942	5.86×10^{-2}	DER354	9.9092	5.86×10^{-2}	100.0%	3 h
1,3-BAC	1.9177	5.39×10^{-2}	DER354	9.1267	5.39×10^{-2}	100.0%	2 h
PXDA	2.9875	8.77×10^{-2}	DER354	14.8443	8.77×10^{-2}	100.0%	1 h [a]
1,4-BAC	3.4214	9.62×10^{-2}	DER354	16.2699	9.62×10^{-2}	100.0%	2 h
MXDA	1.8467	5.42×10^{-2}	E828	10.2163	5.42×10^{-2}	100.0%	2.5 h
MXDA	1.9395	5.70×10^{-2}	PY306	9.5015	5.69×10^{-2}	100.1%	3 h

Table 3.2: Quantities used in cures for solvent sorption/desorption studies. [a]PXDA is a solid hardener, and therefore the pot was held at an elevated temperature (30 °C) in order to reduce the likelihood of crystallisation—see Section 3.2.3

further mixed using a stirring rod. The resulting mixture was covered using parafilm and held, with further mixing (initially every five minutes, then less regularly), at 30 °C.

Application to glass slides After 75 mins, the mixture was removed from the heat and then drawn-down onto prepared glass slides (see section 3.2.3) heated to 30 °C using the heated drawdown block described in Section 3.1.2, using a drawdown cube. The drawdown cube was obtained from Sheen Instruments, with a 400 μm slot. The slides were then placed in an oven and cured under a nitrogen atmosphere. Oxygen free nitrogen, obtained from BOC, was purged through the oven at $\sim$5 cm^3 min^{-1}. The cure schedule was an initial temperature of 60 °C, with a ramp of 1 °C min^{-1} to 160 °C, where the oven was held for three hours. Upon completion of the three hours, the samples were removed from the oven and allowed to cool. Any samples not immediately analysed were placed in a desiccator over phosphorus pentoxide to prevent moisture uptake.

Network preparation for dynamic mechanical analysis and helium pycnometry

All networks were formulated as in the previous sections (liquid isomers as in Section 3.2.3 and PXDA as in Section 3.2.3). After the pot-time, specified in Table 3.3, these mixtures were then poured into PTFE moulds (for DMA bars), spotted onto release film (for helium pycnometry), and cured under a nitrogen atmosphere. Oxygen free nitrogen,

obtained from BOC, was purged through the oven at ~5 cm^3 min^{-1}. The cure schedule was an initial temperature of 60 °C, with a ramp of 1 °C min^{-1} to 160 °C, where the oven was held for three hours. Upon completion of the three hours, the samples were removed from the oven and allowed to cool. Prior to analysis, samples were then placed in a desiccator over phosphorus pentoxide to prevent moisture uptake.

Amine	Mass (amine) /g	Moles (amine) /mol	Epoxy	Mass (epoxy) /g	Moles (epoxy) /mol	Stoich	Pot time
MXDA	2.2584	6.63×10^{-2}	DER354	11.2228	6.63×10^{-2}	100.0%	3 h
1,3-BAC	2.8368	7.98×10^{-2}	DER354	13.4864	7.97×10^{-2}	100.1%	2 h
PXDA	2.9875	8.77×10^{-2}	DER354	14.8443	8.77×10^{-2}	100.0%	1.25 h [a]
1,4-BAC	2.1566	6.06×10^{-2}	DER354	10.2604	6.06×10^{-2}	100.0%	2 h
MXDA	2.7971	8.22×10^{-2}	E828	15.4733	8.21×10^{-2}	100.0%	2.5 h
MXDA	3.0718	9.02×10^{-2}	PY306	15.0585	9.02×10^{-2}	100.0%	3 h

Table 3.3: Quantities used in cures for dynamic mechanical analysis and helium pycnometry. [a] PXDA is a solid hardener, and therefore the pot was held at an elevated temperature (30 °C) in order to reduce the likelihood of crystallisation—see Section 3.2.3

3.2.4 Near-Infrared (NIR) spectroscopy

Degree of cure was measured by NIR spectroscopy, as described in Chapter 2—see Section 2.2.4.

3.2.5 Solvent sorption/desorption

Same method as in Chapter 2: Coated glass slides were placed in solvent (methanol or ethanol) and weighed at time intervals, ranging from 2 hours to 65 weeks (See Table 3.4). Intervals between measurements were increased as time increased due to the slowing of mass uptake. Upon reaching a plateau in mass, these samples were removed from solvent and placed in an oven at 40 °C, and weighed at time intervals, until a reasonable plateau was obtained. No plateau was achieved for ethanol immersed slides, and therefore no cycling was performed. In order to repeat the sorption and desorption process, samples

were placed in a vacuum oven above their T_g (approx. 130 °C), under vacuum, and left until a stable mass, approximate to their original mass was obtained. The process was then repeated.

No. in series	Time (days) - Methanol uptake	Time (days) - Ethanol uptake
0	0	0
1	0.25	3
2	1	20
3	2	39
4	4	63
5	7	90
6	11	120
7	17	160
8	25	200
9	36	260
10	50	320
11	86	400

Table 3.4: Example weighing schedule for methanol and ethanol sorption

3.2.6 Dynamic mechanical analysis (DMA)

Dynamic mechanical analysis was performed on a PerkinElmer DMA8000, using single cantilever mode, heated at a rate of 3 °C. Three beams were prepared for each sample formulation, approximately 10 mm wide and 1.6 mm thick and the dynamic response to a sinusoidal force applied at a frequency of 1 s^{-1} recorded. The T_g was taken as the peak in the tan δ trace, from a Lorentzian fit of the peak using OriginLab 2017. For the β-transition measurements, the sample chamber was cooled to approximately -192 °C, before the measurement was performed. The area of the peak was obtained using a fitted cubic baseline and integrating the area beneath the curve.

3.2.7 Helium pycnometry

Helium pycnometry was performed as described in Chapter 2, see Section 2.2.9.

References

[1] Domke, W.-D. 1H NMR spectroscopic determination of the isomeric ratios of bisphenol-F diglycidyl ethers. *Organic Magnetic Resonance*, **18**(4), 193–196 (1982).

[2] Garcia, F. G. & Soares, B. G. Determination of the epoxide equivalent weight of epoxy resins based on diglycidyl ether of bisphenol A (DGEBA) by proton nuclear magnetic resonance. *Polymer Testing*, **22**(1), 51–56 (2003).

[3] Pontén, A., Zimerson, E., Sörensen, O. & Bruze, M. Chemical analysis of monomers in epoxy resins based on bisphenols F and A. *Contact dermatitis*, **50**(5), 289–97 (2004).

[4] Armarego, W. L. F. & Chai, C. L. L. *Purification of Laboratory Chemicals*. Butterworth-Heinemann (2003). ISBN 9780080515465.

[5] Chen, C.-C., Cheng, S. & Jang, L.-Y. Dual-functionalized large pore mesoporous silica as an efficient catalyst for bisphenol-A synthesis. *Microporous and Mesoporous Materials*, **109**(1-3), 258–270 (2008).

[6] Ramsdale-Capper, R. & Foreman, J. P. Internal antiplasticisation in highly crosslinked amine cured multifunctional epoxy resins. *Polymer*, **146**, 321–330 (2018).

[7] Neogi, P. Transport phenomena in polymer membranes. *Plastics Engineering (New York)*, **32**(Diffusion in Polymers), 173–209 (1996).

[8] Tu, J., Tucker, S. J., Christensen, S., Sayed, A. R., Jarrett, W. L. & Wiggins, J. S. Phenylene ring motions in isomeric glassy epoxy networks and their contributions to thermal and mechanical properties. *Macromolecules*, **48**(6), 1748–1758 (2015).

[9] Brandrup, J., Immergut, E. H. & Grulke, E. A. *Polymer Handbook*. Wiley-Interscience (1999). ISBN 9780471479369.

[10] Cameron, C. Private communication. *AkzoNobel* (2014).

Chapter 4

Isolation of the individual isomers of diglycidyl ether of bisphenol F

4.1 Results and Discussion

Overview

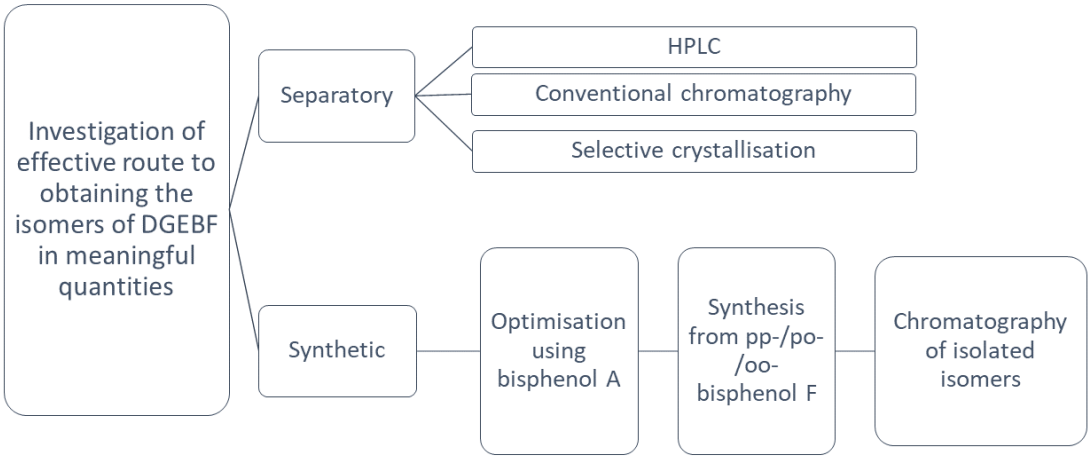

When considering the ultimate aims of this work, we have shown that diglycidyl ether of bisphenol F (DGEBF) based resins have a good degree of variability in their composition (Section 3.1.1). This makes them a useful tool in identifying how subtle chemical changes influence subsequent network properties. A clear starting point would be in producing networks varying the regioisomers of n=0 DGEBF (ortho-ortho- (oo), para-ortho- (po) & para-para- (pp)) or the relative quantities of these isomers, rather than considering any of the complications caused by chain extension (where different regioisomeric substitution might be present in one molecule). This allows for a comparison of otherwise identical networks, aside from a difference in molecular geometry and a small change in mass between crosslinks (M_c). The effect of the higher MW components is also of interest - their presence produces a network with a larger average M_c, but again otherwise identical in terms of chemical composition.

This chapter deals with the purification of DGEBF based mixtures and the isolation of the constituent regioisomers—by both separatory and synthetic means.

4.1.1 Separation of isomers

Preparatory high performance liquid chromatography

Separation of the isomers of DGEBF in DER 354 using HPLC was demonstrated in Section 3.1.1. Using prepatory-HPLC approximately 50 mg ortho-ortho- (oo) and 150 mg of each of the para-ortho- (po) & para-para- (pp) DGEBF were obtained. ^{1}H NMR spectroscopy confirmed the identities of the species in each peak and their purity. Therefore, a method of separation was established. However, HPLC is extremely costly, both in terms of solvent and instrumental costs, so other approaches were targeted. In any case, producing sizeable quantities is extremely time-consuming.

Conventional Chromatography

The normal phase thin layer chromatography of DER 354 initially showed two spots under UV light, when using ethyl acetate/hexane solvent mixtures, from 20:80 to 50:50. The best separation was found using a solvent mixture of ethyl acetate and hexane (35:65), where the two spots were found at R_f values of 0.42 and 0.49. The lower R_f spot was substantially bolder than the higher spot. When another plate was loaded with a higher concentration of DER 354, a faint smear from $R_f = 0$ to $R_f = 0.27$ was observed. This ordering shows the influence of molecular weight on both this technique and reverse-phase HPLC, where irrespective of polarity of the stationary phase, we see the chain extended species eluting slowest.

An initial column (run 1) showed that the two major spots could be separated using column chromatography, using the same solvent mixture. Characterisation of the two components by ^{1}H NMR spectroscopy (Figure 4.1) showed the faster eluting spot (fraction 1(F1)) to be ooDGEBF, and the bolder spot (fraction 2 (F2)) to be a 1:1 mixture of the po- and pp- DGEBF. Within F2, there was a gradient of the po and pp isomers, initially richer in po, and then moving towards richer in pp. In light of the HPLC results, it might be expected that there might be a larger amount of po. However, there is a small overlap of the oo and the mixed fractions and so to eliminate any contamination of the pp/po mixture, any mixed sample vials were discarded. This leads to a slight

reduction in the amount of po.

No full separation between all three isomers was obtained. The faintness of the spot produced by F1 (i.e. ooDGEBF) is as a result of the relative quantities of the isomers within DER 354. If po and pp are considered as a single entity (as they behave in conventional chromatography), the ratio is 1:6 between F1 and F2.

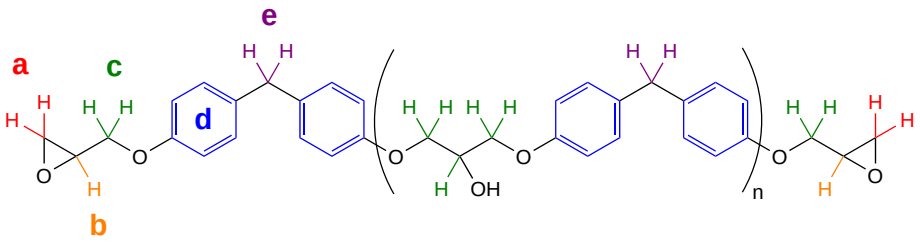

(a) The structure of DGEBF with generalised proton environments

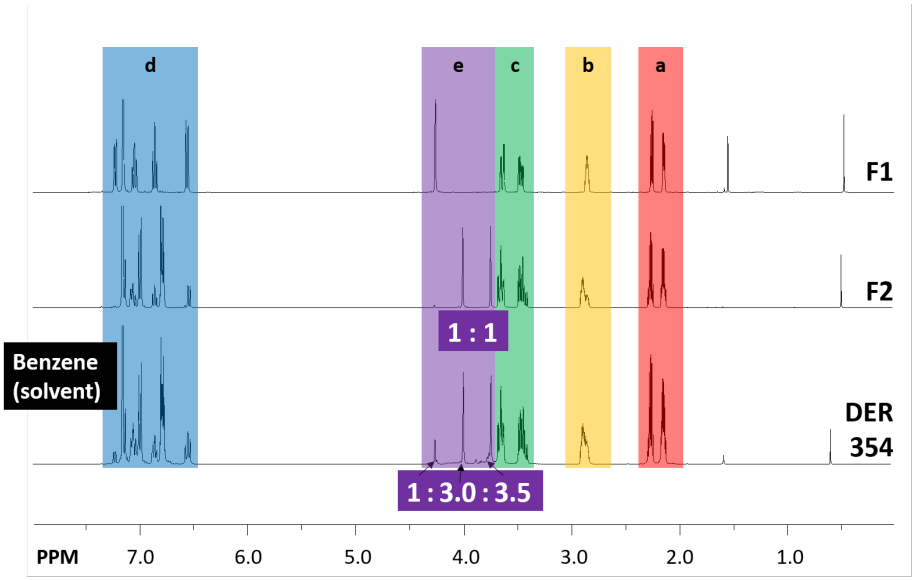

(b) ^{1}H NMR spectra of DER 354 and of fractions one and two (F1 and F2) obtained from column chromatography of DER 354. Fraction one is ooDGEBF, and fraction two an equal ratio of the po- and pp- isomers of DGEBF, as determined by integration of the bridging methylene signal (singlet at 3.7 - 4.3 ppm depending on isomer).

Figure 4.1

The higher MW components of any of the isomers are removed in column chromatography - neither fractions show the associated NMR signals for n>0 isomers. This was confirmed by EEW measurements- with equivalent weights being much closer to that expected for the n=0 isomers (156 g mol^{-1}), rather than the higher EEW obtained for DER 354 (169 g mol^{-1}). This, if F1 and F2 are considered as a single entity, gives a route to separation of the n=0 isomers from any n>0 molecules.

Column chromatography, then, presents two main opportunities:

(a) the production of a 1:1 mixture of pp and po in good quantity

(b) the removal of the higher MW components of DER 354

Therefore, the appropriate work was undertaken in order to obtain the above described samples. Its limitations lie in its cost - a column can process around 11 g of resin per run, using approximately 5 L of solvent and 700 g silica. It is for this reason that it was not pursued as a method to obtain ooDGEBF. As the oo isomer represents less than a seventh of the mixture, of which 10% is higher MW, if a column was 100% efficient, the yield would be less than 1.5 g.

In spite of this, columns were completed in order realise the two possibilities outlined above. With regard to **part (a)**, two columns yielded approximately 5.5 g of the 1 : 1 pp/po mixture each, giving a total of 11 g. ^{1}H NMR spectroscopy and HPLC showed the mixture to be almost entirely the n = 0 isomers of pp and po DGEBF, with the majority of the oo isomer removed. The EEW was found by titration to be 159.4 g mol^{-1}, corresponding to a value of n = 0.03.

With regard to **part (b)**, initially two columns were completed ("Run 1"), which successfully removed the higher MW components. Both yielded approximately 7.5 g, giving a total of 15 g. The EEW was found to be 162.6 g mol^{-1}, corresponding to n = 0.05. However, the ratio of the pp isomer relative to the po and oo was found to be lower than in the original resin. By HPLC it was found to be 33 % rather than the 40 % in DER 354 (see Figure 4.2). This was because there was a small overlap between the end of the pp containing fraction and the higher MW components, which was not included in the final collected fraction.

A second pair of columns was completed with a mobile phase of higher polarity in order to give improved separation of the n = 0 isomers from the higher MW species ("Run 2"). In addition, pppo containing sample tubes where the contamination by higher MW species was minimal (as measured by intensity of spot on the TLC plate) were included in the fraction. This gave a very limited contamination by high MW

components - observed by minor bumps in the HPLC chromatogram (see Figure 4.2), but a material of the same degree of extension as measured by EEW titration. The pp-ratio (of 37 %) remained lower than in DER 354 (40 %), but closer than that obtained in run 1.

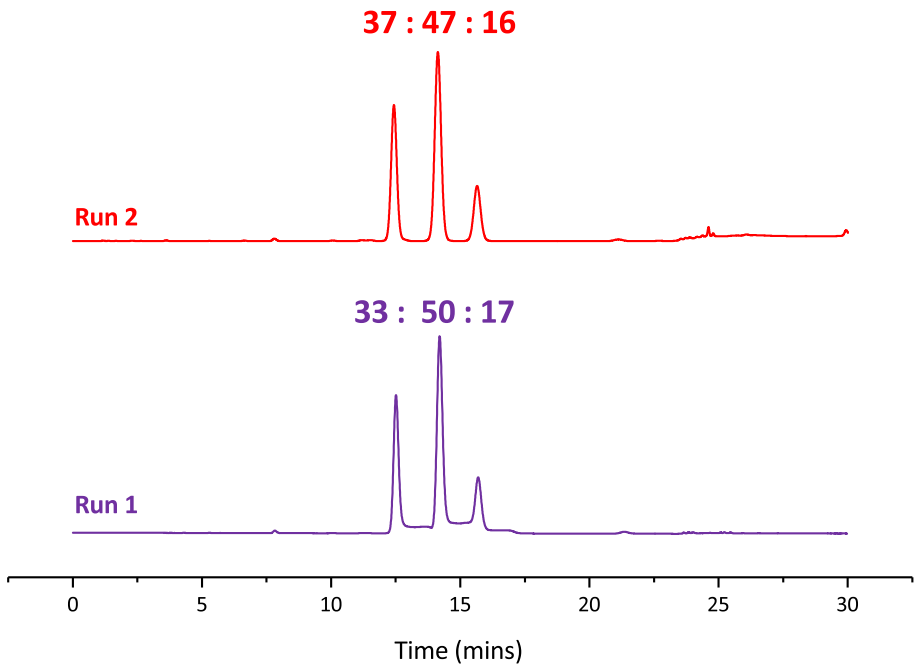

Figure 4.2: HPLC chromatograms for the isomeric mixtures obtained from column chromatography used in order to remove higher MW components.

Computational solubility study

Any differences in the solubility of the isomers may give another possible route to separation. In order to get an idea of whether this approach might be profitable, a computational study was performed.

Quantum chemistry based calculations were performed initially for each of the DGEBF isomers (see Figure 4.3) in acetone, and then dichloromethane. The free energies following optimisation were given, and in both cases showed the pp isomer to be around 4 kJ mol^{-1} more stable than the oo, which in turn was 1 kJ mol^{-1} more stable than the po. This is comparable to the energy at room temperature (2.4 kJ mol^{-1}), and therefore varied behaviour, which would be required for separation, is unlikely.

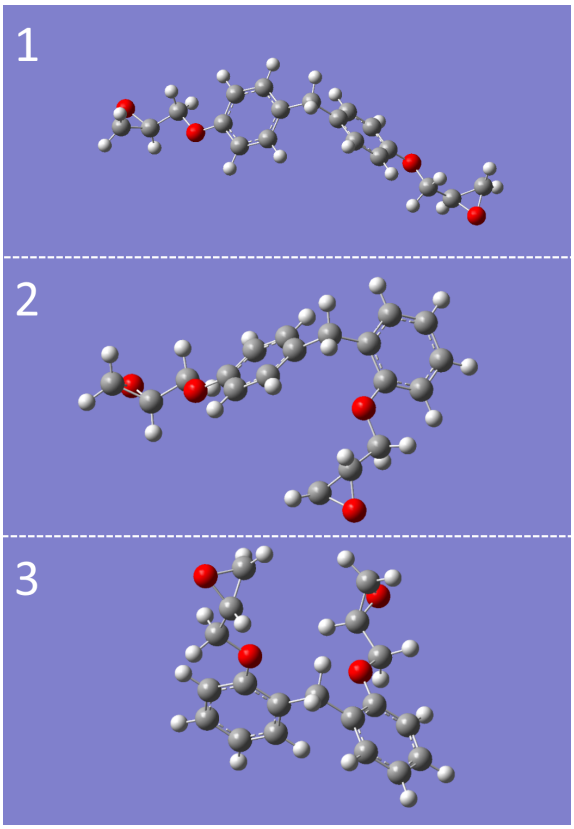

Figure 4.3: The optimised configurations of the three isomers of DGEBF in acetone (1) para-para, 2) para-ortho, 3) ortho-ortho)

Following this, the starting configurations were adjusted in order to ascertain the presence of local minima. Indeed, these were found, but the initially found structures were the lowest in energy and the adjusted structures tended to move to local minima at higher energies. They ranged from around 1 kJ mol^{-1} higher in energy, to 20 kJ mol^{-1} higher. Particularly investigated was the possibility of enhanced hydrogen bonding in the oo isomer. Should there be variation in the amount of hydrogen bonding between the isomers, the selection of solvent could be tuned to increase the energetic difference between isomers.

By rotating appropriate bonds, potential hydrogen bond acceptors, oxygen atoms, and potential donors, hydrogen atoms bonded to the epoxy were moved into closer proximity. This was to ensure that the final structure obtained was not simply a local minimum. However, it became clear that maximising the $\pi - \pi$ overlap by ensuring planarity between the ether fragment and the phenyl ring was preferable to any gains achieved by other means (Figure 4.4).

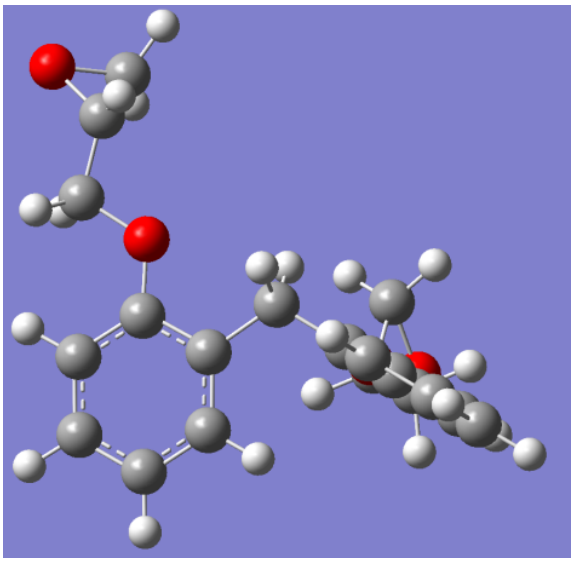

Figure 4.4: The optimised configuration of ortho-ortho DGEBF. Note the planarity of the glycidyl ether moieties, which results in $\pi - \pi$ overlap.

Therefore, it was decided that selective crystallisation from solution was very unlikely, due to the isomers having very similar energies and thus solubilities in both polar and non-polar solvents.

Crystallisation

As shown in Figure 4.5, the po isomer of DGEBF (middle) is resinous, where the other two are solids (left and right). This invites the question as to whether at some point the two solid isomers might crystallise from the mixture. Hence, differential scanning calorimetry (DSC) was used to observe whether this might be the case.

The results from the DSC did not show crystallisation out of the pp/ooDGEBF isomers, instead a glass transition is seen at around -25 °C, that is present in the pure poDGEBF DSC trace, as shown by Figure 4.6.

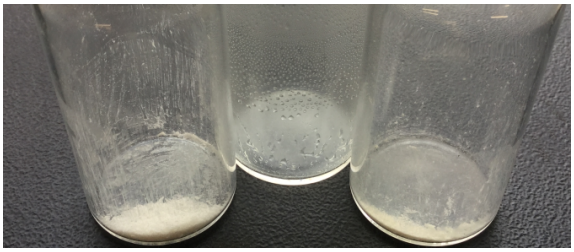

Figure 4.5: Image of the three isomers of DGEBF as produced by preparatory-HPLC. From left to right, para-para, para-ortho, ortho-ortho.

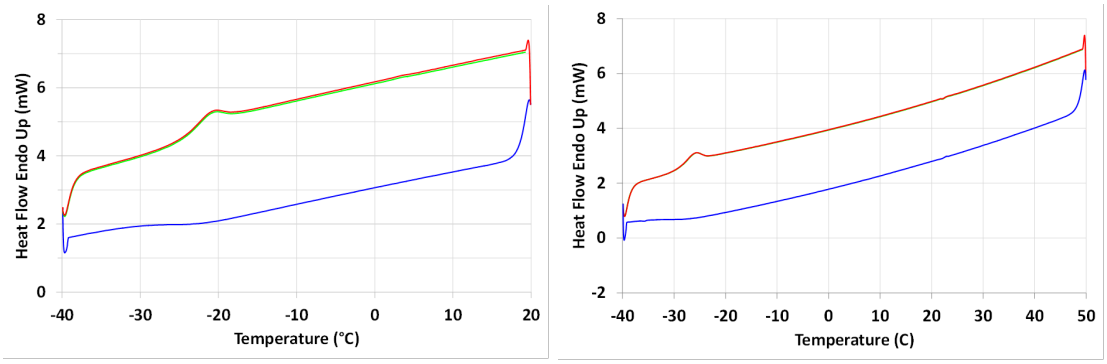

Figure 4.6: DSC traces of (l) D.E.R 354 and (r) poDGEBF. The glass transition can be seen on both at approximately -25 °C.

Separation summary

Partial separation was successfully achieved by chromatographic methods. HPLC gave the clearest separation, but the associated costs were also the highest. Any attempt to use HPLC to produce quantities necessary for test samples would not be viable. Column chromatography was not limited by scale in the same way and was employed as a route to the removal of the oo isomer. However, full separation was not as successful, with the pp and po isomers not separated. The process also remains costly as large volumes of solvents and silica are used. The results from other speculative approaches to crystallisation, whether from solvent or the bulk, did not show promise.

Therefore, it was concluded that it would not be efficient to continue to investigate separation, having exhausted a number of the most commonly employed routes.

4.1.2 Synthetic approach

In order to obtain the individual isomers, a synthetic approach was decided upon. First, a starting point had to be identified. Syntheses of bisphenols is generally achieved by mixing of phenol with a carbonyl containing compound (such as acetone or formaldehyde), in acidic conditions.[1] However, this method produces a mixture of the three isomers. It is this method that is used to produce the mixture as found in DER 354.[2] The literature shows many approaches to individual isomers of bisphenol F.[3–5] There are also routes to selectively catalysing the traditional phenol and aldehyde reaction, such

as with zeolites, in order to adjust the relative amounts of each isomer.[6–9] However, any chemical synthesis takes time to optimise and then complete. Therefore, it was decided to buy the individual bisphenol isomers as they were available at an expensive but not prohibitive price. These would then be epoxidised and then cured and analysed.

Optimisation using bisphenol-A → DGEBA as a model system

Two methods for the epoxidation of bisphenols from the literature were compared as outlined in Scheme 4.1, and optimised using the analogue of bisphenol-F, bisphenol-A, due to its ready availability and low cost.

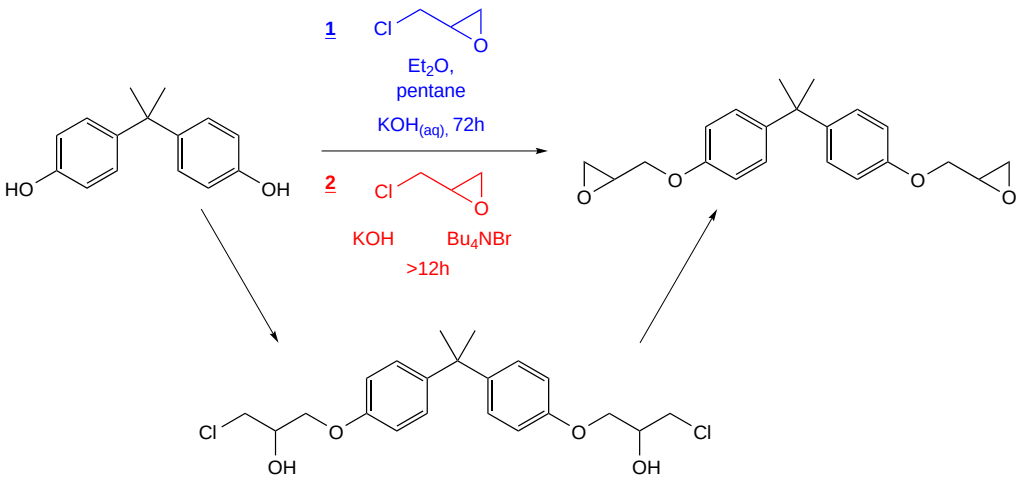

Scheme 4.1: Two methods for the epoxidation of Bisphenol A, showing the intermediate by which the reaction proceeds.

Both methods entail the addition of epichlorohydrin with a potassium hydroxide catalyst. The first is perhaps more conventional in that the potassium hydroxide is made up as an aqueous solution and then added to the bisphenol and epichlorohydrin, and is derived from Wengert *et al.*[10] This method had limited success. ^{1}H NMR spectroscopic analysis of the reaction mixture showed that whilst successfully producing DGEBA (the diglycidyl ether analogue for bisphenol A), there was still a meaningful quantity of reactant in the mixture. In addition, chain extension to longer isomers was also found, as shown in Scheme 4.2.

Adjusting conditions and the concentration of the reactant made no meaningful improvement on this system and therefore the second method was investigated. This

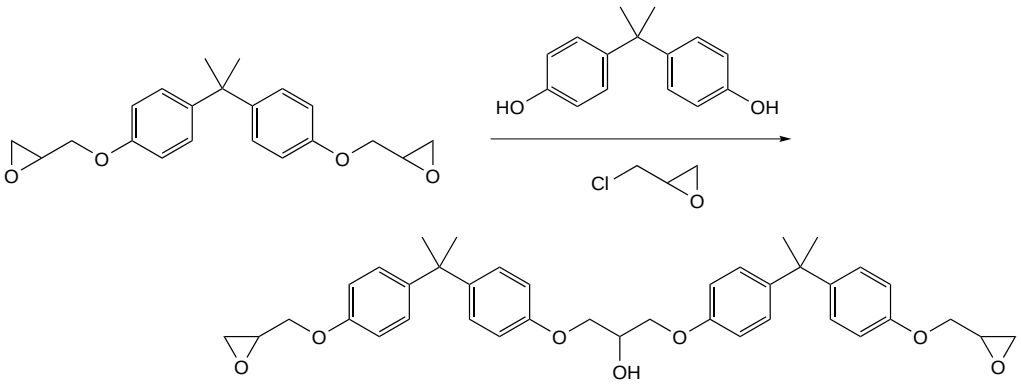

Scheme 4.2: Chain extension of the diglycidyl ether of bisphenol A by a second bisphenol A molecule and epichlorohydrin.

method contains the use of the phase transfer catalyst tetrabutylammonium bromide (TBAB) to partially solubilise the potassium hydroxide in organic solvent, making the need for water superfluous.[11] Hence mixing is much more efficient and indeed the resulting product mixture is much improved. The ^{1}H NMR spectrum showed the product to be mainly DGEBA, with a small amount of chain extension (which would be difficult to eliminate completely) - n $\approx$ 0.1. Assuming all of the substance was product, a 75 % yield was obtained. One final impurity remained, however, identified by 2 peaks in the ^{1}H NMR spectrum at 6.0 and 6.3 ppm. This indicated the presence of a vinyl chloride, with the splitting of the peaks confirming this hypothesis. A reduction in the concentration of hydroxide lead to the removal of this impurity, with a 72 % yield obtained. Finally, it was noted that the workup method might be resulting in lower yields than possible as a result of the presence of TBAB. Within the workup is washing the product with water. Higher concentrations of TBAB solubilise the product in water as it is an amphiphile. Hence, the concentration of TBAB was reduced from 20 mol % (of bisphenol A) to 10 mol %, 5 mol % and 1 mol %. The largest yield obtained was for the 10 mol % formulation, where the 1 mol % caused complete failure. The final optimised yield obtained was 89 %. Further optimisation was deemed unnecessary.

Epoxidation of bisphenol F

Following optimisation, the epoxidation of bisphenol F was completed following a similar method. With the hazards related to epichlorohydrin, it was completed over a number

of different runs. A crude yield of 76 % over eight runs was obtained for ppDGEBF. An improved 87 % yield was obtained for poDGEBF over eight runs and 86 % for ooDGEBF over six runs. Due to the long term air sensitivity of oo-bisphenol F, the runs completed were on a slightly larger scale.

The purity of the three isomers varied somewhat. The ^{1}H NMR spectrum and HPLC chromatogram showed the obtained ppDGEBF to be of good purity, with a small degree of chain extension. There were two main peaks in the HPLC data. The measurement of epoxide equivalent weight (EEW) by titration showed an EEW of 162.3 g mol^{-1}, n = 0.05. If all molecules are considered to be active (i.e. capped by two epoxide groups), then this gives an average n value (for extension) of 0.05. It was decided this was a good level of purity and no further purification would be necessary.

The poDGEBF obtained also gave a ^{1}H NMR spectrum and HPLC chromatogram consistent with the only products being the n=0 isomer and the three possible n=1 isomers (if bonding is considered to be between two bisphenol units, the possibilities are as follows: po-op po-po op-po). However, the EEW was found to be higher, at 170.6 g mol^{-1}, n=0.11.

The ooDGEBF obtained gave analytical results indicating the presence of unwanted material within the product. There were a large number (>10) of distinct signals in the HPLC in the region where chain extended isomers would be expected. We would only expect to see a singular peak in this region as the oo-oo n=1 isomer would be the only molecule produced in any large quantity. The ^{1}H NMR spectrum also showed integrations not consistent with a pure compound. Most notably, the integration of the doublet at 7.35 ppm relative to the epoxide proton multiplet at 2.97 ppm was 0.76 - indicating that there were some other molecules with epoxide functionality within the product mixture. An unassigned broader signal at 4.04-3.92 ppm also showed variability from the spectrum obtained for ooDGEBF obtained from HPLC, as well as broadening of the majority of the expected signals.

Column chromatography of synthesised isomers

Therefore, column chromatography was performed on both the po and oo isomers. Despite the reasonably good results obtained for poDGEBF, it was decided that in order to produce a good comparison between the isomers, the substantial variation in EEW between poDGEBF and ppDGEBF needed to be addressed.

The columned poDGEBF showed a HPLC chromatogram with no peaks in the chain extended region. The EEW was found to be 161.3 g mol^{-1}, which is much more similar to that obtained for ppDGEBF. Also, column chromatography was successful in substantially improving the purity of the ooDGEBF. The ^{1}H NMR spectrum integrations were very close to those obtained for the HPLC-purified equivalent, and HPLC showed some chain extension, but only one peak in the region expected for the chain extended isomers. The EEW was found to be 164.8 g mol^{-1}, $n = 0.07$.

4.2 Methods/Materials

4.2.1 Dow Epoxy Resin 354

Dow Epoxy Resin 354 (DER 354) was obtained from the Olin Corporation and used as supplied. It is the reaction product of bisphenol F and epichlorohydrin.

4.2.2 High performance liquid chromatography (HPLC)

Analytical HPLC system

A Varian Pro Star HPLC system was used, with a 230 pump and a 310 UV detector. The autosampler used was a 410 model, with a 100 μl injection loop. The column (4.6 x 250 mm) was a Waters XBridge™ C18 5 μm. The detector was operated at 280 nm, and the system was run at a flow rate of 1.0 ml min^{-1}. Samples of $\sim$1 mg were dissolved in $\sim$1 cm^3 of acetonitrile, and injected into the column. A 50:50 acetonitrile:water mixture was used for 19 minutes, whereupon the system was moved to 100 % acetonitrile for a further 10 minutes.

Preparatory HPLC system

A Varian Pro Star HPLC system was used, with two 210 pumps and a 320 UV detector. The autosampler used was a 410 model, with a 1000 μl injection loop. The column (19 x 250 mm) was a Waters XBridge™ Prep C18 5 μm OBD. The detector was operated at 280 nm, and the system was run at a flow rate of 17.0 ml min^{-1}. Samples of $\sim$100 mg were dissolved in $\sim$1 cm^3 of acetonitrile, and injected into the column. A 50:50 acetonitrile:water mixture was used for 19 minutes, whereupon the system was moved to 100 % acetonitrile for a further 10 minutes.

4.2.3 Thin layer chromatography

Standard silica thin layer chromatography plates were supplied by Sigma Aldrich Co. LLC. DER 354 and the individual isomers obtained by HPLC were dissolved in ethyl

acetate and spotted onto the silica plates. Mobile phases used were acetone, ethyl acetate, methanol, 1,4-dioxane and ethyl acetate:n-hexane mixtures in ratios ranging from 20:80 to 50:50.

4.2.4 Column chromatography of DER 354

For all columns, Silica (40-63 μm) was obtained from Fisher Scientific and used as supplied.

Initial small-scale DER 354 column

The components of DER 354 (3.5 g) were separated by a standard column chromatography procedure, with a column volume of approximately 700 cm^3. The stationary phase was 0.6 Å silica for flash chromatography. The mobile phase was 35:65 ethyl acetate:hexane. Two main fractions were obtained. The faster eluting fraction (F1) was found to match the ^{1}H NMR spectrum and HPLC chromatogram of ooDGEBF (0.3 g). The slower eluting fraction (F2) was found by ^{1}H NMR and HPLC to be a mixture of poDGEBF and ppDGEBF (1.4 g).

DER 354 column to separate isomers - two runs

The low molecular weight components of DER 354 (11 g) [the isomers of bisphenol F] were separated by a standard column chromatography procedure, with a column volume of approximately 1400 cm^3. The stationary phase was 0.6 Å silica for flash chromatography. The mobile phase was 35:65 ethyl acetate:hexane. As with the initial column, two main fractions were obtained (F1 & F2 - quantities in Table 4.1).

Run	F1	F2
Run 1	1.0 g	5.3 g
Run 2	1.1 g	5.6 g

Table 4.1: Quantities of fractions one and two (F1 and F2) produced in two runs of column chromatography of DER 354 using a 1400 cm^3 column.

DER 354 column to remove higher MW species - four runs

The lower molecular weight components of DER 354 (11 g) were separated from the higher molecular weight components by a standard column chromatography procedure, with a column volume of approximately 1400 cm^3. The stationary phase was 0.6 Å silica for flash chromatography. For runs 1a & b, the mobile phase was 35:65 ethyl acetate:hexane. Overlap between the desired fraction and contaminants (higher MW species) was high and therefore the chromatography was repeated with a more polar mobile phase - runs 2a and b used a mobile phase of 45:55 ethyl acetate:hexane. One main fraction was obtained (F1 - quantities in Table 4.2).

Run	F1
Run 1a	7.3 g
Run 1b	7.5 g
Run 2a	7.6 g
Run 2b	8.1 g

Table 4.2: Quantities of fraction one (F1) produced in two runs of column chromatography of DER 354 using a 1400 cm^3 column.

4.2.5 Nuclear magnetic resonance (NMR) spectroscopy

All nuclear magnetic resonance spectroscopy was completed using a Bruker Avance 400 MHz spectrometer. Chemical shifts are given relative to the lock solvent.

4.2.6 Computational study

The 3 regioisomers of DGEBF were modelled using GaussView 5.0.8, and their energies compared. The models were built using the molecule builder inbuilt into the application and then calculations were performed to find the global energy minimum. Density functional theory, using the B3LYP hybrid functional, was applied with the 6-311G basis set.[12] Solvent-solute interactions were modelled using the polarisation continuum model.[13] This model produces a cavity with solvent specific parameters, rather than

modelling individual solvent molecules. Dichloromethane and acetone were the solvents modelled.

4.2.7 Differential Scanning Calorimetry

DSC measurements were made on a PerkinElmer DSC 8500, and analysis performed on Pyris DSC software. Samples of 5 $\pm$ 2 mg were weighed into an aluminium pan and then measurements taken using the calorimeter.

4.2.8 Optimisation of epoxidation of bisphenol A

Bisphenol A was obtained from Tokyo Chemical Industry UK Ltd., epichlorohydrin (99 %) was obtained from Alfa Aesar, tetrabutylammonium bromide (>98 %) was obtained from Sigma Aldrich Co. LLC. and potassium hydroxide (SLR) was obtained from Fisher Scientific Ltd.

For the following section, all calculations of yield will be simplified by only considering the n = 0 isomer of the bisphenol, irrespective of the complications that have been shown to be present.

Method 1 (biphasic aqueous/organic) run 1

Bisphenol A (2.279 g, 9.98 mmol) was dissolved in epichlorohydrin (8 mL, 102 mmol) and stirred for six hours at room temperature. To this, potassium hydroxide (0.7g, 12.5 mmol) in water (6 mL), pentane (10 mL) and diethyl ether (10 mL) were added. The mixture was stirred for a further 12 hours. The organic layer was separated and washed with water and dried over magnesium sulfate. The solvent and epichlorohydrin were removed under vacuum to give a yellowish resin (2.90 g).

Method 1 run 2

Bisphenol A (2.280 g, 9.99 mmol) was dissolved in epichlorohydrin (8 mL, 102 mmol) and stirred for four days at room temperature. To this, potassium hydroxide (0.77g, 13.7 mmol) in water (6.5 mL), pentane (10.5 mL) and diethyl ether (10.5 mL) were added.

The mixture was stirred for a further four days. The organic layer was separated and washed with water and dried over magnesium sulfate. The solvent and epichlorohydrin were removed under vacuum to give a yellowish resin (2.91 g).

Method 1 run 3

Bisphenol A (2.28 g, 9.99 mmol) was dissolved in epichlorohydrin (8 mL, 102 mmol) and stirred for four days at room temperature. ^{1}H NMR spectra were collected at intervals to measure progress of reaction. No reaction was observed.

Method 1 run 4

Bisphenol A (2.28 g, 9.99 mmol) was dissolved in epichlorohydrin (8 mL, 102 mmol) and stirred for four days at room temperature. To this, potassium hydroxide (1.55 g, 27.6 mmol) in water (10 mL), pentane (10.5 mL) and diethyl ether (10.5 mL) were added. The mixture was stirred for a further four days. The organic layer was separated and washed with water and dried over magnesium sulfate. The solvent and epichlorohydrin were removed under vacuum to give a yellowish resin (2.96 g).

Method 2 (using a phase transfer catalyst) run 1

Ground potassium hydroxide (2.92 g, 52.0 mmol) and tetrabutylammonium bromide (0.70 g, 2.17 mmol) was added with stirring to Bisphenol A (2.280 g, 9.99 mmol) dissolved in epichlorohydrin (8 mL, 102 mmol). This solution was then stirred overnight. Water was added to the solution, and the organic layer separated. The aqueous layer was extracted with diethyl ether three times. The four organic layers were combined and washed three times with water, before drying over magnesium sulfate. Finally the solvent and epichlorohydrin was removed under vacuum to give a yellowish resin (2.69 g, 7.90 mmol, 79 %).

Method 2 run 2

Ground potassium hydroxide (1.548 g, 27.6 mmol) and tetrabutylammonium bromide (0.483 g, 1.49 mmol) was added with stirring to Bisphenol A (1.99 g, 8.72 mmol) dissolved in epichlorohydrin (10 mL, 128 mmol). This solution was then stirred overnight. Water was added to the solution, and the organic layer separated. The aqueous layer was extracted with diethyl ether twice and ethyl acetate once. The four organic layers were combined and washed three times with water, before drying over magnesium sulfate. Finally the solvent and epichlorohydrin was removed under vacuum to give a colourless resin (2.13 g, 6.26 mmol, 72 %).

Method 2 run 3

Ground potassium hydroxide (1.50 g, 26.7 mmol) and tetrabutylammonium bromide (0.32 g, 0.993 mmol) was added with stirring to Bisphenol A (2.00 g, 8.76 mmol) dissolved in epichlorohydrin (10 mL, 128 mmol). This solution was then stirred overnight. Water was added to the solution, and the organic layer separated. The aqueous layer was extracted with diethyl ether twice and ethyl acetate once. The four organic layers were combined and washed three times with water, before drying over magnesium sulfate. Finally the solvent and epichlorohydrin was removed under vacuum to give a colourless resin (2.63 g, 7.73 mmol, 89 %).

Method 2 run 4

Ground potassium hydroxide (1.53 g, 27.3 mmol) and tetrabutylammonium bromide (0.14 g, 0.435 mmol) was added with stirring to Bisphenol A (2.00 g, 8.76 mmol) dissolved in epichlorohydrin (11 mL, 140 mmol). This solution was then stirred overnight. Water was added to the solution, and the organic layer separated. The aqueous layer was extracted with diethyl ether twice and ethyl acetate once. The four organic layers were combined and washed three times with water, before drying over magnesium sulfate. Finally the solvent and epichlorohydrin was removed under vacuum to give a colourless resin (2.40 g, 7.05 mmol, 81 %).

4.2.9 Epoxidation of para-para-bisphenol F

Bisphenol F isomers was obtained from Tokyo Chemical Industry UK Ltd. (pp: >99 %; po: >98 %; oo: >99 %) epichlorohydrin (99 %) was obtained from Alfa Aesar, tetrabutylammonium bromide (>98 %) was obtained from Sigma Aldrich Co. LLC. and potassium hydroxide (SLR) was obtained from Fisher Scientific Ltd. All were used as received, for all three bisphenol epoxidations.

For the following section, all calculations of yield will be simplified by only considering the n = 0 isomer of the bisphenol, irrespective of the complications that have been shown to be present.

Run 1

Ground potassium hydroxide (1.58 g, 28.2 mmol) and tetrabutylammonium bromide (0.312 g, 0.967 mmol) was added with stirring to para-para-Bisphenol F (1.75 g, 8.79 mmol) dissolved in epichlorohydrin (11 mL, 140 mmol). This solution was then stirred for 29 hours. Water was added to the solution, and the organic layer separated. The aqueous layer was extracted with diethyl ether twice and ethyl acetate once. The four organic layers were combined and washed three times with water, before drying over magnesium sulfate. Finally the solvent and epichlorohydrin was removed under vacuum to give an off-white waxy solid (1.58 g, 5.06 mmol, 58 %).

Run 2

Ground potassium hydroxide (1.55 g, 27.6 mmol) and tetrabutylammonium bromide (0.293 g, 0.909 mmol) was added with stirring to para-para-Bisphenol F (1.754 g, 8.76 mmol) dissolved in epichlorohydrin (11 mL, 140 mmol). This solution was then stirred for three days. Water was added to the solution, and the organic layer separated. The aqueous layer was extracted with diethyl ether once and ethyl acetate twice. The four organic layers were combined and washed three times with water, before drying over magnesium sulfate. Finally the solvent and epichlorohydrin was removed under vacuum to give an off-white waxy solid (2.30 g, 7.36 mmol, 58 %).

Runs 3-8

Ground potassium hydroxide (3 g, 54 mmol) and tetrabutylammonium bromide (0.6 g, 1.81 mmol) was added with stirring to para-para-Bisphenol F (3.5 g, 17.5 mmol) dissolved in epichlorohydrin (20 mL, 255 mmol). This solution was then stirred for three to seven days. Water was added to the solution, and the organic layer separated. The aqueous layer was extracted with diethyl ether once and ethyl acetate twice. The four organic layers were combined and washed three times with water, before drying over magnesium sulfate. Finally the solvent and epichlorohydrin was removed under vacuum to give an off-white waxy solid (Average yield 77 %). (Quantities are approximate. See Table 4.3 for exact quantities in each run)

Runs 9-10

Ground potassium hydroxide (6 g, 108 mmol) and tetrabutylammonium bromide (1.2 g, 3.62 mmol) was added with stirring to para-para-Bisphenol F (7 g, 35 mmol) dissolved in epichlorohydrin (40 mL, 510 mmol). This solution was then stirred for three days. Water was added to the solution, and the organic layer separated. The aqueous layer was extracted with diethyl ether once and ethyl acetate twice. The four organic layers were combined and washed three times with water, before drying over magnesium sulfate. Finally the solvent and epichlorohydrin was removed under vacuum to give an off-white waxy solid (Average yield 93 %). (Quantities are approximate. See Table 4.3 for exact quantities in each run)

4.2.10 Epoxidation of para-ortho-bisphenol F

Run 1

Ground potassium hydroxide (1.741 g, 27.0 mmol) and tetrabutylammonium bromide (0.304 g, 0.944 mmol) was added with stirring to para-ortho-Bisphenol F (1.741 g, 8.69 mmol) dissolved in epichlorohydrin (10 mL, 128 mmol). This solution was then stirred for six days. Water was added to the solution, and the organic layer separated. The

Run #	Substance	Mass (g) /Volume (mL) for ECH	Moles	Yield
3	BisF	3.52	1.76×10^{-2}	
	ECH	20	2.55×10^{-1}	
	KOH	3.238	5.77×10^{-2}	
	Bu4NBr	0.584	1.81×10^{-3}	
	DGEBF	4.70	1.50×10^{-2}	86 %
4	BisF	3.557	1.78×10^{-2}	
	ECH	20	2.55×10^{-1}	
	KOH	3.2	5.70×10^{-2}	
	Bu4NBr	0.605	1.88×10^{-3}	
	DGEBF	4.28	1.37×10^{-2}	77 %
5	BisF	3.502	1.75×10^{-2}	
	ECH	20	2.55×10^{-1}	
	KOH	3.036	5.41×10^{-2}	
	Bu4NBr	0.609	1.89×10^{-3}	
	DGEBF	3.627	1.16×10^{-2}	66 %
6	BisF	3.511	1.75×10^{-2}	
	ECH	20	2.55×10^{-1}	
	KOH	2.993	5.33×10^{-2}	
	Bu4NBr	0.594	1.84×10^{-3}	
	DGEBF	4.547	1.46×10^{-2}	83 %
7	BisF	3.509	1.75×10^{-2}	
	ECH	20	2.55×10^{-1}	
	KOH	2.982	5.32×10^{-2}	
	Bu4NBr	0.587	1.82×10^{-3}	
	DGEBF	4.598	1.47×10^{-2}	84 %
8	BisF	2.975	1.49×10^{-2}	
	ECH	20	2.55×10^{-1}	
	KOH	2.55	4.54×10^{-2}	
	Bu4NBr	0.51	1.58×10^{-3}	
	DGEBF	4.118	1.32×10^{-2}	89 %
9	BisF	7.034	3.51×10^{-2}	
	ECH	40	5.10×10^{-1}	
	KOH	6.016	1.07×10^{-2}	
	Bu4NBr	1.196	3.71×10^{-3}	
	DGEBF	10.289	3.29×10^{-2}	94 %
10	BisF	7.001	3.50×10^{-2}	
	ECH	30	5.10×10^{-1}	
	KOH	6.000	1.07×10^{-2}	
	Bu4NBr	1.200	3.72×10^{-3}	
	DGEBF	10.162	3.29×10^{-2}	93 %

Table 4.3: Quantities of reagents used and percentage yields of runs 3-10 of the epoxidation of para-para-bisphenol F

aqueous layer was extracted with diethyl ether twice and ethyl acetate once. The four organic layers were combined and washed three times with water, before drying over magnesium sulfate. Finally the solvent and epichlorohydrin was removed under vacuum to give a colourless resin (1.987 g, 6.36 mmol, 73 %).

Runs 2-8

Ground potassium hydroxide (3 g, 54 mmol) and tetrabutylammonium bromide (0.6 g, 1.81 mmol) was added with stirring to para-para-Bisphenol F (3.5 g, 17.5 mmol) dissolved in epichlorohydrin (20 mL, 255 mmol). This solution was then stirred for six to ten days. Water was added to the solution, and the organic layer separated. The aqueous layer was extracted with diethyl ether once and ethyl acetate twice. The four organic layers were combined and washed three times with water, before drying over magnesium sulfate. Finally the solvent and epichlorohydrin was removed under vacuum to give a yellowish clear resin (Average yield 87 %). (Quantities are approximate. See Table 4.4 for exact quantities in each run) Column chromatography was performed in order to purify this solid (Section 4.2.12). This yielded a yellowish liquid which slowly solidified (over a few hours) to an off-white waxy solid (10.9290 g)

Run #	Substance	Mass (g) /Volume (mL) for ECH	Moles	Yield
2	BisF	3.5142	1.76×10^{-2}	
	ECH	20	2.55×10^{-1}	
	KOH	2.9951	5.34×10^{-2}	
	Bu4NBr	0.6042	1.87×10^{-3}	
	DGEBF	4.4507	1.42×10^{-2}	81%
3	BisF	3.5222	1.76×10^{-2}	
	ECH	20	2.55×10^{-1}	
	KOH	2.9744	5.30×10^{-2}	
	Bu4NBr	0.5981	1.86×10^{-3}	
	DGEBF	3.062	9.80×10^{-3}	56%
4	BisF	3.6135	1.80×10^{-2}	
	ECH	20	2.55×10^{-1}	
	KOH	2.9965	5.34×10^{-2}	
	Bu4NBr	0.6375	1.98×10^{-3}	
	DGEBF	4.82	1.54×10^{-2}	86%
5	BisF	3.4854	1.74×10^{-2}	
	ECH	20	2.55×10^{-1}	
	KOH	3.0423	5.42×10^{-2}	
	Bu4NBr	0.6141	1.90×10^{-3}	
	DGEBF	4.45	1.42×10^{-2}	82%
6	BisF	3.5529	1.77×10^{-2}	
	ECH	20	2.55×10^{-1}	
	KOH	3.0414	5.42×10^{-2}	
	Bu4NBr	0.5964	1.85×10^{-3}	
	DGEBF	5.15	1.65×10^{-2}	93%
7	BisF	3.4934	1.74×10^{-2}	
	ECH	20	2.55×10^{-1}	
	KOH	3.03	5.40×10^{-2}	
	Bu4NBr	0.6047	1.88×10^{-3}	
	DGEBF	4.97	1.59×10^{-2}	91%
8	BisF	3.422	1.71×10^{-2}	
	ECH	20	2.55×10^{-1}	
	KOH	2.9201	5.20×10^{-2}	
	Bu4NBr	0.5864	1.82×10^{-3}	
	DGEBF	4.99	1.60×10^{-2}	92%

Table 4.4: Quantities of reagents used and percentage yields of runs 2-8 of the epoxidation of para-ortho-bisphenol F

4.2.11 Epoxidation of ortho-ortho-bisphenol F

Runs 1-7

Ground potassium hydroxide (reactants in same ratio but varying quantities in each run – see Table 4.5) and tetrabutylammonium bromide was added with stirring to ortho-ortho-Bisphenol F dissolved in epichlorohydrin. This solution was then stirred for six days. Water was added to the solution, and the organic layer separated. The aqueous layer was extracted with diethyl ether twice and ethyl acetate once. The four organic layers were combined and washed three times with water, before drying over magnesium sulfate. Finally the solvent and epichlorohydrin was removed under vacuum to give an off-white waxy solid (average yield 86%). Column chromatography was performed in order to purify this solid (Section 4.2.12). This yielded a white solid (10.6628 g).

4.2.12 Column chromatography of ortho-ortho- and para-ortho-DGEBF

para-ortho-DGEBF

Crude poDGEBF (see Table 4.6 for quantities used per run) was purified by a standard column chromatography procedure, with a column volume of approximately 1400 cm^3. The stationary phase was 0.6 Å silica for flash chromatography. The mobile phase was 35:65 ethyl acetate:hexane. The total poDGEBF obtained was 10.9290 g.

ortho-ortho-DGEBF

Crude ooDGEBF (see Table 4.7 for quantities used per run) was purified by a standard column chromatography procedure, with a column volume of approximately 1400 cm^3. The stationary phase was 0.6 Å silica for flash chromatography. The mobile phase was 35:65 ethyl acetate:hexane. The total ooDGEBF obtained was 10.6628 g.

4.2.13 Titration for epoxide equivalent weight[2]

Titration for epoxide equivalent weight was performed as in Chapter 2—see Section 2.2.2.

Run #	Substance	Mass (g) /Volume (mL) for ECH	Moles	Yield
1	BisF	1.7251	8.62 x 10-3	
	ECH		1.28 x 10-1	
	KOH	1.53	2.73 x 10-2	
	Bu4NBr	0.3118	9.67 x 10-4	
	DGEBF	2.3627	7.56 x 10-3	88%
2	BisF	2.7307	1.36 x 10-2	
	ECH		2.55 x 10-1	
	KOH	2.3316	4.16 x 10-2	
	Bu4NBr	0.4751	1.47 x 10-3	
	DGEBF	4.07	1.30 x 10-2	96%
3	BisF	2.4127	1.20 x 10-2	
	ECH		2.55 x 10-1	
	KOH	2.1062	3.75 x 10-2	
	Bu4NBr	0.4147	1.29 x 10-3	
	DGEBF	3.23	1.03 x 10-2	86%
4	BisF	3.52	1.76 x 10-2	
	ECH		2.55 x 10-1	
	KOH	3.0281	5.40 x 10-2	
	Bu4NBr	0.6031	1.87 x 10-3	
	DGEBF	4.69	1.50 x 10-2	85%
5	BisF	3.4985	1.75 x 10-2	
	ECH		2.55 x 10-1	
	KOH	3.0252	5.39 x 10-2	
	Bu4NBr	0.5981	1.86 x 10-3	
	DGEBF	4.71	1.51 x 10-2	86%
6	BisF	3.3872	1.69 x 10-2	
	ECH		2.55 x 10-1	
	KOH	2.97	5.29 x 10-2	
	Bu4NBr	0.57706	1.79 x 10-3	
	DGEBF	4.1	1.31 x 10-2	78%

Table 4.5: Quantities of reagents used and percentage yields of runs 2-8 of the epoxidation of para-ortho-bisphenol F

	Crude loaded (approx)	Product obtained
Run 1	8 g	5.91 g
Run 2	7 g	5.03 g

Table 4.6: Amount of poDGEBF obtained from two runs of column chromatography using a 1400 cm^3 column.

	Crude loaded (approx)	Product obtained
Run 1	10 g	5.58 g
Run 2	11 g	5.12 g

Table 4.7: Amount of ooDGEBF obtained from two runs of column chromatography using a 1400 cm^3 column.

References

[1] Grüttner, C., Boehmer, V., Assmus, R. & Scherf, S. A convenient and general synthesis of alkanediyl diphenols. *Journal of the Chemical Society, Perkin Transactions 1*, (2), 93 (1995).

[2] Cameron, C. Private communication. *AkzoNobel* (2014).

[3] Hejaz, H. A. M., Woo, L. W. L., Purohit, A., Reed, M. J. & Potter, B. V. L. Synthesis, in vitro and in vivo activity of benzophenone-based inhibitors of steroid sulfatase. *Bioorganic & medicinal chemistry*, **12**(10), 2759–72 (2004).

[4] Buehler, C. A., Cooper, D. E. & Scrudder, E. O. The stability of 2,2'-dihydroxydiphenylmethane. *Journal of Organic Chemistry*, **8**, 316–319 (1943).

[5] Casiraghi, G., Casnati, G., Cornia, M., Pochini, A., Sartori, G. & Ungaro, R. Selective reactions using metal phenoxides. Part 2. Reactions with aromatic alcohols. *Journal of the Chemical Society, Perkin Transactions 1*, (4), 322 (1978).

[6] Smith, K., Alotaibi, M. H. & El-Hiti, G. A. Highly regioselective dinitration of toluene over reusable zeolite Hβ. *Journal of Catalysis*, **297**, 244–247 (2013).

[7] Jana, S. K., Okamoto, T., Kugita, T. & Namba, S. Selective synthesis of bisphenol F catalyzed by microporous H-beta zeolite. *Applied Catalysis A: General*, **288**(1-2), 80–85 (2005).

[8] Dubois, R. A., Malzman, A. J. & Ohnishi, H. Epoxy resins comprising moieties derived from high ortho bisphenol F. (1997).

[9] Tan, Y., Li, Y., Wei, Y., Wu, Z., Yan, J., Pan, L. & Liu, Y. The hydroxyalkylation of phenol with formaldehyde over mesoporous M(Al, Zr, Al–Zr)-SBA-15 catalysts: The effect on the isomer distribution of bisphenol F. *Catalysis Communications*, **67**, 21–25 (2015).

[10] Wengert, M., Sanseverino, A. M. & de Mattos, M. C. S. Trichloroisocyanuric acid: an alternate green route for the transformation of alkenes into epoxides (2002).

[11] Zhou, Y., Jiang, C., Zhang, Y., Liang, Z., Liu, W., Wang, L., Luo, C., Zhong, T., Sun, Y., Zhao, L., Xie, X., Jiang, H., Zhou, N., Liu, D. & Liu, H. Structural optimization and biological evaluation of substituted bisphenol A derivatives as beta-amyloid peptide aggregation inhibitors. *Journal of medicinal chemistry*, **53**(15), 5449–66 (2010).

[12] Becke, A. D. Density-functional thermochemistry. III. The role of exact exchange. *The Journal of Chemical Physics*, **98**(7), 5648 (1993).

[13] Miertuš, S., Scrocco, E. & Tomasi, J. Electrostatic interaction of a solute with a continuum. A direct utilizaion of AB initio molecular potentials for the prevision of solvent effects. *Chemical Physics*, **55**(1), 117–129 (1981).

Chapter 5

Networks produced using purer epoxy resin monomers

5.1 Results/Discussion

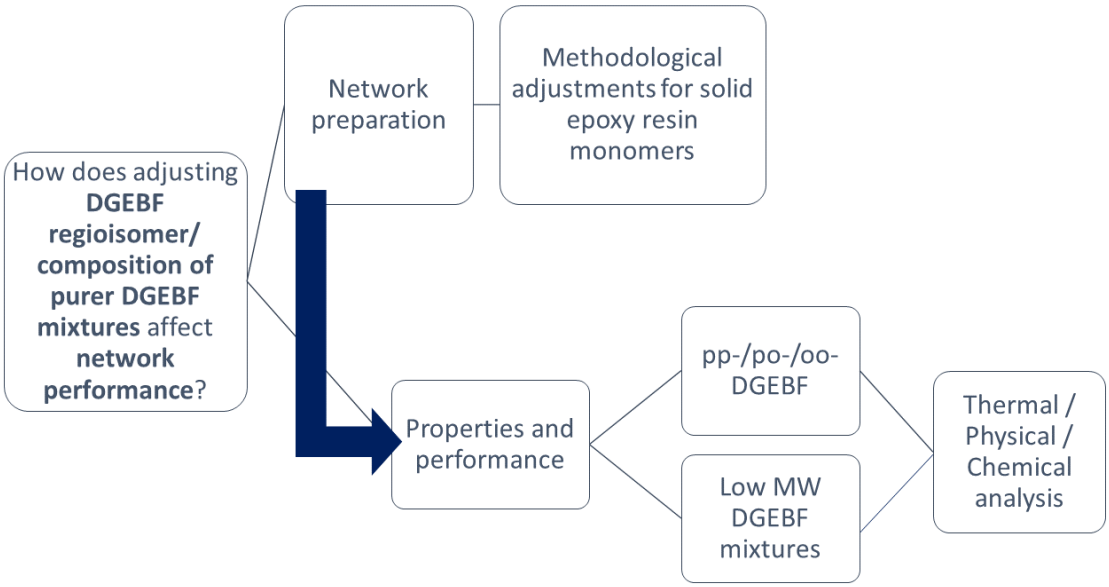

In Chapter 4, separatory and synthetic routes were explored to isolate the different components of DER 354. The three isomers of diglycidyl ether of bisphenol F (DGEBF—Figure 5.1) were synthesised, and the high molecular weight components of DER 354 were removed to yield three different isomeric compositions of n = 0 isomers. These six different isolated mixtures are summarised in Tables 5.1 & 5.2. This chapter will investigate the properties obtained from networks made with these epoxy resin monomers and meta-xylylenediamine (MXDA).

	pp	**po**	**oo**
EEW /g mol^{-1}	164.8	161.3	162.3
n	0.07	0.04	0.05

Table 5.1: The epoxide equivalent weights of the synthesised isomers of DGEBF, and the degree of chain extension (as described by n value) that the EEW corresponds to.

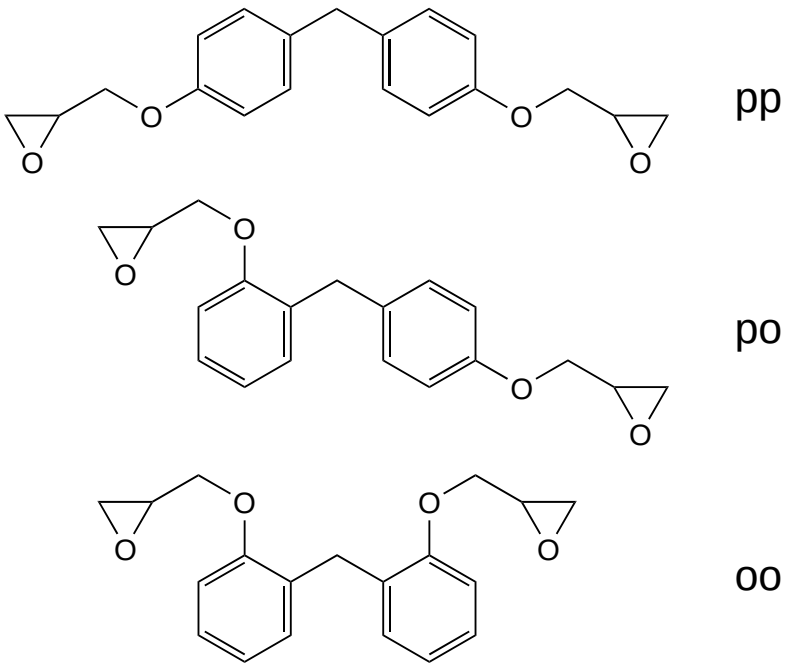

Figure 5.1: The three isomers of DGEBF: para-para- (pp), para-ortho- (po) & ortho-ortho- (oo)

	pppo	**LM37**	**LM33**
EEW /g mol^{-1}	159.4	162.6	162.4
n	0.03	0.05	0.05
pp : po : oo	45 : 52 : 03	37 : 47 : 16	33 : 50 : 17

Table 5.2: Epoxide equivalent weights (& corresponding degree of chain extension) and pp : po : oo ratios for the chromatographically purified DGEBF mixtures. LM33 & LM37 represent the two low molecular weight (LM) samples with differing pp : po : oo ratios, where the number represents the proportion of pp.

5.1.1 Network preparation

Methodological considerations

As has been shown in the Section 3.1.2, the physical state of reactive components will impact on the method that can be used to produce a uniform network. For the DER 354 / PXDA network (where PXDA is a solid amine), the mixing method and pot conditions were adjusted to a higher temperature to prevent recrystallisation. In this chapter all networks were prepared using the liquid amine MXDA, but with an adjusted method relative to Chapters 2 & 3

All of the isolated isomers were found to be solid, rather than liquid. Both the tendency to crystallise and melting points of the chemistries produced varied markedly. The least waxy and highest melting isomer was the oo, with a melting peak in the DSC trace at $\sim$80 °C. The pp showed a lower melting peak at $\sim$60°C, and recrystallisation of the whole sample after removing from heat generally required a few minutes. If left to reach equilibrium, the po would eventually crystallise, though this process is of the order of days. As shown in Section 4.1.1, the po appears as a liquid resin after evaporation of solvent or melting. As would then be expected, increased po content led to a waxier and therefore less likely to crystallise substance for the three isomeric mixtures described in Table 5.2. In all cases, for these mixtures, crystallisation was markedly slower than for the pure pp or oo isomers.

In order to ensure that the chance of recrystallisation was minimal for all network formulations, an elevated pot temperature was used (that is the temperature the reactive mixture was held at prior to cure). For all but the oo isomer, this was 33 °C; for the oo it was 40 °C. Where any clouding was observed, the mixture was heated to melting, before rapidly returning to the pot temperature. Effective control of temperature was crucial to prevent a runaway exothermic reaction, which would prevent the preparation of appropriate samples for testing. Where too high a temperature was used ($>$50 °C) the pot-time was shorter than ten minutes. In all cases the heated drawdown block (as described in Section 3.1.2) was used to drawdown onto slides held at 30 °C.

The oo presented a particularly high propensity to crystallise even when held at

40 °C. Instead of heating at the first observation of clouding, as much reaction as possible was allowed to complete (almost complete recrystallisation), before re-melting with a heat gun. Cooling back to 40 °C as soon as melting had occurred was crucial in avoiding runaway reaction. Although oo samples were successfully prepared, there were insufficient samples for ethanol measurements.

NIR spectroscopy

As in Chapter 3, no new extinction coefficients need to be calculated, since the local chemical environment of the epoxide is identical in all of the epoxides used, with the chemical structure as a whole only adjusted very slightly. The conversions for all networks produced were in excess of 97 % and are shown in Table 5.3. The slightly reduced degree of cure obtained for ooDGEBF and the LM37 might be expected to cause a slight reduction in properties, but not a dramatic shift (as is illustrated in Figure 2.27).

Epoxy	Amine	Final Conversion
pp	MXDA	100.0 %
po	MXDA	100.0 %
oo	MXDA	97.3 %
pppo	MXDA	100.0 %
LM33	MXDA	99.9 %
LM37	MXDA	98.1 %

Table 5.3: The epoxide conversion obtained for each network prepared by NIR spectroscopy

5.1.2 Properties and performance

The below analyses will generally be divided into two main sections—comparing the isolated isomers first and then the chromatographically purified mixtures. However, the pppo mixture will be included in both comparisons, to observe the impact of introducing limited complexity to purer systems.

Thermal and physical properties

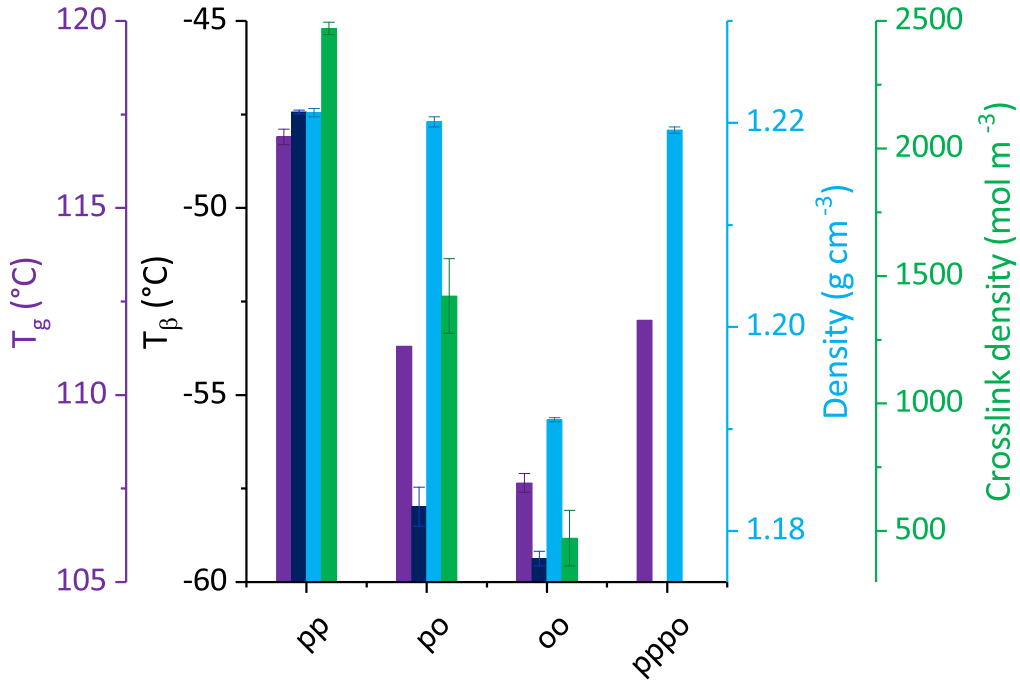

*Figure 5.2: The T_g, T_β, crosslink density (all as found by DMA) and density (as found by helium pycnometry) of the networks prepared with the isolated isomers of DGEBF (and MXDA). Error bars show standard error of three measurements for the values obtained by DMA, and standard deviation of ten measurements of a single sample for density. *There was insufficient sample to obtain T_β and crosslink density data for the pppo resin*

Figure 5.2 shows the extensive variation between network properties for the networks prepared with the regioisomers of DGEBF (and MXDA). T_g is shown to decrease with increasing ortho- content (as was suggested in Section 3.1.3). Similarly, there is a decrease in T_β, indicating that the energetic barrier to molecular motion is lower in the ortho- containing isomers. The area of the β-transition was found to be heavily reduced

for the network based on oo isomer (Figure 5.3), relative to the (very similar to one another) pp and po isomers—this suggests that there is a molecular motion related to the para- phenylene ring which is not possible for the ortho- substituted rings—Tu *et al.* show that there is a phenylene ring flip in DGEBA based resins.[1] Density is very similar for the networks based on the pp and po isomers (as well as the mixture of those two isomers-pppo), but is much lower for the oo based network. This indicates that the space filling of the bisphenol moiety in a network is substantially limited by adjacent ortho- substitution. Finally, crosslink density is also shown to decrease with increasing ortho- content. The picture this presents is that whilst molecular motion is limited, the oo network is less well-packed than networks produced with para- containing isomers. The change in T_β between po and pp based networks suggests the ortho- rings have an impact upon the onset of the phenylene motion.

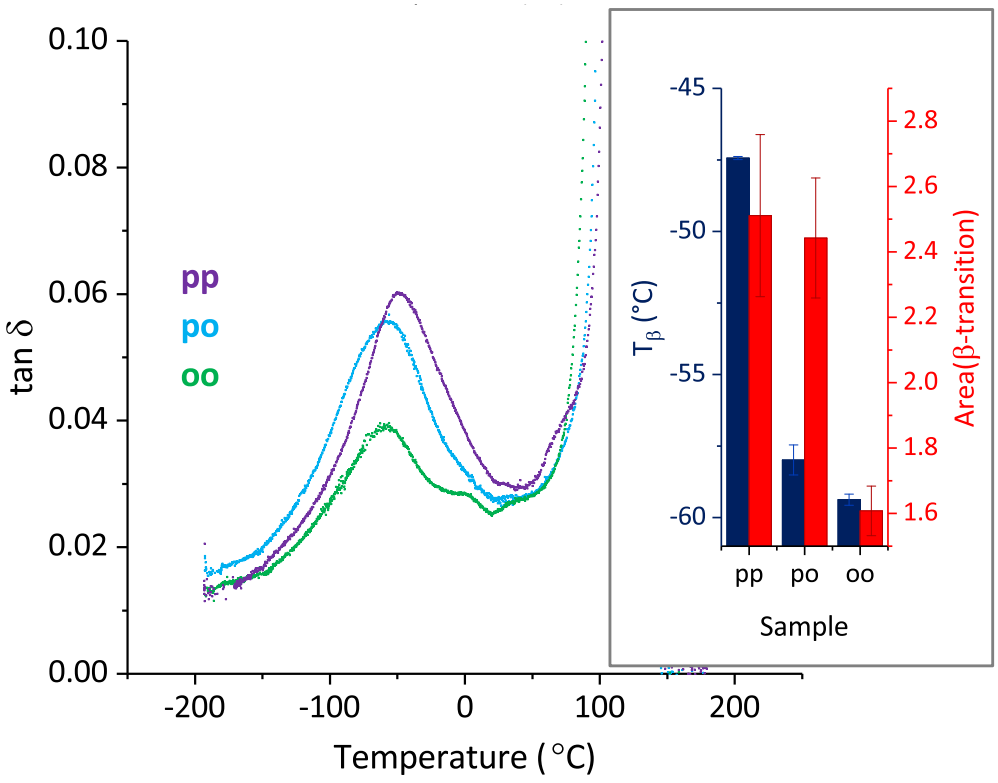

Figure 5.3: DMA traces of tan δ against temperature for networks prepared with the isomers of DGEBF (and MXDA), showing the response for the β-transition. Inset: The T_β and area of the β-transition for those networks. Error bars show standard error of two samples

For the networks based on chromatographically purified DGEBF mixtures, the varia-

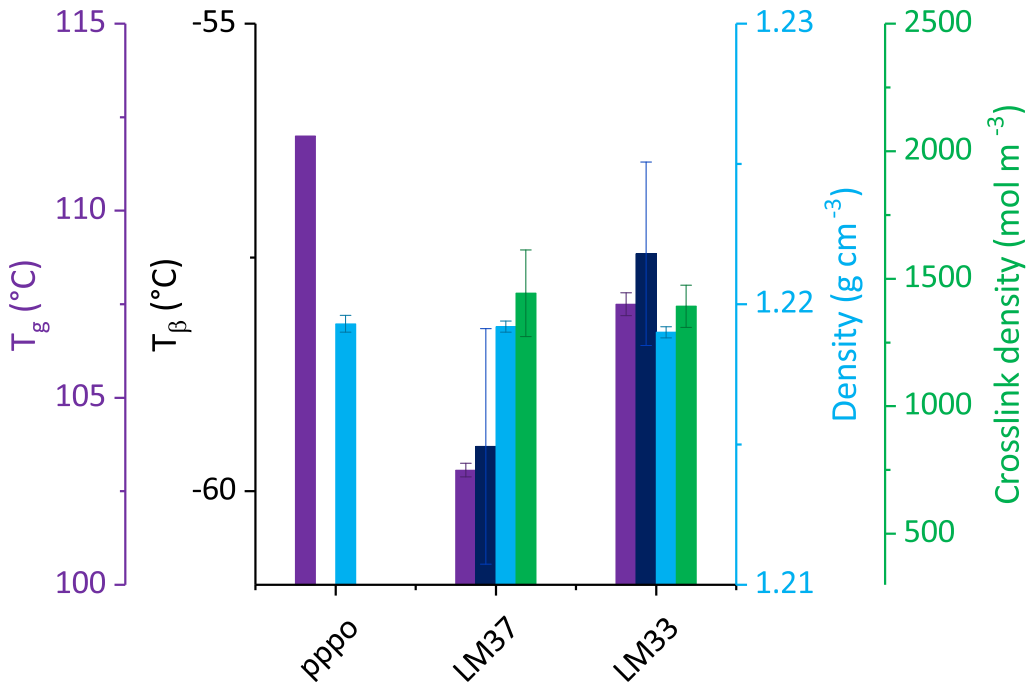

*Figure 5.4: The T_g, T_β, crosslink density (all as found by DMA) and density (as found by helium pycnometry) of the networks prepared with the chromatographically purified DGEBF mixtures (and MXDA). Error bars show standard error of three measurements for the values obtained by DMA, and standard deviation of ten measurements of a single sample for density. *There was insufficient sample to obtain T_β and crosslink density data for the pppo network*

tion was much more limited (Figure 5.4). There is no change in density although perhaps unexpectedly, the T_g and T_β are shown to decrease as ortho- content decreases (LM33 vs LM37), though the areas of β-transition were found to be very similar. The basis for this decrease in T_g might lie in the slightly reduced degree of cure found for the LM37 network, which was found to be 98.1 %

There is no significant change in crosslink density—it is higher for the LM37 but within error.

Methanol uptake

DGEBF isomers The uptake of methanol for the networks prepared with the individual isomers of DGEBF in Figure 5.5, shows some unexpected trends. Unusually the trends in sorption and desorption diffusion coefficients (D_{sor} and D_{des} respectively) are the opposite of one another. The lowest D_{sor} value was obtained for ppDGEBF / MXDA, which also had the lowest ultimate uptake. The oo isomer had the highest D_{sor} and ultimate uptake, with a large increase in both relative to the changes observed across this work. poDGEBF / MXDA showed an intermediate value for both. The network based on the mixture of po and pp isomers (pppo) exhibited very similar properties to that of the pure poDGEBF. However, the highest D_{des} was obtained from the network based on ppDGEBF, then the pppo, then the po and finally the oo had the lowest.

As is shown in Figure 5.5, the sorption profiles of the po and pppo networks are dissimilar to one another, but yield very similar parameters. Further, the initial uptake for all of the networks based on each of the pure isomers (pp/po/oo) are initially very similar but marked changes become evident from 500 $s^{\frac{1}{2}}$. Figure 5.6 shows the profile changes more clearly. In the case of pppo, (Figure 5.6a), the sorption is of the two-step mode, which is contrasted to the Fickian behaviour observed for ppDGEBF. As explored for Epikote 828 / MXDA in Section 3.1.3, this is attributed to a heterogeneous network structure, where there are regions of differing accessibility for the solvent. This is conceivable, as the network consists of the pp and po isomers in an approximately equal ratio, which are shown in this study to perform differently to one another. As with the comparison of the networks based on E828 and DER 332, the gradient of the second "step" of sorption for the two-step system is similar to the initial gradient of the Fickian system. This suggests regions richer in po uptake faster, and then the regions richer in pp uptake in that second step.

Figure 5.6b shows the varied performance of the three isomers—what is immediately clear is the sigmoidal nature of the uptake for the po and oo isomers relative to the Fickian ppDGEBF. This mode is attributed to swelling processes, which the oo network is most susceptible to (since it has the largest change in gradient).

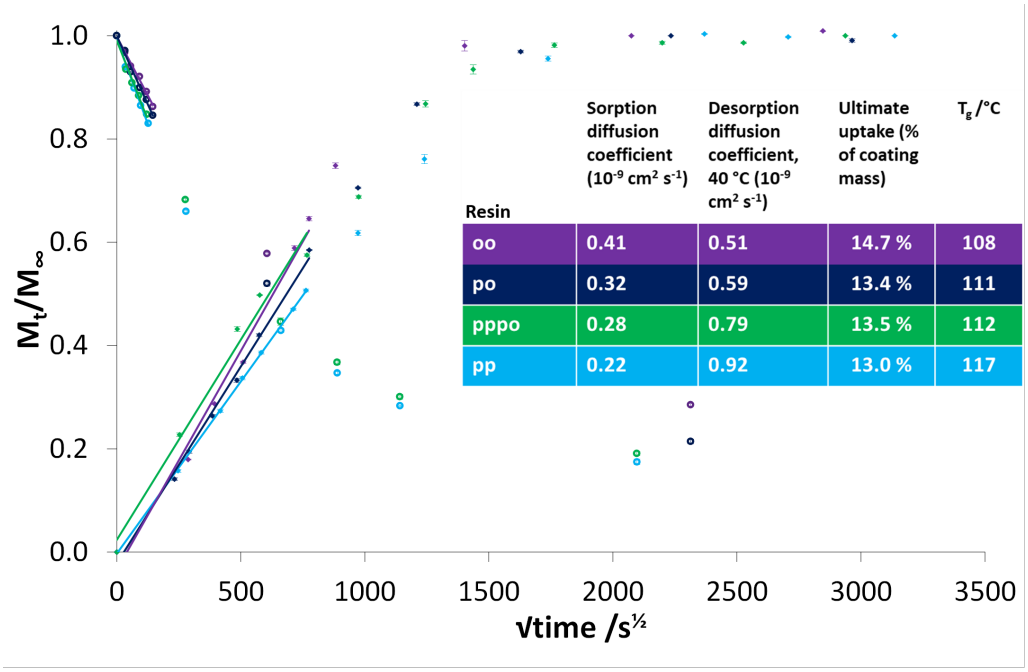

Resin	Sorption diffusion coefficient (10^{-9} cm^2 s^{-1})	Desorption diffusion coefficient, 40 °C (10^{-9} cm^2 s^{-1})	Ultimate uptake (% of coating mass)	T_g /°C
oo	0.41	0.51	14.7 %	108
po	0.32	0.59	13.4 %	111
pppo	0.28	0.79	13.5 %	112
pp	0.22	0.92	13.0 %	117

(a) Methanol sorption and desorption of DGEBF / MXDA networks on glass slides made with the different isomers of DGEBF (para-para- (pp), para-ortho- (po) and ortho-ortho (oo)), and an approximately even mixture of pp and po DGEBF (pppo). Sorption begins at the origin with a positive slope and desorption at $\frac{M_t}{M_\infty} = 1$, with a negative slope. Error bars show standard error from three samples. The diffusion coefficients, D, were calculated from the gradient of the initial linear fits and are shown in the inset table. Ultimate uptake and glass transition temperature, T_g, are shown for each sample.

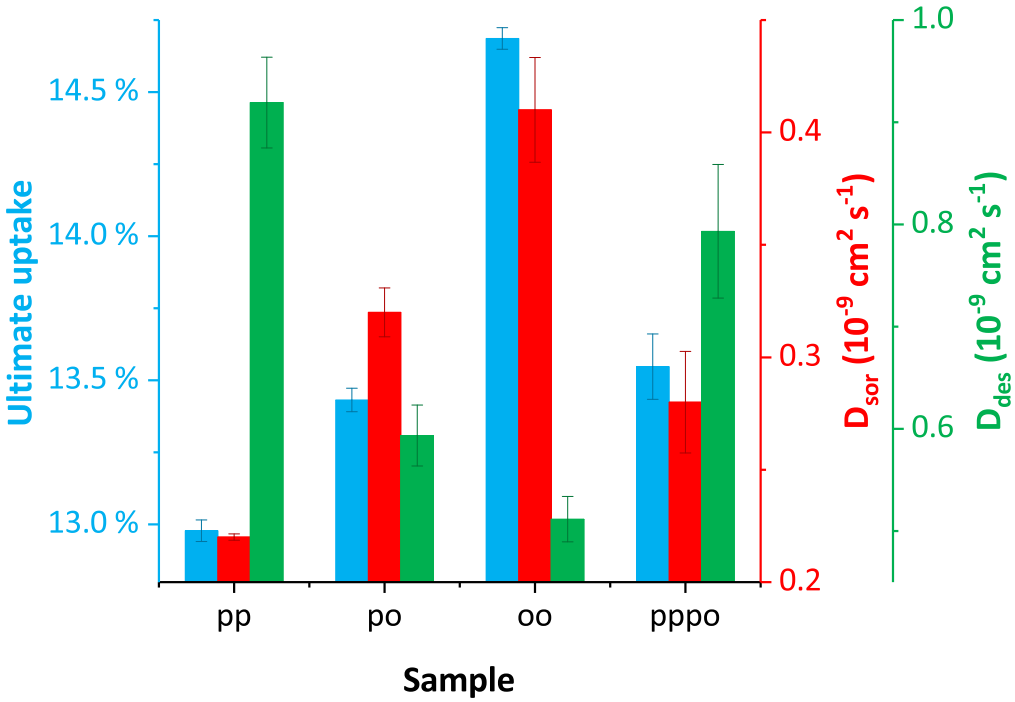

(b)

Figure 5.5: Summary of methanol uptake parameters for networks of the different isomers (pp, po & oo) of DGEBF and an approximately even mixture of pp and po DGEBF (pppo) (cured with MXDA). Error bars show standard error of three samples.

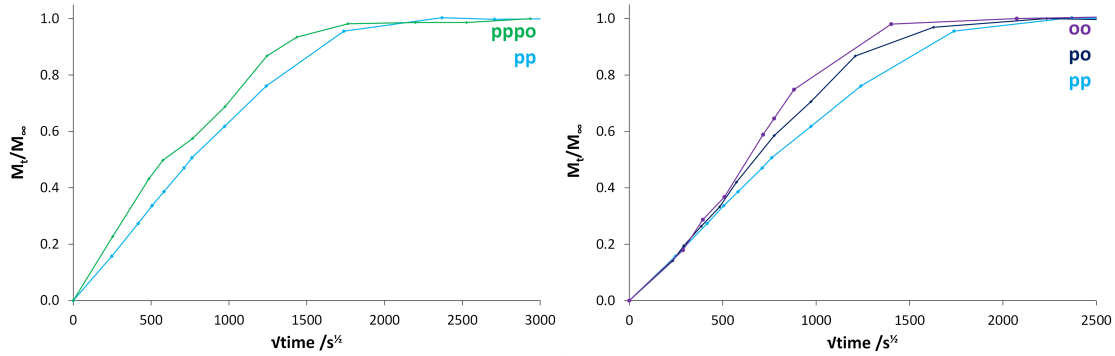

Figure 5.6: Methanol sorption of DGEBF / MXDA networks made with the different isomers of DGEBF (para-para- (pp), para-ortho- (po) and ortho-ortho (oo)), and an approximately even mixture of pp and po DGEBF (pppo). The individual data points are shown joined with straight lines.

Chromatographically purified DGEBF mixtures Figure 5.7a shows the similarity of the networks based on the two chromatographically purified DGEBF mixtures, LM33 and LM37. When considered with the pppo based network, D_{sor} is observed to decrease slightly for the lower ortho- content LM37, and then still further for the pppo based network. Ultimate uptake shows a slight minimum with the LM37 sample. If compared to the pure isomers, the performance is intermediate between the po and oo based networks in terms of rate of sorption, but in terms of ultimate uptake, the LM37 is only inferior to the pp network. The LM33 network shows a similar performance to the po & pppo networks. In the context of the measured T_g, this is perhaps unexpected, though the degree of cure by NIR was found to be high (>99.5 %) so provides more evidence for the finding in Chapter 2, that T_g accurately illustrates degree of cure at high conversions.

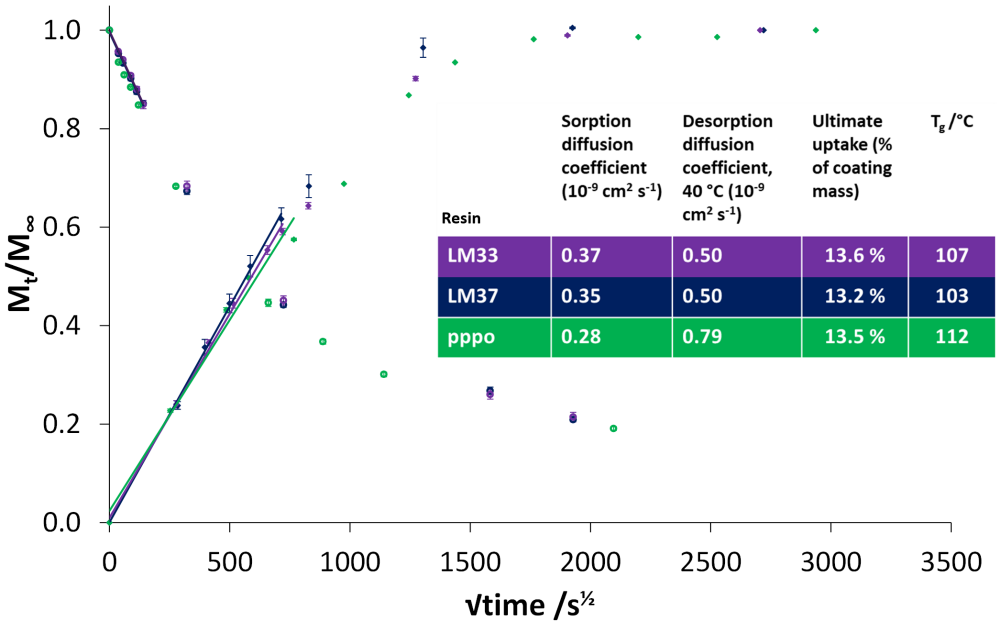

Resin	Sorption diffusion coefficient (10^{-9} cm^2 s^{-1})	Desorption diffusion coefficient, 40 °C (10^{-9} cm^2 s^{-1})	Ultimate uptake (% of coating mass)	T_g /°C
LM33	0.37	0.50	13.6 %	107
LM37	0.35	0.50	13.2 %	103
pppo	0.28	0.79	13.5 %	112

(a) Methanol sorption and desorption of DGEBF / MXDA networks on glass slides made with the chromatographically purified DGEBF mixtures (LM33 & LM37), and an approximately even mixture of pp and po DGEBF (pppo). Sorption begins at the origin with a positive slope and desorption at $\frac{M_t}{M_\infty} = 1$, with a negative slope. Error bars show standard error from three samples. The diffusion coefficients, D, were calculated from the gradient of the initial linear fits and are shown in the inset table. Ultimate uptake and glass transition temperature, T_g, are shown for each sample.

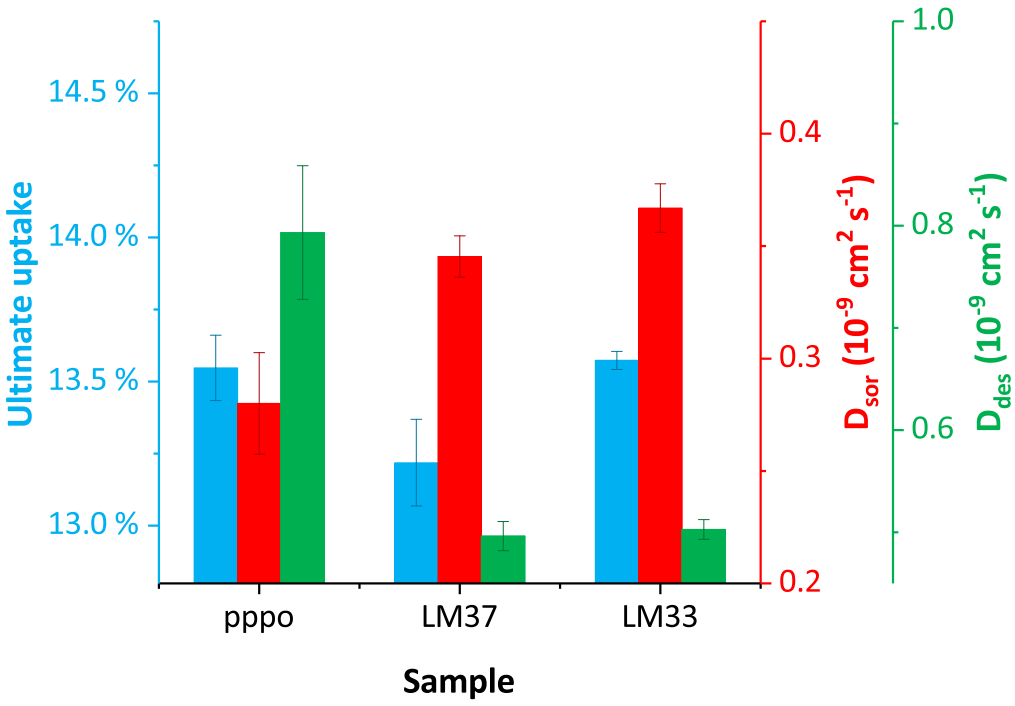

(b) Summary of methanol uptake parameters for networks made with the chromatographically purified DGEBF mixtures (LM33 & LM37), and an approximately even mixture of pp and po DGEBF (pppo) (cured with MXDA). Error bars show standard error of three samples.

Figure 5.7

Ethanol uptake

DGEBF isomers Ethanol uptake data was only possible for the pp, po and pppo samples, due to the added difficulties in preparing the ooDGEBF network. The worst performing was the poDGEBF, which not only showed increased uptake relative to the other two, but wholescale failure was visible in the form of cracking (as is shown inset in Figure 5.8). This cracking was different to that observed for air cured DER 354 / MXDA systems—for poDGEBF it was much more prevalent, where the DER 354 based samples only showed isolated star cracks.

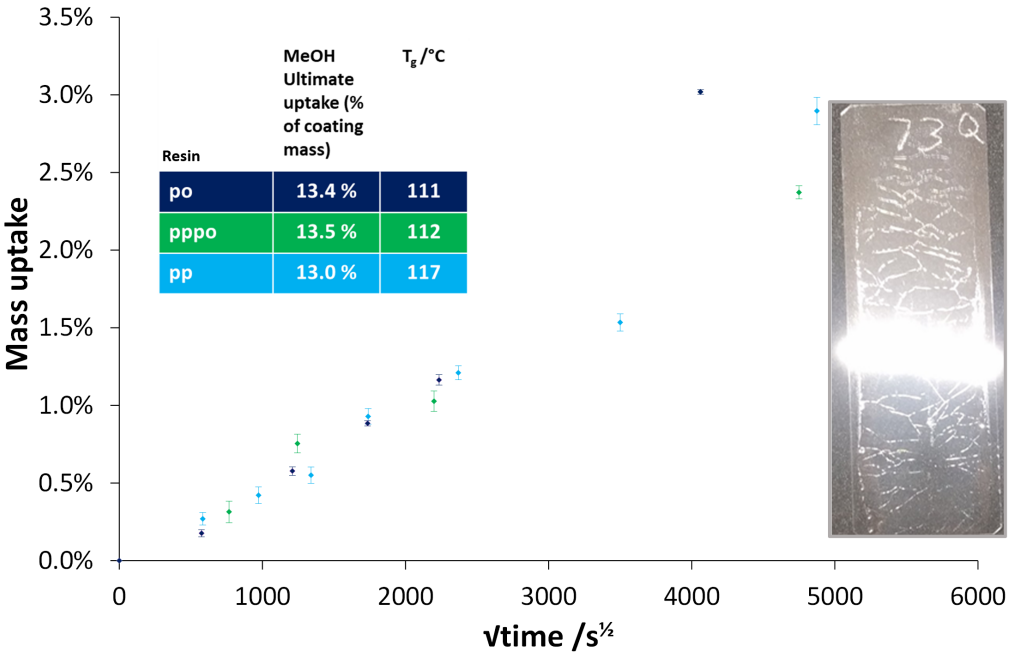

Figure 5.8: Ethanol sorption for networks made with pp- and po- DGEBF and an approximately equal ratio of those two isomers (pppo) (all cured with MXDA). For reference, the methanol ultimate uptake and T_g for each sample is shown. Error bars show standard error of three samples. Inset: cracking observed in po samples after ∼190 days. Slide is 26mm wide.

Chromatographically purified DGEBF mixtures Ethanol uptake appeared similar between the networks based on the low molecular weight mixtures LM37 and LM33, but they performed better than the pppo, especially at short times. The rate of sorption after 1500 $s^{\frac{1}{2}}$ did accelerate. Further measurements would be required to draw firm conclusions—time limitations meant a full analysis was not possible.

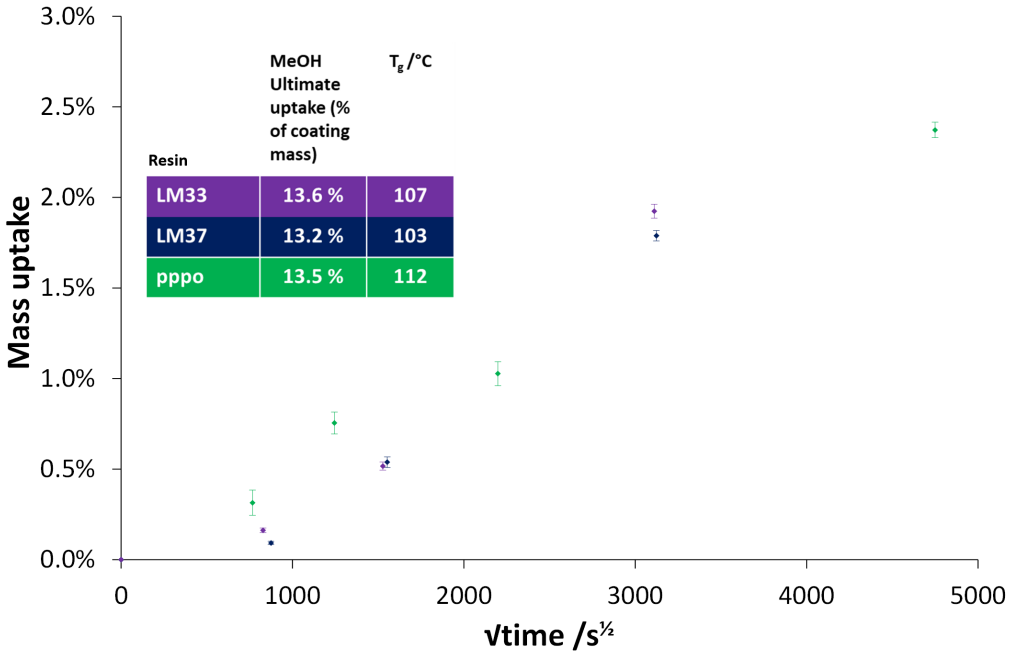

Figure 5.9: Ethanol uptake for networks made with the chromatographically purified DGEBF mixtures (LM33 & LM37), and an approximately even mixture of pp and po DGEBF (pppo) (cured with MXDA). Error bars show standard error of three samples.

Summary

DGEBF isomers Ortho- content was found to be a major influence on the chemical and thermal/physical properties of an epoxy network. ooDGEBF was found to produce a network which was inferior to the network made with poDGEBF, which in turn was inferior to the ppDGEBF-based network, in terms of all three parameters measured—the pp had the lowest ultimate uptake, lowest D_{sor}, and counterintuitively, the highest D_{des} (Figure 5.5). The chemical performance results can be explained in terms of the thermal and physical properties. The pp network had the highest T_g and crosslink density, indicating a more tightly packed network, also supported by its high density (Figure 5.2). T_β measurements also indicated that the ambient molecular motions had a higher energetic barrier. The oo network, by comparison, exhibited a low crosslink density and T_g, as well as a particularly low density when compared to all other DGEBF based resins across this work. This, coupled with a smaller observed β-transition, presents us with evidence that the network is both less well-packed and less mobile. The po network showed intermediate kinetics of diffusion (i.e. D_{sor} & D_{des}), though the ultimate uptake

was more similar to the pp network (Figure 5.5). This similarity is also observed in the density, though the thermal properties (T_g & T_β) are more similar to the oo—accounting for the values of D_{sor} & D_{des}. In ethanol uptake, an unexpected failure was observed for the po network, which was not seen for the pp network, nor the network based on 1:1 mixture of pp and po (Figure 5.8). The decrease in crosslink density observed for the po relative to the pp could cause this variation.

Both the oo and po based networks showed some degree of swelling in methanol (the oo greater than the po), with sigmoidal sorption plots, where the pp network showed a Fickian plot (Figure 5.6). This is attributed to the variation in crosslink density—the pp had a very high crosslink density preventing extensive swelling, where the oo had the lowest degree of crosslinking.

In comparing the properties of the network based on the pppo mixture to the pp and po networks, intermediate values for some properties are obtained—such at T_g, D_{sor} and D_{des} (Figures 5.5 & 5.2). However, there is an increase in ultimate uptake (for pppo) with a small simultaneous decrease in density. The mode of sorption also varies for the pppo based network, with two-step uptake indicating some level of inhomogeneity (Figure 5.6a).

Chromatographically purified DGEBF mixtures Again ortho- content was shown to influence the chemical performance, where the best performing network was that based on the approximately 1:1 mixture of the po and pp isomers ("pppo"), when compared to two mixtures which also had ooDGEBF in a meaningful proportion (LM33 & LM37). A higher T_g provides evidence that the pppo produced a more effectively packed network, though the densities between the three networks are very similar.

Limited variation was observed between the two LM samples, though that might be expected considering their relative similarity. However, slightly improved chemical performance was obtained for the lower ortho- content LM37, in spite of a reduced degree of cure and T_g—again suggesting the negative impact that ortho- content can have upon a network's chemical performance.

5.2 Methods/Materials

5.2.1 Materials

Meta-xylylenediamine (MXDA, 99%) was obtained from Sigma Aldrich Co. LLC., and used as supplied. All resins were obtained as described in Chapter 4.

5.2.2 Network Preparation

Glass slide preparation

Hydrogen peroxide was added with care and gentle stirring to sulfuric acid in a 1:3 ratio to produce "piranha solution". Slides (as supplied) were placed in the "piranha solution" and left for 15 minutes before rinsing thoroughly with deionised water. The treated slides were placed in a rack and dried at 50 °C in an oven, and stored there until use.

General network preparation for solvent sorption/desorption studies

Formulation Epoxy resin was added to MXDA (for identities/quantities see Table 5.4), and then mixed using a stirring rod. The resulting mixture was covered using parafilm, and held, with further mixing (initially every five minutes, then less regularly), at 33 °C. Upon any clouding, the mixture was heated with a heat gun until melted—and then returned immediately to 33 °C

Application to glass slides/Cure After a pot-time of 75 minutes, the mixture was drawn-down onto prepared glass slides (see section 5.2.2), held at 30 °C, using a drawdown cube. The drawdown cube was obtained from Sheen Instruments, with a 400 μm slot. The slides were then placed in an oven and cured under a nitrogen atmosphere. Oxygen free nitrogen, obtained from BOC, was purged through the oven at $\sim$5 cm^3 min^{-1}. The cure schedule was an initial temperature of 60 °C, with a ramp of 1 °C min^{-1} to 160 °C, where the oven was held for three hours. Upon completion of the three hours, the samples were removed from the oven and allowed to cool. Any

samples not immediately analysed were placed in a desiccator over phosphorus pentoxide to prevent moisture uptake.

Amine	Mass (amine) /g	Moles (amine func group) /mol	Epoxy	Mass (epoxy) /g	Moles (epoxy func group) /mol	Stoich
MXDA	1.5153	4.45×10^{-2}	pp	7.1591	4.41×10^{-2}	100.9%
MXDA	1.1382	3.34×10^{-2}	po	5.3821	3.34×10^{-2}	100.2%
MXDA	1.0285	3.02×10^{-2}	oo[a]	4.9450	3.00×10^{-2}	100.7%
MXDA	1.6748	4.92×10^{-2}	pppo	7.8262	4.91×10^{-2}	100.2%
MXDA	1.7416	5.12×10^{-2}	LM33	8.2911	5.10×10^{-2}	100.0%
MXDA	2.4277	7.13×10^{-2}	LM37	11.5648	7.12×10^{-2}	100.1%

Table 5.4: Quantities used in cures for solvent sorption/desorption studies. [a]oo has a higher melting point and greater tendency to crystallise, therefore the pot-temeperature used was higher (40 °C) in order to reduce the likelihood of crystallisation—see Section 5.2.2

Network preparation for solvent sorption/desorption studies - ooDGEBF

Formulation ooDGEBF was added to MXDA (for quantities see Table 5.4), and then mixed using a stirring rod. The resulting mixture was covered using parafilm, and held, with further mixing (initially every five minutes, then less regularly), at 40 °C. As described in Section 5.1.1, as much reaction as possible was allowed to complete in spite of crystallisation, before re-melting with a heat gun followed by immediate cooling back to 40 °C.

Application to glass slides and cure was conducted as in Section 5.2.2, though the pot-time was reduced to 20 minutes.

Network preparation for dynamic mechanical analysis and helium pycnometry

All networks were formulated as in the previous sections (all but ooDGEBF as in the general description above and ooDGEBF as in the specific section directly above). After the relevant pot-time, these mixtures were then poured into PTFE moulds (for DMA bars), spotted onto release film (for helium pycnometry), and cured under a nitrogen

atmosphere. Oxygen free nitrogen, obtained from BOC, was purged through the oven at $\sim$5 cm^3 min^{-1}. The cure schedule was an initial temperature of 60 °C, with a ramp of 1 °C min^{-1} to 160 °C, where the oven was held for three hours. Upon completion of the three hours, the samples were removed from the oven and allowed to cool. Prior to analysis, samples were then placed in a desiccator over phosphorus pentoxide to prevent moisture uptake.

5.2.3 Near-Infrared (NIR) spectroscopy

Degree of cure was measured by NIR spectroscopy, as described in Chapter 2—see Section 2.2.4.

5.2.4 Solvent sorption/desorption

Solvent uptake was performed in the same manner as in Chapters 2 & 3, see Section 3.2.5.

5.2.5 Dynamic mechanical analysis (DMA)

DMA was performed as in Chapter 3, see Section 3.2.6.

5.2.6 Helium pycnometry

Helium pycnometry was performed as described in Chapter 2, see Section 2.2.9.

References

[1] Tu, J., Tucker, S. J., Christensen, S., Sayed, A. R., Jarrett, W. L. & Wiggins, J. S. Phenylene ring motions in isomeric glassy epoxy networks and their contributions to thermal and mechanical properties. *Macromolecules*, **48**(6), 1748–1758 (2015).

Chapter 6

Themes and conclusions

6.1 Overview

This investigation sought to investigate the effects of changing the following features upon chemical performance of an epoxy resin network:

A. Geometry of molecules - generally edited by the position of substituents on six-membered rings

B. Nature of chemistry - by changing the nature of six-membered rings from aromatic to aliphatic, and changing the type of bisphenol

C. Distance between bonds - inherent to a change of geometry, the distance between reactive groups will also be varied. This can also be achieved by editing the epoxy resin.

These areas have been explored in the individual chapters, of which brief summaries will be given. Further, there are comparisons to be drawn between the work of various chapters in order to fully explore the findings of this work.

6.2 Discussion of research aims

In order to answer the aforementioned aims, a range of networks was produced. Initially, optimisation of the curing process was performed, including examining the effect of cure atmosphere and stoichiometry of mixing. A full list of the networks produced for Chapters 3-6 is shown in Table 6.1. These were prepared with 100 % stoichiometry (1:1 ratio of epoxy : amine hydrogens), and cured under a nitrogen atmosphere, above the ultimate T_g of the networks, at 160 °C.

Name(s)	Epoxy	Amine
DER 354 / MXDA	Dow Epoxy Resin 354 (DGEBF based)	meta-Xylylenediamine
PY306	Araldite PY306 (DGEBF based)	meta-Xylylenediamine
E828	Epikote 828 (DGEBA based)	meta-Xylylenediamine
DER 332	Dow Epoxy Resin 332 (DGEBA based)	meta-Xylylenediamine
1,3-BAC	Dow Epoxy Resin 354	1,3-bis(Aminomethyl)cyclohexane
1,4-BAC	Dow Epoxy Resin 354	1,4-bis(Aminomethyl)cyclohexane
PXDA	Dow Epoxy Resin 354	para-Xylylenediamine
PACM	Dow Epoxy Resin 354	bis(para-Aminocyclohexyl) methane
pp	para-para-DGEBF	meta-Xylylenediamine
po	para-ortho-DGEBF	meta-Xylylenediamine
oo	ortho-ortho-DGEBF	meta-Xylylenediamine
pppo	DGEBF isomers*	meta-Xylylenediamine
LM37	DGEBF isomers*	meta-Xylylenediamine
LM33	DGEBF isomers*	meta-Xylylenediamine

*Table 6.1: The chemical basis for networks produced in this study. DGEBF and DGEBA are the diglycidyl ethers of bisphenol F and A respectively. *The final three samples are chromatographically purified DGEBF mixtures, the compositions of which are shown in Table 6.2.*

	pppo	**LM33**	**LM37**
pp : po : oo	.45 : .52 : .03	.33 : .50 : .17	.37 : .47 : .16

Table 6.2: pppo, LM33 and LM37 represent mixtures of the three n=0 isomers of DGEBF (pp,po and oo - defined in Table 6.1), as obtained from column chromatography. This table shows pp : po : oo ratios for these chromatographically purified DGEBF mixtures. LM33 and LM37 represent the two low molecular weight (LM) samples with differing pp : po : oo ratios, the number represents the proportion of pp.

6.2.1 A. Geometry of molecules

Where the geometry of the molecules involved in network structure is considered, we have observed the effects of changes to both the epoxide (Chapter 5 and to a lesser extent, Section 3.1.3) and amine (Section 3.1.4). With regards to epoxides, the variation considered was ortho- versus para- susbstitution of the bisphenol unit. Meta- substitution is not present, due to the mechanism of formation of bisphenols from phenol and a carbonyl group—the hydroxyl group present in phenol directs the substitution to ortho- and para-.[1] In the case of the amines investigated the key change was 1,3- to 1,4- substitution, in both aromatic (i.e. meta- to para-) and aliphatic systems.

Ortho- and para- substitution in DGEBF

Broadly, increasing the proportion of ortho- substitution in diglycidyl ether of bisphenol F (DGEBF) based resins was found to be detrimental to the chemical performance of the network (Figure 6.1), which was reflected in the measured physical properties. In Section 5.1.2, the comparison of networks made with the three pure isomers of DGEBF (para-para- (pp), para-ortho- (po) & ortho-ortho- (oo)) showed particular deterioration of chemical performance for the completely ortho- substituted oo network, and the pp was found to be better performing than the po (Figure 6.1a).

Regarding mixtures of the DGEBF isomers, in Chapter 2, a network based on Dow Epoxy Resin 354 (DER 354) was shown to be better performing than one based on the higher ortho- content Araldite PY306 (PY306)—Figure 6.1. This trend was also observed for the networks based on chromatographically purified isomers in Section 5.1.2, where the pppo and LM37 performed better than the more ortho- containing LM33. However, this trend is less marked, indeed, the trend is only seen for D_{sor} and not ultimate uptake. Changes observed in the ultimate uptake showed a much greater reliance on other factors—e.g. while LM37 has a greater ortho- content, it also has a reduced chain-extended content, the effects of which are discussed in more detail below (Section 6.2.3). Generally, a reduction of the distance between bonds results in a better-performing network, which would explain the lower than expected ultimate uptake.

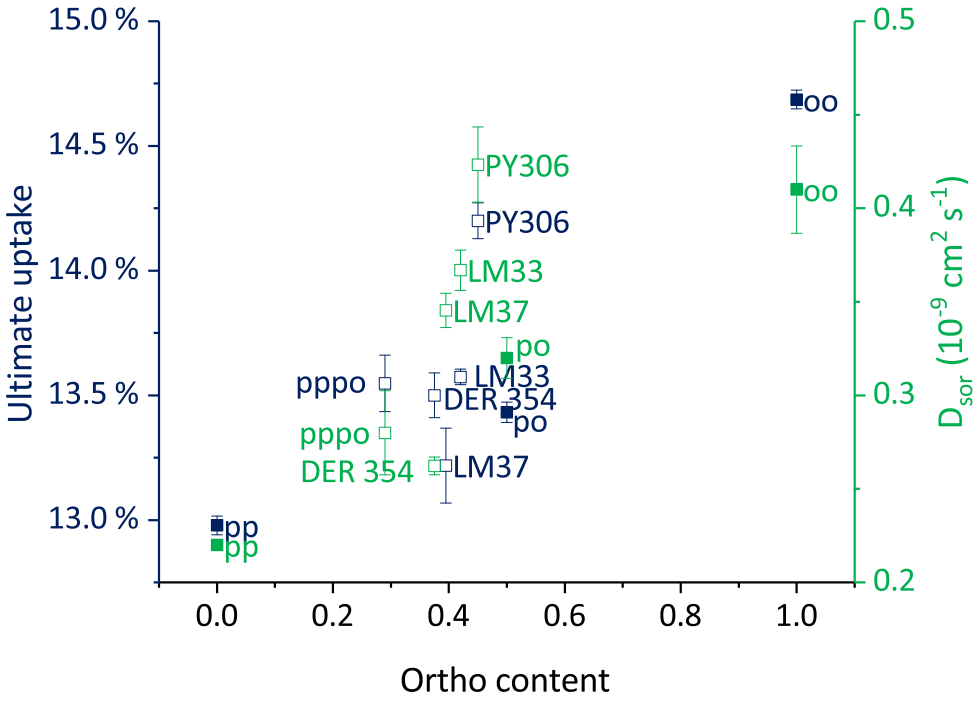

(a)

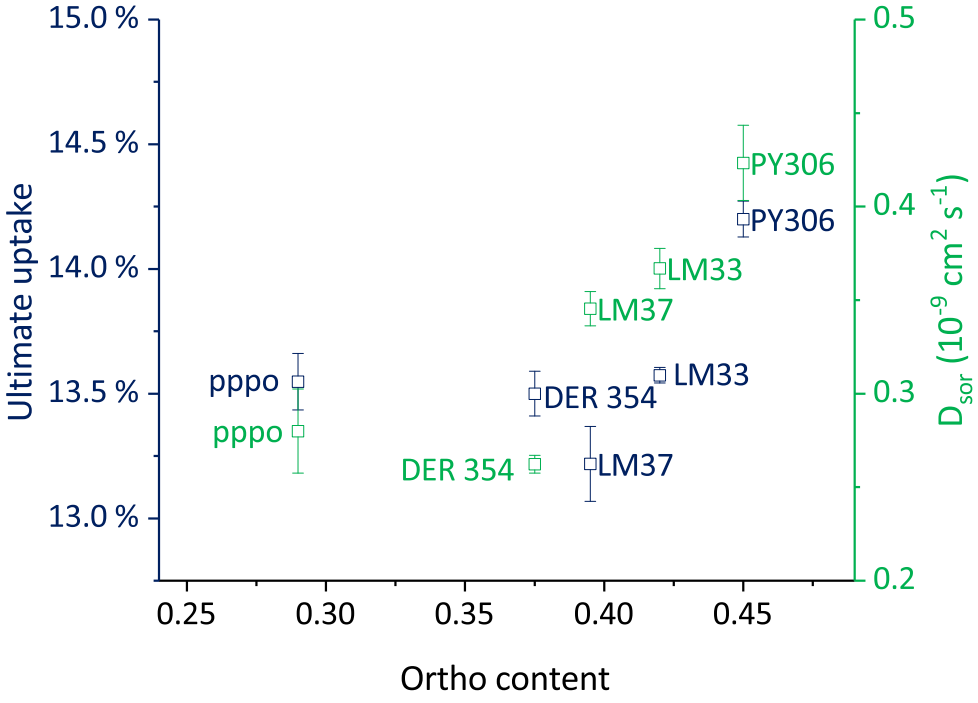

(b)

Figure 6.1: Ultimate uptake and sorption diffusion coefficient for all of the DGEBF based networks with differing amounts of ortho- substitution. Pure isomers are solid colours, and mixtures are outlined. Each sample is labelled—all were cured with MXDA as the amine. (b) shows a zoomed picture of the isomeric mixtures.

1,3- and 1,4- substitution in amines

This comparison is discussed in full in Chapter 3—a short summary is given here. Regardless of the nature of the bonding, 1,3- substituted species performed better than 1,4- substituted species, when forming a network with DER 354. MXDA and 1,3-BAC based networks performed markedly better than those based on their 1,4- analogues PXDA and 1,4-BAC, irrespective of the thermal/physical properties of the material. For example, while MXDA and PXDA based networks had near-identical densities, the uptake of methanol and ethanol was lower for the MXDA.

6.2.2 B. Nature of chemistry

DGEBF/DGEBA based networks

Section 3.1.3 shows a comparison of networks based on some industrially available DGEBF and DGEBA based resins, when cured with MXDA. The DGEBF based network DER 354 showed the best performance in both methanol and ethanol, and that based on Epikote 828 (E828 - based on DGEBA) showed the worst. PY306 (DGEBF based) and Dow Epoxy Resin 332 (DER 332 - DGEBA based) based networks showed intermediate properties, where identifying the better performing depends on the measure/solvent used. However, these comparisons are not completely fair, since the DGEBA based resin consists of a single regioisomer, but the DGEBF based resins have the mixture of regioisomers discussed above. Therefore, the most accurate comparison to draw would be between networks based on the synthesised ppDGEBF and DER 332 (which could also be described as ppDGEBA), as both have very low degrees of chain extension and represent the same regioisomers for the different chemistries.

Figure 6.2 compares both the thermal & physical properties and the chemical performance in methanol of the network produced when cured with MXDA. Clearly, the ppDGEBF network performs substantially better in terms of uptake and D_{sor}. D_{des} is also reduced. The density of the ppDGEBF network is much higher than the DER 332 network, which would suggest a more tightly packed network, and T_{β} is higher, suggesting a network which has molecular motions with a higher energetic barriers. Both of these factors would predict the improved performance. However, it does contradict the literature that suggests a higher crosslink density leads to reduced chemical performance.[2,3] In any case, the results show the methyl groups present on the bridging carbon of the bisphenol unit in DGEBA causes a clear disruption of chain packing, which results in a lower density and, in turn, a reduced chemical performance.

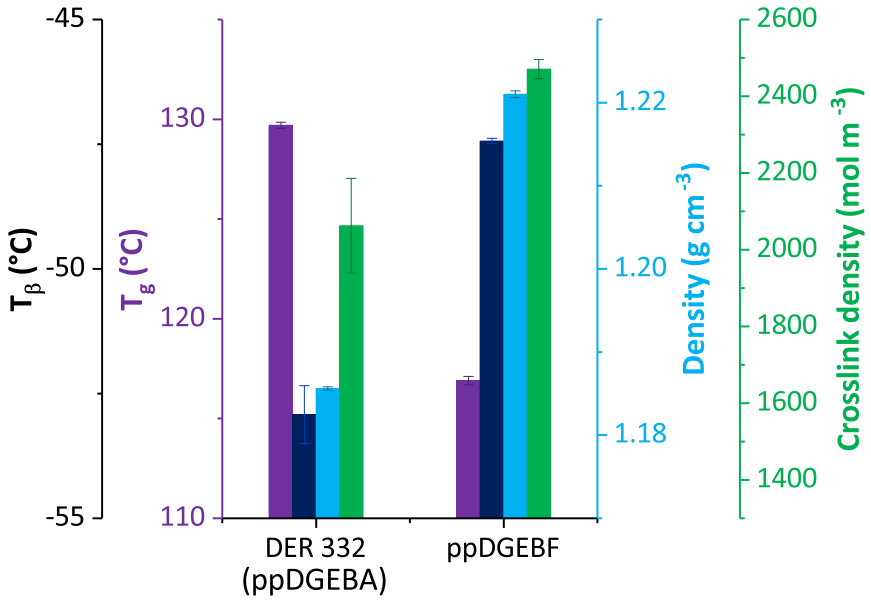

(a)

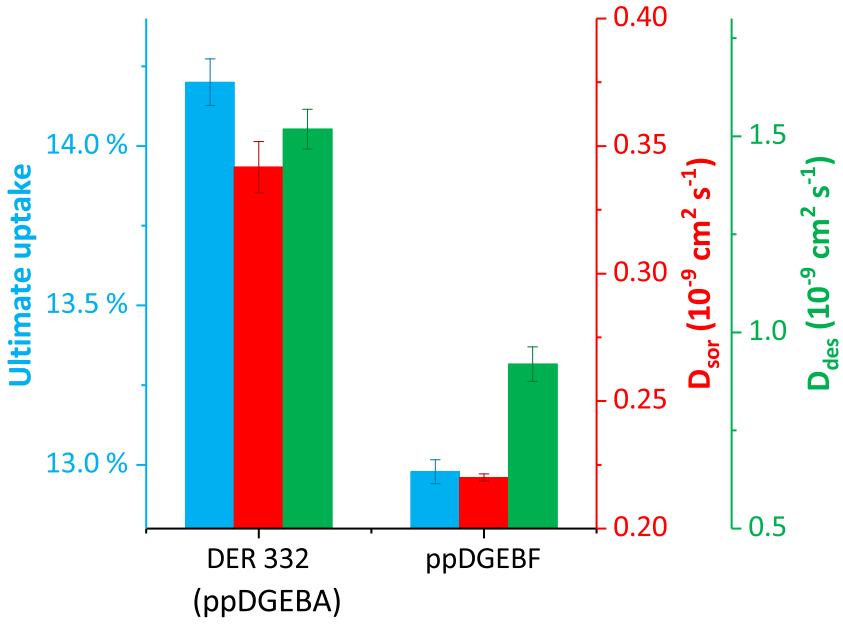

(b)

Figure 6.2: Summary of (a) thermal & physical properties and (b) methanol uptake properties for ppDGEBF and DER 332 (ppDGEBA) based networks (cured with MXDA). (a) shows the glass transition temperature (T_g), β-transition temperature (T_β) & crosslink density (as measured by dynamic mechanical analysis) and density (as measured by helium pycnometry). (b) shows the ultimate uptake, and diffusion coefficients for sorption (D_{sor}) and desorption (D_{des}) of methanol.

Aromatic/Aliphatic amine

Again, this comparison is discussed in full in Chapter 3, though a short summary will again be given. Unexpectedly, the T_gs of the networks produced with aromatic amines were found to be lower than their aliphatic analogues. In spite of this, their performance in both methanol and ethanol was found to be markedly better. The density of the aromatic systems were substantially higher than the aliphatic equivalents, which again is an indicator of a better packed network, confirmed by the methanol uptake. Further, for ethanol uptake, networks based on aliphatic amines exhibited greater swelling (see Section 3.1.4 for more detail). Little variation is observed between the samples in crosslink density or T_β. The PXDA and 1,3-BAC networks were found to be quite similar in performance, indicating that the change from aromatic to aliphatic bonding had a similar effect to the change from meta- to para-.

6.2.3 C. Distance between bonds

The isomeric study indicates that this is not the primary driver, since ortho- substitution inherently results in a shorter distance between crosslinks, but is detrimental to the network. However, the added distance between crosslinks caused by chain extension of the epoxy resin monomer can also be observed through comparison of DER 332 and E828. As discussed in Section 3.1.3, the E828 based network is worse-performing, both in terms of ultimate uptake and rate of uptake. E828 / MXDA also exhibits "two-step" uptake, which suggests some degree of inhomogeneity throughout the network—which we might attribute to the presence of the chain extended isomers.

A second opportunity to examine the effects of chain extension is to compare the chromatographically purified DGEBF mixtures used in Section 5.1.2 to the industrial mixtures used in Section 3.1.3. In terms of regioisomeric composition, LM33 bears a good semblance to PY306 ($\pm$ 3 % per isomer), and likewise, LM37 to the DER 354 ($\pm$ 3 % per isomer). The changes in both thermal/physical properties and uptake properties of networks made with these resins (cured with MXDA) are shown in Figure 6.3. Each individual comparison is isolated by the grey box, the mixture containing chain extended isomers on the left of each box. In all cases, there is a small but measurable increase in density and a simultaneous reduction in the ultimate uptake. For the comparisons of the networks based on PY306 & LM33 and E828 & DER 332, similar reductions are observed in D_{sor} and D_{des}, though there is an increase in D_{sor} when comparing the DER 354 & LM37 networks. This is justified as a result of the higher ortho- content of LM37, which causes a deterioration in chemical performance, as discussed in Section 6.2.1. Therefore, the distance between crosslinks is shown to have a greater impact upon the ultimate uptake than D_{sor}, where the change to molecular packing caused by regioisomerism has a greater impact upon the rate of sorption.

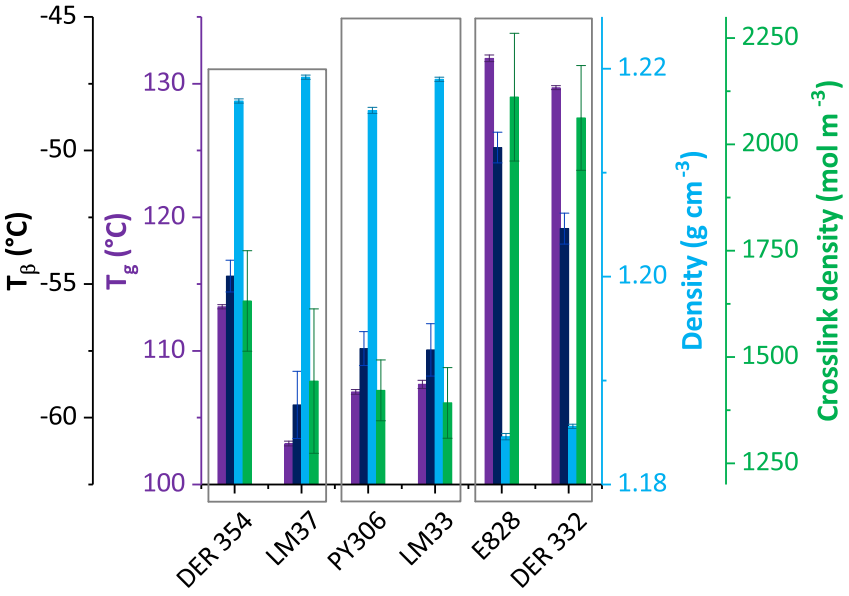

(a)

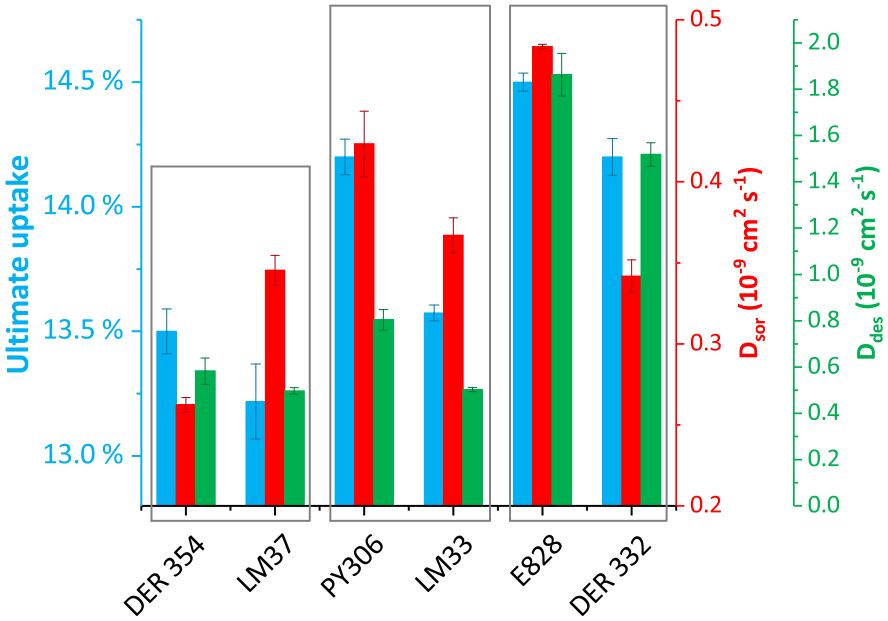

(b)

Figure 6.3: Summary of (a) thermal & physical properties and (b) methanol uptake properties examining the influence of chain extended isomers upon both DGEBF (DER 354/LM37, & PY306/LM33) and DGEBA (E828/DER 332) based networks (all were cured with MXDA). (a) shows the glass transition temperature (T_g), β-transition temperature (T_β) & crosslink density (as measured by dynamic mechanical analysis) and density (as measured by helium pycnometry). (b) shows the ultimate uptake, and diffusion coefficients for sorption (D_{sor}) and desorption (D_{des}) for methanol.

Unusual desorption trends

A final feature of note which appears to be related to both the geometry / distance between bonds is the relationship between D_{des} and D_{sor}. The expectation for chemically similar networks is that a material with a high rate of sorption would have a high rate of desorption also, as the free volume which allowed rapid sorption would also allow rapid desorption. Clearly, any specific solvent-polymer interactions would change this relationship, but for the networks considered in this study, that possibility is judged unlikely as a result of their chemical similarity. Section 5.1.2 showed that the expected relationship between sorption and desorption rates was not observed for the networks based on individual isomers of DGEBF (and MXDA). Figure 6.4 shows the ratio of D_{des}/D_{sor}. While a definitive trend is absent, generally, it appears networks consisting of monomers with more linear molecular structures (i.e. a higher aspect ratio) exhibit a higher D_{des}/D_{sor} ratio. For example, para- content generally causes an increase in the ratio, as does the shift in hardener from 1,3-BAC to PACM.

The swelling of a network results in the decrease in entropy for the polymer chains, driven by the entropy of the solvent-polymer mixing.[4] A hypothesis for the observed trend would be that the swelling of higher aspect ratio molecules causes a bigger loss of polymer chain entropy which upon removal of solvent produces a system further from equilibrium, leading to a faster rate of desorption.

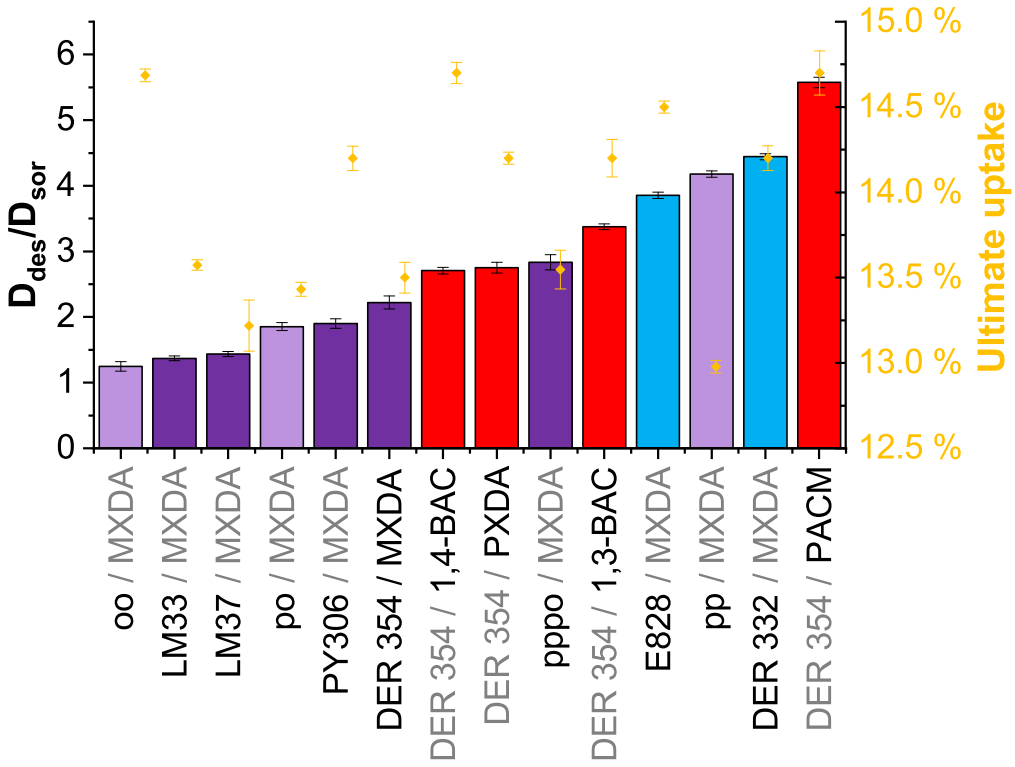

Figure 6.4: The ratio of the desorption and sorption diffusion coefficients (D_{des}/D_{sor}) and ultimate uptake for the networks produced in this study. Networks based on DGEBF & MXDA are coloured purple (with individual isomers a lighter shade); networks based on DGEBF & a different amine to MXDA are red; and networks based on DGEBA & MXDA are blue. Error bars show standard error of three samples.

6.3 Conclusions

6.3.1 Thermal/Physical properties and their relationship to chemical performance

A key finding of this investigation is the absence of one particular physical/thermal property that will accurately predict the chemical performance across all epoxy resins. The properties measured include the glass transition temperature (T_g), the crosslink density, the bulk density of the network and the β-transition temperature (T_β). Simple plots of these properties against the two main chemical performance parameters, ultimate uptake and the sorption diffusion coefficient (D_{sor}), show at best limited correlation (Figure 6.5)—when a linear fit is performed, only two (of six) plots show an R^2 >0.8. No R^2 >0.95 was obtained and therefore in the summaries below, the graphs plotted show the values for each sample discretely, rather than the plots shown in Figure 6.5 so extenuating factors can be considered.

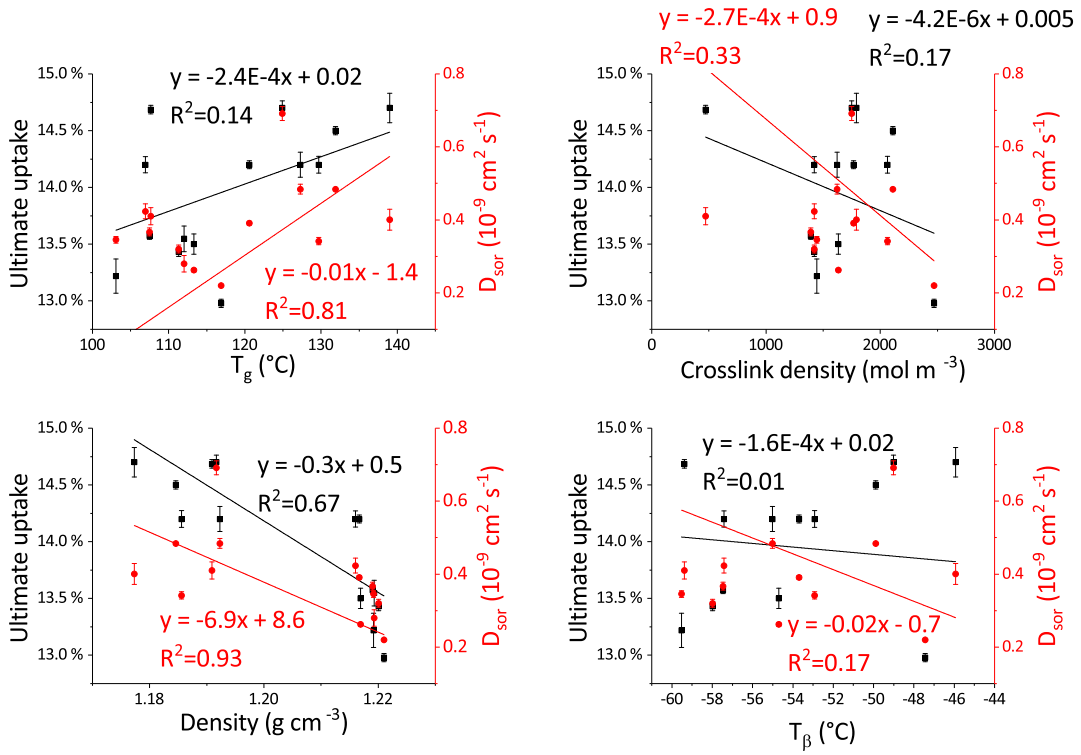

Figure 6.5: Relationship between (a) T_g (top left) / crosslink density (top right) / density (bottom left) / T_β (bottom right) and (b) ultimate uptake (black) / sorption diffusion coefficient (D_{sor} - red)

T_g The T_g was shown to offer an effective measure of degree of cure for a particular chemical system, cured under carefully controlled conditions (i.e. a higher T_g indicates a higher degree of cure). Indeed, where T_g is seen to noticeably deteriorate (e.g. 90 % stoichiometry sample—see Section 2.1.6), it is indicative of a much worse performing network as a result of the reduction in degree of cure. However, even for an identical chemical system (DER 354 / MXDA), samples with the same T_g were shown to perform differently as a result of a change in cure atmosphere. Further, DGEBA based networks had much higher T_gs than DGEBF based networks, but performed worse. This is illustrated in Figure 6.6—all networks based on DGEBF are to the left of the grey line (i.e. lower in T_g) but have better chemical performance. An exception of note is the oo / MXDA network which shows a clear deterioration of performance, with a very high ultimate uptake (compared to those around it with a similar T_g). This indicates a fundamentally different free volume distribution, even if there is some architectural similarity (shown by the T_g).

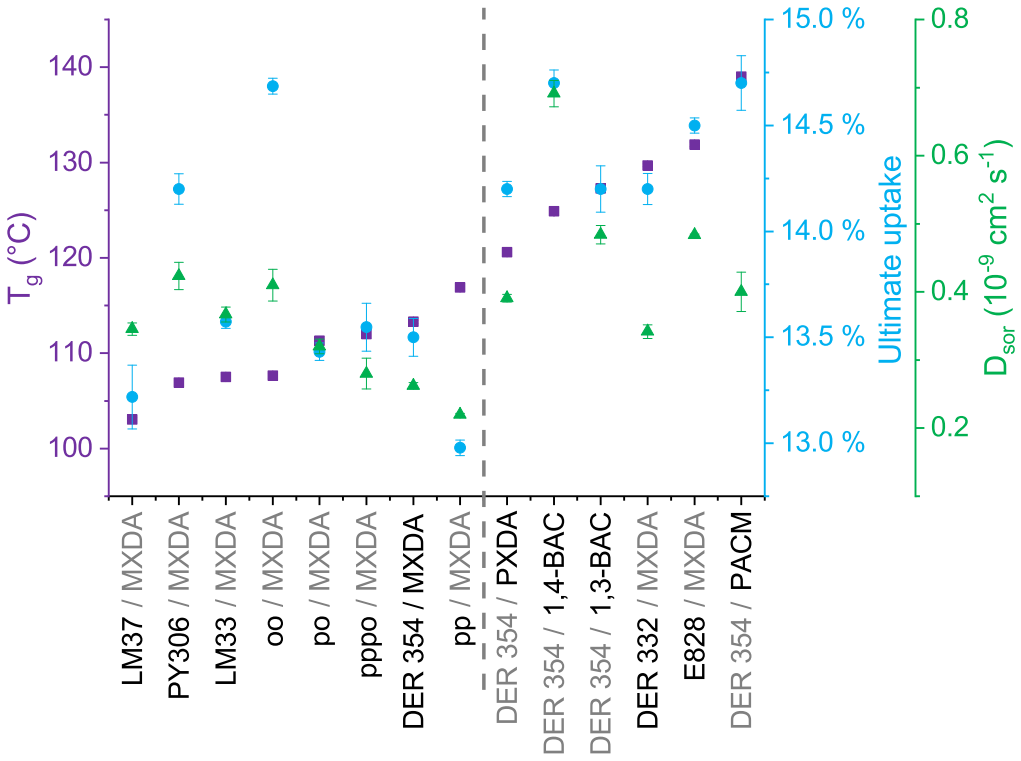

Figure 6.6: Comparison of ultimate uptake and sorption diffusion coefficient (D_{sor}) to T_g for all networks cured across this study. The data is shown in ascending order of T_g, from left to right. See Table 6.1 for information regarding sample naming

Crosslink density Where the isolated ppDGEBF network was found to have the highest crosslink density and best chemical performance, the next five highest crosslink densities exhibited substantially worse performance than the DER 354 / MXDA networks. The trends (or lack thereof) in Figure 6.7 illustrate that the crosslink density cannot be used as a predictor for chemical performance, though again it can be an indicator of an effectively packed network when confined to chemically similar systems. The variation in chemical performance between DER 354 / MXDA and the pp network was markedly smaller than the drastic change in crosslink density. This might be because of the diversity of species, which leads to a variability in the distance between crosslinks which could cause some of the network not to be mechanically active.[5]

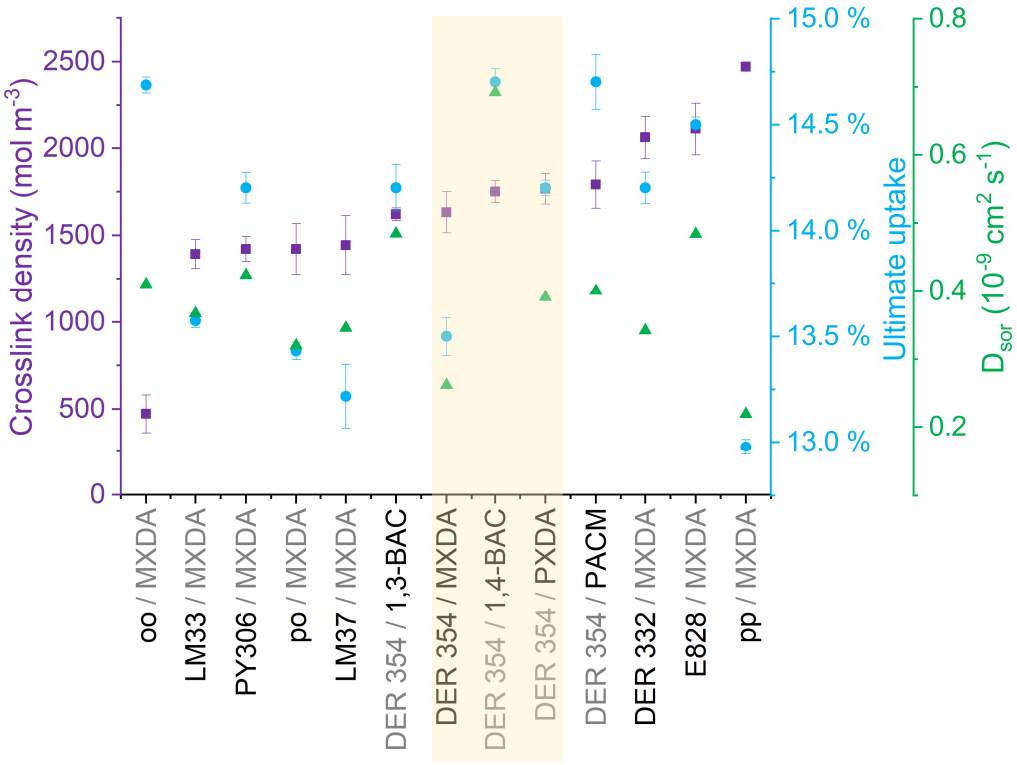

Figure 6.7: Comparison of ultimate uptake and sorption diffusion coefficient (D_{sor}) to crosslink density for the networks produced in this work—shown in ascending order of crosslink density from left to right. Particular attention is drawn to the highlighted region to show a wide range of chemical performance with very limited crosslink density variation. See Table 6.1 for information regarding sample naming.

Density Generally the density represented the best predictor of high chemical performance—the best performing network across the study was also the densest, and generally worse performing networks were found to be lower in density (e.g. 1,4-BAC, E828, oo - see Figure 6.8). However, there were also examples of less dense materials found to be better performing in terms of rate of sorption (e.g. 1,3-BAC, DER 332), though generally their ultimate uptake remained higher than the best networks. Ultimately, density is a good starting point, but again substantial variation in performance can be observed for networks with very similar densities—perhaps a comparison of the MXDA and PXDA networks provides the strongest case for this.

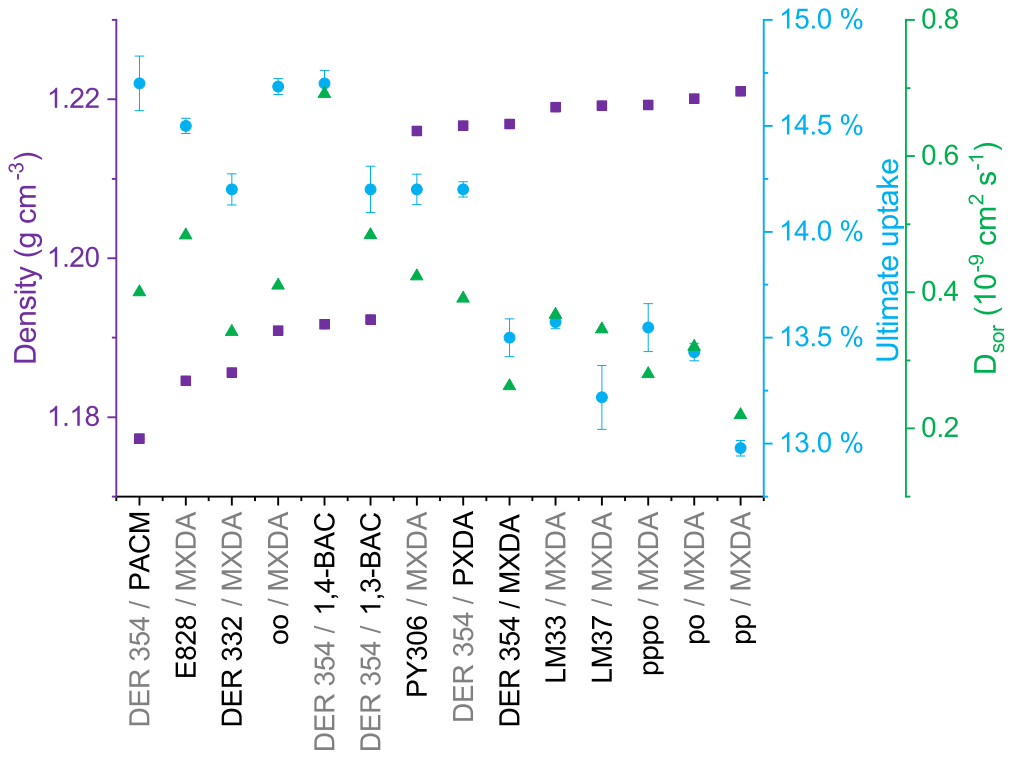

Figure 6.8: Comparison of ultimate uptake and sorption diffusion coefficient (D_{sor}) to density for the networks produced in this work—shown in ascending order of density from left to right. See Table 6.1 for information regarding sample naming.

β-transition Variation of the temperature and area of the β-transition was observed across the samples. As shown by both Figures 6.5 and 6.9a, there is no general trend. However, the marked suppression of the transition when comparing para- substituted species to either meta- (PXDA vs. MXDA - amines) or ortho- (ppDGEBF vs. ooDGEBF - resins) substituted species is of note. This suppression is indicative of a reduction in molecular motion. In the case of MXDA and PXDA (where both were cured with DER 354), this reduction was suggested as a possible justification for the decrease in D_{sor} observed (Section 3.1.4). A decrease in D_{sor} is not observed for oo vs. pp, though there is a large decrease in density—which has a greater influence upon the chemical performance.

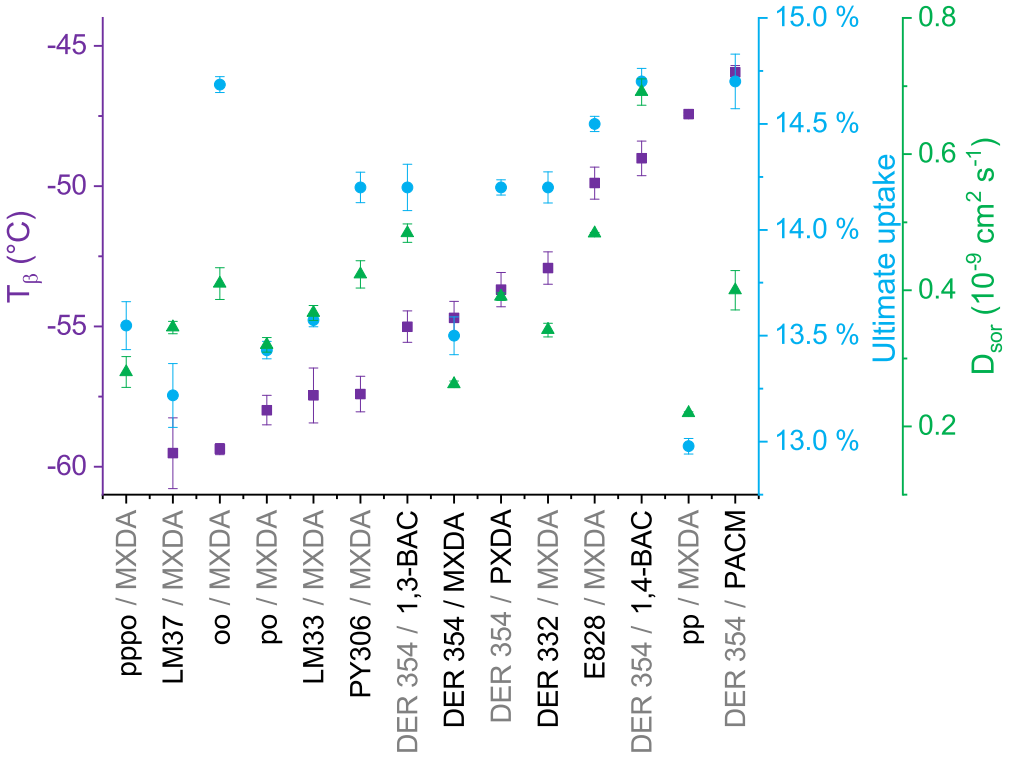

(a)

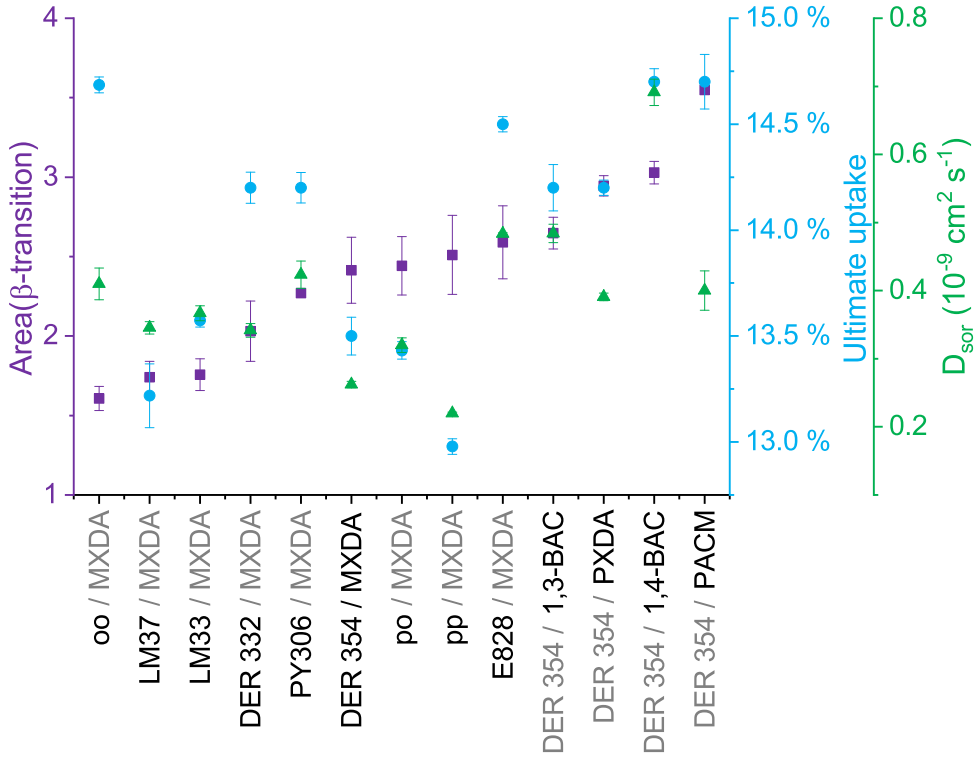

(b)

Figure 6.9: Comparison of ultimate uptake and sorption diffusion coefficient (D_{sor}) to (a) T_β and (b) the area of the β-transition, for the networks produced in this work—shown in ascending order of density from left to right. See Table 6.1 for information regarding sample naming.

6.3.2 Considerations for improving the chemical performance of an epoxy-amine network

The chemical basis of an epoxy network has a strong influence upon its subsequent chemical performance. Even the atmosphere of cure alters how a network responds to a solvent, where the use of an inert atmosphere during cure will improve performance. Across this work, networks based on DGEBF monomers (over DGEBA), aromatic amines (over aliphatic amines) and with a reduced distance between reactive groups (in the epoxy resin monomer) were found to result in denser networks which showed improved chemical performance. Improvements in performance were also offered with 1,3- substitution of amines (over 1,4- substitution) and reducing the proportion of ortho- substituted bisphenol moieties in DGEBF based resins.

The production of networks from the individual isomers of DGEBF particularly illustrated the variation that molecular geometry can cause in terms of chemical performance, where network polarity was virtually identical. The network based on ppDGEBF showed the best chemical performance of any network produced, as well as the highest density and crosslink density.

6.3.3 Application and future work

Key findings This work has shown a range of features to consider when formulating for chemically resistant networks, including;

- The importance of considering regioisomerism in bisphenol F based systems. Primarily to reduce the ortho-ortho content where possible (in order to reduce solvent uptake).
- That where truly analogous systems (and purer) are considered, bisphenol F based systems show substantially reduced solvent uptake in rate and ultimate uptake.
- That 1,3- substitution in amines results in reduced solvent uptake compared to 1,4- substitution.
- That aromatic linkages in amines are preferable to their aliphatic analogues
- Reduction of the degree of chain extension in epoxy resin monomers results in a small but measurable reduction in solvent uptake

Future work Future opportunities include;

(a) The robustness of a formulation - for situations where cure under an inert atmosphere, well above the maximum T_g of the material is not possible (as is the case in an industrial setting). Further study of the effects of oxidation and carbamation could be considered under industrially applicable systems (e.g. varied application temperature and relative humidity)

(b) This work only considers the chemical performance of ideal networks, and gives no regard to processability of the materials involved. Clearly the networks based upon individual isomers presented a much greater challenge to prepare (in terms of melting point), especially the best-performing ppDGEBF / MXDA and worst performing ooDGEBF / MXDA networks. Therefore, a greater understanding of the crystallisation of DGEBF isomers and driving forces relating to this would be of interest.

(c) Since the lowering of ortho- content has been shown to produce better performing DGEBF based networks, synthetic selectivity for greater para- content might be explored, as well as removal of ooDGEBF higher MW components. Acidic zeolites have previously been used as catalysts with other chemistries, and indeed bisphenol F to promote the formation of more linear structures.[6,7] Exploring the control that these methods offer, as well as the properties of the mixtures obtained with these catalysts would be of great interest. Investigations might include some measure of processability.

(d) The unusual trend in D_{des}/D_{sor} presents another opportunity. When applied as a tank coating, epoxy resins are formulated for low solvent uptake and low D_{sor}, but little regard is given to D_{des}. However, contamination of the solvents carried (cargoes) is a major concern. In order to prevent contamination, extensive cleaning procedures are carried out, usually involving rinsing with warm water.[8,9] If a coating with a higher D_{des} is used, the amount of cleaning required is reduced, as the solvent can be removed more easily. Therefore, further work could be carried out in order to further study the fundamental science behind this unusual trend discussed in Section 6.2.3. An initial starting point would be to produce a network combining the highest aspect ratio epoxy and amine and observe whether further increases are observed in D_{des}/D_{sor}, as well as the other extreme to observe whether a lower value is obtained.

(e) The molecular motions probed to some extent in terms of the β-transition could be investigated in much greater detail using solid-state NMR techniques and quasi-elastic neutron scattering, which would give definitive evidence as to which motions were present at a particular temperature. This work would require selectively deuterated networks, and therefore extensive synthetic chemistry in order to obtain the components of such networks.

References

[1] Clayden, J., Greeves, N. & Warren, S. *Organic Chemistry*. OUP Oxford, 1st edition (2001). ISBN 9780199270293.

[2] Pethrick, R. A., Hollins, E. A., McEwan, I., Pollock, E. A., Hayward, D. & Johncock, P. Effect of cure temperature on the structure and water absorption of epoxy/amine thermosets. *Polymer International*, **39**(4), 275–288 (1996).

[3] Morsch, S., Lyon, S., Greensmith, P., Smith, S. & Gibbon, S. Water transport in an epoxy–phenolic coating. *Progress in Organic Coatings*, **78**, 293–299 (2015).

[4] Flory, P. J. & Rehner, J. Statistical mechanics of cross-linked polymer networks II. Swelling. *The Journal of Chemical Physics*, **11**(11), 521–526 (1943).

[5] James, H. M. & Guth, E. Simple presentation of network theory of rubber, with a discussion of other theories. *Journal of Polymer Science*, **4**(2), 153–182 (1949).

[6] Smith, K., Alotaibi, M. H. & El-Hiti, G. A. Highly regioselective dinitration of toluene over reusable zeolite Hβ. *Journal of Catalysis*, **297**, 244–247 (2013).

[7] Jana, S. K., Okamoto, T., Kugita, T. & Namba, S. Selective synthesis of bisphenol F catalyzed by microporous H-beta zeolite. *Applied Catalysis A: General*, **288**(1-2), 80–85 (2005).

[8] Port, A. B. & Cameron, C. Performance Properties of Coatings. In Marrion, A., editor, *The Chemistry and Physics of Coatings*, pages 64–95. Royal Society of Chemistry, Cambridge, 2nd edition (2004).

[9] Cameron, C. Private communication. *AkzoNobel* (2014).